Functionalised Iron(II) Supramolecular Helicates: Design, Synthesis and DNA Binding Studies

Jenna Anne Norman

A thesis submitted to the University of Birmingham for the degree of Doctor of Philosophy

School of Chemistry
University of Birmingham
September 2012

Abstract

The work described in this thesis concerns the design, synthesis and DNA binding activity of functionalised iron(II) supramolecular helicates.

DNA and the ways that organic and metallo-molecules recognise and bind to it are reviewed. The field of supramolecular chemistry and particularly supramolecular helicates is considered, including those developed as anticancer agents.

The design of a novel functionalisation route for the development of functionalised helicates is presented. The synthesis and characterisation of several metallo-helicates functionalised with simple chemical groups, such as hydroxyl and phenyl moieties, is described. Studies reveal that this functionalisation does not inhibit the inherent DNA binding activity of these types of cylinders.

The development of steroid-hormone functionalised iron(II) helicates for targeted delivery to cancerous tissues is also detailed, including their synthesis and characterisation. These steroid functionalised complexes bind to DNA, inducing changes in the DNA conformation.

The design, synthesis and characterisation of several metallo-helicates functionalised with targeting sugar vectors, is also presented. These sugar-conjugates can bind to DNA, causing intramolecular coiling and unwinding of the DNA helix.

Acknowledgements

First of all I would like to thank my supervisor Professor Mike Hannon for the brilliant opportunity he has given me to be part of the Hannon group and to work on such an interesting project. I am grateful for his guidance, wisdom and encouragement and for his advice on life.

I would like to thank all past and present members of the Hannon group with whom I have had the pleasure of working with, especially Carlos Sanchez-Cano my Hannon group father. I am also grateful to the members of the School of Chemistry analytical facility; to Peter, Neil and Graham for their hard work and advice.

The biggest and most heartfelt thanks goes to Natalia Calle Alonso with whom I have spent almost every day for the past four years, sharing every high and every low. For keeping me smiling and working hard, along with all the advice and gossip and for being the best friend I could have asked for.

I would like to express my deepest gratitude to my mum and dad, for everything they have done for me. For their love, support and wisdom throughout these last twenty five years which has been invaluable and will always be treasured. I would also like to thank my sister Lauren for her support and words of encouragement.

To my husband Chris, thank you for always being there, for all the love and support and for being my rock. I couldn't live without you.

I am grateful to the University of Birmingham and the EPSRC for funding.

Contents

Chapter 1: Introduction 1

1.1 DNA structure 1

1.2 DNA recognition 3

1.2.1 Major groove binding 3

1.2.2 Minor groove binding 5

1.2.3 Sugar-phosphate backbone binding 9

1.2.4 Intercalation 10

1.2.5 Coordinative DNA binding: platinum based drugs 13

1.2.5.1 Cisplatin 14

1.2.5.2 Second generation platinum drugs 17

1.2.5.3 Multi-nuclear platinum drugs 18

1.2.5.4 Platinum(IV) prodrugs 19

1.3 Other, non-platinum based transition metal anticancer agents 20

1.3.1 Ruthenium drugs 20

1.3.2 Rhodium drugs 21

1.3.3 Rhenium drugs 22

1.3.4 Iridium drugs 24

1.3.5 Iron drugs 25

1.4 Targeting other DNA structures 27

1.4.1 Targeting the Holliday junction 27

1.4.2 Targeting the three-way junction 28

1.4.3 Targeting G-quadruplexes 29

1.5 Supramolecular chemistry 33

1.5.1 Supramolecular helicates 33

1.5.2 Chirality of helicates 35

1.5.3 Applications of supramolecular helicates 36

1.5.4 Supramolecular cylinders with anticancer activity 37

1.6 Summary and thesis aims 42

1.7 References 43

Chapter 2: Novel Alkyne Metallo-Cylinders 50
2.1 Introduction and aims 50
2.2 Novel functionalisation route 51
2.2.1 Sonogashira cross-coupling 53
2.3 Molecular design 54
2.4 Synthesis 56
2.4.1 Synthesis of Parent cylinder, $[Fe_2L^{P}_3][BF_4]_4$ 56
2.4.2 Synthesis of Triple Bond cylinder, $[Fe_2L^{TB}_3][BF_4]_4$ 58
2.4.3 Synthesis of Propargyl Alcohol cylinder, $[Fe_2L^{PA}_3][BF_4]_4$ 61
2.4.4 Synthesis of Hexyn-ol cylinder, $[Fe_2L^{Hex}_3][BF_4]_4$ 64
2.4.5 Synthesis of Phenylacetylene cylinder, $[Fe_2L^{Phen}_3][BF_4]_4$ 67
2.5 Properties of synthesised alkyne cylinders 70
2.5.1 Complex counterions 70
2.5.2 Solubility of synthesised complexes 71
2.5.3 UV-Vis stability studies 72
2.6 DNA binding studies 75
2.6.1 Circular dichroism 76
2.6.1.1 Circular dichroism studies of the parent cylinder, $[Fe_2L^{P}_3]^{4+}$, with different counterions 78
2.6.1.2 Circular dichroism studies of synthesised alkyne cylinders 81
2.6.2 Linear dichroism 86
2.6.2.1 Linear dichroism studies of the parent cylinder, $[Fe_2L^{P}_3]^{4+}$, with different counterions 88
2.6.2.2 Linear dichroism studies of synthesised alkyne cylinders 91
2.6.3 Gel electrophoresis 96
2.6.3.1 Gel electrophoresis studies of the parent cylinder, $[Fe_2L^{P}_3]^{4+}$, with different counterions 99
2.6.3.2 Gel electrophoresis studies of synthesised alkyne cylinders 102
2.6.4 PAGE studies 106
2.6.4.1 PAGE studies of the parent cylinder, $[Fe_2L^{P}_3]^{4+}$, and bulky cylinder, $[Fe_2L^{CF3}_3]^{4+}$ 107
2.6.4.2 PAGE studies of the parent cylinder, $[Fe_2L^{P}_3]^{4+}$, with different counterions and alkyne cylinders 109
2.7 Conclusions 112

2.8 Experimental: synthesis 115
2.9 Experimental: DNA binding studies 126
2.10 References 131

Chapter 3: Steroid Functionalised Metallo-Cylinders 134
3.1 Introduction and aims 134
3.1.1 Drug targeting strategies 135
3.1.1.1 Biomolecule conjugated supramolecular cylinders 135
3.1.2 Conjugation of chiral substituents and biomolecules 138
3.2 Molecular design 139
3.3 Synthesis 141
3.3.1 Synthesis of Testosterone cylinder, $[Fe_2L^{Test}_3][BF_4]_4$ 141
3.3.2 Synthesis of Estrogen cylinder, $[Fe_2L^{Estro}_3][BF_4]_4$ 145
3.4 Properties of synthesised steroid cylinders 148
3.4.1 Chirality of synthesised helicates, as investigated by ^{1}H NMR studies with Δ-TRISPHAT 148
3.4.1.1 ^{1}H NMR Δ-TRISPHAT studies with the parent cylinder 149
3.4.1.2 ^{1}H NMR Δ-TRISPHAT studies with peptide cylinders 151
3.4.1.3 ^{1}H NMR Δ-TRISPHAT studies with novel steroid cylinders 153
3.4.2 Chirality of helicates, as investigated by circular dichroism 156
3.4.3 Complex counterions 157
3.4.4 Solubility of steroid functionalised cylinders 158
3.4.5 UV-Vis stability studies 159
3.5 DNA binding studies 160
3.5.1 Circular dichroism binding studies 161
3.5.2 Linear dichroism binding studies 163
3.5.3 Gel electrophoresis studies 166
3.5.4 PAGE studies 168
3.6 Conclusions 170
3.7 Experimental: synthesis 172
3.8 Experimental: DNA binding studies 178
3.9 References 183

Chapter 4: Sugar Functionalised Metallo-Cylinders 186
4.1 Introduction and aims 186
4.1.1 Sugar functionalisation 186
4.2 Molecular design 189
4.3 Synthesis 190
4.3.1 Synthesis of Acetyl Sugar cylinder, $[Fe_2L^{OAcSug_3}][BF_4]_4$ 190
4.3.2 Attempted synthesis of Hydroxyl Sugar cylinder, $[Fe_2L^{OHSug_3}][BF_4]_4$ 194
4.4 Properties of synthesised sugar cylinders 198
4.4.1 Chirality of synthesised helicates, as investigated by ^{1}H NMR Δ-TRISPHAT studies 198
4.4.2 Chirality of helicates, as investigated by circular dichroism 201
4.4.3 Solubility of sugar functionalised cylinders 203
4.4.4 UV-Vis stability studies 203
4.5 DNA binding studies 205
4.5.1 Circular dichroism binding studies 205
4.5.2 Linear dichroism binding studies 208
4.5.3 Gel electrophoresis studies 211
4.5.4 PAGE studies 214
4.6 Conclusions 216
4.7 Experimental: synthesis 220
4.8 Experimental: DNA binding studies 227
4.9 References 232

Chapter 5: Conclusions and Future Work 234
5.1 Conclusions 234
5.2 Future work 237
5.3 References 239

Appendix 240

Abbreviations

δ	chemical shift (NMR)
ε	molar absorption coefficient ($mol^{-1}dm^3cm^{-1}$)
Φ	DNA unwinding angle
λ	wavelength
λ_{max}	wavelength maximum
A	adenine (DNA base)
BF_4	tetrafluoroborate
br	broad (in NMR and IR data)
C	circular (form of plasmid DNA)
C	cytosine (DNA base)
CD	circular dichroism
$CDCl_3$	deuterated chloroform
CD_3CN	deuterated acetonitrile
cm	centimetre
^{13}C NMR	carbon nuclear magnetic resonance (spectroscopy)
ct-DNA	calf thymus deoxyribonucleic acid
d	doublet (NMR)
2D-COSY	two dimensional correlation spectroscopy (NMR)
dd	doublet of doublets (NMR)
DNA	deoxyribonucleic acid
D_2O	deuterated water
EI	electron impact (mass spectrometry)

ESI	electrospray ionisation (mass spectrometry)
FW	formula weight
G	guanine (DNA base)
HIV	human immunodeficiency virus
HMG	high mobility group (protein)
^{1}H NMR	proton nuclear magnetic resonance (spectroscopy)
HRMS	high resolution mass spectrometry
hrs	hours
Hz	hertz
ICD	induced circular dichroism
ILD	induced linear dichroism
IR	infra-red (spectroscopy)
J	coupling constant (NMR)
K	Kelvin
LD	linear dichroism
m	medium (in IR data)
m	multiplet (in NMR data)
M	molar (mol dm^{-3})
μM	micromolar
mdeg	millidegrees
MeCN	acetonitrile
MeOH	methanol
MHz	megahertz
MLCT	metal to ligand charge transfer

mM	millimolar
mmol	millimole
MTT	3-(4,5-dimethylthiazol-2-yl)-2,5-diphenyltetrazolium bromide
m/z	mass to charge ratio
nm	nanometre
NMR	nuclear magnetic resonance (spectroscopy)
^{32}P	phosphorus-32 (isotope)
PAGE	polyacrylamide gel electrophoresis
PDB	protein data bank (file)
PF_6	hexafluorophosphate
ppm	parts per million
RNA	ribonucleic acid
s	strong (in IR data)
s	singlet (in NMR data)
SC	supercoiled (form of plasmid DNA)
sh	shoulder (UV-Vis)
T	thymine (DNA base)
t	triplet (NMR)
td	triplet of doublets (NMR)
Δ-TRISPHAT	[Δ-tris(tetrachloro-1,2-benzenediolato)phosphate(V)]
UV	ultraviolet (light/spectroscopy)
UV-Vis	Ultraviolet-visible (spectroscopy)
w	weak (IR)

Chapter 1: Introduction

Deoxyribonucleic acid (DNA) is one of the most important biomolecules in living organisms. DNA allows the storage of genetic information, which is then translated via proteins into essential cellular processes that maintain cell function. It is the role of DNA in encoding these processes, and our increased understanding of these cellular events such as DNA replication and gene expression, that makes it a target for the diagnosis and treatment of disease. A large and varied range of natural and synthetic ligands that bind to DNA, and inhibit or alter the biological activity of DNA, have been discovered or developed as therapeutic agents. The development of drug molecules with a higher specificity for DNA may lead to a greater control of gene expression and therefore an improved therapeutic efficacy of anticancer drugs.

1.1 DNA structure

The structure of DNA was first elucidated in 1953 by Watson and Crick.[1] It is a helical molecule formed of two strands, with each strand composed of a backbone of alternating ribose sugar and phosphate groups (Fig. 1.1).[1,2] An aromatic nitrogenous base is attached to each ribose sugar, with the hydrophobic bases pointing into the helix and the hydrophilic sugar-phosphate units pointing outwards.[2,3] The bases are joined together in pairs, one from each strand, by hydrogen bonds which consequently also hold the two DNA strands together.[2] There are four DNA bases; two of which are purines, adenine (**A**) and guanine

(**G**), and two pyrimidines, cytosine (**C**) and thymine (**T**).[2] Pairing only occurs between a purine base and a pyrimidine base, either **A** with **T** or **C** with **G** (Fig. 1.1).[2] The attachment of the base pairs to the sugar-phosphate backbone is rather asymmetrical, leading to two grooves being formed in the double helix called the major and minor grooves.[4]

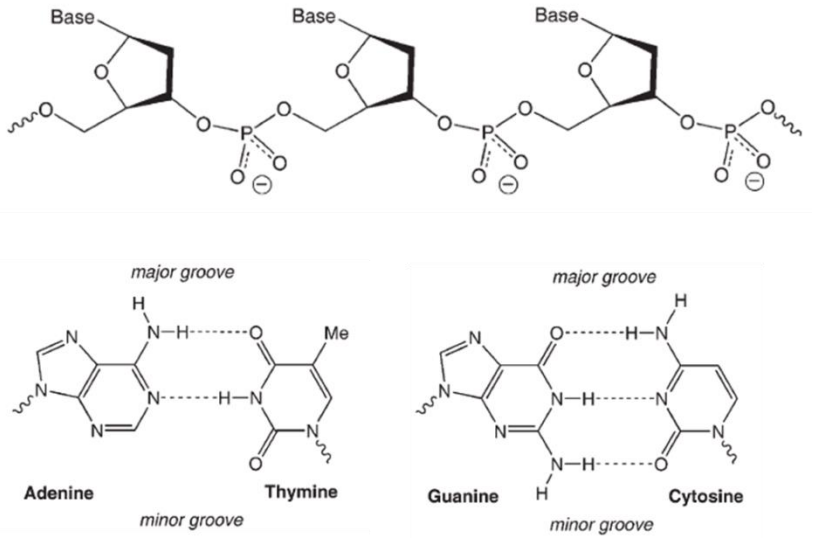

Figure 1.1 Structure of deoxyribose phosphate backbone (top) and DNA bases and their base pairing (bottom). [Reproduced from Ref [3]]

There are many possible conformations of duplex DNA, of which three are more common, the A-form, B-form and Z-form (Fig. 1.2). The B-form of DNA is a right-handed helix, when viewed down the helical axis, consisting of ten base pairs per turn and has a deep and narrow minor groove and a wide and shallow major groove.[5] A-DNA is also a right-handed helix, however it consists of eleven base pairs per turn and so is shorter and fatter than B-DNA.[5] The minor groove of A-DNA is shallow and wide while the major groove is extremely narrow.[5] Z-DNA is a left-handed helix with a zigzag conformation due to an alternating purine-pyrimidine base sequence.[5] It has 12 base pairs per helical turn, with a

single narrow minor groove and no major groove.[5] The B-DNA conformation is believed to be the most prevalent in biological systems.[3]

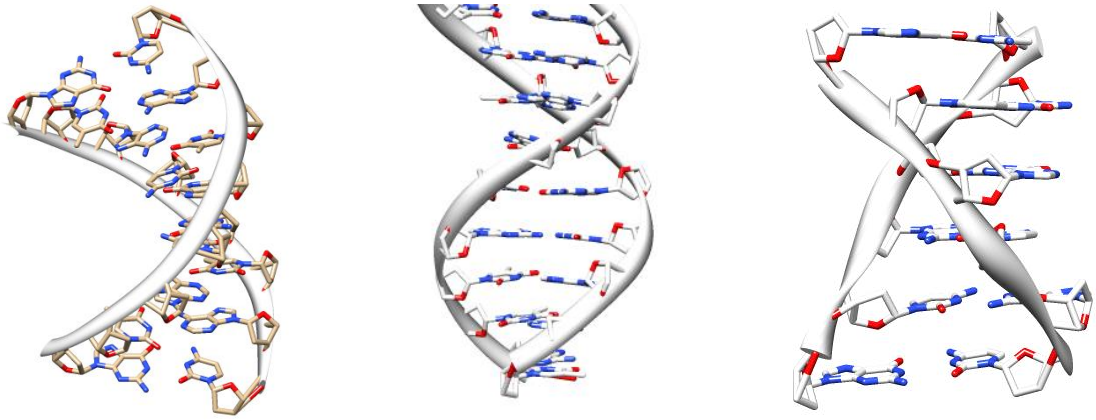

Figure 1.2 Structure of A-DNA (PDB 5ANA)[6] (left), B-DNA (PDB 3BSE)[7] (middle), and Z-DNA (PDB 1DCG)[8] (right).

1.2 DNA recognition

DNA binding by natural and synthetic small molecules can be grouped into five categories; (1) major groove binding, (2) minor groove binding, (3) sugar-phosphate backbone binding, (4) intercalation and (5) coordinative binding.

1.2.1 Major groove binding

Relatively little research has been conducted into major groove recognition by synthetic drugs. This is likely due to the fact that major groove binding is mainly limited to biological macromolecules such as proteins, as the dimensions of the groove are usually too large for synthetic DNA-binders.[9] These protein-DNA interactions allow essential biological processes such as transcription to occur.[10] These interactions are non-covalent in nature and are therefore reversible. Interaction between the protein and the target DNA is

mainly through hydrogen bonding to the DNA base pairs, however the formation of van der Waals contacts plays a role.[11] The protein can recognise the DNA base pairs on the floor of the major groove by their hydrogen bond donor/acceptor functionalities.[10] Binding in the major groove often causes kinking or bending at the interaction site, changing the width and depth of the DNA groove.[11]

The part of the protein that actually interacts with the DNA major groove is most commonly an α-helix moiety (Fig. 1.3).[11] Examples of α-helix proteins that bind in the major groove are helix-turn-helix, zinc-binding and leucine zipper proteins.[11] The majority of zinc-binding proteins are involved in gene regulation and many of these are transcription factor proteins.[11,12] A crystal structure of a Zif268-zinc finger peptide complex containing three zinc fingers crystallised with a short DNA sequence (Fig. 1.3) shows that the α-helix of each finger fits directly into the major groove.[12] Each finger interacts with three base pairs via hydrogen bonding and most of these contacts are made with a **G** rich strand of DNA.[12]

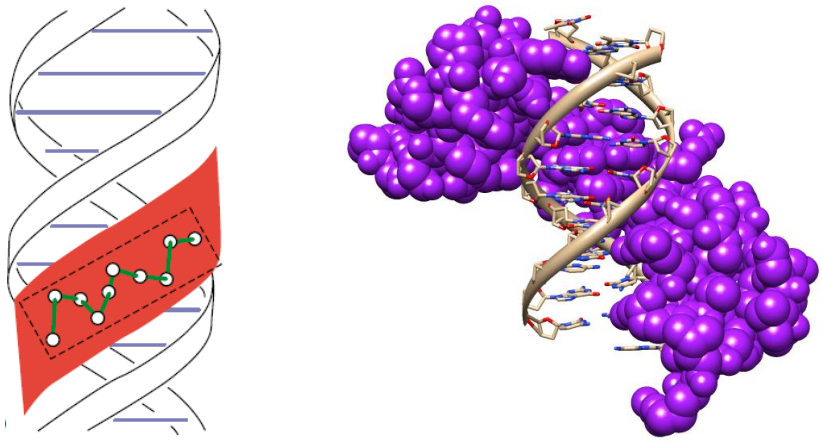

Figure 1.3 Docking of α-helix in DNA major groove [Reproduced from Ref [11]] (left); Crystal structure of Zif268-zinc finger binding in major groove of DNA (PDB 1ZAA)[12] (right).

Small molecule drugs that reside in the major groove usually are anchored there by intercalative interactions (see Section 1.2.4). For example, ditercalinium (Fig. 1.4) is a synthetic major groove binder derived from the natural product ellipticine.[13] It has anticancer activity and binds to DNA in the major groove.[13] The crystal structure of the drug bound to double stranded DNA shows the linker bound in the major groove of the DNA with the two aromatic moieties bis-intercalated between the base pairs.[13]

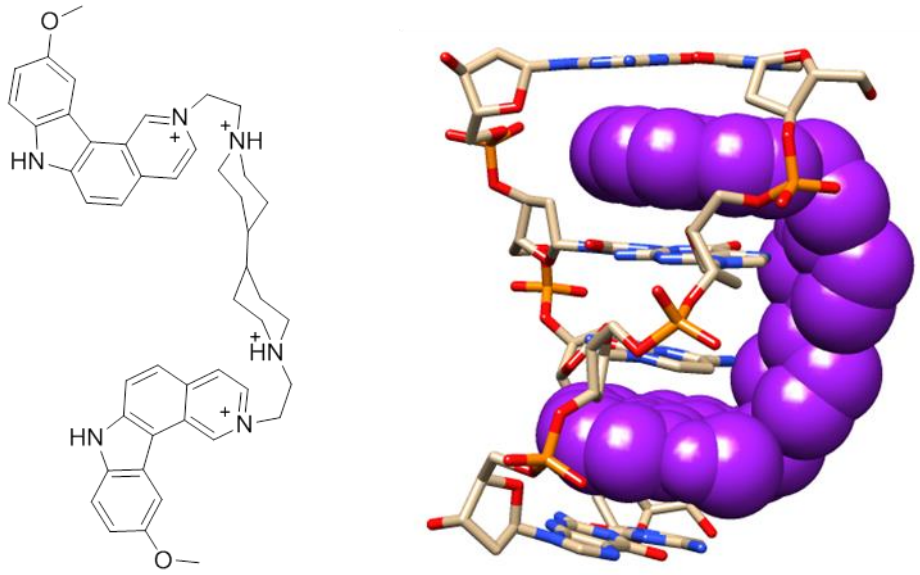

Figure 1.4 Structure of ditercalinium (left); Crystal structure of ditercalinium binding in DNA major groove (PDB 1D32)[13] (right).

1.2.2 Minor groove binding

The minor groove is narrow and deep, with the floor of the groove consisting of the edges of the DNA bases and the walls formed from the sugar-phosphate backbone.[4] The surfaces of the walls of the groove are made up of hydrogen atoms from the sugar-phosphate backbone and so are hydrophobic in nature.[4] Interaction between minor groove binders and DNA occurs mainly through hydrogen bonding, electrostatic and van der Waals interactions and frequently occurs with some degree of sequence specificity.[4,9] **A**/**T** rich

regions of the DNA have an overall negative charge, and are more flexible than **G**/**C** rich regions, and so positively charged DNA binders prefer these sequences of DNA, giving rise to this sequence specificity.[4,9]

Distamycin (Fig. 1.5) has anti-tumour and antibiotic properties.[14] It is a natural minor groove binder, binding with sequence specificity for **A**/**T** rich sequences of DNA via hydrogen bonds.[14] The interaction between distamycin and DNA is further strengthened by hydrophobic and van der Waals interactions between the aromatic rings of the molecule and the walls of the minor groove. Electrostatic interactions between the positively charged propylamidinium group and the negatively charged DNA also contribute.[14]

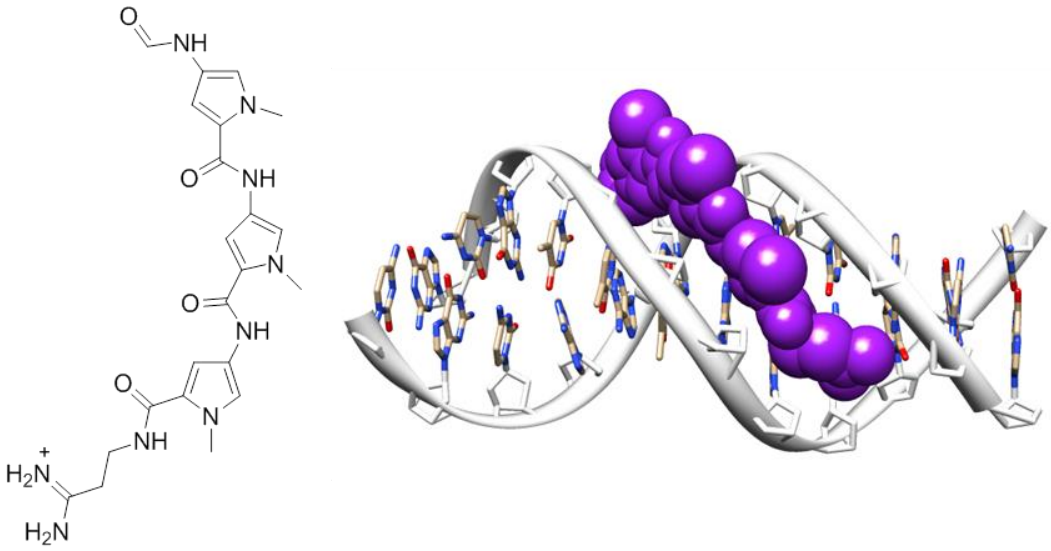

Figure 1.5 Structure of distamycin (left); Crystal structure of distamycin binding in DNA minor groove (PDB 2DND)[14] (right).

Berenil (Fig. 1.6), a synthetic minor groove binder, has anti-protozoal properties and is used to treat parasitic tyrpanosomal infections.[4] It binds to **A**/**T** rich regions of the minor groove with the positively charged amidinium group hydrogen bonded to the oxygens of

the thymine bases.[15] There are also hydrophobic and van der Waals interactions between the molecule and the minor groove walls, which are lined with hydrogen atoms from the sugar-phosphate backbone.[15]

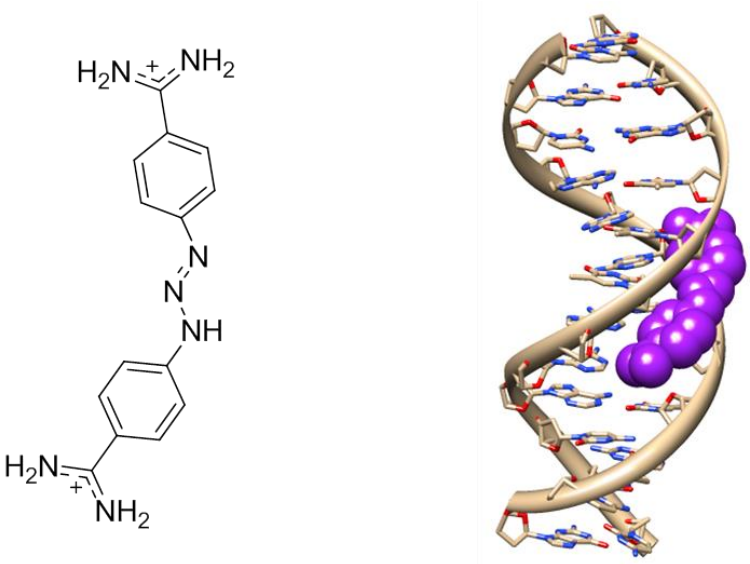

Figure 1.6 Structure of berenil (left); Crystal structure of berenil binding in DNA minor groove (PDB 1D63)[15] (right).

Hoechst (Fig. 1.7) is a synthetic fluorescent DNA stain and also has antibiotic properties.[16] It has a preference for binding to **A**/**T** rich sequences of DNA, forming hydrogen bonds between the amine hydrogens of the benzimidazole and the nitrogens of the adenine bases and oxygens of the thymine bases.[16] Binding of Hoechst to DNA causes the minor groove to widen and the helix to bend slightly.[16]

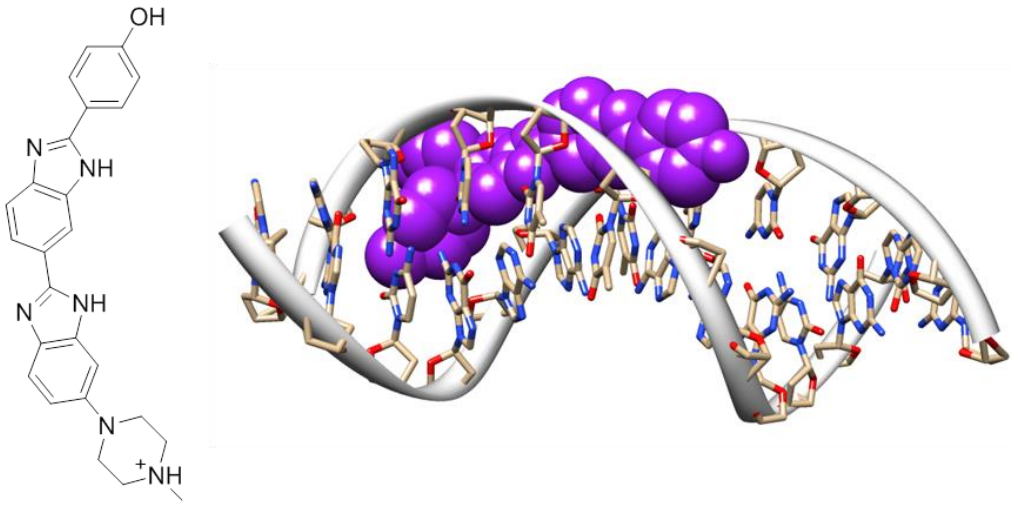

Figure 1.7 Structure of Hoechst (left); Crystal structure of Hoechst binding in DNA minor groove (PDB 8BNA)[16] (right).

Recently, an aromatic aza-bisbenzamidine functionalised with a coumarin fluorophore was developed (Fig. 1.8).[17] The compound shows sequence preference for **A**/**T** rich regions of DNA.[17] It also exhibits some fluorescence emission and this was found to be greatly enhanced in the presence of DNA.[17]

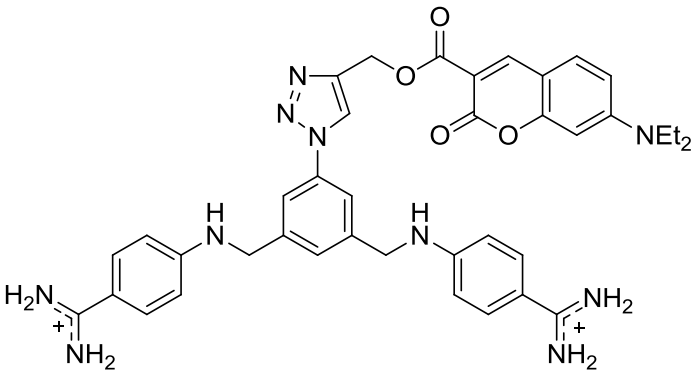

Figure 1.8 Structure of aza-bisbenzamidine functionalised with a coumarin fluorophore.[17]

1.2.3 Sugar-phosphate backbone binding

The sugar-phosphate backbone of DNA is made up of alternating sugar and phosphate units and so is negatively charged and hydrophilic.[3] Natural proteins with cationic charged regions can bind to the sugar-phosphate backbone and form hydrogen bonds with the phosphate units and the DNA bases.[3]

There are few examples of synthetic sugar-phosphate backbone binding molecules, however a cationic trinuclear platinum(II) drug (Fig. 1.9) developed by Farrell binds specifically to the sugar-phosphate backbone.[18] It is made up of three cationic square planar platinum(II) centres, that are unable to bind covalently to the DNA, and hydrophobic linking segments.[18]

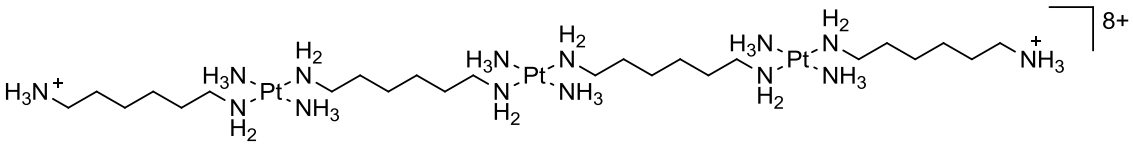

Figure 1.9 Structure of Farrell's trinuclear platinum drug.[18]

This long molecule interacts with the sugar-phosphate backbone of double stranded DNA in a number of ways (Fig. 1.10).[18] It extends along the negatively charged backbone interacting via electrostatics, and spans the minor groove.[18] The complex also forms bidentate hydrogen bonds between its amine and ammine groups and the phosphate oxygens, known as phosphate clamps.[18]

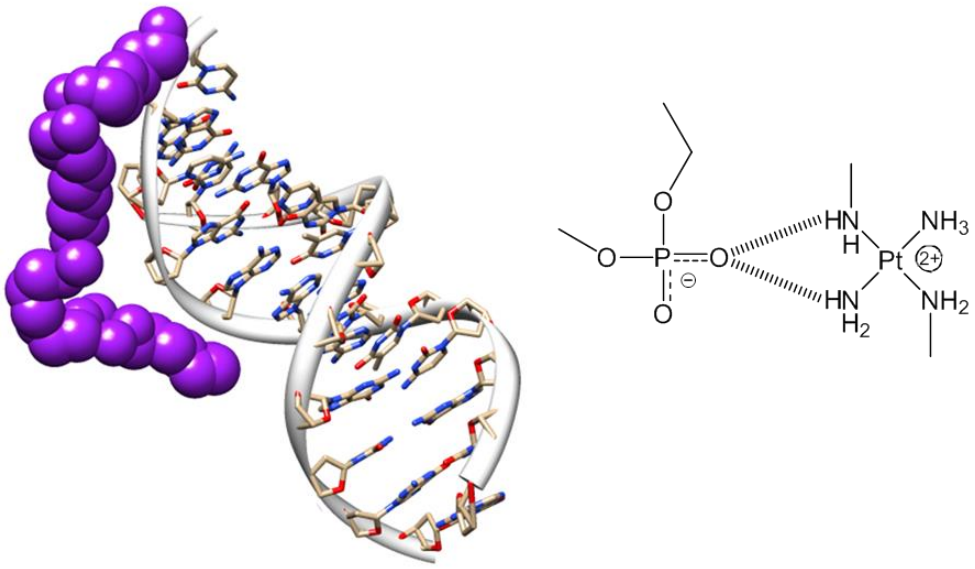

Figure 1.10 Crystal structure of Farrell's trinuclear platinum drug binding to sugar-phosphate backbone of DNA (PDB 2DYW)[18] (left); Schematic diagram of a phosphate clamp (right).

1.2.4 Intercalation

DNA binding by intercalation is the most common way that small molecules interact with DNA and a significant number of therapeutic drugs are intercalators.[9] Intercalation involves the insertion of a planar aromatic molecule, or part of a molecule, between the base pairs of duplex DNA.[9] This space between the base pairs is hydrophobic and the intercalator can form π-π stacking interactions with the bases closest to it.[3] Intercalators are often positively charged and so interact with the negatively charged DNA via electrostatic interactions.[9] Intercalation causes unwinding of the DNA helix and these structural modifications can lead to inhibition of processes such as transcription, replication and DNA repair.[3,19]

Daunorubicin (Fig. 1.11) is a DNA intercalator from the anthracycline family. It is used as an antibiotic and to treat a variety of cancers.[20] This planar aromatic molecule is found to

intercalate between cytosine and guanine DNA bases, with the amino sugar extending into the minor groove making several van der Waals contacts with the DNA bases. Hydrogen bonds formed between daunorubicin and the DNA bases aid in stabilising the interaction.[20]

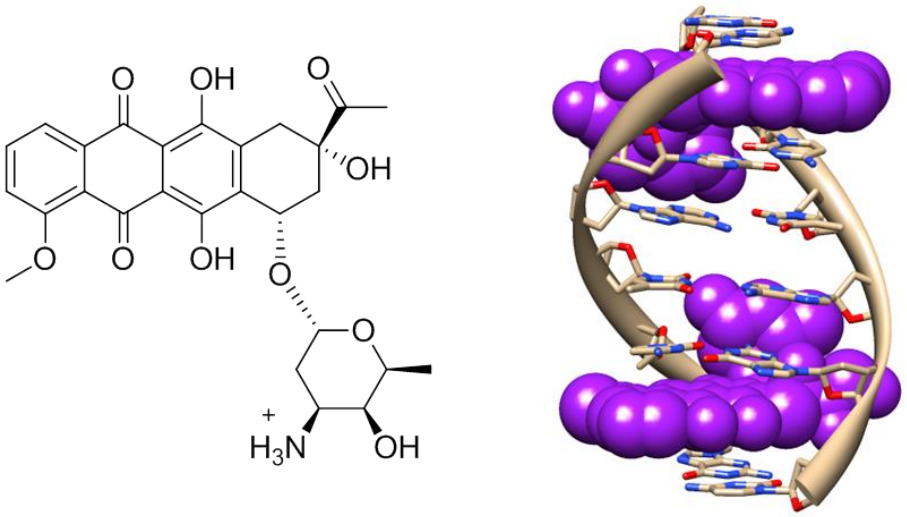

Figure 1.11 Structure of daunorubicin (left); Crystal structure of two daunorubicin molecules intercalating between DNA base pairs (PDB 1D12)[20] (right).

Ellipticine (Fig. 1.12) is also an intercalator and a potent anticancer drug.[21] It intercalates between cytosine and guanine DNA bases, forming π-π stacking interactions.[21] This intercalation causes unwinding and lengthening of the DNA helix.[21]

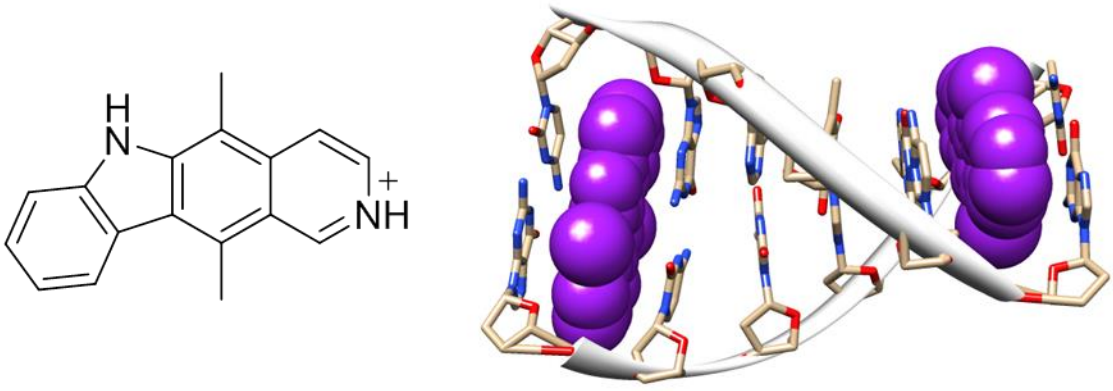

Figure 1.12 Structure of ellipticine (left); Crystal structure of two ellipticine molecules intercalating between DNA base pairs (PDB 1Z3F)[21] (right).

There are also many synthetic metallo-intercalators. The metal, usually a transition metal, is incorporated so as to impart positive charge, increasing the electrostatic interactions of the intercalator with DNA.[3]

One of the first examples of a metallo-intercalator was Lippard's platinum(II) terpyridine complex (Fig. 1.13). It was found to bind strongly to DNA by intercalation, with the π-π stacking interactions with the DNA bases enhanced by the cationic metal centre.[22,23]

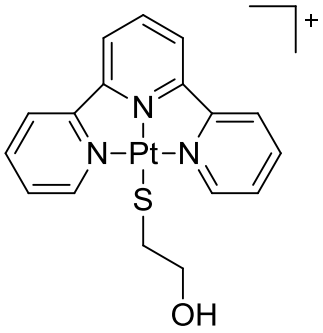

Figure 1.13 Structure of Lippard's platinum(II) terpyridine intercalator.[22]

Another example of a metallo-intercalator is an octahedral ruthenium(II) complex with several aromatic ligands (Fig. 1.14).[24] The dipyridophenazine ligand (dppz) is able to intercalate into the DNA with sequence preference for adenine and thymine DNA bases.[24] Due to the ruthenium centre, the complex is luminescent and this luminescence is significantly enhanced when in the presence of DNA.[24] Therefore this 'light switch' complex has many applications as a diagnostic or therapeutic drug.[24]

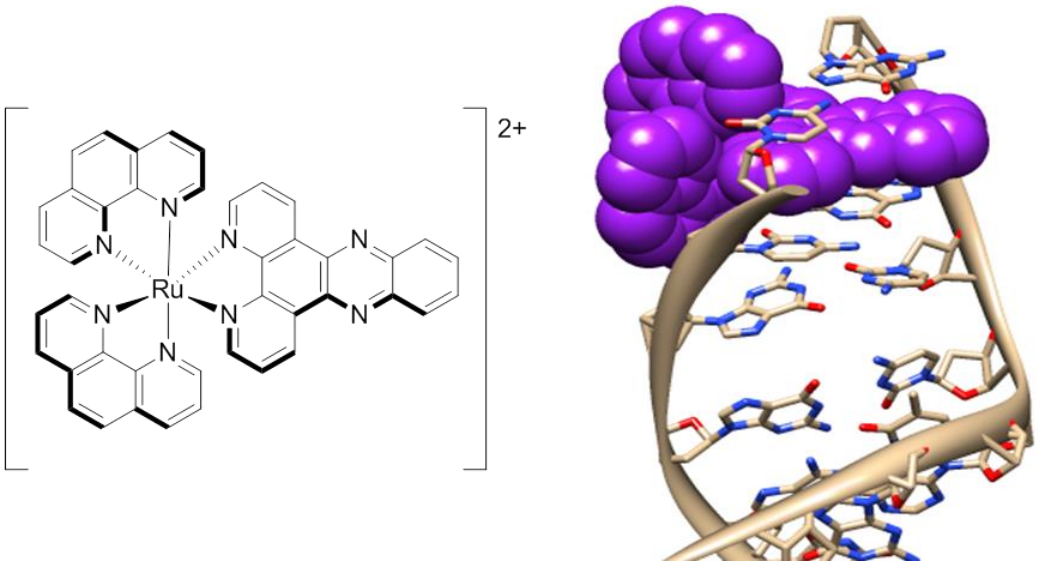

Figure 1.14 Structure of $[Ru(phen)_2(dppz)]^{2+}$ (left); Crystal structure of dppz moiety of $[Ru(phen)_2(dppz)]^{2+}$ intercalating between DNA base pairs (PDB 4E7Y)[24] (right).

1.2.5 Coordinative DNA binding: platinum based drugs

Coordinative binding involves the formation of direct covalent bonds between the DNA binding molecule and the DNA bases.[9] It is normally sequence specific with the preferential binding sites being the N7 position of guanine and adenine bases in the DNA major groove.[9,25] Coordinative binding usually involves cross-linking between DNA strands, inhibiting base pairing and preventing the separation of DNA strands in DNA processes such as replication and transcription.[9] Anti-cancer chemotherapy was founded on alkylating agents that bind coordinatively to DNA, and these compounds are still clinically important today.[9] Cisplatin is one of the most well-known examples of coordinative binding drugs.

1.2.5.1 Cisplatin

Cisplatin, cis-diamminedichloroplatinum(II) (Fig. 1.15), is a very potent anti-tumour drug.[26] Its activity was first discovered accidentally by Rosenberg in 1965 when it was found that platinum salts inhibited cell division in the bacterium *Escherichia coli*.[27] Cisplatin has been a significant drug in the treatment of cancer since its initial use in 1978, and is very effective against tumour types such as testicular, ovarian, small-cell lung cancer and head and neck cancers.[28,29]

The structure of cisplatin consists of two strongly coordinated ammonia ligands and two weakly coordinated chloride ligands, bound to a square-planar platinum(II) centre with *cis* conformation.

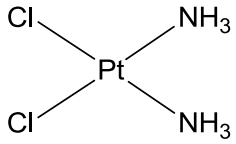

Figure 1.15 Structure of cisplatin.

However, this is not the structure of the complex that actually binds to the DNA once it has crossed the cell membrane by passive diffusion or via copper transporters.[30,31] One of the chloride ligands is first hydrolysed to form the cationic aquated species, cis-$[Pt(NH_3)_2Cl(OH_2)]^+$,[32] and it is this potent electrophile that can react with the DNA bases via its platinum metal centre (Fig. 1.16).[29]

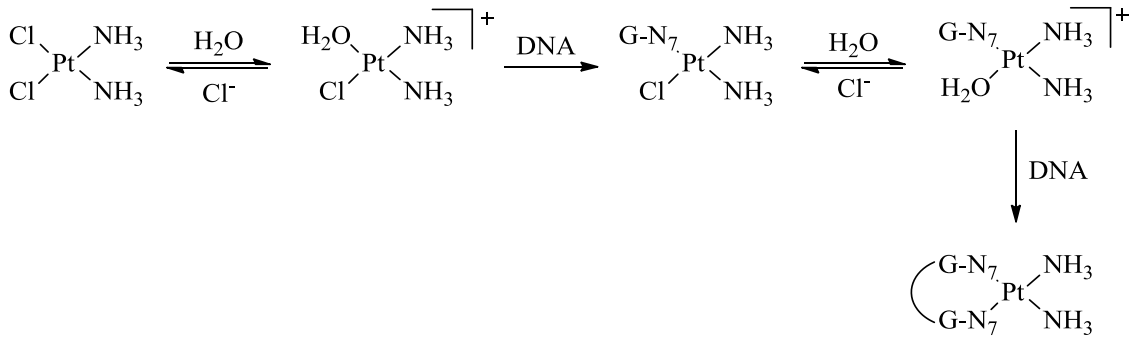

Figure 1.16 Schematic representation of cisplatin hydrolysis and subsequent DNA binding (where N7-G is the N7 atom of **G**).

Two metal coordination bonds are formed with two neighbouring **A** and/or **G** purine bases (Fig. 1.17) on the same strand of DNA, through their N7 atoms, forming a bifunctional adduct.[29,33]

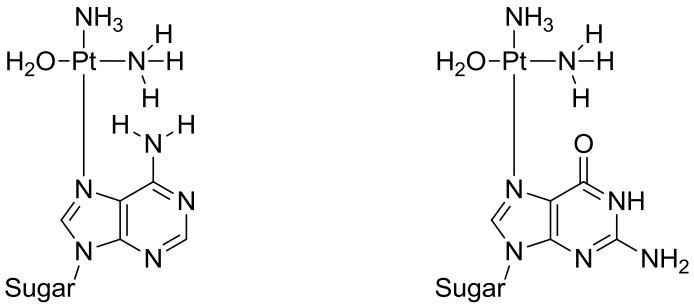

Figure 1.17 Structure of platinum bound to adenine (left) and guanine (right).

Several different adducts are formed between cisplatin and DNA (Fig. 1.18) with the 1,2 intrastrand Pt-**GG** adduct thought to be the most significant in the anti-cancer activity of cisplatin.[34]

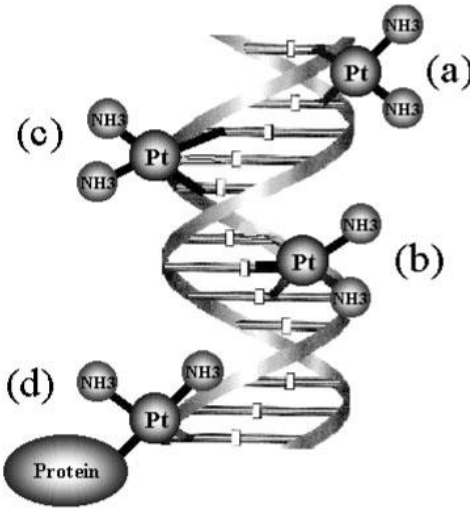

Figure 1.18 Representation of adducts formed between cisplatin and DNA; (a) interstrand crosslink; (b) 1,2-intrastrand crosslink; (c) 1,3-intrastrand crosslink and (d) protein-DNA crosslink. [Reproduced from Ref [26]]

These intrastrand crosslinks have been found to damage DNA by causing a kink in the double helix at around 45º, towards the site of platination.[33,35] This kinking produces a specific structural motif [36] which is recognised by nuclear high-mobility group (HMG) proteins.[29] These HMG proteins bind to the kinked parts of the DNA preventing the binding of normal DNA repair proteins, such as those that carry out nucleotide excision repair, which may hinder transcription and DNA replication activities.[25,37]

Although cisplatin has worldwide clinical approval, is one of the foremost anti-cancer drugs,[25] and is used to treat 50-70% of all cancer patients[38] there are several major disadvantages of this drug.[39] Many tumours develop cisplatin resistance[25,40] and the drug does not work for all primary tumours, for example breast and prostate cancer, the two most frequent cancers.[25] Treatment with cisplatin causes severe side effects such as nephrotoxicity, neurotoxicity, loss of sensation to the extremities and nausea,[25,41] due to the

poor specificity of cisplatin for tumour cells. Platination occurs in all cells leading to normal cells and tissues being damaged.[25,42]

1.2.5.2 Second generation platinum drugs

Due to the limiting factors of cisplatin, there has been a vast amount of research in the last few decades to discover new anti-cancer drugs with reduced side effects and improved properties.

Carboplatin (Fig. 1.19) has worldwide clinical approval.[43] It forms the same adducts with DNA as cisplatin, and has shown cytotoxic activity against the same tumour types.[44] The bidentate leaving group renders the drug less toxic than cisplatin.[43, 44] Consequently carboplatin is only used in cases where the patient is otherwise compromised, for example the elderly or those with HIV.[25]

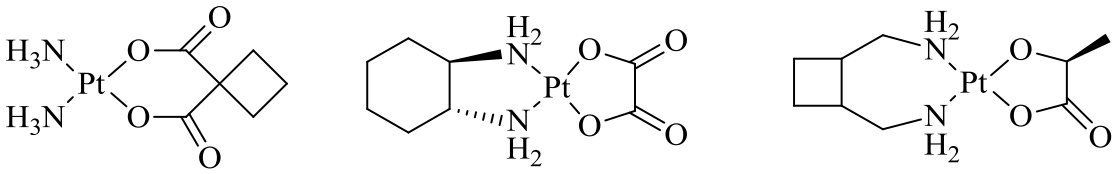

Figure 1.19 Structure of carboplatin (left), oxaliplatin (middle) and lobaplatin (right).[43,45]

Oxaliplatin (Fig. 1.19) has a carboxylato leaving group and a 1,2-diaminocyclohexane (DACH) non-leaving group.[45] This leaving group is hydrolysed less readily and so oxaliplatin is less toxic than cisplatin, and the side effects of the drug are much reduced.[45,46] Oxaliplatin forms [Pt(dach)] adducts with DNA and so has a different

spectrum of activity than that of cisplatin.[25, 45] It is cytotoxic against tumour types that are not treatable with cisplatin or that are cisplatin resistant.[25, 47]

Lobaplatin (Fig. 1.19) has a 1,2-dimethylaminocyclobutane non-leaving group[44,45] and therefore also forms DNA adducts that differ from those of cisplatin.[44,45] It is less toxic than cisplatin due to its leaving group.[45] Lobaplatin has no clinical advantages over cisplatin.[25]

1.2.5.3 Multi-nuclear platinum drugs

Multi-nuclear platinum drugs are structurally very different from cisplatin and therefore form different types of platinum-DNA adducts and so unsurprisingly have different clinical activity.[48]

Farrell's tri-platinum agent BBR3464 (Fig. 1.20) has undergone phase II clinical trials and has been found to be far more potent than cisplatin and can be used to treat cisplatin-resistant cancers.[49] It has DNA binding and anti-tumour activity distinct from that of cisplatin and other mononuclear platinum agents.[49] The two reactive platinum centres of the complex are spaced far apart and so the platinum-DNA adducts that are formed are long-range adducts.[49] The central platinum centre cannot covalently bind to DNA, however it has a high DNA affinity due to electrostatic interactions and hydrogen bonding with the DNA bases.[49]

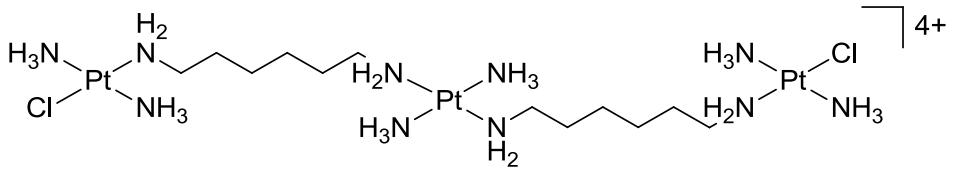

Figure 1.20 Structure of tri-platinum BBR3464.[49]

1.2.5.4 Platinum(IV) prodrugs

Platinum(IV) prodrugs can be used to overcome the problems of cisplatin as they are relatively inactive and kinetically inert when compared to their platinum(II) analogues.[50] They must be activated by reduction and this occurs mainly in the acidic conditions of the tumour cell.[50] The axial ligands also offer the potential to functionalise the drug with bioactive ligands, allowing targeting of specific tumour types.

A very promising example of platinum(IV) prodrugs are two trans-diammine platinum complexes (Fig. 1.21) developed by Sadler.[51] The platinum(IV) complexes are relatively inert and are non-toxic in the dark. However, upon UV irradiation they are photoactivated to their platinum(II) analogues whereby they can form adducts with DNA and exert a potent cytotoxicity.[51] It is known that platinum drugs with leaving groups *trans* to one another, as in transplatin, are usually inactive[52] however these compounds have very similar activity to that of cisplatin in a human cancer cell line.[51]

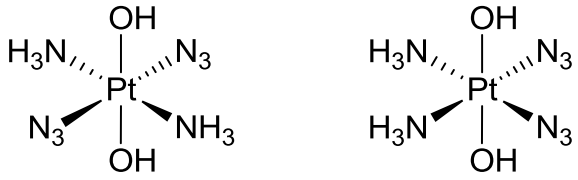

Figure 1.21 Structure of platinum(IV) prodrugs.[51]

1.3 Other, non-platinum based transition metal anticancer agents

Inspired by the success of the metallo-drug cisplatin, a vast array of other transition metal-based drugs have been developed as therapeutic agents. Transition metals have a range of coordination numbers and geometries and can consequently be used as scaffolds to obtain architectures not possible with organic molecules.[50] The metal centre can impart a cationic charge to the molecule which is very favourable for DNA binding.[39] Some transition metal complexes also have photophysical properties such as luminescence and so metallo-drugs can be used for diagnostic applications as well as therapeutic ones.[53]

1.3.1 Ruthenium drugs

Ruthenium complexes are often less toxic than platinum drugs and have a different mode of action due to being octahedral in geometry rather than square planar.[54] It is thought that they are taken up into cells via transferrin receptor-mediated endocytosis.[54,55] Two ruthenium drugs are currently undergoing clinical trials, NAMI-A and KP1019 (Fig. 1.22).

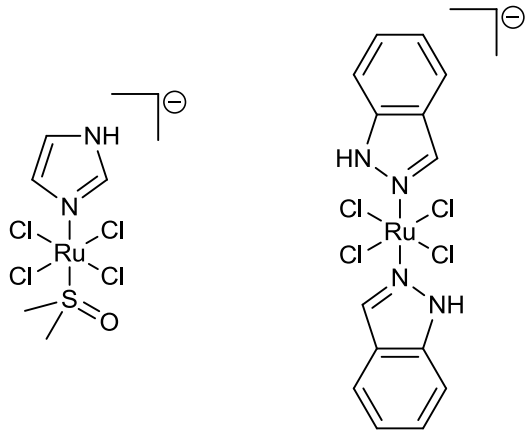

Figure 1.22 Structure of ruthenium drugs NAMI-A (left) and KP1019 (right).[55,56]

NAMI-A shows very promising activity *in vitro* and has been found to be less toxic than cisplatin and is also less toxic to healthy cells.[56] It has a different mechanism of action than platinum drugs, and other ruthenium drugs, in that it is not cytotoxic to tumour cells.[56] However it has strong efficacy in the treatment of solid tumours, even those in an advanced stage of growth.[56] The mechanism for this anti-tumour activity has not been fully elucidated as yet.

KP1019 is a potent anti-tumour agent against many different cancers, including colon cancer. It rapidly enters tumour cells, causing cell death by apoptosis.[55] It is thought that DNA is not the main target for this drug but that its interaction with cellular proteins is responsible for its activity.[55]

1.3.2 Rhodium drugs

Rhodium-based metallo-drugs show potential as anticancer agents as many have potent anticancer activity and show limited side effects.[57] They are attractive due to their possible photophysical properties and many rhodium(III) complexes have been found to perform photoinduced DNA cleavage.[58]

A rhodium(III)-polypyridyl complex (Fig. 1.23) was found to be very cytotoxic against breast and colon cancer cell lines, with an activity greater than that of cisplatin.[57] The complex was also found to affect cellular oxygen consumption, and therefore cell respiration, indicating an anti-mitochondrial mode of action.[57]

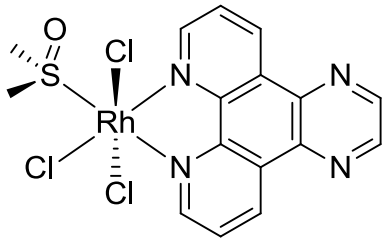

Figure 1.23 Structure of rhodium(III)-polypyridyl complex.[57]

One example of a photoactivated rhodium-based drug is a rhodium(III)-dipyridophenazine complex (Fig. 1.24).[59] It has been found to penetrate tumour cell membranes and is phototoxic when irradiated with UVA light.[59] The complex forms adducts with DNA and acts as a photonuclease, cleaving the DNA strands.[59] This rhodium(III) complex can also penetrate the protein shell of the Sindbis alphavirus and after photoactivation renders the viral genome non-infectious.[59]

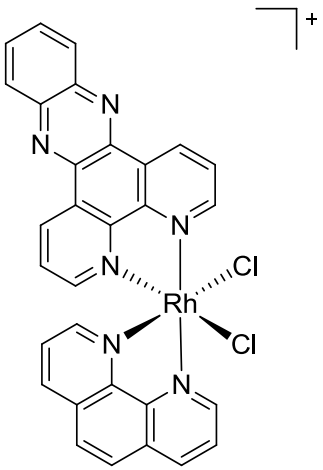

Figure 1.24 Structure of rhodium(III)-dipyridophenazine complex.[59]

1.3.3 Rhenium drugs

Luminescent rhenium-based drugs are also of great interest as they have many possible applications in diagnostic and therapeutic medicine.[60]

One example is a luminescent rhenium(I)-polypyridine complex (Fig. 1.25) designed as a biological sensor for cadmium(II) and zinc(II) ions.[61] Studies showed that the compound was taken up by a human cervix epithelioid carcinoma cancer cell line and was far more cytotoxic than cisplatin.[61] The compound could be used as a cellular stain, with increased luminescence emission upon addition of zinc(II) or cadmium(II) ions indicating its potential use as a biological probe.[61]

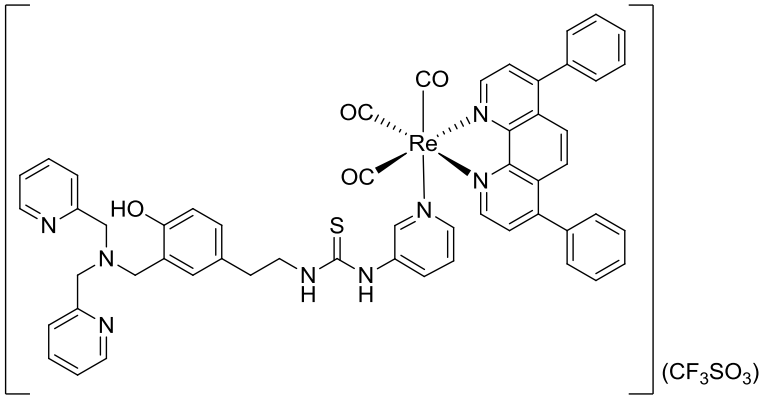

Figure 1.25 Structure of rhenium(I)-polypyridine complex.[61]

Other examples of rhenium complexes developed as anticancer compounds are two rhenium(IV) compounds with bipyridine and dimethyl-bipyridine ligands (Fig. 1.26).[62] These mononuclear complexes show potent cytotoxicity towards breast, ovarian and prostate cancer cell lines, with a higher anti-proliferative activity than cisplatin.[62] It was also found that the bipyridine-rhenium(IV) complex causes cell death by apoptosis.[62]

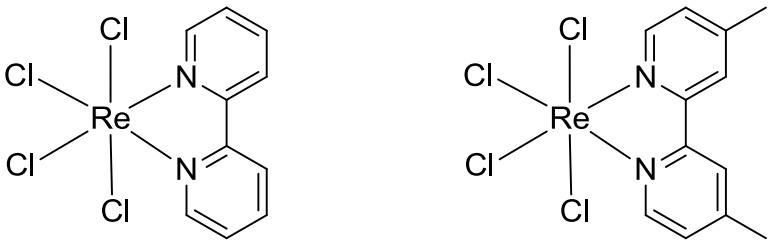

Figure 1.26 Structure of rhenium(IV)-bipyridine complexes.[62]

1.3.4 Iridium drugs

Iridium metallo-complexes are often designed as biological probes due to their luminescent properties.[63]

One example of a luminescent iridium complex that also possesses anticancer activity is an iridium(III)-polypyridine-indole complex (Fig. 1.27).[63] Excitation of this complex gave rise to long-lived luminescence in the visible region, which makes it suitable for biological applications.[63] *In vitro* studies confirmed that the complex has potent cytotoxicity, significantly greater than that of cisplatin, in a human cervix epithelioid carcinoma cancer cell line.[63] Cellular uptake and microscopy studies indicated good uptake and localisation of the complex in the perinuclear area of the cell.[63]

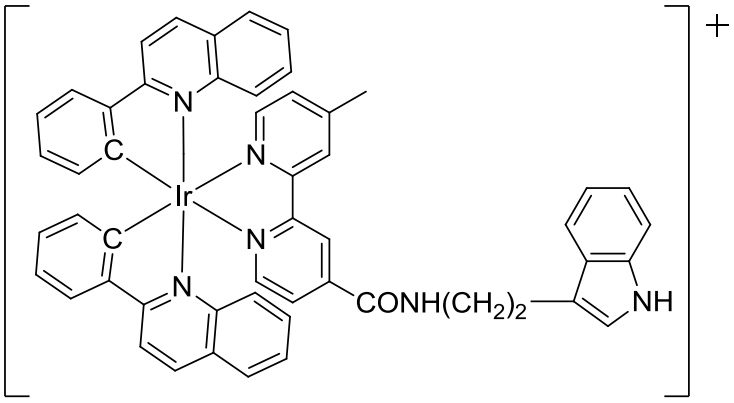

Figure 1.27 Structure of iridium(III)-polypyridyl-indole complex.[63]

One recently developed iridium(III) complex (Fig. 1.28) has been found to act as a kinase inhibitor and possesses light-activated cytotoxicity.[64] The complex inhibits vascular endothelial growth factor kinases, a possible novel anticancer target, which may lead to tumour growth inhibition.[64] Cytotoxic activity of the compound was assessed in a human cervix epithelioid carcinoma cancer cell line and was found to be light dependent.[64] In the

dark the compound was not cytotoxic, whereas when irradiated with UV light the compound was found to reduce cellular survival to 12.5%.[64]

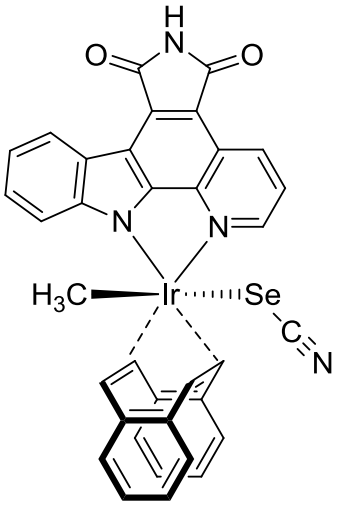

Figure 1.28 Structure of iridium(III) complex.[64]

1.3.5 Iron drugs

Metallo-complexes containing iron are of great interest, as iron is found abundantly in the body and is essential for many biological processes.[65]

One example is an iron(II) complex with a pentadentate pyridyl ligand (Fig. 1.29) that is cytotoxic in breast and human cervix epithelioid carcinoma cancer cell lines with activity greater than that of cisplatin.[65] This cell death is caused by DNA damage by the compound. The complex is also able to cleave DNA, inducing single strand cleavage of supercoiled DNA.[65]

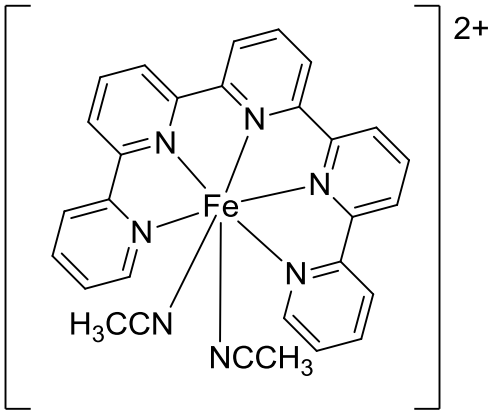

Figure 1.29 Structure of iron(II) complex with pentadentate pyridyl ligand.[65]

A bis(Fe(II)-EDTA-distamycin)fumaramide complex (Fig. 1.30) can bind to DNA with sequence preference for **A**/**T** rich regions of DNA and can also cleave DNA.[66]

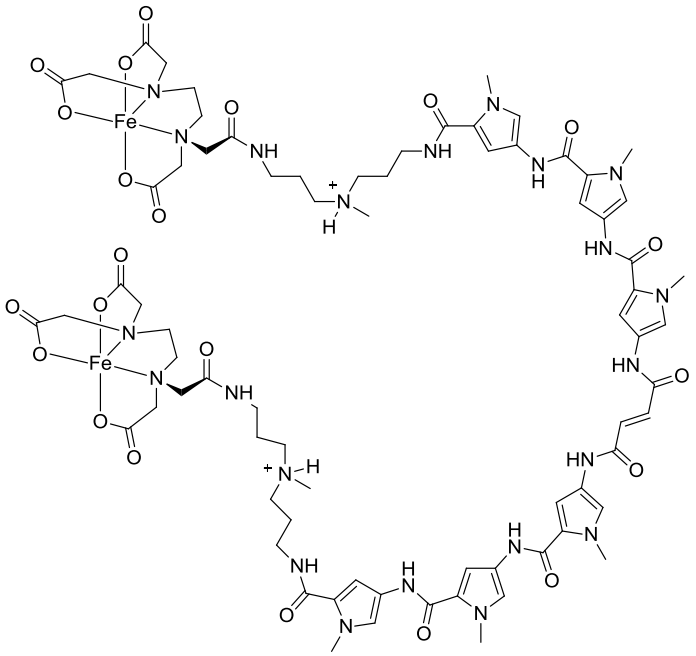

Figure 1.30 Structure of bis(Fe(II)-EDTA-distamycin)fumaramide complex.[66]

1.4 Targeting other DNA structures

Although the majority of classical drugs bind to duplex DNA, a greater understanding of DNA processes has shown that DNA structures other than duplex DNA are often involved in DNA replication, transcription and recombination.[67,68] These DNA structures are exciting new targets for therapeutic agents.

1.4.1 Targeting the Holliday junction

A Holliday junction, or four-way junction, is formed from two intertwined DNA duplexes that have exchanged strands (Fig. 1.31).[3] The Holliday junction is an integral intermediate in homologous recombination; the process in which DNA is repaired.[69] Targeting the Holliday junction may provide a new class of drugs with a different method of action to those of conventional duplex DNA binding drugs.

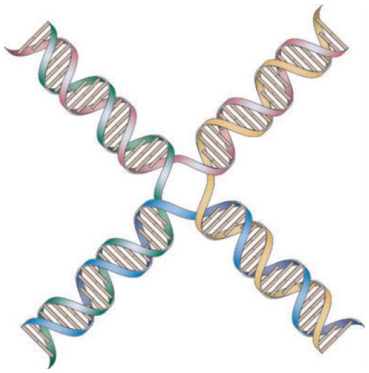

Figure 1.31 Structure of Holliday junction. [Reproduced from Ref [70]]

A bis-acridine compound that can bind across the centre of this junction has been developed (Fig. 1.32).[69] The molecule can interact with the junction in several ways, with the two acridine moieties extensively π-π stacking with the DNA bases of the crossover DNA strands.[69] The hydrophobic side chains of the compound are positioned in the minor grooves of the junction and the positive charge of the compound neutralises the high

negative charge density of the junction, stabilising the structure by electrostatic interactions.[69]

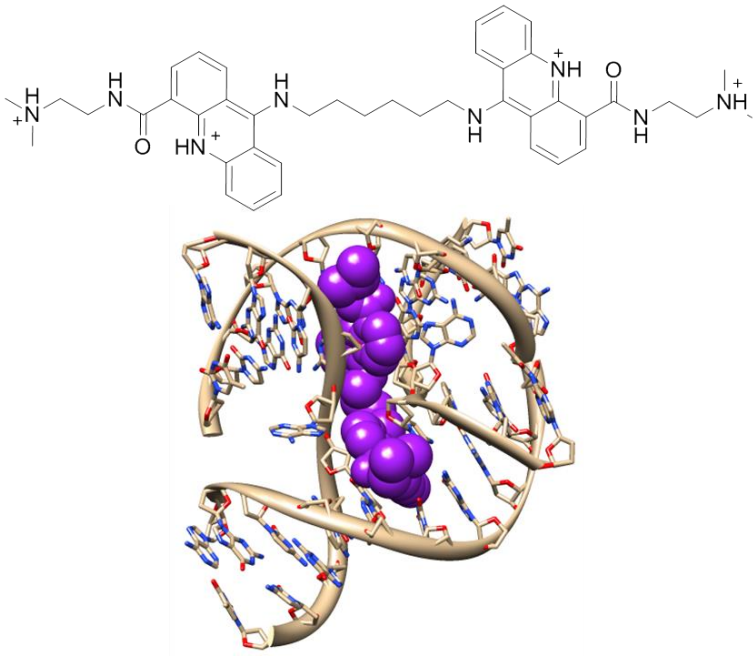

Figure 1.32 Structure of bis-acridine compound (top); Crystal structure of bis-acridine compound binding to Holliday junction (PDB 2GWA)[69] (bottom).

1.4.2 Targeting the three-way junction

Three-way, or Y-shaped, junctions are another type of junction and are found in DNA and RNA.[71] They are formed, like the four-way Holliday junction, from duplex DNA strands that converge at a point.[71] Y-shaped junctions are thought to be the most abundant junctions and play important roles in DNA replication, RNA translation and are present in several diseases such as myotonic dystrophy type I and Huntington's disease.[72,73,74] Consequently they may be an interesting target for the design of new therapeutic agents with a different mode of activity than conventional drugs.

One known compound that can bind to DNA three-way junctions is a dinuclear iron(II) triple stranded complex (Fig. 1.33) developed by Hannon.[71] The cylindrical complex is of the correct size and shape to fit neatly into the cavity in the centre of the three-way junction.[71] The phenyl rings of the compound π-π stack with the DNA bases, and electrostatic interactions between the cationic compound and the negatively charged DNA help to stabilise the non-covalent binding interactions.[71] The iron(II) complex is a potent cytotoxic agent, however this has yet to be directly linked to this DNA binding mode.[71] This compound, and its analogues, will be further discussed in Section 1.5.4.

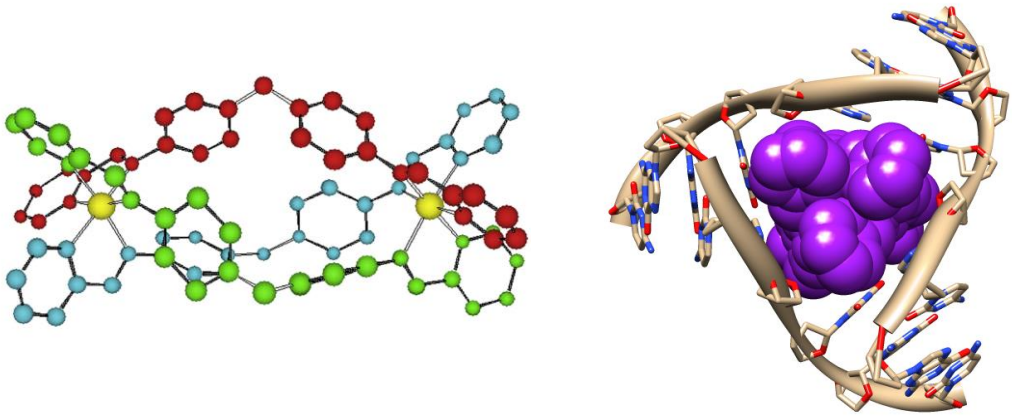

Figure 1.33 Structure of iron(II) triple stranded complex [Reproduced from Ref [75]] (left); Crystal structure of iron(II) complex bound in the heart of a DNA three-way junction (PDB 2ET0)[71] (right).

1.4.3 Targeting G-quadruplexes

Recently there has been much interest in G-quadruplex DNA structures. These are another example of non-classical DNA that may be targeted with more specificity and may provide a new mode of action for therapeutic agents.

G-quadruplexes are found at the telomere ends of chromosomes and are formed of several stacked G-tetrads, which are themselves formed of four guanine DNA bases interacting by Hoogsteen base pairing in a planar arrangement (Fig. 1.34).[9]

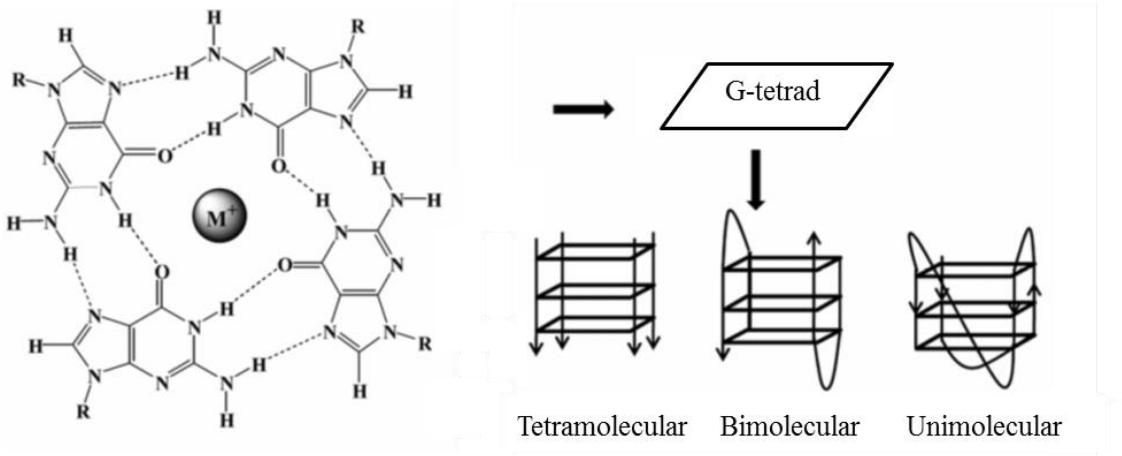

Figure 1.34 G-tetrad where $M^+ = K^+$, Na^+ or NH_4^+ (left); Tetrameric, dimeric and monomeric G-quadruplexes composed of three G-tetrads (right). [Reproduced from Ref [9]]

In normal cells telomeric DNA shortens after every cell division and when the telomeres get too short, the cells stop dividing and commit suicide.[50] This is to maintain the DNA and prevent mutations. Telomerase is an enzyme that catalyses the synthesis of telomeric DNA and is overexpressed in cancerous cells, allowing indefinite replication and so a high proliferation rate.[9] The formation of G-quadruplexes at the telomere ends of DNA stops telomerase action, and so if these G-quadruplexes can be induced or stabilised, cancer cell replication may be inhibited.[76] Therefore, many small molecules have been designed to bind to and stabilise G-quadruplexes.

One example is a manganese(III) porphyrin (Fig. 1.35) which has been found to preferentially bind to G-quadruplexes over duplex DNA.[76] The complex interacts by π-π

stacking with the last G-tetrad and the four cationic arms interact with the loops of the G-quadruplex.[76] Electrostatic interactions occur between the positively charged complex and the negative G-quadruplex, strengthening the interaction.[76]

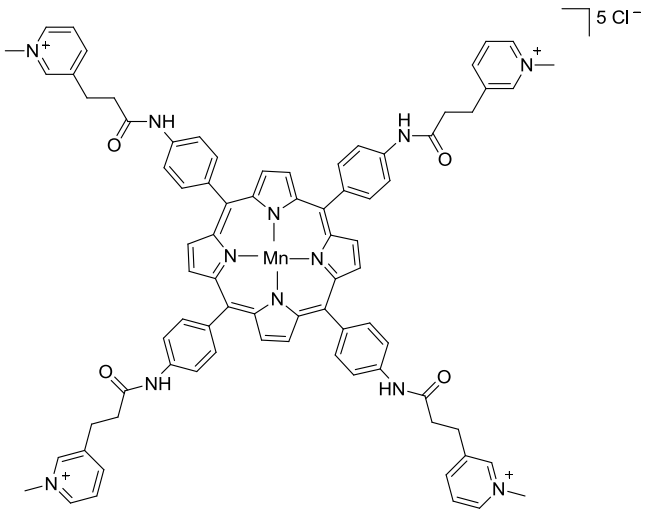

Figure 1.35 Structure of manganese(III) porphyrin.[76]

Another example is that of a tetra-substituted naphthalene diimide compound (Fig. 1.36), which binds to the terminal G-tetrad of G-quadruplexes and thermally stabilises the structure.[77] Extensive π-π stacking can be observed between the compound and the G-tetrad, and the four side chains are positioned within the G-quadruplex groove regions and can hydrogen bond to the guanine bases.[77] The compound has been found to be a potent inhibitor of cell growth, however this has not been formally linked to the stabilisation of the G-quadruplex structure.[77]

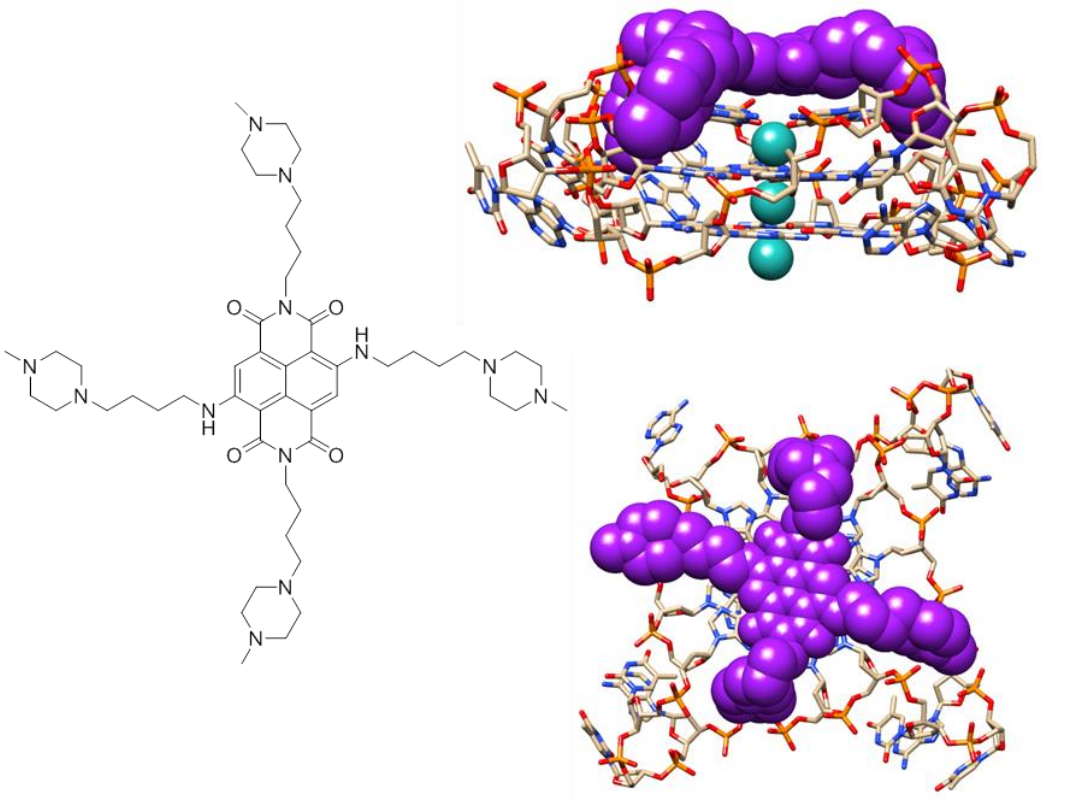

Figure 1.36 Structure of naphthalene diimide compound (left); Crystal structure of naphthalene diimide compound (purple) interacting with G-quadruplex (turquoise spheres are potassium ions) (PDB 3T5E)[77]; side view (top right) and top view (bottom right).

An N,N'-bis(quinolinyl)pyridine-2,6-dicarboxamide compound (Fig. 1.37) has been found to stabilise a human telomeric G-quadruplex, while no stabilisation was found for double stranded DNA, showing high selectivity.[78] The compound could induce long-term inhibition of cell growth in several cancer cell lines.[78]

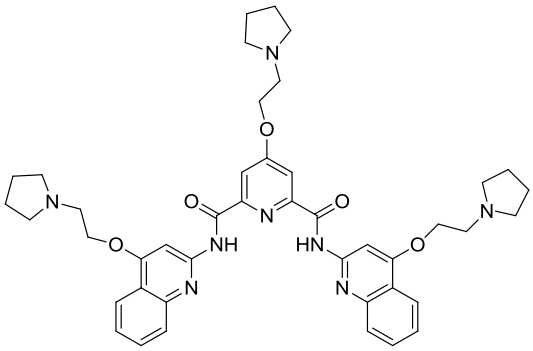

Figure 1.37 Structure of N,N'-bis(quinolinyl)pyridine-2,6-dicarboxamide compound.[78]

1.5 Supramolecular chemistry

Supramolecular chemistry was defined as the 'chemistry of molecular assemblies and of the intermolecular bond' by its founder J.M. Lehn.[79] It is the study of highly-organised and sometimes extremely complex molecular species that are formed from several discrete chemical components through intermolecular, non-covalent interactions rather than covalent bonds.[80,81] Supramolecular chemistry involves the self-assembly of carefully designed molecular components, forming large highly functional molecular architectures with novel properties.[82] The most impressive examples of supramolecular assembly can be seen in nature. For example, ferritin is a large and complex iron storage protein which is composed of many subunits that contain the inherent information that allows the formation of the whole supermolecule by self-assembly.[83]

Supramolecular chemistry involves the formation of molecular architectures through non-covalent interactions, including hydrogen bonding, electrostatics, π-π stacking, van der Waals and hydrophobic interactions.[81] These interactions are weaker than covalent bonds, however collectively they are strong enough to allow the formation of large and complex structures.[81]

1.5.1 Supramolecular helicates

Supramolecular chemistry encompasses a broad range of architectures, but one area of particular interest is that of supramolecular helicates as many helical motifs appear in nature and important biological molecules.[84] Supramolecular helicates are formed from the spontaneous self-assembly of organic ligands and metal ions, with one or more ligands

wrapping around and coordinating to one or more central metal ions.[85] It is the intrinsic structural information encompassed within these components that allows the formation of a specific, directed architecture.[86] The specific stereochemical requirements of the metal ion and the position of the binding sites on the ligand dictate the structure of the helicate that is formed.[84,86]

The helicate ligand is made up of several metal ion polydentate binding sites with spacer groups between these units.[85] The spacer must be flexible enough to allow the formation of the helical complex, yet rigid enough to prevent coordination of one metal ion to several binding units.[85] Helicates can be classed as homotopic; if the metal binding units of the ligand are the same, or heterotopic; if the ligand contains different metal binding units (Fig. 1.38).[85] Heterotopic helicates exist as two isomeric forms, head-to-head (HH) or head-to-tail (HT).[85]

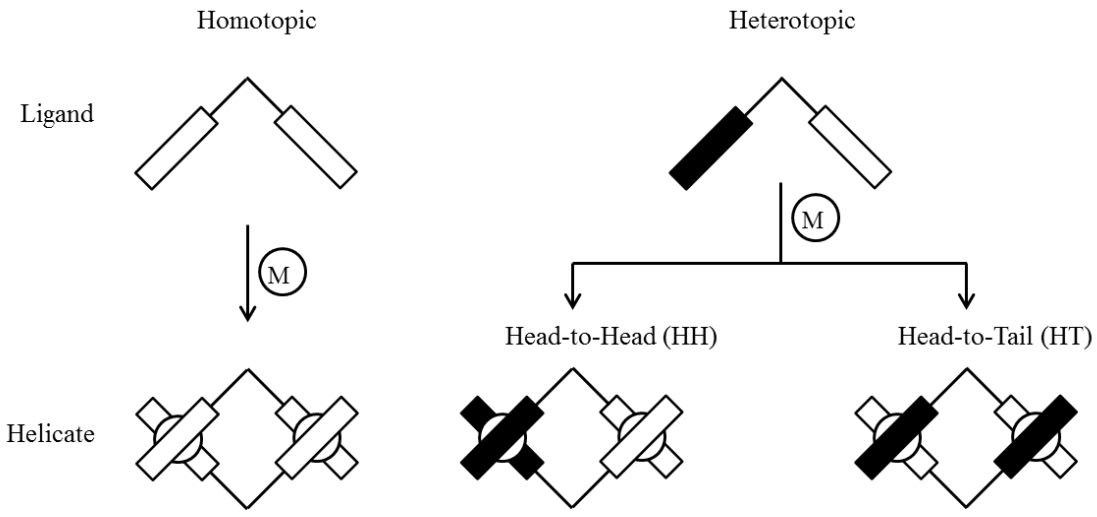

Figure 1.38 Configurations of homotopic and heterotopic helicates. [Adapted from Ref [85]]

1.5.2 Chirality of helicates

Supramolecular helicates are intrinsically chiral due to the way the ligands are wrapped around the central metal ions. If the ligands are wound in a clockwise direction, when viewed down the helical axis, they are right handed (P or plus) and if they are wound in an anti-clockwise manner they are left handed (M or minus) (Fig. 1.39).[86]

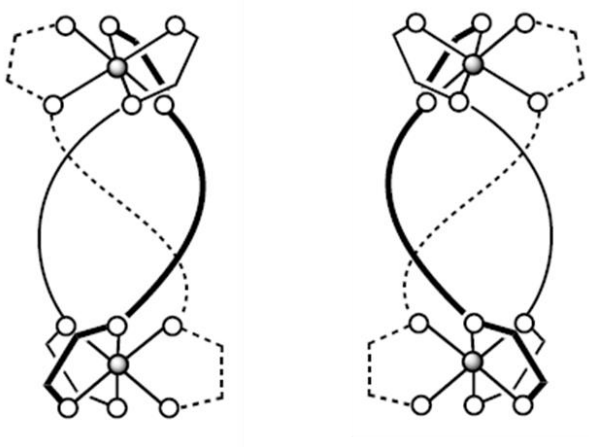

Figure 1.39 P (left) and M (right) helicity of a dinuclear helicate. [Reproduced from Ref [87]]

If the helicate is formed from achiral ligands, a racemic mixture of M and P enantiomers will result.[87] These may be separated by chiral resolving agents or chiral chromatography.[87] However, there are many examples of enantiopure helicates synthesised from chiral, enantiopure ligands.[87] Stereoselectivity can be forced by the rigidity of the ligand, the length of the ligand spacer or by introducing chiral moieties on the ligand coordinating units or spacer.[87,88]

One example of an enantiopure helicate is a trinuclear triple stranded titanium(IV) complex synthesised from a chiral ligand (Fig. 1.40).[89] The introduction of chiral groups to the

ligand spacer allowed the complete control of the stereochemistry of the resulting helicate.[89]

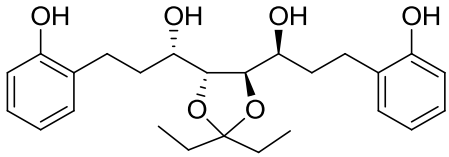

Figure 1.40 Structure of chiral ligand used to form enantiopure Ti(IV) helicate.[89]

1.5.3 Applications of supramolecular helicates

Although a vast array of supramolecular helicates have been developed, research into their applications is less established. One application of helicates is for the recognition and capture of anions, with helicates being designed to include an anion binding cavity. An example of this is a triple stranded dinuclear iron(II) helicate which has a cavity in which chloride ions can bind (Fig. 1.41).[90]

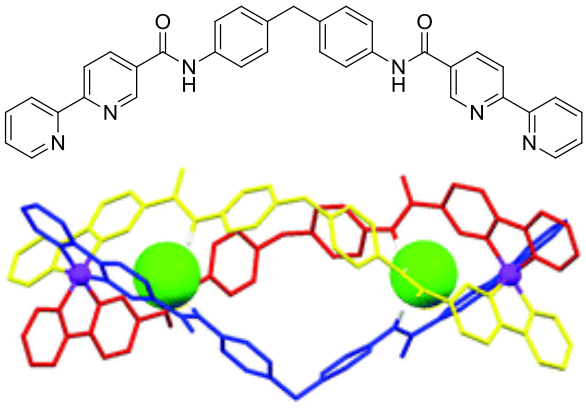

Figure 1.41 Structure of ligand of iron(II) triple stranded helicate (top); Molecular model of chloride anions (green) bound in anion cavities of helicate [Reproduced from Ref [90]] (bottom).

Helicates have also been developed for use as catalysts. A chiral dinuclear silver(I) helicate (Fig. 1.42) was synthesised to be used as a catalyst for an asymmetric allylation reaction.[91]

The helicate afforded the desired product of the reaction in good yield but with low enantiomeric excess.[91]

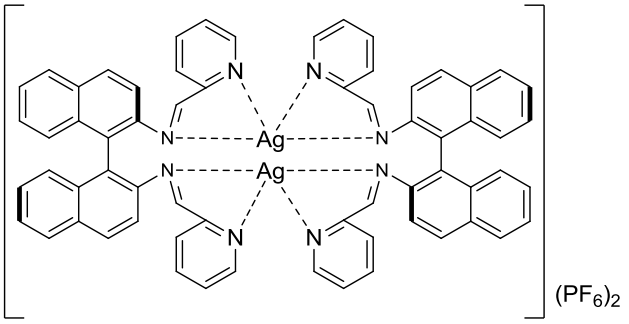

Figure 1.42 Structure of chiral dinuclear Ag(I) helicate.[91]

Hannon *et al* have developed double and triple stranded metallo-helicates that are potent cytotoxic[75] and anti-microbial [92] agents for use in therapeutic applications, as discussed in the next section.

1.5.4 Supramolecular cylinders with anticancer activity

Over the past decade supramolecular metallo-cylinders have been developed as potential anticancer agents in the Hannon group. These helicates are formed of pyridylimine ligands wrapped around two central metal ions (Fig. 1.43).[93] The ligand is synthesised from commercially available, inexpensive starting materials and can be complexed with a range of metal salts to yield double or triple stranded dinculear helicates.[93]

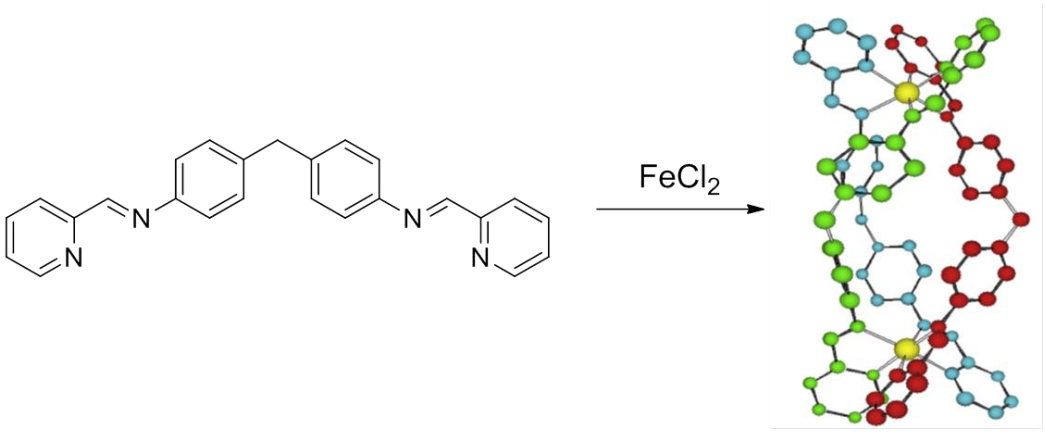

Figure 1.43 Synthesis of iron(II) triple stranded supramolecular cylinder from pyridylimine ligand, L. [Reproduced from Ref [75]]

Modelling and DNA binding studies revealed that the triple stranded iron(II) cylinder, $[Fe_2L_3]^{4+}$ (Fig. 1.43), is of the correct size and shape, 2 nm in length by 1 nm diameter, to bind in the major groove of DNA.[94] This DNA binding is with some sequence preference for **A**/**T** rich regions and induces bending and intramolecular coiling of the DNA helix.[94,95] Atomic force microscopy (AFM) images of the cylinder with linearized plasmid DNA show dramatic intramolecular coiling of the DNA at moderate cylinder loading (Fig. 1.44).[94]

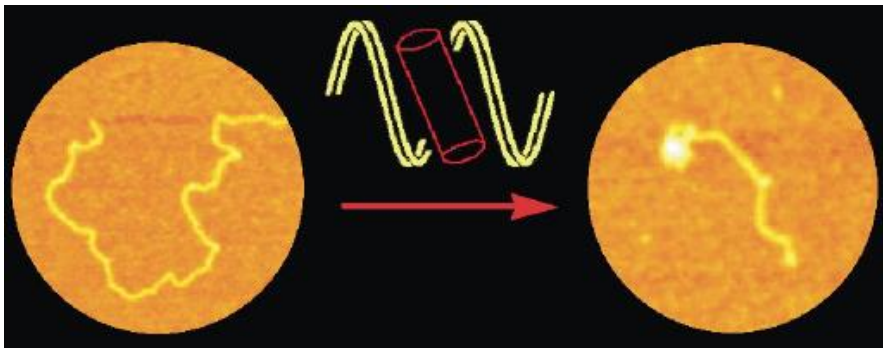

Figure 1.44 AFM images of linearized plasmid DNA in absence and presence of iron(II) triple stranded cylinder. [Reproduced from Ref [94]]

Further studies revealed that the cylinder can also unwind duplex DNA, with an unwinding angle of 27°, and can do so rather extensively compared to other non-intercalative compounds.[95] This indicates that the cylinder could have an effect on any cellular processes that require opening of the DNA helix, such as DNA transcription and replication.[96]

Attempts to crystallise the iron(II) cylinder with a DNA palindromic hexanucleotide led to the discovery of an unprecedented mode of non-covalent DNA recognition. The crystal structure revealed a DNA three-way junction with the cylinder bound in its central cavity (Fig. 1.45) (as discussed in Section 1.4.2).[71]

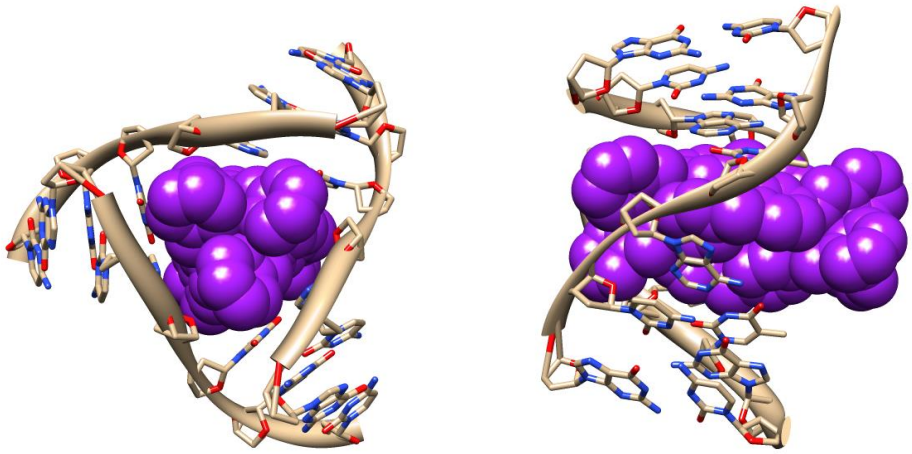

Figure 1.45 Crystal structure of $[Fe_2L_3]^{4+}$ bound in heart of DNA three-way junction (PDB 2ET0)[71]; front view (left) and side view (right).

Further studies revealed that the cylinder can bind to and stabilise a variety of three-way junction, and other Y-shaped junction, structures formed from palindromic and non-palindromic oligonucleotide sequences of varying lengths.[97]

This novel DNA recognition has many applications, as three-way junctions and other Y-shaped junctions play a role in many biological processes, as previously discussed.

Perhaps unsurprisingly, for a molecule that exhibits such strong DNA binding, the cylinder has been found to be a potent inhibitor of cellular proliferation in several cancer cell lines, with an activity IC_{50} (the drug concentration needed to inhibit cellular proliferation by fifty percent) only five times less than that of cisplatin.[75]

Interestingly the cylinder is not genotoxic or mutagenic, properties that cause severe side effects in existing anti-cancer compounds such as cisplatin.[75,98] The iron(II) complex also possesses antimicrobial activity[92] and has been shown to inhibit the DNA binding of proteins involved in DNA replication.[99]

These supramolecular cylinders are a racemic mixture of M and P enantiomers (Fig. 1.46), which can be separated by cellulose column chromatography with sodium chloride solution as the eluent.[100] Studies have revealed that the two enantiomers have different DNA binding modes, with the M enantiomer having a stronger binding affinity for DNA due to its ability to partially insert one of its chelates between the DNA bases in the major groove.[95] The M enantiomer has been found to be more efficient at DNA coiling and unwinding, and can stabilise DNA three-way junctions more effectively than the P enantiomer.[95,97,101]

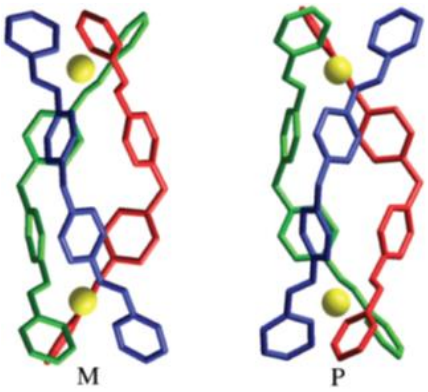

Figure 1.46 Structure of M and P enantiomers of $[Fe_2L_3]^{4+}$. [Reproduced from Ref [95]]

Double stranded dinuclear cylinders can also be formed, using tetrahedral metal ions such as copper(I) and silver(I). The copper(I) cylinder $[Cu_2L^1{}_2]^{2+}$ (Fig. 1.47) binds to DNA, although less strongly compared to the iron(II) triple stranded cylinder, likely due to its reduced charge.[102] However, it can act as an artificial nuclease in the presence of peroxide, causing unusual double strand DNA cleavage at the same site.[102]

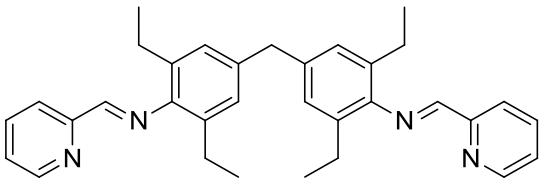

Figure 1.47 Structure of ligand L^1 in double stranded complex $[Cu_2L^1{}_2]^{2+}$.[102]

A luminescent triple stranded ruthenium(II) cylinder, $[Ru_2L_3]^{4+}$, has also been developed that is highly stable due to its inert ruthenium centres.[103] This cylinder can bind to DNA, induce intramolecular coiling and is cytotoxic, with IC_{50} values only 2-5 times less than cisplatin, against several cancer cell lines.[103] More excitingly, this complex can cleave DNA in a sequence dependent manner upon irradiation with visible or UVA light.[104] This

observed DNA photocleavage activity makes the ruthenium(II) cylinder a potential candidate for use in photodynamic therapy applications.[104]

1.6 Summary and thesis aims

There has been a vast amount of research conducted to try to understand the structure and function of DNA, to investigate the action of natural therapeutic agents and to develop synthetic agents with similar or enhanced efficacy.

The work undertaken and presented in this thesis is an extension of the research on supramolecular helicates with anticancer activity, discussed in section 1.5.4. The aim of the work herein is to develop novel helicates, functionalised with a variety of DNA binding groups and biomolecules, to further probe the DNA binding activity of this class of metallo-drugs. In order to achieve a range of functionalised cylinders, a new functionalisation route is needed for the easy modification of the cylinder. Helicates with tumour-targeting steroid and sugar vectors will also be designed and synthesised in order to improve the specificity of these metallo-cylinders for their target, cancerous tissue. Their DNA binding and activity will be assessed using circular and linear dichroism, and agarose and polyacrylamide gel electrophoresis.

1.7 References

(1) Watson, J. D.; Crick, F. H. C., *Nature* **1953**, *171*, 737.

(2) Watson, J. D.; Crick, F. H. C., *Nature* **1953**, *171*, 964.

(3) Hannon, M. J., *Chem. Soc. Rev.* **2007**, *36*, 280.

(4) Neidle, S. *Nat. Prod. Rep.*, **2001**, *18*, 291.

(5) Neidle, S., Nucleic Acid Structure and Recognition, *Oxford University Press* **2002**.

(6) Takusagawa, F. *J., Biomol. Struct. Dyn.* **1990**, *7*, 795.

(7) Narayana, N.; Weiss, M. A., *J. Mol. Biol.* **2009**, *385*, 469.

(8) Gessner, R. V.; Frederick, C. A.; Quigley, G. J.; Rich, A.; Wang, A. H., *J. Biol. Chem.* **1989**, *264*, 7921.

(9) Paul, A.; Bhattacharya, S., *Curr. Sci.* **2012**, *102*, 212.

(10) Hamilton, P. L.; Arya, D. P., *Nat. Prod. Rep.* **2012**, *29*, 134.

(11) Xiong, Y.; Sundaralingam, M., Encyclopedia of Life Sciences, *John Wiley & Sons* **2001**.

(12) Pavletich, N.; Pabo, C., *Science* **1991**, *252*, 809.

(13) Gao, Q.; Williams, L. D.; Egli, M.; Rabinovich, D.; Chen, S. L.; Quigley, G. J.; Rich, A., *Proc. Natl. Acad. Sci. USA.* **1991**, *88*, 2422.

(14) Coll, M.; Frederick, C. A.; Wang, A. H.; Rich, A., *Proc. Natl. Acad. Sci. USA* **1987**, *84*, 8385.

(15) Brown, D. G.; Sanderson, M. R.; Garman, E.; Neidle, S., *J. Mol. Biol.* **1992**, *226*, 481.

(16) Pjura, P. E.; Grzeskowiak, K.; Dickerson, R. E., *J. Mol. Biol.* **1987**, *197*, 257.

(17) Sanchez, M. I.; Vazquez, O.; Martinez-Costas, J.; Vazquez, M. E.; Mascarenas, J. L., *Chem. Sci.* **2012**, *3*, 2383.

(18) Komeda, S.; Moulaei, T.; Woods, K. K.; Chikuma, M.; Farrell, N. P.; Williams, L. D., *J. Am. Chem. Soc.* **2006**, *128*, 16092.

(19) Liu, H.-K.; Sadler, P. J., *Acc. Chem. Res.* **2011**, *44*, 349.

(20) Frederick, C. A.; Williams, L. D.; Ughetto, G.; Van der Marel, G. A.; Van Boom, J. H.; Rich, A.; Wang, A. H. J., *Biochemistry* **1990**, *29*, 2538.

(21) Purciolas, M.; Canals, A.; Coll, M.; Aymamí, J., *Acta Crystallogr., Sect. D:Biol. Crsytallogr.* **2005**, *61*, 1009.

(22) Jennette, K. W.; Lippard, S. J.; Vassiliades, G. A.; Bauer, W. R., *Proc. Natl. Acad. Sci. USA.* **1974**, *71*, 3839.

(23) Bond, P. J.; Langridge, R.; Jennette, K. W.; Lippard, S. J., *Proc. Natl. Acad. Sci. USA.* **1975**, *72*, 4825.

(24) Niyazi, H.; Hall, J. P.; O'Sullivan, K.; Winter, G.; Sorensen, T.; Kelly, J. M.; Cardin, C. J., *Nature Chem.* **2012**, *4*, 621.

(25) Hannon, M. J., *Pure Appl. Chem.* **2007**, *79*, 2243.

(26) Ho, Y. P.; Au-Yeung, S. C.; To, K. K., *Med. Res. Rev.* **2003**, *23*, 633.

(27) Rosenberg, B.; Van Camp, L.; Krigas, T., *Nature* **1965**, *205*, 698.

(28) Ahmad, S.; Isab, A. A.; Ali, S., *Transition Met. Chem.* **2006**, *31*, 1003.

(29) Kartalou, M.; Essigmann, J. M., *Mutat. Res.* **2001**, *478*, 1.

(30) Ghezzi, A.; Aceto, M.; Cassino, C.; Gabano, E.; Osella, D., *J. Inorg. Biochem.* **2004**, *98*, 73.

(31) Kuo, M. T.; Chen, H. H. W.; Song, I.-S.; Savaraj, N.; Ishikawa, T., *Cancer Mestastasis Rev.* **2007**, *26*, 71.

(32) Jamieson, E. R.; Lippard, S. J., *Chem. Rev.* **1999**, *99*, 2467.

(33) Takahara, P. M.; Frederick, C. A.; Lippard, S. J., *J. Am. Chem. Soc.* **1996**, *118*, 12309.

(34) Flchtlnger-Schepman, A. M. J.; van Dijk-Knijnenburg, H. C. M.; van der Velde-Visser, S. D.; Berends, F.; Baan, R. A., *Carcinogenesis* **1995**, *16*, 2447.

(35) Rice, J. A.; Crothers, D. M.; Pinto, A. L.; Lippard, S. J., *Proc. Natl. Acad. Sci. USA.* **1988**, *85*, 4158.

(36) Pil, P.; Lippard, S., *Science* **1992**, *256*, 234.

(37) Trimmer, E. E.; Essigmann, J. M., *Essays Biochem.* **1999**, *34*, 191.

(38) Dyson, P. J.; Sava, G., *Dalton Trans.* **2006**, 1929.

(39) Zhang, C. X.; Lippard, S. J., *Curr. Opin. Chem. Biol.* **2003**, *7*, 481.

(40) Reedijk, J., *Chem. Commun.* **1996**, 801.

(41) Wong, E.; Giandomenico, C. M., *Chem. Rev.* **1999**, *99*, 2451.

(42) Hannon, M. J.; Green, P. S.; Fisher, D. M.; Derrick, P. J.; Beck, J. L.; Watt, S. J.; Ralph, S. F.; Sheil, M. M.; Barker, P. R.; Alcock, N. W.; Price, R. J.; Sanders, K. J.; Pither, R.; Davis, J.; Rodger, A., *Chem. Eur. J.* **2006**, *12*, 8000.

(43) Fuertes, M. A.; Alonso, C.; Pérez, J. M., *Chem. Rev.* **2003**, *103*, 645.

(44) Barefoot, R. R., *J. Chromatogr. B: Biomed. Sci. Appl.* **2001**, *751*, 205.

(45) Saris, C. P.; van de Vaart, P. M.; Rietbroek, R. C.; Bloramaert, F., *Carcinogenesis* **1996**, *17*, 2763.

(46) Lippert, B., Cisplatin, Chemistry and Biochemistry of a Leading Anticancer Drug, *Wiley-VCH* **1999.**

(47) Kraker, A. J.; Moore, C. W., *Cancer Res.* **1988**, *48*, 9.

(48) Pizarro, A. M.; Sadler, P. J., *Biochimie* **2009**, *91*, 1198.

(49) Brabec, V.; Kašpárková, J.; Vrána, O.; Nováková, O.; Cox, J. W.; Qu, Y.; Farrell, N., *Biochemistry* **1999**, *38*, 6781.

(50) Bruijnincx, P. C. A.; Sadler, P. J., *Curr. Opin. Chem. Biol.* **2008**, *12*, 197.

(51) Mackay, F. S.; Woods, J. A.; Moseley, H.; Ferguson, J.; Dawson, A.; Parsons, S.; Sadler, P. J., *Chem. Eur. J.* **2006**, *12*, 3155.

(52) Rosenberg, B.; Van Camp, L.; Grimley, E. B.; Thomson, A. J., *J. Biol. Chem.* **1967**, *242*, 1347.

(53) Zeglis, B. M.; Pierre, V. C.; Barton, J. K., *Chem. Commun.* **2007**, 4565.

(54) Jakupec, M. A.; Galanski, M.; Arion, V. B.; Hartinger, C. G.; Keppler, B. K., *Dalton Trans.* **2008**, 183.

(55) Heffeter, P.; Böck, K.; Atil, B.; Reza Hoda, M.; Körner, W.; Bartel, C.; Jungwirth, U.; Keppler, B.; Micksche, M.; Berger, W.; Koellensperger, G., *J. Biol. Inorg. Chem.* **2010**, *15*, 737.

(56) Bergamo, A.; Gagliardi, R.; Scarcia, V.; Furlani, A.; Alessio, E.; Mestroni, G.; Sava, G., *J. Pharmacol. Exp. Ther.* **1999**, *289*, 559.

(57) Harlos, M.; Ott, I.; Gust, R.; Alborzinia, H.; Wölfl, S.; Kromm, A.; Sheldrick, W. S., *J. Med. Chem.* **2008**, *51*, 3924.

(58) Schatzschneider, U., *Eur. J. Inorg. Chem.* **2010**, *2010*, 1451.

(59) Menon, E. L.; Perera, R.; Navarro, M.; Kuhn, R. J.; Morrison, H., *Inorg. Chem.* **2004**, *43*, 5373.

(60) Fernandez-Moreira, V.; Thorp-Greenwood, F. L.; Coogan, M. P., *Chem. Commun.* **2010**, *46*, 186.

(61) Louie, M.-W.; Liu, H.-W.; Lam, M. H.-C.; Lau, T.-C.; Lo, K. K.-W., *Organometallics* **2009**, *28*, 4297.

(62) Martinez-Lillo, J.; Mastropietro, T. F.; Lappano, R.; Madeo, A.; Alberto, M. E.; Russo, N.; Maggiolini, M.; De Munno, G., *Chem. Commun.* **2011**, *47*, 5283.

(63) Lau, J. S.-Y.; Lee, P.-K.; Tsang, K. H.-K.; Ng, C. H.-C.; Lam, Y.-W.; Cheng, S.-H.; Lo, K. K.-W., *Inorg. Chem.* **2008**, *48*, 708.

(64) Kastl, A.; Wilbuer, A.; Merkel, A. L.; Feng, L.; Di Fazio, P.; Ocker, M.; Meggers, E., *Chem. Commun.* **2012**, *48*, 1863.

(65) Wong, E. L.-M.; Fang, G.-S.; Che, C.-M.; Zhu, N., *Chem. Commun.* **2005**, 4578.

(66) Youngquist, R. S.; Dervan, P. B., *J. Am. Chem. Soc.* **1985**, *107*, 5528.

(67) Duckett, D. R.; Lilley, D. M., *EMBO J.* **1990**, *9*, 1659.

(68) Han, H.; Hurley, L. H., *Trends Pharmacol. Sci.* **2000**, *21*, 136.

(69) Brogden, A. L.; Hopcroft, N. H.; Searcey, M.; Cardin, C. J., *Angew. Chem. Int. Ed.* **2007**, *46*, 3850.

(70) Reynolds, J., *Nat. Cell Biol.* **2004**, *6*, 184.

(71) Oleksi, A.; Blanco, A. G.; Boer, R.; Usón, I.; Aymamí, J.; Rodger, A.; Hannon, M. J.; Coll, M., *Angew. Chem. Int. Ed.* **2006**, *45*, 1227.

(72) Pearson, C. E.; Tam, M.; Wang, Y. H.; Montgomery, S. E.; Dar, A. C.; Cleary, J. D.; Nichol, K., *Nucleic Acids Res.* **2002**, *30*, 4534.

(73) Singleton, M. R.; Scaife, S.; Wigley, D. B., *Cell* **2001**, *107*, 79.

(74) Nikulin, A.; Serganov, A.; Ennifar, E.; Tishchenko, S.; Nevskaya, N.; Shepard, W.; Portier, C.; Garber, M.; Ehresmann, B.; Ehresmann, C.; Nikonov, S.; Dumas, P., *Nat. Struct.Mol. Biol.* **2000**, *7*, 273.

(75) Hotze, A. C.; Hodges, N. J.; Hayden, R. E.; Sanchez-Cano, C.; Paines, C.; Male, N.; Tse, M. K.; Bunce, C. M.; Chipman, J. K.; Hannon, M. J., *Chem. Biol.* **2008**, *15*, 1258.

(76) Dixon, I. M.; Lopez, F.; Tejera, A. M.; Estève, J.-P.; Blasco, M. A.; Pratviel, G.; Meunier, B., *J. Am. Chem. Soc.* **2007**, *129*, 1502.

(77) Collie, G. W.; Promontorio, R.; Hampel, S. M.; Micco, M.; Neidle, S.; Parkinson, G. N., *J. Am. Chem. Soc.* **2012**, *134*, 2723.

(78) Muller, S.; Sanders, D. A.; Di Antonio, M.; Matsis, S.; Riou, J.-F.; Rodriguez, R.; Balasubramanian, S., *Org. Biomol. Chem.* **2012**, *10*, 6537.

(79) Lehn, J. M., *Pure Appl. Chem.* **1978**, *50*, 871.

(80) Lehn, J., *Science* **1993**, *260*, 1762.

(81) Cragg, P. J., Supramolecular Chemistry: From Biological Inspiration to Biomedical Applications, *Springer* **2010**.

(82) Pfeil, A.; Lehn, J.-M., *J. Chem. Soc., Chem. Commun.* **1992**, 838.

(83) Davis, A. V.; Yeh, R. M.; Raymond, K. N., *Proc. Natl. Acad. Sci. USA.* **2002**, *99*, 4793.

(84) Constable, E. C., *Angew. Chem. Int. Ed. Engl.* **1991**, *30*, 1450.

(85) Piguet, C.; Bernardinelli, G.; Hopfgartner, G., *Chem. Rev.* **1997**, *97*, 2005.

(86) He, C.; Zhao, Y.; Guo, D.; Lin, Z.; Duan, C., *Eur. J. Inorg. Chem.* **2007**, *2007*, 3451.

(87) Jodry, J. J.; Lacour, J., *Chem. Eur. J.* **2000**, *6*, 4297.

(88) Albrecht, M., *Chem. Eur. J.* **2000**, *6*, 3485.

(89) Corey, E. J.; Cywin, C. L.; Noe, M. C., *Tetrahedron Lett.* **1994**, *35*, 69.

(90) Goetz, S.; Kruger, P. E., *Dalton Trans.* **2006**, 1277.

(91) Zhang, H.; Chen, L.; Song, H.; Zi, G., *Inorg. Chim. Acta* **2011**, *366*, 320.

(92) Richards, A. D.; Rodger, A.; Hannon, M. J.; Bolhuis, A., *Int. J. Antimicrob. Agents* **2009**, *33*, 469.

(93) Hannon, M. J.; Painting, C. L.; Jackson, A.; Hablin, J.; Errington, W., *Chem. Commun.* **1997**, 1807.

(94) Hannon, M. J.; Moreno, V.; Prieto, M. J.; Moldrheim, E.; Sletten, E.; Meistermann, I.; Isaac, C. J.; Sanders, K. J.; Rodger, A., *Angew. Chem. Int. Ed.* **2001**, *40*, 879.

(95) Malina, J.; Hannon, M. J.; Brabec, V., *Nucleic Acids Res.* **2008**, *36*, 3630.

(96) Karp, G., Cell and Molecular Biology: Concepts and Experiments, *Wiley* **2009**.

(97) Malina, J.; Hannon, M. J.; Brabec, V., *Chem. Eur. J.* **2007**, *13*, 3871.

(98) Yarema, K. J.; Lippard, S. J.; Essigmann, J. M., *Nucleic Acids Res.* **1995**, *23*, 4066.

(99) Ducani, C.; Leczkowska, A.; Hodges, N. J.; Hannon, M. J., *Angew. Chem. Int. Ed.* **2010**, *49*, 8942.

(100) Hannon, M. J.; Meistermann, I.; Isaac, C. J.; Blomme, C.; Aldrich-Wright, J. R.; Rodger, A., *Chem. Commun.* **2001**, 1078.

(101) Meistermann, I.; Moreno, V.; Prieto, M. J.; Moldrheim, E.; Sletten, E.; Khalid, S.; Rodger, P. M.; Peberdy, J. C.; Isaac, C. J.; Rodger, A.; Hannon, M. J., *Proc. Natl. Acad. Sci. USA.* **2002**, *99*, 5069.

(102) Childs, L. J.; Malina, J.; Rolfsnes, B. E.; Pascu, M.; Prieto, M. J.; Broome, M. J.; Rodger, P. M.; Sletten, E.; Moreno, V.; Rodger, A.; Hannon, M. J., *Chem. Eur. J.* **2006**, *12*, 4919.

(103) Pascu, G. I.; Hotze, A. C.; Sanchez-Cano, C.; Kariuki, B. M.; Hannon, M. J., *Angew. Chem. Int. Ed. Engl.* **2007**, *46*, 4374.

(104) Malina, J.; Hannon, M. J.; Brabec, V., *Chem. Eur. J.* **2008**, *14*, 10408.

Chapter 2: Novel Alkyne Metallo-Cylinders

2.1 Introduction and aims

As detailed in Chapter 1 (Section 1.5.4), double and triple stranded di-nuclear metallo-cylinders (Fig. 2.1) have been developed as potential anticancer agents in the Hannon group.[1]

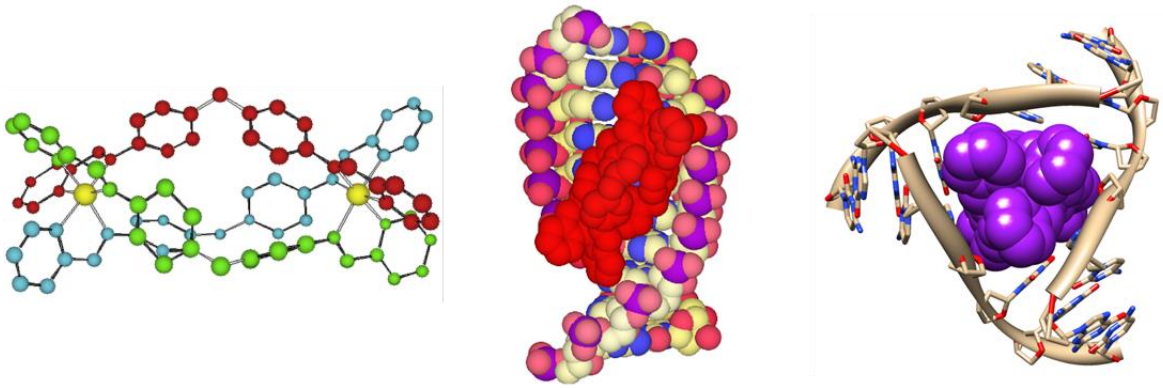

Figure 2.1 Structure of triple stranded supramolecular cylinder [Reproduced from Ref [2]] (left); Model of cylinder bound in major groove [Reproduced from Ref [3]] (middle); Crystal structure of cylinder bound in the heart of a DNA three-way junction (PDB 2ET0)[4] (right).

These cylindrical structures are of the correct size and shape to bind in the major groove of DNA[5] and in the centre of DNA three-way junctions.[4] They are able to unwind duplex DNA[6] and are cytotoxic against several cancer cell lines.[2]

Inspired by the successes of the parent cylinder, the aim of the work described herein was to design and synthesise functionalised supramolecular helicates (Fig. 2.2) that could be used to further probe, and possibly improve, the DNA recognition properties of this

exciting class of anticancer agents. Modification of these cylinders, by the addition of a variety of functional groups, R, may give further insight into the structural requirements of the DNA sites that these cylinders preferentially bind.

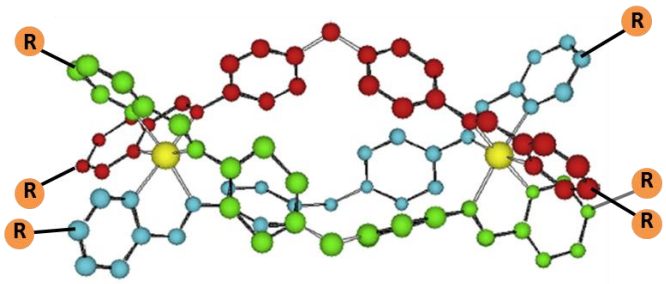

Figure 2.2 Functionalised supramolecular cylinder. [Adapted from Ref [2]]

To achieve a range of functionalised cylinders, a novel functionalisation route was needed to allow the easy and varied modification of the cylinder, over few reaction steps. Functionalisation of these supramolecular helicates has been accomplished in the past, however the synthetic route used is less than ideal due to the many reaction steps needed.[7]

2.2 Novel functionalisation route

To synthesise these modified cylinders, a simple coupling procedure was needed so that many different functional groups could be attached using the same reaction conditions, over few reaction steps. Sonogashira cross-coupling is a well-known and documented procedure for the coupling of terminal alkynes and aryl/alkenyl halides, catalysed by palladium(0) and copper(I) catalysts, under mild conditions.[8] The proposed synthesis (Scheme 2.1) involves Sonogashira coupling of the new functional moiety, R, to commercially available 5-bromopyridine-2-carboxaldehyde over one step.

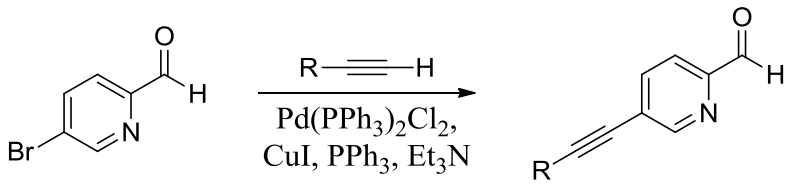

Scheme 2.1 Sonogashira coupling of functional moiety, R, to 5-bromopyridine-2-carboxaldehyde.

The triple stranded iron(II) cylinder can then be synthesised from the functionalised pyridine carboxaldehyde in a one-pot reaction (Scheme 2.2).

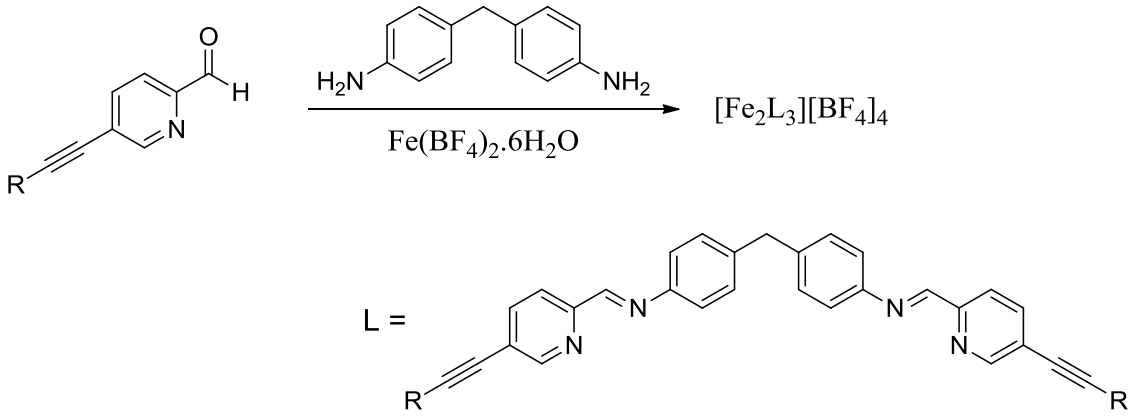

Scheme 2.2 One-pot synthesis of functionalised iron(II) helicate.

This synthesis route allows a variety of chemical groups to be conjugated to the cylinder, and many compounds containing an alkyne functional group are commercially available. However these compounds can also be easily synthesised. An alkyne group can be added in many ways, including via a palladium catalysed cross-coupling reaction (Scheme 2.3).

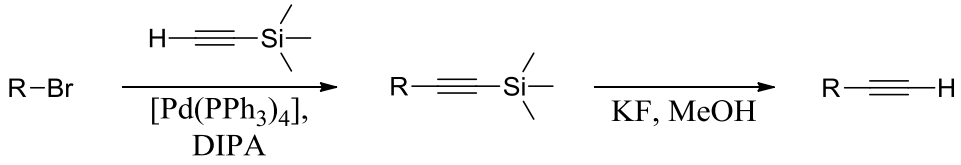

Scheme 2.3 Proposed synthetic route for addition of an alkyne group, via a palladium catalysed cross-coupling reaction, and subsequent silyl deprotection.

2.2.1 Sonogashira cross-coupling

Sonogashira cross coupling involves the use of a palladium catalyst, either a Pd(0) catalyst such as [$Pd(PPh_3)_4$] or alternatively a Pd(II) pre-catalyst such as [$Pd(PPh_3)_2Cl_2$], and a copper(I) catalyst such as CuI.[9] The presence of an organic base such as triethylamine or diisopropylamine is also needed.[9] The proposed mechanism of the cross-coupling reaction proceeds via a dual catalytic cycle (Scheme. 2.4) with the first step being an oxidative addition (A) of Pd(0) **(f)** into the C-X bond of an aryl or vinyl halide **(b)** to form the Pd(II) species **(j)**.[9] Transmetallation (B) then occurs, where the Pd(II) electron deficient metal centre accepts a terminal alkyne donor ligand, to form **(k)**.[9] It is thought that a copper catalytic cycle is responsible for the formation of copper acetylide **(e)**, which transfers the alkyne to the palladium, from the alkyne reactant **(a)** via an intermediate **(d)**.[9] The reductive elimination step (C) produces the disubstituted alkyne **(c)**, the reaction product, by forming a new carbon-carbon bond and at the same time regenerates the catalyst Pd(0).[9]

If a palladium(II) pre-catalyst **(g)** is used, this must first be activated by phosphine or excess alkyne to form Pd(0) species **(f)**.[9] This is facilitated by a copper cycle that aids the sequential transfer of two alkyne ligands **(a)**, and then reductive carbon-carbon bond formation to expel the diacetylene side product **(i)**.[9] An organic base is needed to remove the acid formed in the reductive elimination step of the palladium cycle.[9]

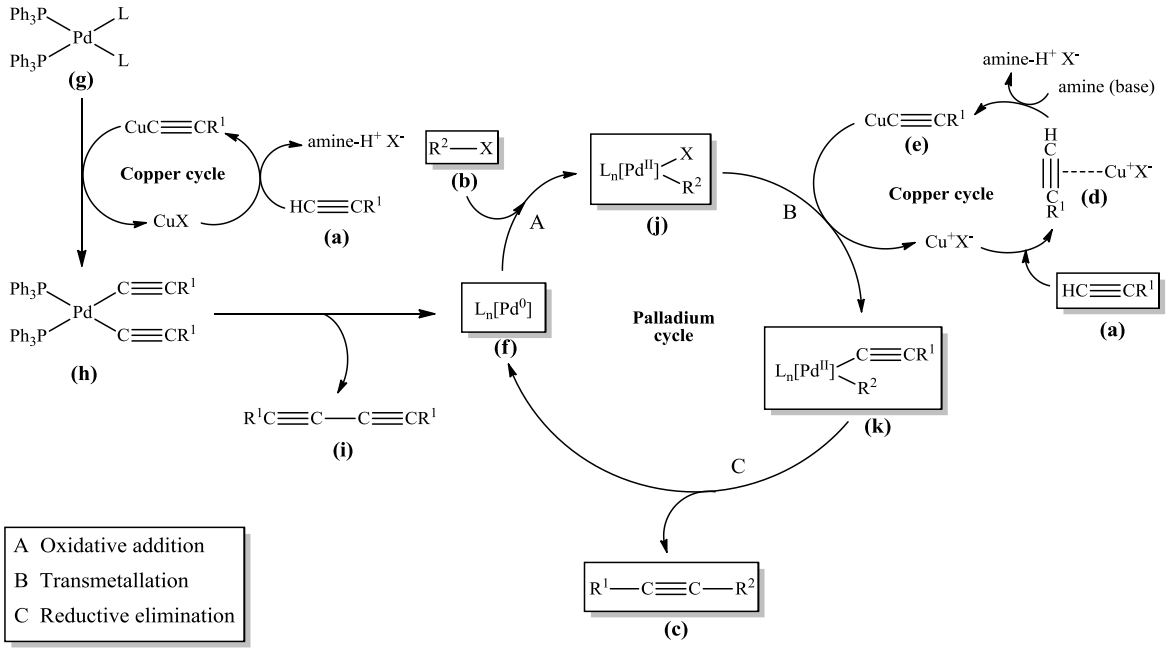

Scheme 2.4 Outline of reaction scheme and proposed catalytic cycles of Sonogashira coupling. [Adapted from Ref [9]]

2.3 Molecular design

Several iron(II) cylinders functionalised with simple chemical groups were designed. The 5-position of the pyridine carboxaldehyde was used as it is known that modification at this site, which has the effect of increasing the length of the cylinder, has the least effect on its DNA recognition properties.[10] Widening of the cylinder by modification at the 3-position was found to weaken the DNA binding strength of the cylinder[10] and this may also be the case for the 4-position. Modification at the 6-position of the pyridine ring was also ruled out due to possible steric hindrance of the iron coordination site, or inhibition of the formation of the triple stranded cylinder.

The first cylinder to be synthesised, $[Fe_2L^{TB}_3]^{4+}$, was functionalised with an alkyne group only (Fig. 2.3). The DNA binding studies of this cylinder would indicate whether or not the

alkyne linker, present in all of the functionalised cylinders, would adversely affect the DNA recognition properties of these cylinders.

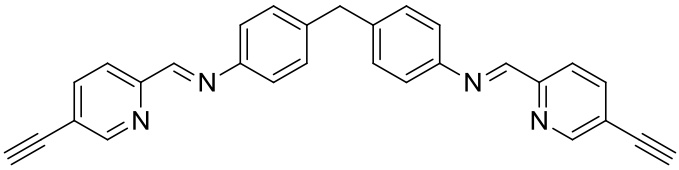

Figure 2.3 Structure of L^{TB} ligand of complex $[Fe_2L^{TB}_3]^{4+}$.

Two iron(II) cylinders, $[Fe_2L^{PA}_3]^{4+}$ and $[Fe_2L^{Hex}_3]^{4+}$, functionalised with alcohol groups at different distances from the helicate core were then designed (Fig. 2.4). It was hoped that these hydroxyl groups would increase solubility and may be able to hydrogen-bond with the DNA, increasing the interaction between the complex and the DNA. A flexible alkyl linker was incorporated into the hexyn-ol complex, $[Fe_2L^{Hex}_3]^{4+}$, which may have some effect on the interaction of the alcohol group with the DNA.

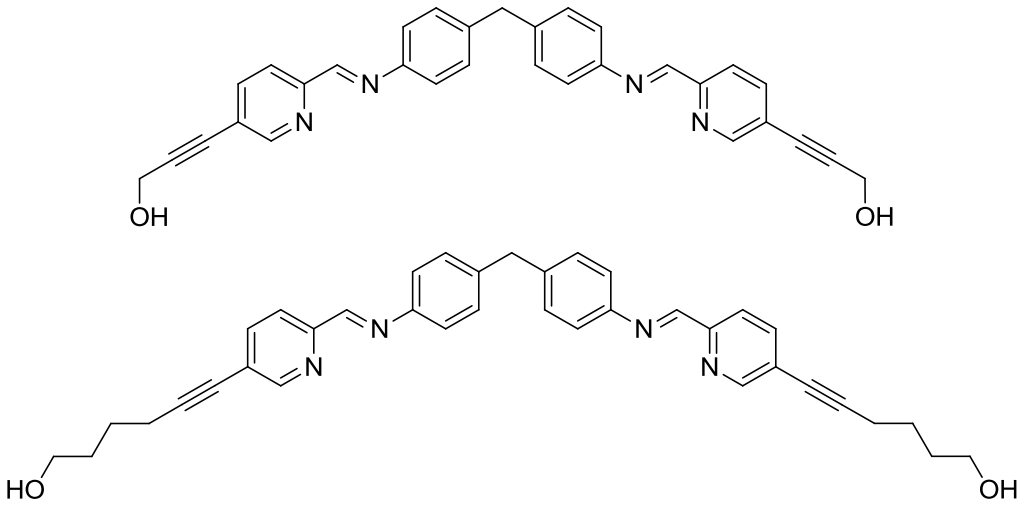

Figure 2.4 Structures of L^{PA} (top) and L^{Hex} (bottom) ligands of complexes $[Fe_2L^{PA}_3]^{4+}$ and $[Fe_2L^{Hex}_3]^{4+}$.

Finally, a cylinder functionalised with aromatic phenyl groups, $[Fe_2L^{Phen}{}_3]^{4+}$, (Fig. 2.5) was designed. It was thought that this group would allow any effects on the DNA binding of introducing aromatic substituents onto the cylinder to be explored.

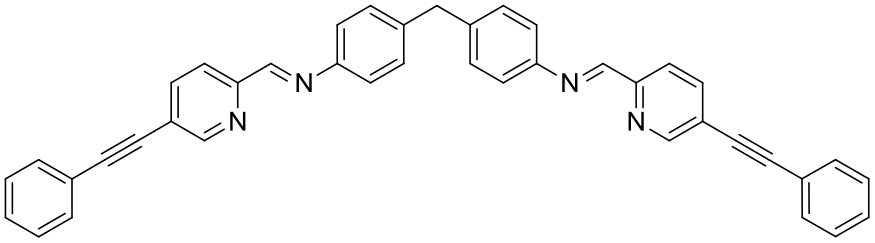

Figure 2.5 Structure of ligand L^{Phen} of complex $[Fe_2L^{Phen}{}_3]^{4+}$.

2.4 Synthesis

2.4.1 Synthesis of parent cylinder, $[Fe_2L^{P}{}_3][BF_4]_4$ [11]

The parent cylinder with tetrafluoroborate counterions has previously been synthesised[11] however the synthesis method described herein has not been reported. A one-pot synthesis was employed between the commercially available starting materials 2-pyridinecarboxaldehyde, 4,4'-methylenedianiline and iron(II) tetrafluoroborate hexahydrate (Scheme 2.5) in a 6:3:2 stoichiometry. The reaction was performed in ethanol, with the starting materials added sequentially and dropwise, and an immediate colour change from pale yellow to deep purple was observed. Although this colour change signals the formation of the iron(II) complex, the reaction mixture was stirred at room temperature for 12 hours, to make sure that as much of the starting materials had reacted as possible. The product, which had precipitated from the reaction solution, was then collected by filtration. Washing with copious amounts of chloroform resulted in a light purple solid in 81% yield.

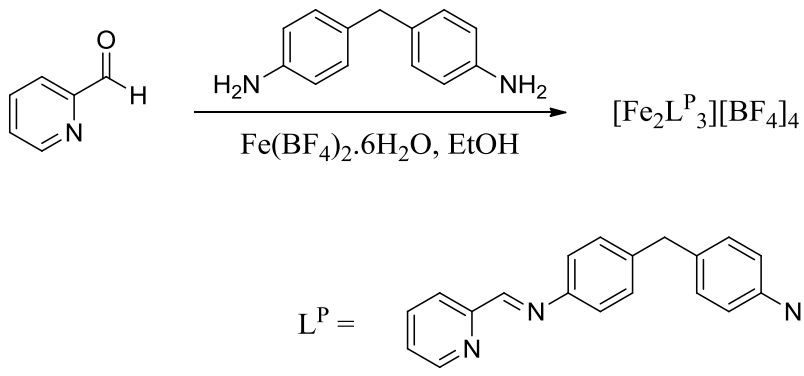

Scheme 2.5 Synthetic route for preparation of $[Fe_2L^P_3][BF_4]_4$.

In the ^{1}H NMR spectrum (Fig. 2.6), assigned using a 2D-COSY (see Appendix), a peak corresponding to the imine (H_{im}) proton is observed, giving evidence for the formation of the product. The four phenyl protons give rise to two peaks in the spectrum corresponding to H_{Pha} and H_{Phb} due to rotation of the phenylene rings at room temperature.

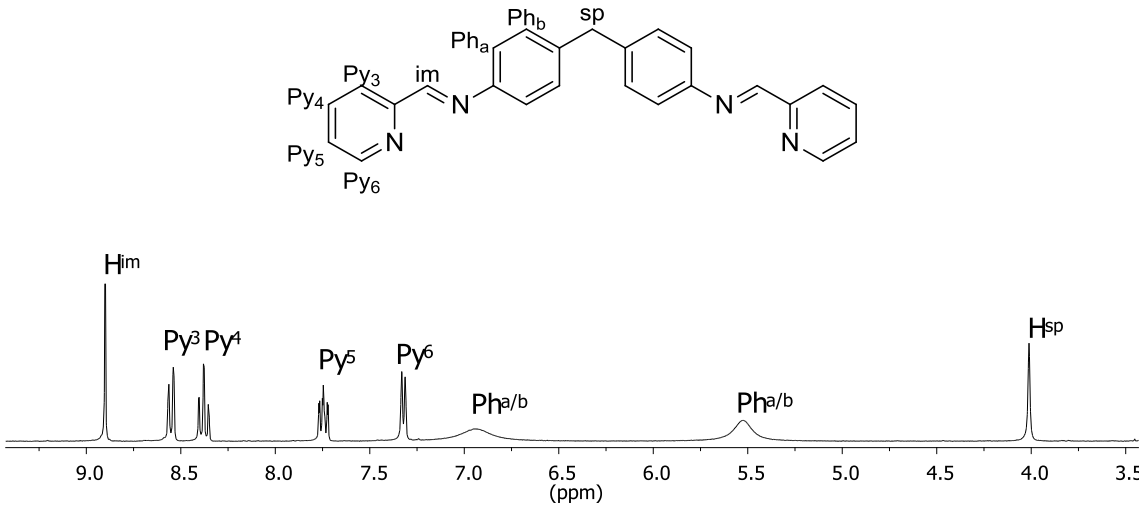

Figure 2.6 ^{1}H NMR (300 MHz, CD_3CN, 298 K) of $[Fe_2L^P_3][BF_4]_4$.

The ESI mass spectrum (see Appendix) shows several multiply charged peaks with an isotopic distribution pattern corresponding to the species $[Fe_2(C_{25}H_{20}N_4)_3]^{4+}$, $[Fe_2(C_{25}H_{20}N_4)_3]^{3+}$ and $[Fe_2(C_{25}H_{20}N_4)_3]^{2+}$.

2.4.2 Synthesis of triple bond cylinder, $[Fe_2L^{TB}_3][BF_4]_4$

2.4.2.1 Synthesis of 5-ethynyl-2-pyridinecarboxaldehyde (2) [12]

As 5-ethynyl-2-pyridinecarboxaldehyde (2) is not commercially available, it was synthesised in two steps from 5-bromo-2-pyridinecarboxaldehyde (Scheme 2.6) according to literature procedure.[12]

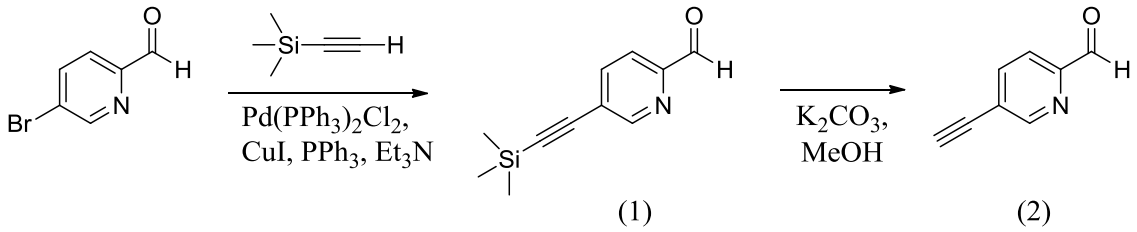

Scheme 2.6 Synthetic route for preparation of 5-ethynyl-2-pyridinecarboxaldehyde (2).

A Sonogashira coupling reaction was employed to couple trimethylsilylacetylene with the bromo-pyridine starting material in the presence of the catalysts bis(triphenylphosphine)palladium(II) dichloride and copper iodide in basic conditions. This was achieved by heating the reaction mixture at 80°C for 5 hours under an argon atmosphere. The triphenylphosphine oxide impurity from this reaction was removed by protonating the product with hydrochloric acid, partitioning the product and impurity using water and diethyl ether, neutralising the aqueous phase and extracting with ethyl acetate. The product (1) could then be purified using column chromatography on silica. In the second step of the synthesis, potassium carbonate was used to deprotect the silyl group of 5-[(trimethylsily)ethyny])-2-pyridinecarboxaldehyde (1) to give the expected product (2) in an overall yield of 56%.

The off-white solid was characterised by ^{1}H NMR (Fig. 2.7), high resolution EI mass spectrometry and elemental analysis which confirm the formation of the triple bond aldehyde (2) and are consistent with the literature.[12]

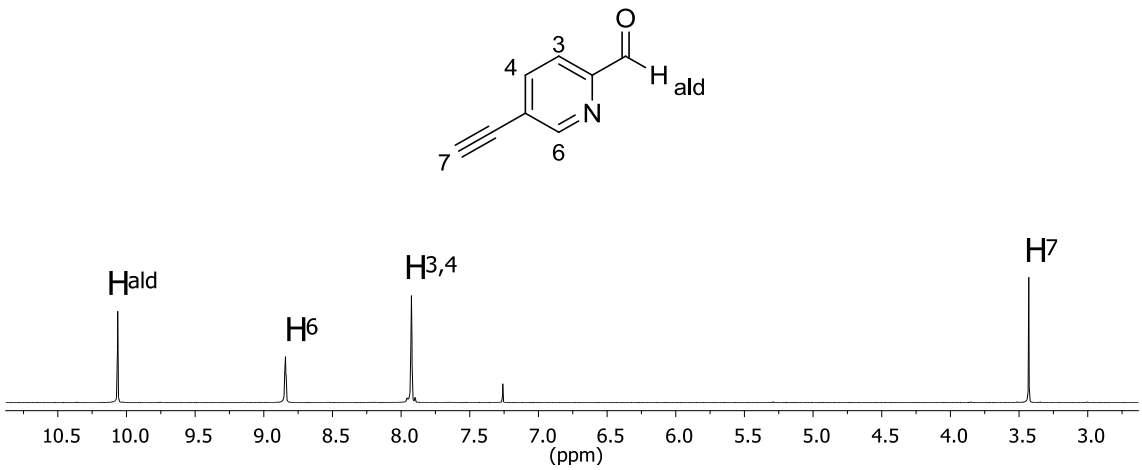

Figure 2.7 ^{1}H NMR (300 MHz, $CDCl_3$, 298 K) of 5-ethynyl-2-pyridinecarboxaldehyde (2).

2.4.2.2 Synthesis of $[Fe_2L^{TB}_3][BF_4]_4$

To prepare the functionalised cylinder, a one-pot reaction using six equivalents of 5-ethynyl-2-pyridinecarboxaldehyde (2), three equivalents of the spacer 4,4'-methylenedianiline and two equivalents of iron(II) tetrafluoroborate hexahydrate, mixed sequentially and dropwise, was stirred for 12 hours in ethanol (Scheme 2.7). An immediate colour change from pale yellow to purple after addition of the starting materials was observed, indicating the formation of the iron(II) helicate. The resulting purple precipitate was collected by filtration and purified by washing with a large volume of chloroform. A yield of 73% was obtained for this synthesis.

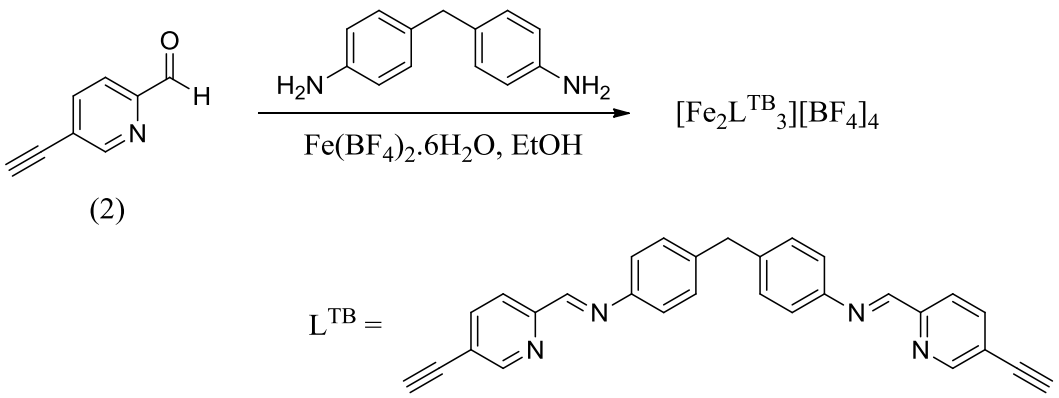

Scheme 2.7 Synthetic route for preparation of $[Fe_2L^{TB}{}_3][BF_4]_4$.

The product was characterised using ESI mass spectrometry, in which peaks corresponding to multiply charged species $[Fe_2(C_{29}H_{20}N_4)_3]^{4+}$ and $[Fe_2(C_{29}H_{20}N_4)_3]^{3+}$ were observed with the expected isotopic distribution patterns (see Appendix). In the ^{1}H NMR spectrum (Fig. 2.8), assigned using a 2D-COSY (see Appendix), characteristic peaks corresponding to the imine (H_{im}), spacer (H_{sp}) and phenyl ($H_{Pha,Phb}$) protons are observed with the expected integration. The proton of the triple bond moiety is also observed.

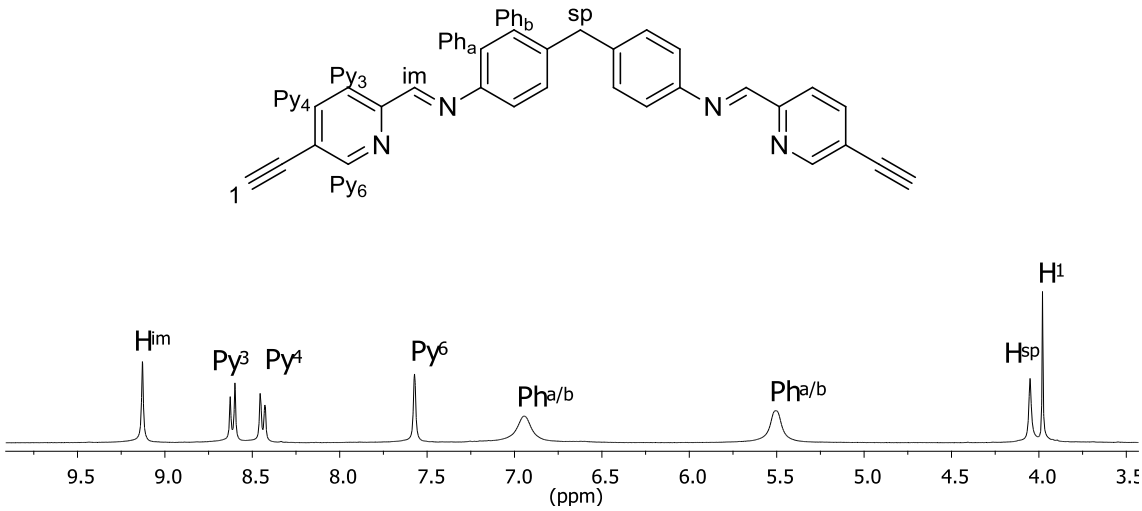

Figure 2.8 ^{1}H NMR (300 MHz, CD_3CN, 298 K) of $[Fe_2L^{TB}{}_3][BF_4]_4$.

An overall yield of 41% was obtained, with respect to the 5-bromo-2-pyridinecarboxaldehyde starting material, for the synthesis of the triple bond cylinder, $[Fe_2L^{TB}_3][BF_4]_4$.

2.4.3 Synthesis of propargyl alcohol cylinder, $[Fe_2L^{PA}_3][BF_4]_4$

2.4.3.1 Synthesis of 5-(3-hydroxyprop-1-ynyl)-2-pyridinecarboxaldehyde (3)

As 5-(3-hydroxyprop-1-ynyl)-2-pyridinecarboxaldehyde (3) is not commercially available, it was synthesised in one step (Scheme 2.8). A Sonogashira coupling, with catalysts bis(triphenylphosphine)palladium(II) dichloride and copper iodide, between 5-bromo-2-pyridinecarboxaldehyde and propargyl alcohol was performed in basic conditions under an argon atmosphere. The reaction mixture was heated to 80°C for 5 hours, after which time the crude product was purified by column chromatography on silica, to remove unreacted starting materials. The triphenylphosphine oxide impurity was removed by protonation of the product with hydrochloric acid, partitioning of the product and impurity, and subsequent neutralisation and extraction of the solution of 5-(3-hydroxyprop-1-ynyl)-2-pyridinecarboxaldehyde. An off-white solid was produced, in a yield of 58%.

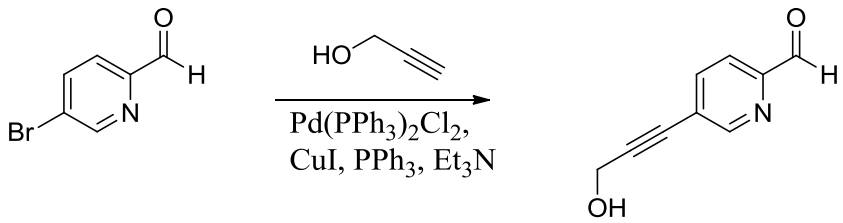

(3)

Scheme 2.8 Synthetic route for preparation of 5-(3-hydroxyprop-1-ynyl)-2-pyridinecarboxaldehyde (3).

High resolution EI mass spectrometry data was consistent with the formation of the product. The ^{1}H NMR spectrum (Fig. 2.9) provides further evidence for the formation of the compound, as peaks corresponding to the aldehyde (H_{ald}) and H_7 protons are observed at the correct integration.

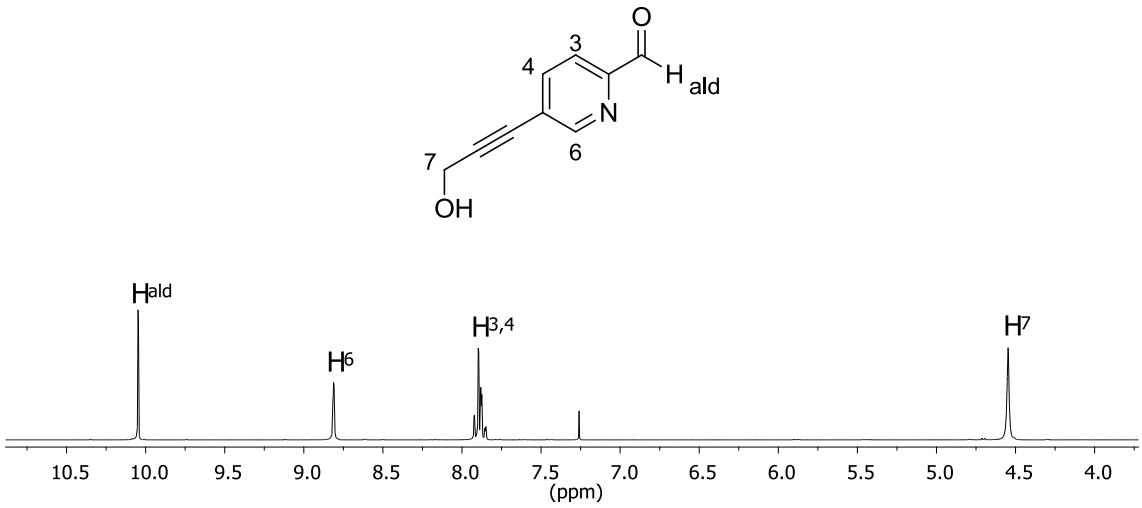

Figure 2.9 ^{1}H NMR (300 MHz, $CDCl_3$, 298 K) of 5-(3-hydroxyprop-1-ynyl)-2-pyridinecarboxaldehyde (3).

2.4.3.2 Synthesis of $[Fe_2L^{PA}{}_3][BF_4]_4$

A one-pot reaction between the propargyl alcohol aldehyde (3), 4,4'-methylenedianiline and iron(II) tetrafluoroborate hexahydrate with stoichiometry of 6:3:2 (Scheme 2.9) yielded the desired product in a very good yield of 96%.

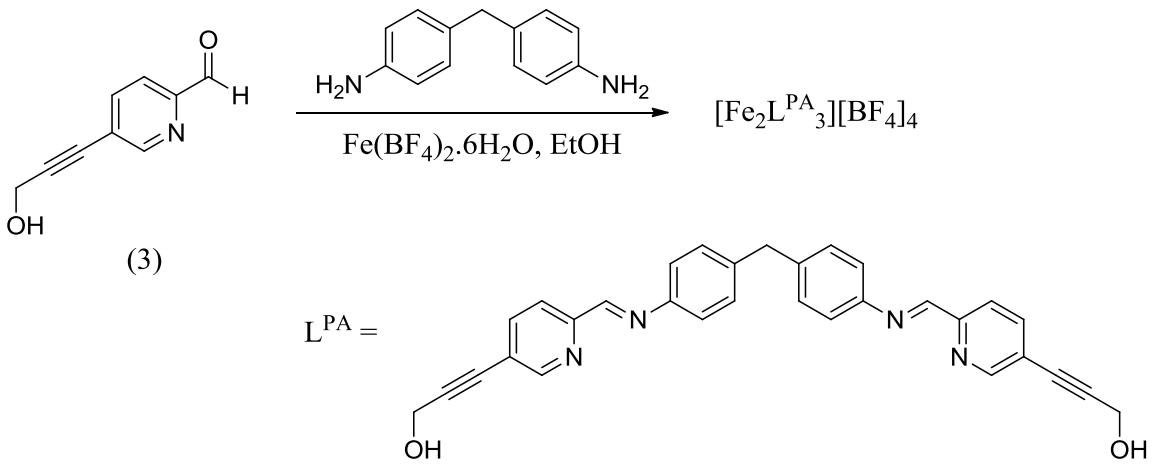

Scheme 2.9 Synthetic route for preparation of $[Fe_2L^{PA}{}_3][BF_4]_4$.

The purple solid was purified simply by washing with copious volumes of chloroform. Characterisation by ESI mass spectrometry confirmed the cylinder had been formed, with species $[Fe_2(C_{31}H_{24}N_4O_2)_3]^{4+}$, $[Fe_2(C_{31}H_{24}N_4O_2)_3]^{3+}$ and $[Fe_2(C_{31}H_{24}N_4O_2)_3]^{2+}$ being identified (see Appendix). The ^{1}H NMR spectrum (Fig. 2.10), assigned using 2D-COSY (see Appendix), contains the characteristic peaks corresponding to the imine (H_{im}), spacer (H_{sp}) and phenyl ($H_{Pha,Phb}$) protons at the expected chemical shifts and integrations. The propargyl alcohol moiety can be identified by the peak corresponding to the H_1 protons.

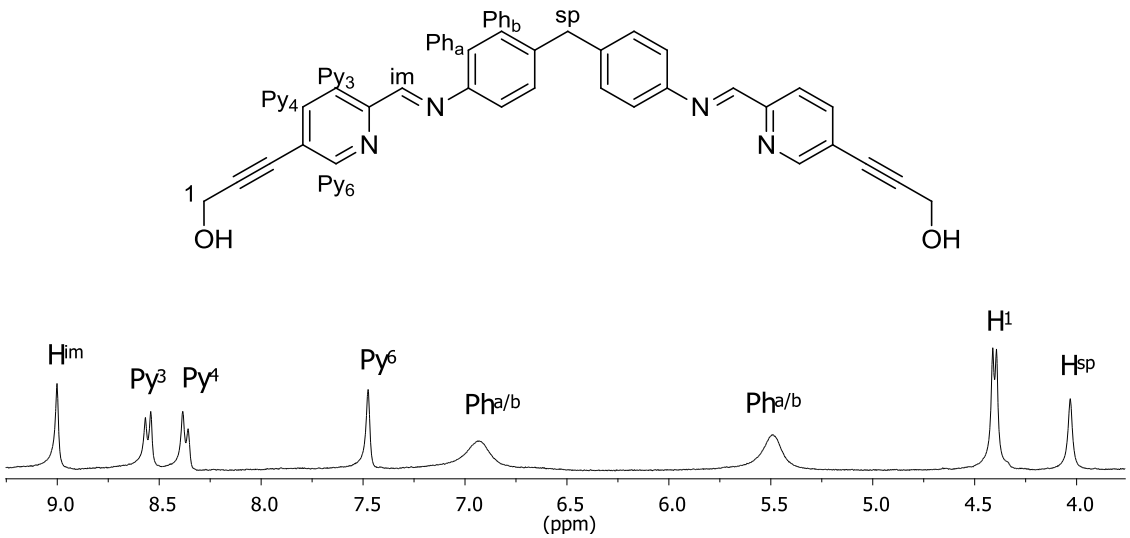

Figure 2.10 ^{1}H NMR (300 MHz, CD_3CN, 298 K) of $[Fe_2L^{PA}{}_3][BF_4]_4$.

An overall yield of 56% was obtained, with respect to the 5-bromo-2-pyridinecarboxaldehyde starting material, for the synthesis of the propargyl alcohol cylinder, $[Fe_2L^{PA}_3][BF_4]_4$.

2.4.4 Synthesis of hexyn-ol cylinder, $[Fe_2L^{Hex}_3][BF_4]_4$

2.4.4.1 Synthesis of 5-(hex-5-yn-1-ol)-2-pyridinecarboxaldehyde (4)

As 5-(hex-5-yn-1-ol)-2-pyridinecarboxaldehyde (4) is not commercially available it was synthesised by coupling 5-bromo-2-pyridinecarboxaldehyde and 5-hexyn-1-ol using a Sonogashira procedure (Scheme 2.10). In the presence of the catalysts bis(triphenylphosphine)dichloropalladium(II) and copper iodide, the reaction was stirred for seventy two hours under an inert atmosphere. The triphenylphosphine oxide impurity, introduced by the palladium catalyst, was removed by a short silica column with diethyl ether as eluent. The product could then be purified further using column chromatography on silica to remove unreacted starting materials, yielding an off-white solid in 42% yield.

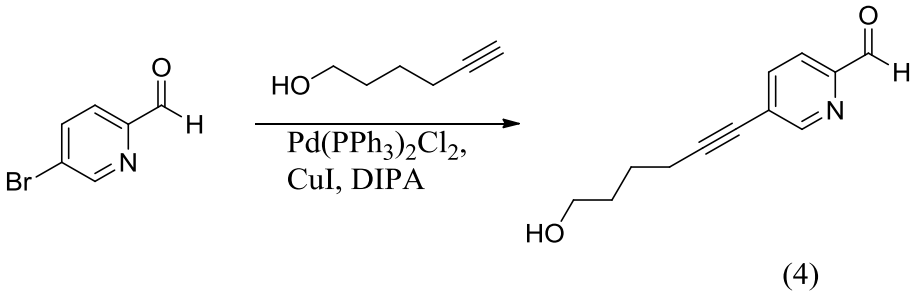

(4)

Scheme 2.10 Synthetic route for preparation of 5-(hex-5-yn-1-ol)-2-pyridinecarboxaldehyde (4).

Characterisation by high resolution EI mass spectrometry confirmed the expected product, 5-(hex-5-yn-1-ol)-2-pyridinecarboxaldehyde (4), had been formed. The ^{1}H NMR spectrum

(Fig. 2.11) shows peaks corresponding to the pyridine-carboxaldehyde and also to the hexyn-ol moiety. The H_{10} proton is found furthest downfield as it is closest to the electronegative oxygen, and one peak is observed for the H_8 and H_9 protons due to their similar chemical environments.

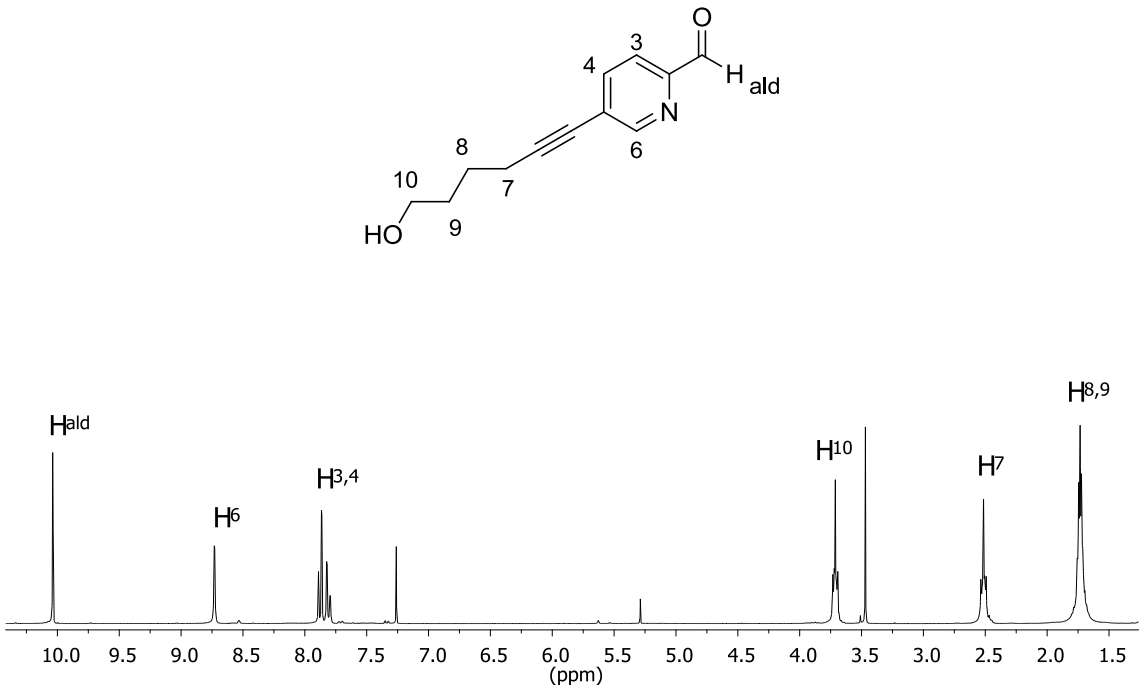

Figure 2.11 ^{1}H NMR (300 MHz, $CDCl_3$, 298 K) of 5-(hex-5-yn-1-ol)-2-pyridinecarboxaldehyde (4).

2.4.4.2 Synthesis of $[Fe_2L^{Hex}{}_3][BF_4]_4$

As with the previously synthesised alkyne cylinders, a one-pot reaction was used with the sequential and dropwise addition of six equivalents of 5-(hex-5-yn-1-ol)-2-pyridinecarboxaldehyde (4), three equivalents of 4,4'-methylenedianiline and two equivalents of iron(II) tetrafluoroborate hexahydrate in ethanol (Scheme 2.11). An immediate precipitation of a purple species was observed which is consistent with the formation of an iron(II) cylinder. The reaction mixture was stirred overnight to allow the maximum amount of starting materials to react, and then the resulting precipitate was

collected by filtration and washed with chloroform. A 58% yield was obtained for this one-pot reaction.

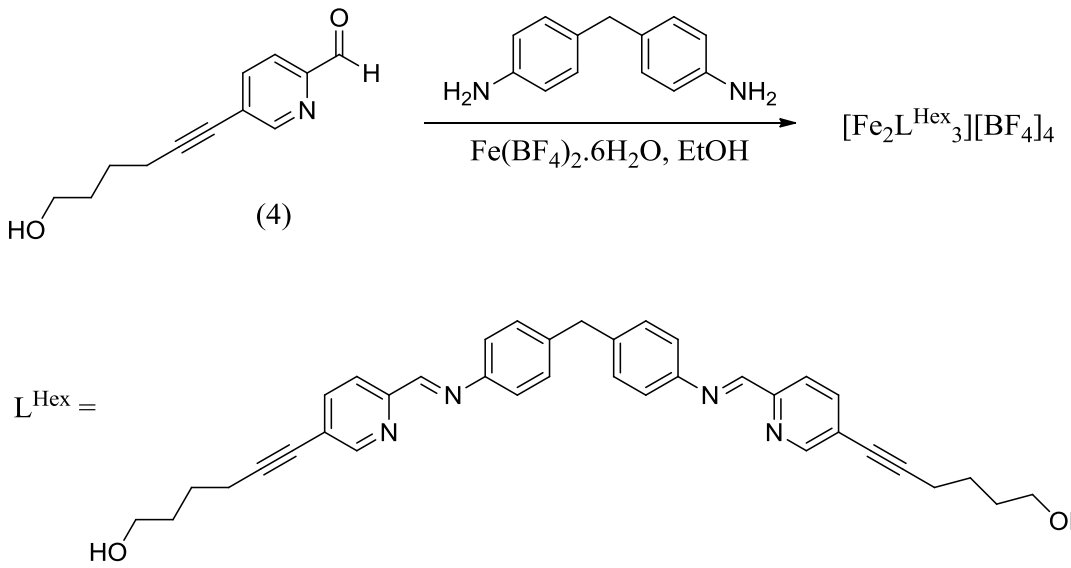

Scheme 2.11 Synthetic route for preparation of $[Fe_2L^{Hex}{}_3][BF_4]_4$.

The cylinder $[Fe_2L^{Hex}{}_3][BF_4]_4$ was characterised by ESI mass spectrometry, in which three species corresponding to the multiply charged $[Fe_2(C_{37}H_{36}N_4O_2)_3]^{4+}$, $[Fe_2(C_{37}H_{36}N_4O_2)_3]^{3+}$ and $[Fe_2(C_{37}H_{36}N_4O_2)_3]^{2+}$ were observed with the correct isotopic pattern (see Appendix). The ^1H NMR (Fig. 2.12), assigned using a 2D-COSY (see Appendix), has peaks characteristic of these types of metallo-cylinders, including those corresponding to the imine (H_{im}), spacer (H_{sp}) and phenyl ($H_{Pha,Phb}$) protons at expected chemical shifts and integrations.

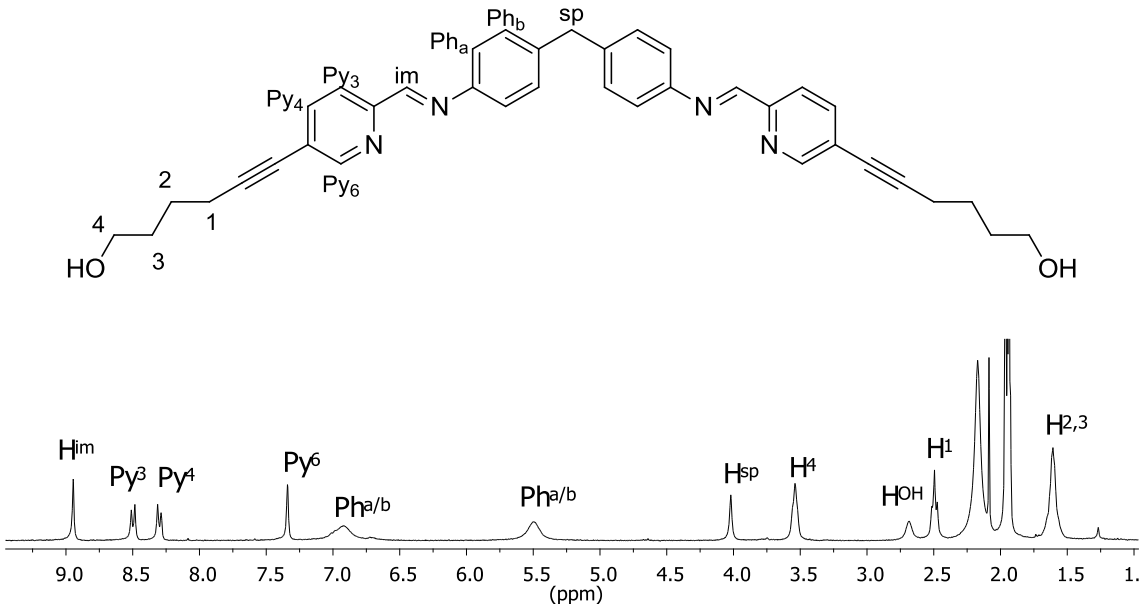

Figure 2.12 ^{1}H NMR (300 MHz, CD_3CN, 298 K) of $[Fe_2L^{Hex}{}_3][BF_4]_4$.

An overall yield of 24% was obtained, with respect to the 5-bromo-2-pyridinecarboxaldehyde starting material, for the synthesis of the hexyn-ol cylinder, $[Fe_2L^{Hex}{}_3][BF_4]_4$.

2.4.5 Synthesis of phenylacetylene cylinder, $[Fe_2L^{Phen}{}_3][BF_4]_4$

2.4.5.1 Synthesis of 5-(ethynylphenyl)-2-pyridinecarboxaldehyde (5)

As 5-(ethynylphenyl)-2-pyridinecarboxaldehyde (5) is not commercially available it was synthesised by Sonogashira coupling of 5-bromo-2-pyridinecarboxaldehyde and phenylacetylene (Scheme 2.12). The catalysts bis(triphenylphosphine)-dichloropalladium(II) and copper iodide were used, as well as basic conditions and an inert atmosphere. The reaction mixture was stirred for 72 hours at room temperature. The triphenylphosphine oxide impurity, resulting from the palladium catalyst, was removed by

a short silica column with diethyl ether as eluent. Unreacted starting materials were then removed by column chromatography on silica, to yield a pale brown solid in 72% yield.

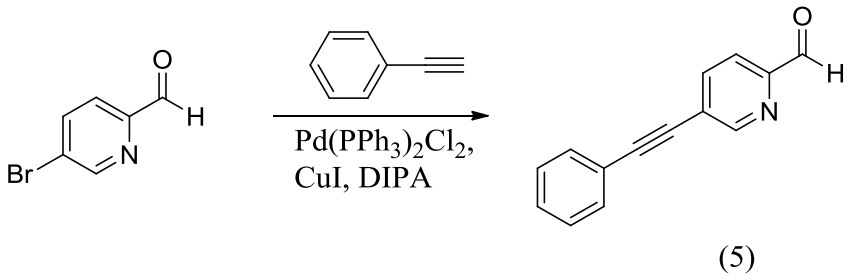

(5)

Scheme 2.12 Synthetic route for preparation of 5-(ethynylphenyl)-2-pyridinecarboxaldehyde (5).

The compound was characterised by high resolution EI mass spectrometry, which confirmed the formation of the product. The ^{1}H NMR spectrum (Fig. 2.13) also confirms the formation of the desired product, 5-(ethynylphenyl)-2-pyridinecarboxaldehyde (5). The pyridine-carboaxaldehyde peaks can be observed, as well as the peaks corresponding to the attached aromatic ring moiety at the expected chemical shifts and integration.

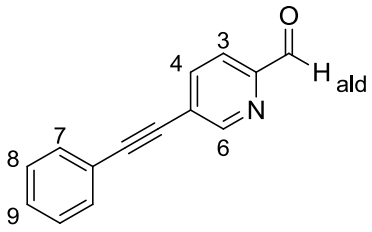

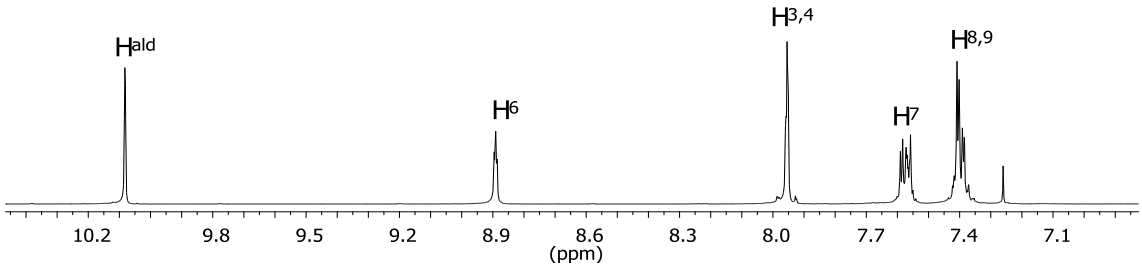

Figure 2.13 ^{1}H NMR (300 MHz, $CDCl_3$, 298 K) of 5-(ethynylphenyl)-2-pyridinecarboxaldehyde (5).

2.4.5.2 Synthesis of $[Fe_2L^{Phen}{}_3][BF_4]_4$

The synthesis of $[Fe_2L^{Phen}{}_3][BF_4]_4$ was achieved using a one-pot reaction with six equivalents of 5-(ethynylphenyl)-2-pyridinecarboxaldehyde (5), three equivalents of 4,4'-methylenedianiline and two equivalents of iron(II) tetrafluoroborate hexahydrate being mixed sequentially and dropwise in ethanol (Scheme 2.13). An immediate colour change from pale yellow to deep purple indicated the formation of an iron(II) cylinder, however the reaction mixture was stirred at room temperature overnight to ensure maximum yield of the product. The purple precipitate was collected by filtration and purified by washing with a large volume of chloroform to yield the desired product in 21% yield.

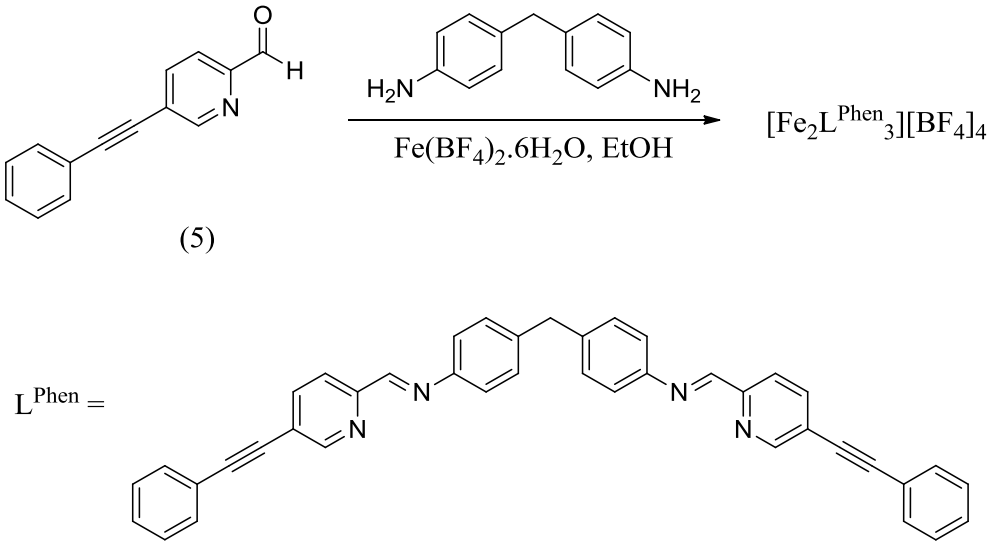

Scheme 2.13 Synthetic route for preparation of $[Fe_2L^{Phen}{}_3][BF_4]_4$.

The $[Fe_2L^{Phen}{}_3][BF_4]_4$ cylinder was characterised by ESI mass spectrometry, in which one peak corresponding to the species $[Fe_2(C_{41}H_{28}N_4)_3]^{4+}$ was observed with the correct isotopic pattern (see Appendix). Observation of the characteristic cylinder peaks, in the ^1H NMR spectrum (Fig. 2.14), corresponding to the imine (H_{im}), spacer (H_{sp}) and phenyl

($H_{Pha,Phb}$) protons is evidence of the desired product being formed. Peaks originating from the phenyl ring are also apparent, with the H_2 and H_3 protons overlapping.

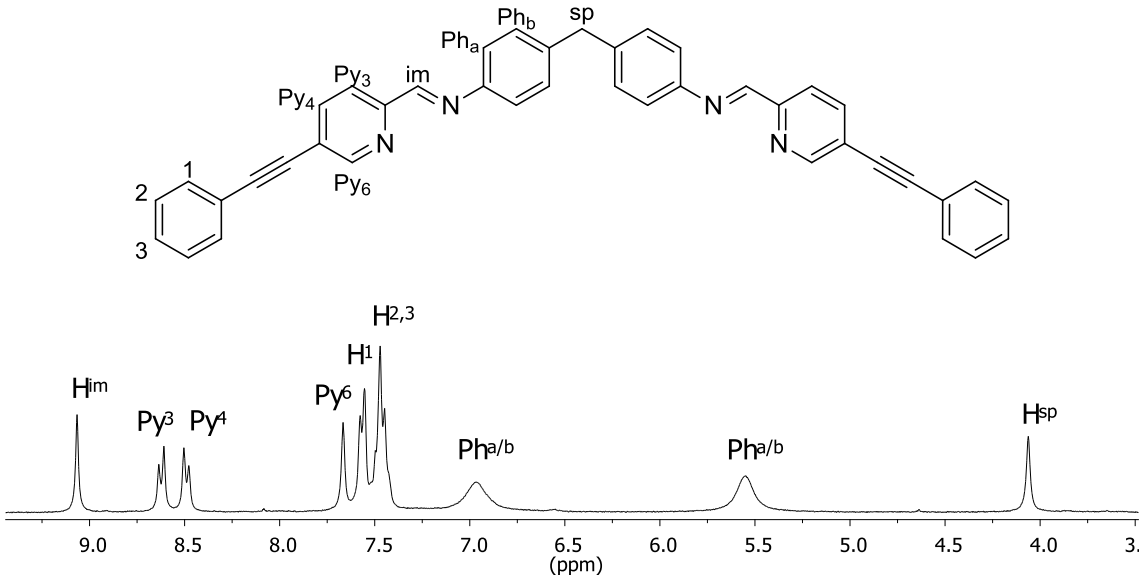

Figure 2.14 ^{1}H NMR (300 MHz, CD_3CN, 298 K) of $[Fe_2L^{Phen}{}_3][BF_4]_4$.

An overall yield of 15% was obtained, with respect to the 5-bromo-2-pyridinecarboxaldehyde starting material, for the synthesis of the phenylacetylene cylinder, $[Fe_2L^{Phen}{}_3][BF_4]_4$.

2.5 Properties of synthesised alkyne cylinders

2.5.1 Complex counterions

The novel alkyne cylinders synthesised in this chapter are all dinuclear triple stranded cylinders with tetrafluoroborate counterions. The most favoured counterion would be chloride for these complexes, as the majority of the parent and later generation iron(II) cylinders have chloride counterions,[1,7] however synthesis of these cylinders with chloride counterions was unsuccessful. One-pot syntheses with iron(II) chloride tetrahydrate, as

used in the formation of the parent cylinder,[1] gave an immediate green precipitate which could not be identified by mass spectrometry or NMR spectroscopy. This observation suggests that the triple-stranded iron(II) helicate with chloride counterions is unstable and therefore does not form. This theory was further investigated by the addition of tetrabutylammonium chloride, a compound often used in the ion exchange of the parent cylinder, to a solution of the tetrafluoroborate alkyne cylinders. The deep purple solution immediately became a pale yellow colour, indicating degradation of the iron(II) cylinder. The addition of a solution of sodium chloride to the tetrafluoroborate alkyne cylinders had the same effect. These studies indicate that the chloride counterions somehow destabilise these alkyne triple-stranded cylinders, whereas the tetrafluoroborate counterions do not.

2.5.2 Solubility of synthesised complexes

Due to the nature of the desired application of these metallo-cylinders, as anti-cancer drugs, solubility is an important factor. The therapeutic effectiveness of a drug is linked to its ability to reach its target site in the body at an appropriate dose, and this is dependent on the aqueous solubility of the drug.[13] However, there are many water-insoluble therapeutic drugs in development and therefore much research is on-going into methods of improving their bioavailability. Numerous drug carriers have been developed, such as water soluble polymers, microcapsules, liposomes and micelles, that can solubilise poorly soluble drugs.[14]

The parent cylinder with chloride counterions, $[Fe_2L^P_3][Cl]_4$, is soluble in water as is the tetrafluoroborate complex, $[Fe_2L^P_3][BF_4]_4$, (both in millimolar concentrations). This

aqueous solubility is very advantageous as DNA binding studies are carried out in aqueous solutions. Unfortunately none of the alkyne cylinders synthesised in this chapter are water soluble. The triple bond, propargyl alcohol and hexyn-ol cylinders, $[Fe_2L^{TB}{}_3][BF_4]_4$, $[Fe_2L^{PA}{}_3][BF_4]_4$ and $[Fe_2L^{Hex}{}_3][BF_4]_4$ respectively, are very soluble in methanol and acetonitrile. The phenylacetylene cylinder, $[Fe_2L^{Phen}{}_3][BF_4]_4$, is only soluble in acetonitrile. This solubility in water-miscible solvents allows these complexes to be dissolved in water, with the assistance of a small percentage of methanol or acetonitrile, and so DNA binding studies can be carried out.

2.5.3 UV-Vis stability studies

When designing a metallo-drug, one pharmacokinetic consideration must be its stability when administered into the body. After entering the bloodstream, metallo-drugs will undergo some hydrolysis leading to unwanted metabolites that could cause side effects.[15] The stability of the synthesised cylinders is also important when investigating their DNA binding activity, as any degradation of the complex will affect the results of the DNA binding studies. The stability of the cylinders synthesised in this chapter were assessed using UV-Vis spectroscopy.

The UV-Vis absorption of solutions of these cylinders in water (and sometimes a small percentage of methanol due to solubility issues) was measured every hour for twelve hours at room temperature. As the stability of metallo-cylinders has been known to improve in the presence of DNA,[16] this was also measured, using a ct-DNA:complex ratio of 6:1, over

a twelve hour period at room temperature. Any loss of absorbance over time indicates degradation of the complex.

Firstly, the stability of the parent cylinder in water was investigated. As the cylinders synthesised in this work have tetrafluoroborate counterions, the stabilities of the parent complex with both chloride and tetrafluoroborate counterions was investigated to see if the counterion has any effect. It was found that the complexes $[Fe_2L^P_3][Cl]_4$ and $[Fe_2L^P_3][BF_4]_4$ have remarkably different stabilities at room temperature (Fig. 2.15). Over a 12 hour period the tetrafluoroborate complex loses 10% of its original absorbance, compared to only 2% for the chloride complex. However, in the presence of ct-DNA (calf thymus DNA) the complexes have a much greater and more comparable stability, with hardly any degradation for either compound. This is evidence that although the counterion has an effect on the complex stability at room temperature, in the presence of DNA the tetrafluoroborate counterion has no significant disadvantages.

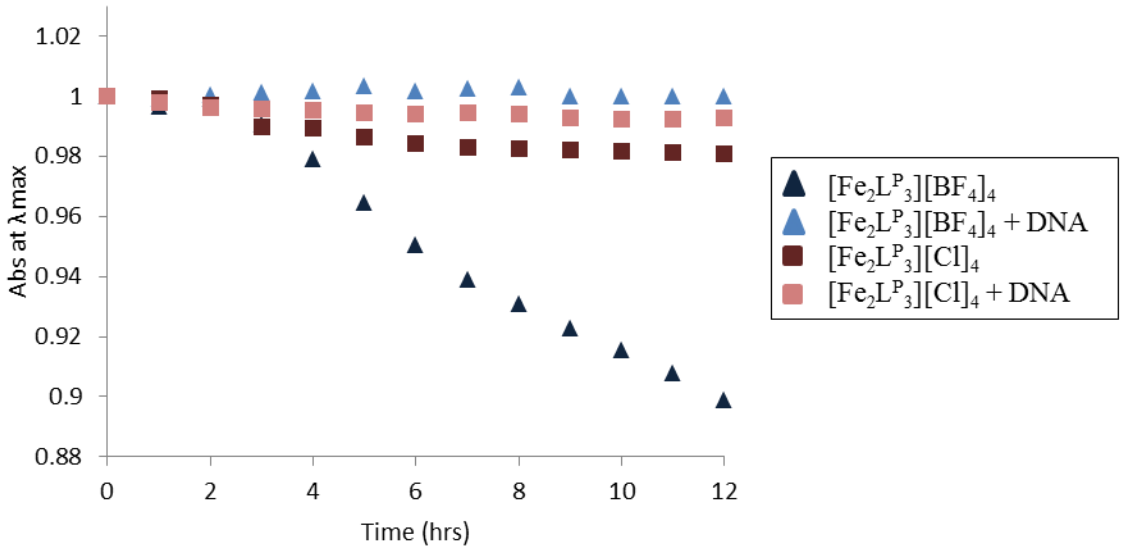

Figure 2.15 Normalised UV-Vis stability studies of complexes $[Fe_2L^P_3][Cl]_4$ and $[Fe_2L^P_3][BF_4]_4$ at room temperature (10 μM, water) and in presence of ct-DNA in 6.7 mM NaCl and 0.33 mM $Na(CH_2)_2AsO_2.3H_2O$ (pH 6.8) (ratio 6:1 ct-DNA:complex). λ_{max} = 573 nm.

The stability of the alkyne cylinders synthesised in this chapter was also explored. Due to these complexes not being completely water soluble, a small percentage of methanol or acetonitrile was needed to solubilise them. All four complexes showed degradation at room temperature, with $[Fe_2L^{PA}{}_3][BF_4]_4$ being the most stable with a loss of 8% of absorbance over 12 hours. The $[Fe_2L^{Phen}{}_3][BF_4]_4$ cylinder was the least stable, with a loss of 54% of its original absorbance and a half-life of 11 hours (Fig. 2.16). The stability of all of the complexes, apart from $[Fe_2L^{Phen}{}_3][BF_4]_4$, was greatly improved in the presence of ct-DNA. The complex with the greatest stability improvement was $[Fe_2L^{TB}{}_3][BF_4]_4$, with a loss of only 2% of its original absorbance in the presence of DNA over 12 hours, compared to a loss of 49% without DNA.

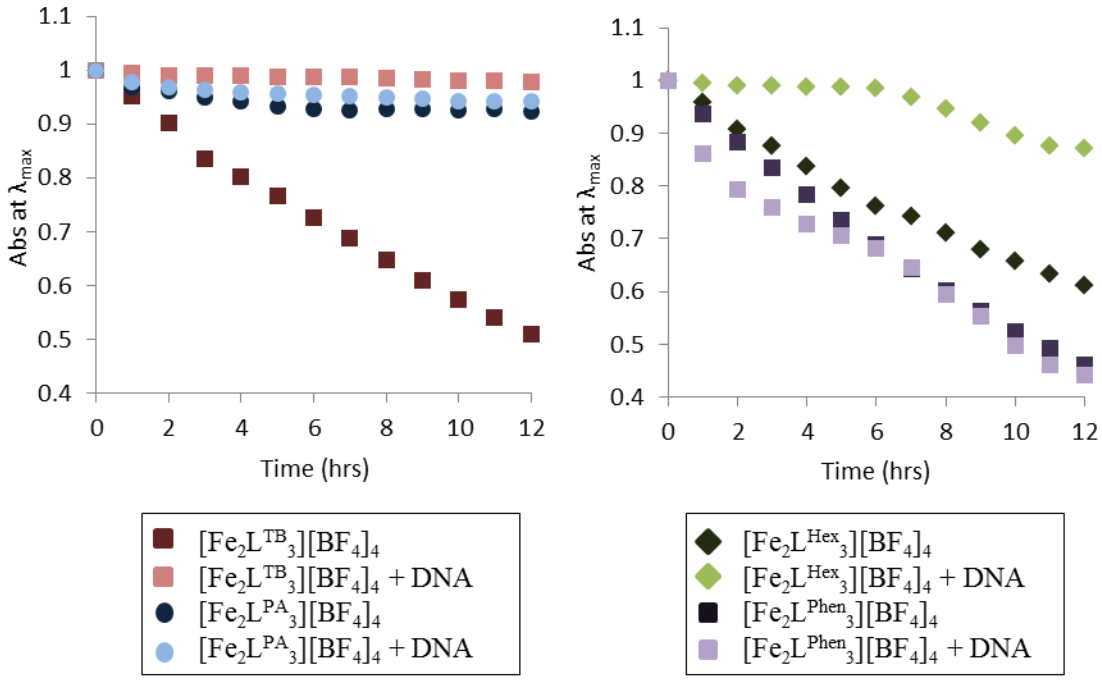

Figure 2.16 Normalised UV-Vis stability studies of (left) complexes $[Fe_2L^{TB}{}_3][BF_4]_4$ and $[Fe_2L^{PA}{}_3][BF_4]_4$ at room temperature (10 µM, 3% MeOH:water) and in presence of ct-DNA in 6.7 mM NaCl and 0.33 mM $Na(CH_2)_2AsO_2.3H_2O$ (pH 6.8) (ratio 6:1 ct-DNA:complex, 1.9% MeOH:water). λ_{max} = 591 nm.
And (right) complexes $[Fe_2L^{Hex}{}_3][BF_4]_4$ and $[Fe_2L^{Phen}{}_3][BF_4]_4$ at room temperature (8 µM, 2.4% MeOH:water, 2.4% MeCN:water respectively) and in presence of ct-DNA in 6.7 mM NaCl and 0.33 mM $Na(CH_2)_2AsO_2.3H_2O$ (pH 6.8) (ratio 6:1 ct-DNA:complex, 1.9% MeOH:water and 1.9% MeCN:water respectively). λ_{max} 589 nm and 605 nm respectively.

This apparent stabilising effect of DNA to these complexes has previously been observed with other iron(II) supramolecular cylinders.[16] As these types of cylinders are known to bind in the major groove of DNA,[5,16] it is possible that the DNA groove shields or protects the cylinders from attack by solvent molecules, slowing down their degradation. This may explain why the stability of $[Fe_2L^{Phen}{}_3][BF_4]_4$ with and without ct-DNA is very similar. As this cylinder is more bulky in shape than the other alkyne cylinders described, it may not fit into the major groove of the DNA as well and therefore will not be as shielded to solvent attack.

Taking into account that the DNA binding studies detailed herein involve maximum experimental times of 5 hours, it can be concluded that the stabilities of these alkyne cylinders should not significantly affect any conclusions that may be drawn from them, except perhaps for $[Fe_2L^{Phen}{}_3][BF_4]_4$.

2.6 DNA binding studies

Four novel iron(II) supramolecular cylinders functionalised with small chemical groups have been synthesised and characterised. The DNA binding properties of these novel cylinders were investigated by several techniques. DNA binding studies of the parent cylinder with tetrafluoroborate counterions, $[Fe_2L^{P}{}_3][BF_4]_4$, were also carried out for comparison as this complex had not been investigated previously.

2.6.1 Circular dichroism

Circular dichroism (CD) is a highly sensitive spectroscopic technique used to investigate DNA conformation in solution and drug-DNA interactions.[17] CD measures the difference in absorption of left (A_l) and right (A_r) circularly polarised light:

$$CD = A_l - A_r$$

Circularly polarised light consists of two linearly polarised light beams oscillating perpendicularly to each other.[18] The rotating electric field vector maintains a constant magnitude but rotates about the propagation direction in the form of a helix (Fig. 2.17).[18] If the vector forms a right-handed helix the light is right-circularly polarised, whereas a left-handed helix is left-circularly polarised. At each point in space and time the magnetic field vector is perpendicular to the electric field.[19]

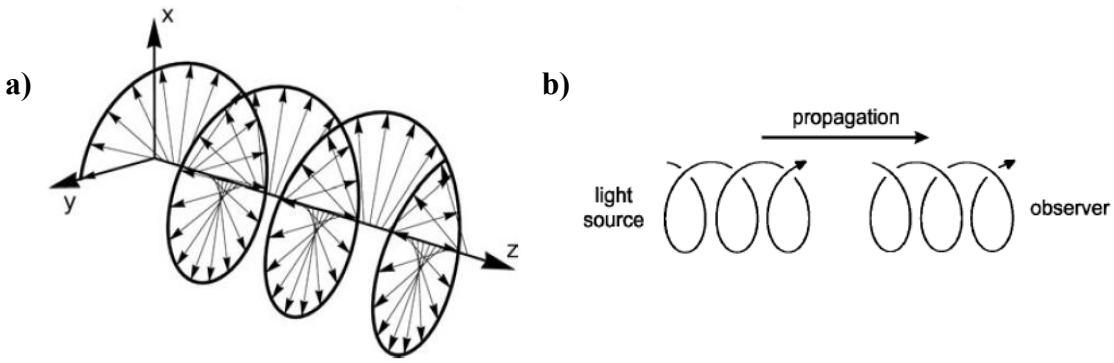

Figure 2.17 a) Left-circularly polarised light, propagating in z direction. Arrows show rotating electric field vector, the magnetic field vector is perpendicular to the electric field vector. [Reproduced from Ref [20]]
b) Left- and right-circularly polarised light. [Reproduced from Ref [18]]

Circular dichroism is used to study chiral molecules. Chiral molecules, defined as being non-superimposable on their mirror image, do not have a plane of reflection therefore any rearrangement of electrons occurs in a helical nature.[19] As CD uses circularly polarised light, with electric field vectors propagating in a helical manner, the molecule will interact

differently with left and right handed circularly polarised light.[19] This difference in absorption of left and right circularly polarised light is plotted against wavelength, resulting in a CD spectrum.[18]

DNA is a chiral molecule, due to the chiral sugar units that make up the sugar-phosphate backbone, and therefore has its own CD spectrum (Fig. 2.18). The CD spectrum of the B-form of ct-DNA exhibits positive and negative bands of nearly equal magnitudes between 200-300 nm. The CD signals in the UV region do not result from the chiral sugar-phosphate backbone, as it has no important transitions in this region, but from transitions of the purine and pyrimidine bases that are in a chiral environment created by the sugar-phosphate backbone.[19]

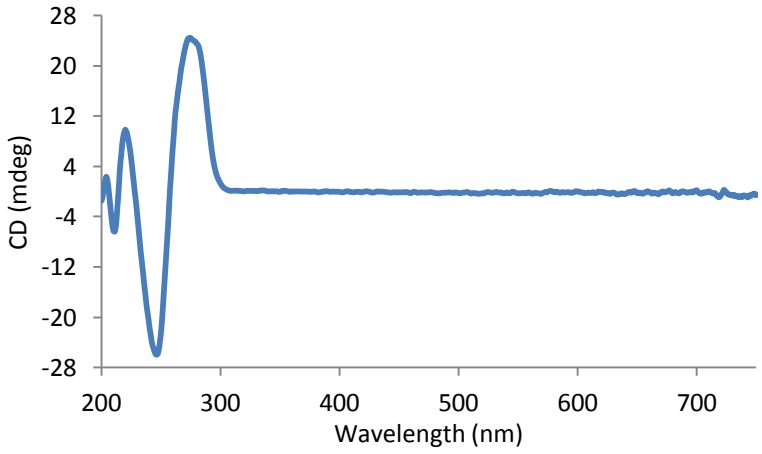

Figure 2.18 CD spectrum of ct-DNA (B-conformation).

As mentioned previously, circular dichroism is a valuable technique in probing drug-DNA interactions. Many DNA-binding molecules are achiral and so do not have a CD spectrum of their own. However by binding to DNA, the drug acquires an induced chirality from its environment, giving rise to an induced CD (ICD) signal.[19] The resulting CD spectrum

gives information about the conformation of DNA, if it is retained or altered due to the drug binding, and gives an insight into the binding mode of the drug, indicated by characteristic ICD signals.[19]

In the work detailed in this thesis, CD titrations with calf thymus DNA are carried out in an aqueous buffered solution, keeping a constant DNA concentration and decreasing the ratio of ct-DNA:complex by adding aliquots of a stock solution of complex. CD spectra are measured after each addition of complex and overlaid to give a CD titration spectrum as shown in figure 2.19.

2.6.1.1 Circular dichroism studies of the parent cylinder, $[Fe_2L^P_3]^{4+}$, with different counterions

In recent work, the DNA binding activity of the parent iron(II) metallo-cylinder, $[Fe_2L^P_3][Cl]_4$, as studied by circular dichroism was reported.[5,21] The CD spectrum of the titration of $[Fe_2L^P_3][Cl]_4$ with ct-DNA (Fig. 2.19) has several features which show that the cylinder is binding to DNA without perturbing its B-conformation. There are several induced CD (ICD) signals in the MLCT region of the metal complex, at 315 nm, 375 nm, 541 nm and 610 nm, which show that the cylinder is binding to the DNA. As the concentration of complex in solution increases, so too does the ICD signal suggesting an additive effect.[5,21] In the DNA region of the spectrum (200-300 nm) there is no significant change to the CD signal showing that the binding of $[Fe_2L^P_3][Cl]_4$ does not alter the DNA geometry.[5,21]

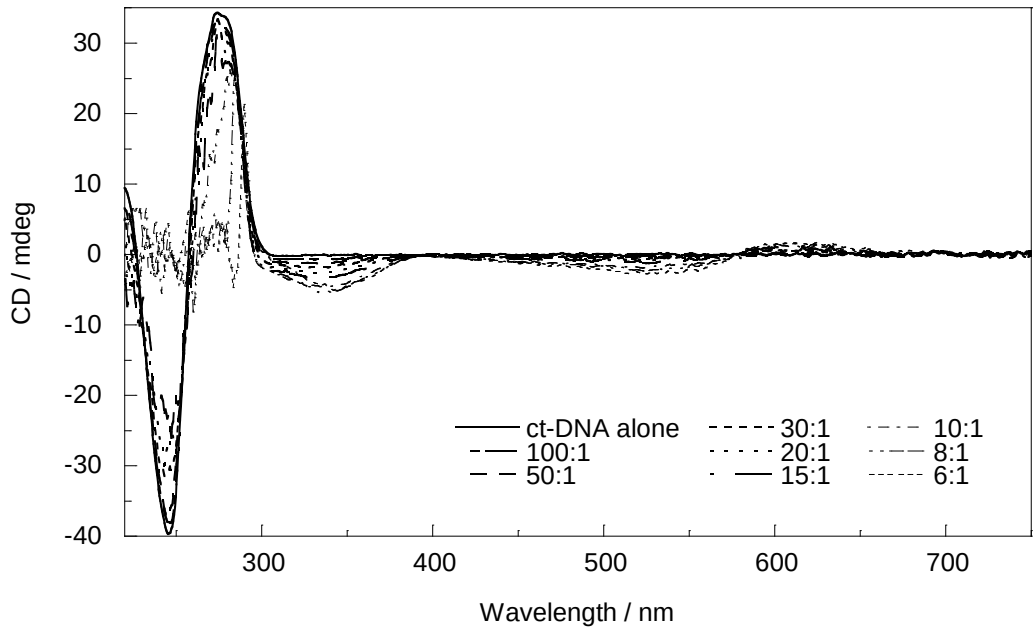

Figure 2.19 CD spectrum of 500 μM ct-DNA in 20 mM NaCl and 1 mM $Na(CH_2)_2AsO_2.3H_2O$ (pH 6.8) with increasing concentrations of $[Fe_2L^P_3][Cl]_4$. Legend shows ct-DNA:complex ratios. [Reproduced from Ref [21]]

The parent cylinder with tetrafluoroborate counterions, $[Fe_2L^P_3][BF_4]_4$ has previously been synthesised,[11] however its DNA binding activity had not been investigated. As the functionalised cylinders presented in this thesis have tetrafluoroborate counterions the DNA binding activity of the parent cylinder with tetrafluoroborate counterions, and its comparison with the parent cylinder with chloride counterions, is of great interest.

As already discussed (Section 2.5.3) the stability of $[Fe_2L^P_3][Cl]_4$ is significantly greater than that of $[Fe_2L^P_3][BF_4]_4$, however in the presence of ct-DNA the stabilities of these complexes are very similar. This allows comparison of the results of DNA binding studies carried out for both cylinders, as their degradation is very similar in an environment where DNA is present.

CD titrations with ct-DNA were carried out for the complexes $[Fe_2L^P_3][Cl]_4$ and $[Fe_2L^P_3][BF_4]_4$ and the resulting CD titration spectra were found to be almost identical as expected. The spectrum for $[Fe_2L^P_3][BF_4]_4$ is shown below (Fig. 2.20). As previously discussed, characteristic ICD signals in the MLCT region of the complexes are observed which indicate binding to ct-DNA, with no change to the DNA B-conformation.

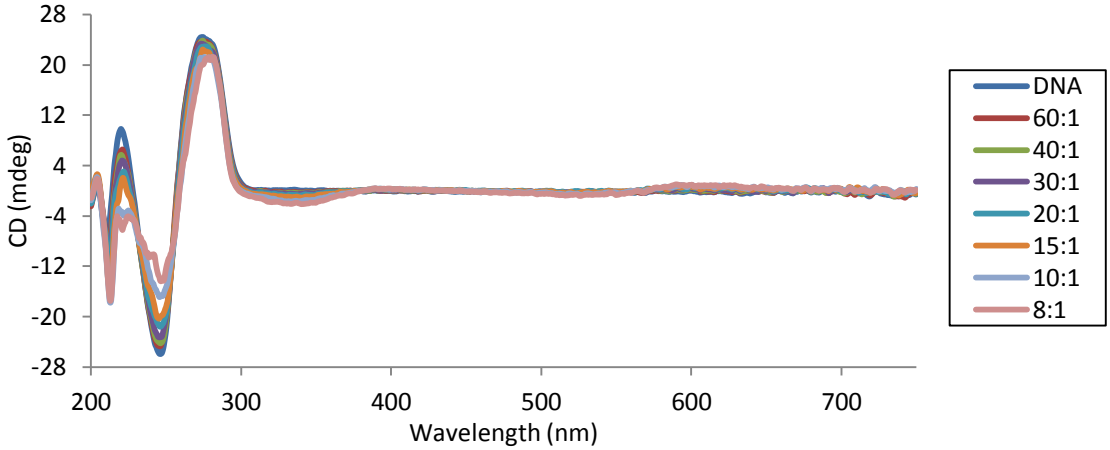

Figure 2.20 CD of 295 μM ct-DNA in 20 mM NaCl and 1 mM $Na(CH_2)_2AsO_2.3H_2O$ (pH 6.8) with increasing concentrations of complex $[Fe_2L^P_3][BF_4]_4$. Legend shows ct-DNA:complex ratios. Analysed in a 1cm pathlength cuvette.

When the ICD signals at 338 nm and 622 nm are plotted against complex concentration (Fig. 2.21), it is apparent that both complexes have a very similar behaviour towards DNA.

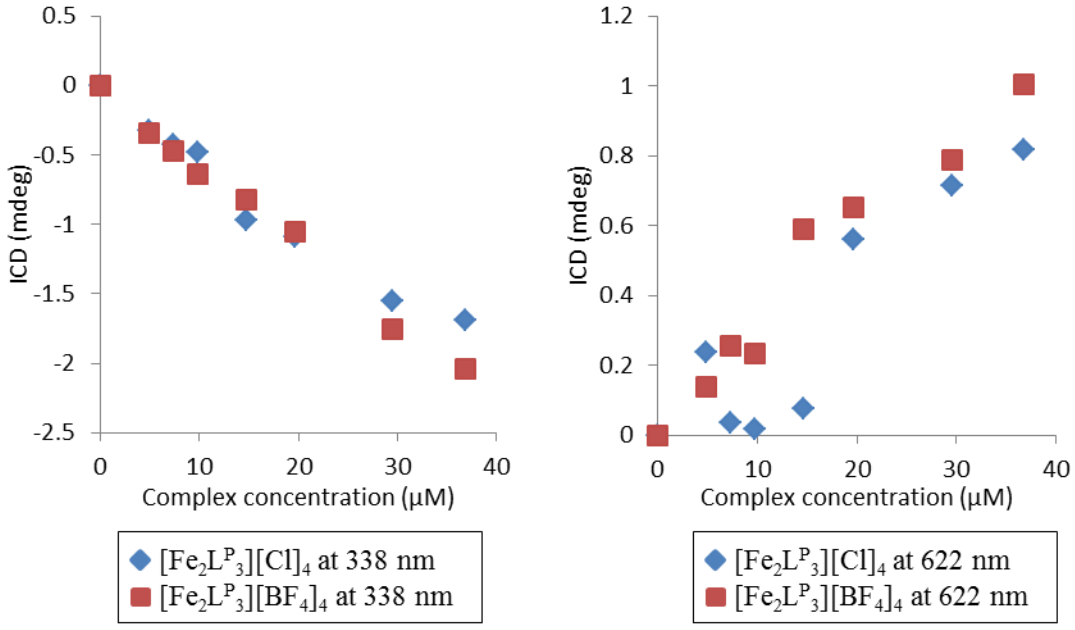

Figure 2.21 Normalised ICD signal vs complex concentration for complexes $[Fe_2L^P{}_3][Cl]_4$ and $[Fe_2L^P{}_3][BF_4]_4$ at 338 nm and 622 nm.

These CD studies provide evidence that the counterion of these iron(II) helicates does not significantly alter their DNA binding activity.

2.6.1.2 Circular dichroism studies of synthesised alkyne cylinders

CD titrations analogous to those performed with the parent cylinder were carried out for the synthesised alkyne cylinders in order to assess their DNA binding activity. Due to their poor solubility in water, concentrated stock solutions of the alkyne cylinders in methanol, or acetonitrile for $[Fe_2L^{Phen}{}_3][BF_4]_4$, were made. These were then diluted with water to achieve the final complex solutions used in the CD titration experiments. The percentage of methanol, or acetonitrile, at the end of each titration was calculated to be 6% at most. Control experiments were carried out to assess whether the solvent had any effect on the CD spectroscopy of ct-DNA. The titration was performed as usual, but instead of titrating

in a stock solution of complex, a solution of water with the corresponding percentage of methanol or acetonitrile was added. The resulting CD spectra showed that the small percentage of solvent had no effect on the ct-DNA.

For each complex, two equal titrations were carried out using the same stock solutions of DNA and complex. One titration was performed in a 1cm pathlength cuvette, so as to analyse the less intense MLCT region. However as more complex is titrated into the DNA-complex solution, the concentration increases, and so the CD signal in the UV region becomes saturated. This is usually observed when a DNA:complex ratio of 10:1 is reached. To study the UV region at higher complex concentrations, the titration is also carried out in a 0.1 cm pathlength cuvette. This can be explained using the Beer Lambert law:

$$A = \varepsilon c l$$

Where A = absorbance, ε = molar absorption coefficient ($mol^{-1}dm^3cm^{-1}$), c = concentration ($moldm^3$) and l = pathlength (cm).

If the pathlength, l, is shortened the absorbance, and consequently the saturation, of the sample will be lower.

None of the alkyne cylinders has an intrinsic CD signal as they exist as a racemic mixture of M and P enantiomers. As a result, the CD signals that are observed in the spectroscopic regions of the complex are due to interaction with DNA.

The CD titration spectra of the triple bond cylinder, $[Fe_2L^{TB}_3][BF_4]_4$, (Fig. 2.22) reveal an ICD signal at 312 nm. This indicates that the cylinder is binding to ct-DNA. The B-

conformation of DNA is retained upon cylinder binding. However at higher complex loading, with a ratio of DNA:complex of 6:1 (0.1 cm pathlength spectrum), a new peak arises at approximately 241 nm, overlapping the DNA signature. This is most likely due to the complex in-ligand spectroscopy.

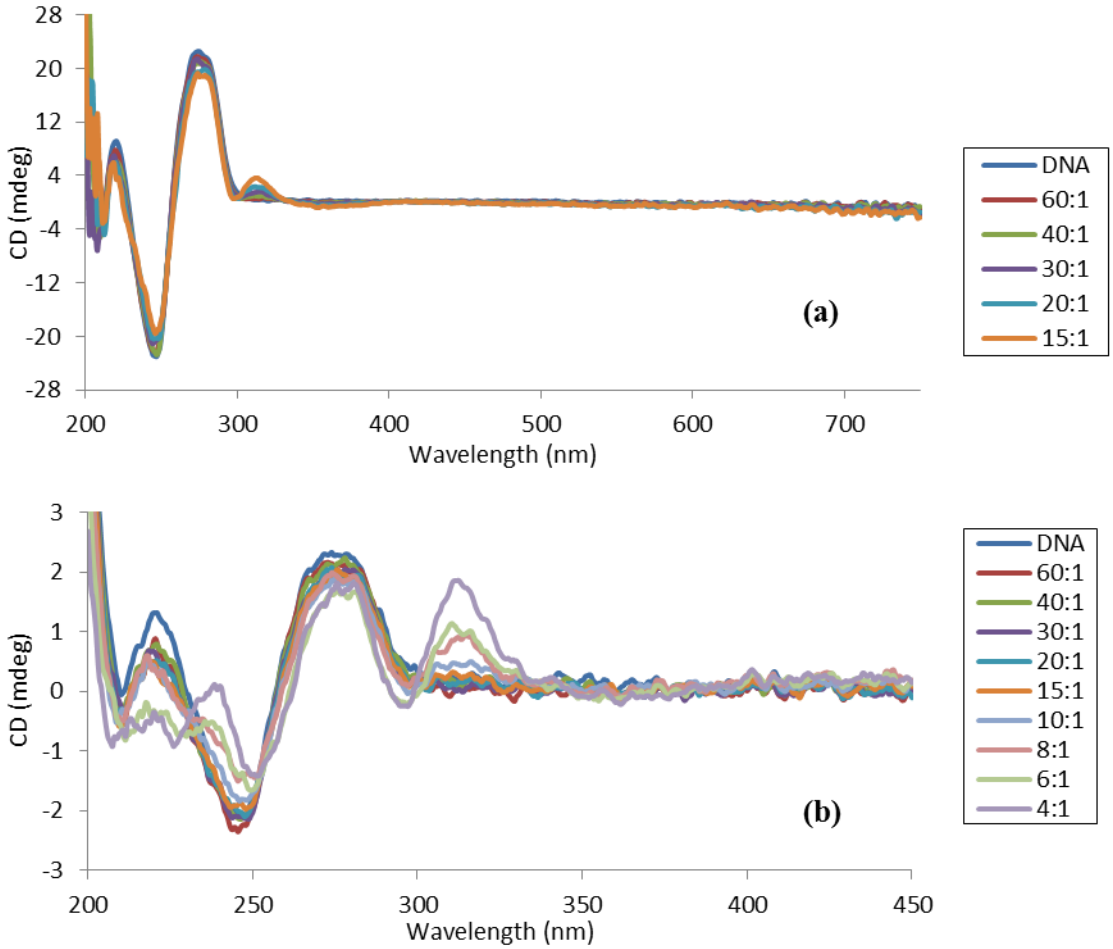

Figure 2.22 CD of 266 μM ct-DNA in 20 mM NaCl and 1 mM $Na(CH_2)_2AsO_2.3H_2O$ (pH 6.8) with increasing concentrations of complex $[Fe_2L^{TB}{}_3][BF_4]_4$. Legend shows ct-DNA:complex ratios. 5.3% max. MeOH. Analysed in 1cm (a) and 0.1cm (b) pathlength cuvettes.

An induced CD signal at 326 nm can be observed in the CD titration spectra of the propargyl alcohol cylinder, $[Fe_2L^{PA}{}_3][BF_4]_4$, (Fig. 2.23). This ICD signal arises from the interaction between the cylinder and DNA, and indicates a binding event. The characteristic B-DNA signal between 200-300 nm is unaffected by this binding, apart from

small decreases in its intensity. At the lowest DNA:complex ratio of 4:1, an extra band arises at 241 nm due to in-ligand complex spectroscopy, which overlaps the DNA spectroscopy.

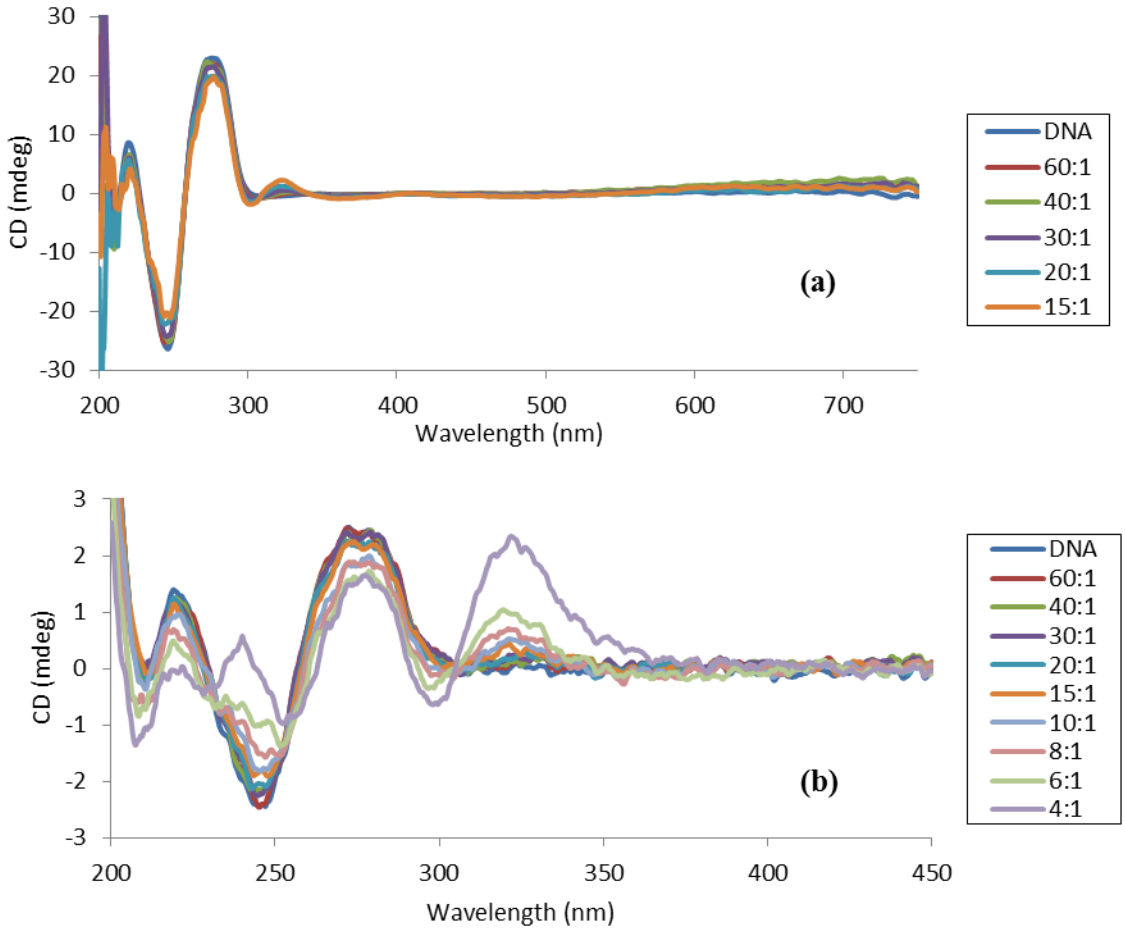

Figure 2.23 CD of 295 μM ct-DNA in 20 mM NaCl and 1 mM $Na(CH_2)_2AsO_2.3H_2O$ (pH 6.8) with increasing concentrations of complex $[Fe_2L^{PA}{}_3][BF_4]_4$. Legend shows ct-DNA:complex ratios. 5.9% max. MeOH. Analysed in 1cm (a) and 0.1cm (b) pathlength cuvettes.

The CD titration spectra for the hexyn-ol cylinder, $[Fe_2L^{Hex}{}_3][BF_4]_4$, (Fig. 2.24) indicate that the complex binds to ct-DNA as an ICD signal at 330 nm can be observed. The B-conformation of ct-DNA is retained throughout the titration and is not affected by the cylinder binding. From a ratio of DNA:complex of 10:1 a band corresponding to the in-ligand spectroscopy appears at approximately 246 nm, overlapping the DNA transitions.

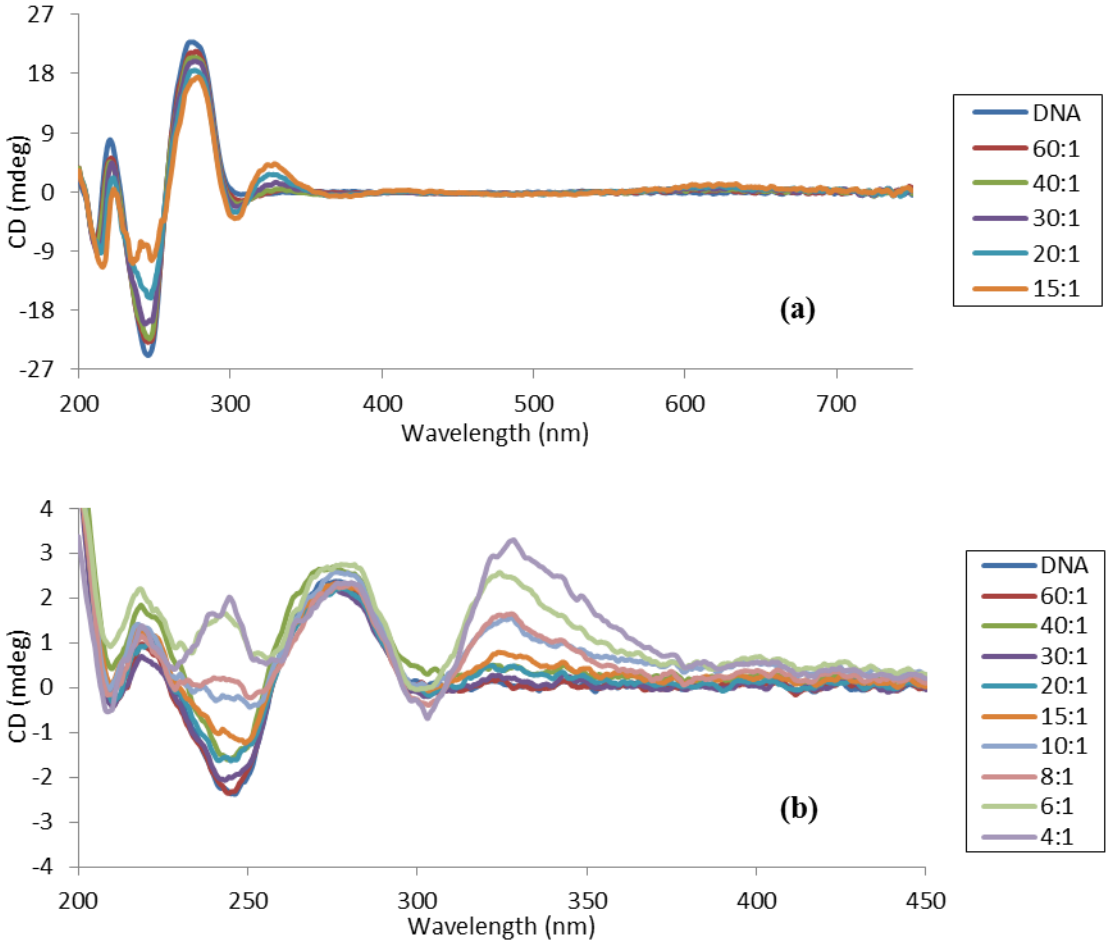

Figure 2.24 CD of 285 μM ct-DNA in 20 mM NaCl and 1 mM $Na(CH_2)_2AsO_2.3H_2O$ (pH 6.8) with increasing concentrations of complex $[Fe_2L^{Hex}{}_3][BF_4]_4$. Legend shows ct-DNA:complex ratios. 5.7% max. MeOH. Analysed in 1cm (a) and 0.1cm (b) pathlength cuvettes.

Induced CD signal at 348 nm is apparent in the CD titration spectra of the phenylacetylene cylinder, $[Fe_2L^{Phen}{}_3][BF_4]_4$, (Fig. 2.25) giving evidence that the complex binds to ct-DNA. As more and more complex binds to the ct-DNA, the shape of the DNA signal remains unchanged therefore the B-conformation of DNA is retained upon cylinder binding. As the ICD signal for this complex is less intense than for the other cylinders, it cannot be observed in the 0.1 cm pathlength cuvette.

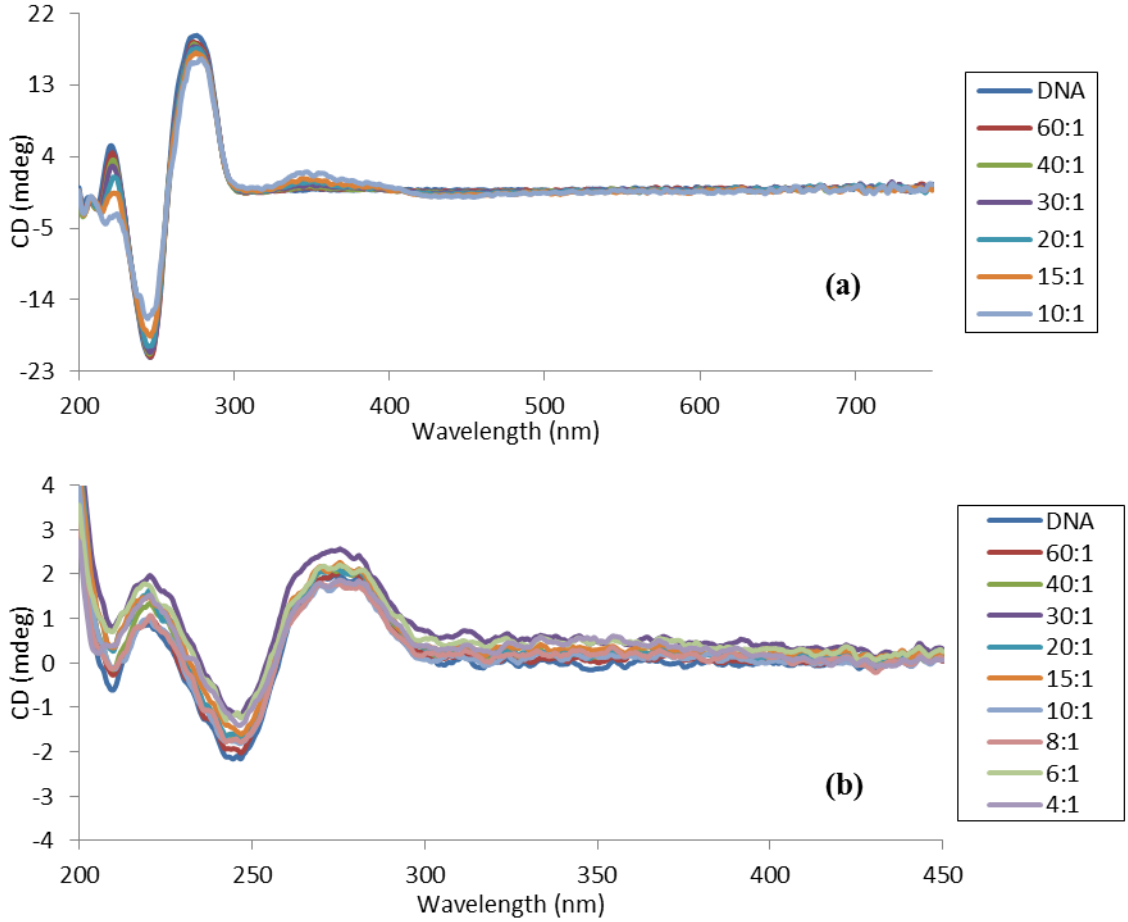

Figure 2.25 CD of 241 μM ct-DNA in 20 mM NaCl and 1 mM $Na(CH_2)_2AsO_2.3H_2O$ (pH 6.8) with increasing concentrations of complex $[Fe_2L^{Phen}{}_3][BF_4]_4$. Legend shows ct-DNA:complex ratios. 6% max. MeCN. Analysed in 1cm (a) and 0.1cm (b) pathlength cuvettes.

2.6.2 Linear Dichroism

Linear dichroism (LD) is another technique used to study DNA conformation and drug-DNA interactions. LD measures the difference in absorption of light linearly polarised parallel and perpendicular to an orientation axis:

$$LD = A_{parallel} - A_{perpendicular}$$

In linearly polarised light the electric field vector oscillates in the same plane (Fig. 2.26).[19]

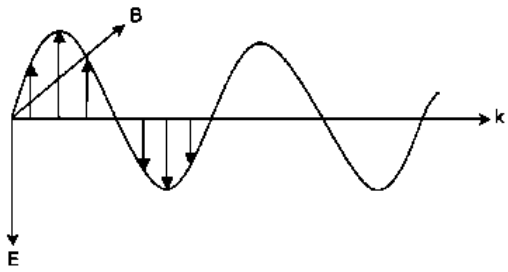

Figure 2.26 Linearly polarised light. [Reproduced from Ref [19]]

LD is used to probe molecules that are long enough to be oriented, such as DNA. A couette cell can be used to orient a sample by viscous drag.[22] Linearly polarised light can interact with the oriented DNA molecules producing an LD spectrum (Fig. 2.27). The DNA bases are situated perpendicular to the helix axis and therefore the transitions of the bases are also perpendicular to the helix axis, giving rise to a negative signal in the DNA absorbance region, between 200-300 nm.[22]

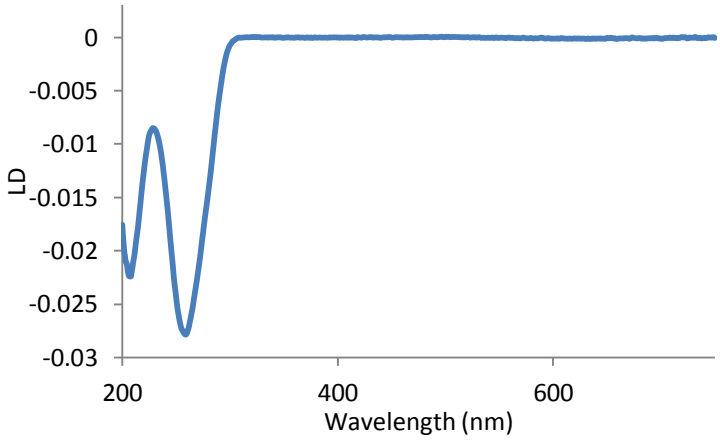

Figure 2.27 LD spectrum of ct-DNA (B-conformation).

As most DNA-binding molecules are too small to be oriented themselves they do not have their own LD spectrum. However when these molecules bind to DNA they become oriented and an induced LD signal (ILD) results from the interaction.[22] The LD spectrum

gives information about the conformation of DNA and how it is affected by the binding of a drug molecule, and characteristic ILD signals can provide evidence of a specific binding mode.

In the work detailed in this thesis, LD titrations with ct-DNA were carried out in aqueous buffered solution, keeping a constant DNA concentration and decreasing the ratio of ct-DNA:complex by adding aliquots of a stock solution of complex. LD spectra are measured after each addition of complex and overlaid to give an LD titration spectrum as shown in figure 2.28.

2.6.2.1 Linear dichroism studies of the parent cylinder, $[Fe_2L^P_3]^{4+}$, with different counterions

The DNA binding activity of the parent cylinder, $[Fe_2L^P_3][Cl]_4$, as investigated by linear dichroism was recently reported.[5,21] The LD spectrum for the titration between ct-DNA and $[Fe_2L^P_3][Cl]_4$ (Fig. 2.28) shows an induced LD (ILD) signal at 569 nm in the MLCT region of the complex. As the concentration of complex increases, the ILD signal also increases confirming that the cylinder is binding to the DNA, not at random sites but in a specific orientation.[5,21] The DNA LD signal at 260 nm, arising from the DNA bases, decreases in magnitude as cylinder concentration increases, showing that the cylinder is binding to the DNA and kinking or coiling it.[5,21]

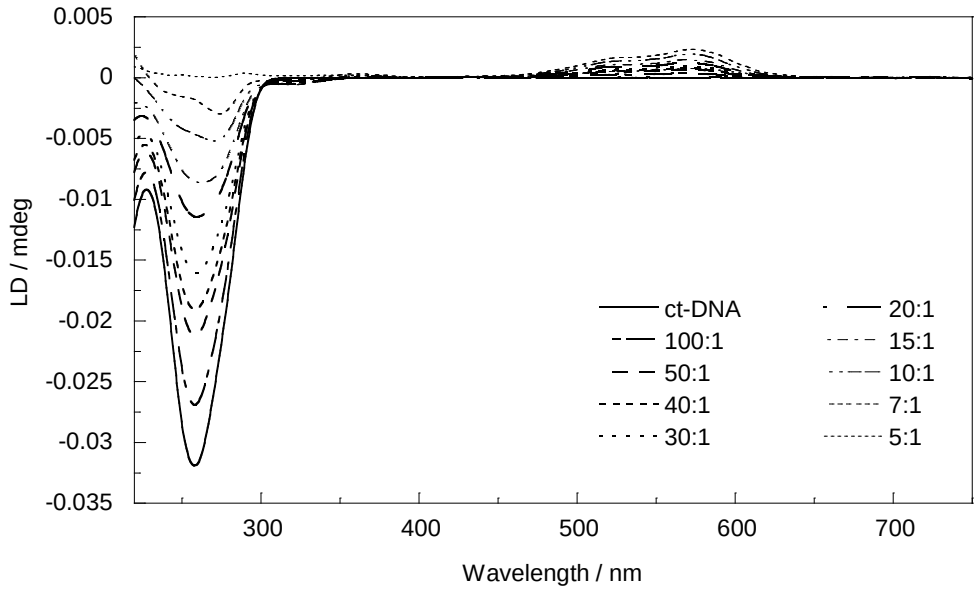

Figure 2.28 LD spectrum of 500 μM ct-DNA in 20 mM NaCl and 1 mM $Na(CH_2)_2AsO_2.3H_2O$ (pH 6.8) with increasing concentrations of $[Fe_2L^P_3][Cl]_4$. Legend shows ct-DNA:complex ratios. [Reproduced from Ref [21]]

Although previously synthesised,[11] the DNA binding of the parent cylinder with tetrafluoroborate counterions, $[Fe_2L^P_3][BF_4]_4$, had not been studied by LD. Due to the synthesised complexes in this work having tetrafluoroborate counterions, it was deemed very important to compare the DNA binding of $[Fe_2L^P_3][Cl]_4$ and $[Fe_2L^P_3][BF_4]_4$ by linear dichroism, to see if altering the counterion can affect the DNA binding activity in any way.

LD titrations with ct-DNA were carried out for both $[Fe_2L^P_3][Cl]_4$ and $[Fe_2L^P_3][BF_4]_4$ complexes and the results compared. The spectra were found to be very similar for both complexes. The spectrum of the LD titration of $[Fe_2L^P_3][BF_4]_4$ (Fig. 2.29) shows, as previously detailed, an ILD signal in the MLCT region that increases with increasing complex concentration, indicating oriented binding. The magnitude of the DNA band at 260 nm decreases with increasing complex concentration, showing kinking or coiling of the DNA upon cylinder binding.

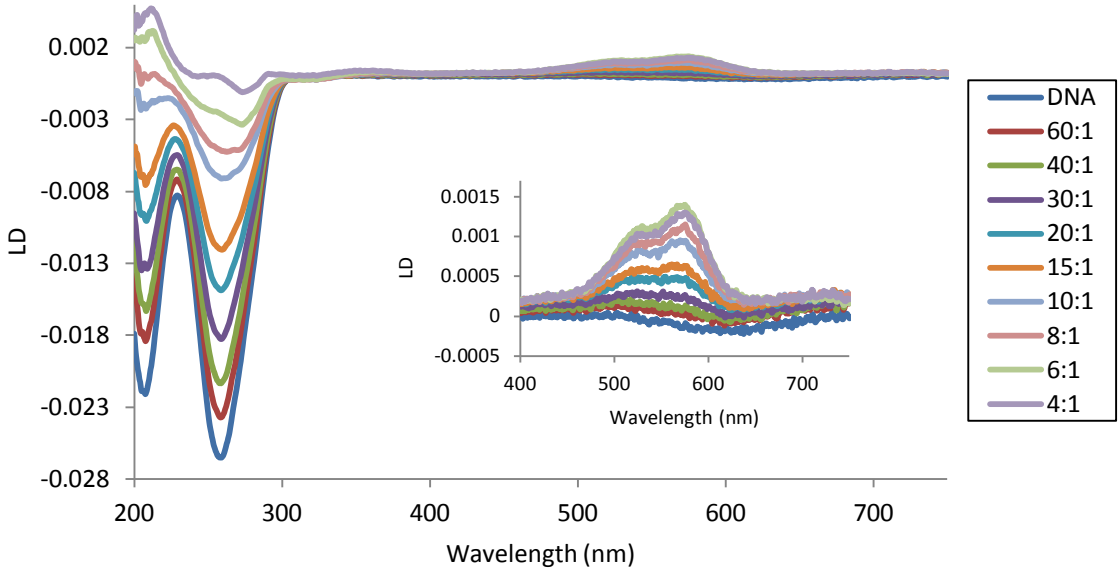

Figure 2.29 LD of 295 μM ct-DNA in 20 mM NaCl and 1 mM $Na(CH_2)_2AsO_2.3H_2O$ (pH 6.8) with increasing concentrations of complex $[Fe_2L^P_3][BF_4]_4$. Inset shows expansion of MLCT region. Legend shows ct-DNA:complex ratios.

To compare the DNA interaction of these complexes, the ILD can be plotted against complex concentration (Fig. 2.30). It is observed that the complexes $[Fe_2L^P_3][Cl]_4$ and $[Fe_2L^P_3][BF_4]_4$ induce a very similar effect on the DNA when they bind.

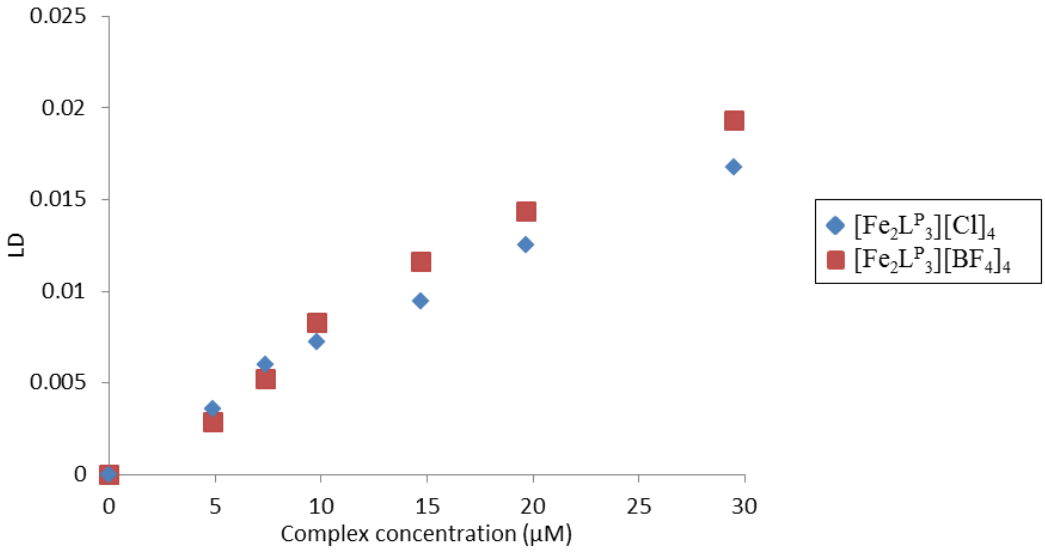

Figure 2.30 Normalised LD signal at 260 nm vs complex concentration for complexes $[Fe_2L^P_3][Cl]_4$ and $[Fe_2L^P_3][BF_4]_4$.

These LD studies demonstrate that the counterion of these iron(II) helicates has no significant effect on the DNA binding.

2.6.2.2 Linear dichroism studies of synthesised alkyne cylinders

Linear dichroism titrations analogous to those performed with the parent cylinder were carried out for the complexes synthesised in this chapter. As these complexes are not water soluble, concentrated stock solutions of the alkyne cylinders in methanol, or acetonitrile for $[Fe_2L^{Phen}{}_3][BF_4]_4$, were made and then diluted with water to achieve the final complex solutions used in the titrations. Maximum percentages of 6% methanol and 7% acetonitrile were used and control LD titrations were carried out in order to ensure that these solvents had no effect on the ct-DNA.

As these iron(II) cylinders are too small to be oriented by the couette cell, no intrinsic LD signal can arise from the cylinders. Consequently any ILD signal observed must come from the interaction between the complex and ct-DNA.

The LD titration spectrum with complex $[Fe_2L^{TB}{}_3][BF_4]_4$ (Fig. 2.31) shows a strong ILD signal between 500-650 nm in the MLCT region of the complex. As the concentration of complex increases so too does the magnitude of this LD signal. This shows that the complex is binding to the DNA in a specific orientation and not just randomly. There is also induced LD signal apparent at 298 nm, but only at higher complex loading. It is observed that the magnitude of the negative DNA band at 260 nm decreases as the complex concentration increases. This indicates that the complex is binding to the DNA and causing a loss of orientation by coiling or bending the DNA. Even on addition of a

very small concentration of complex there is an immediate effect on this negative DNA band, showing that this coiling occurs at very low complex loading.

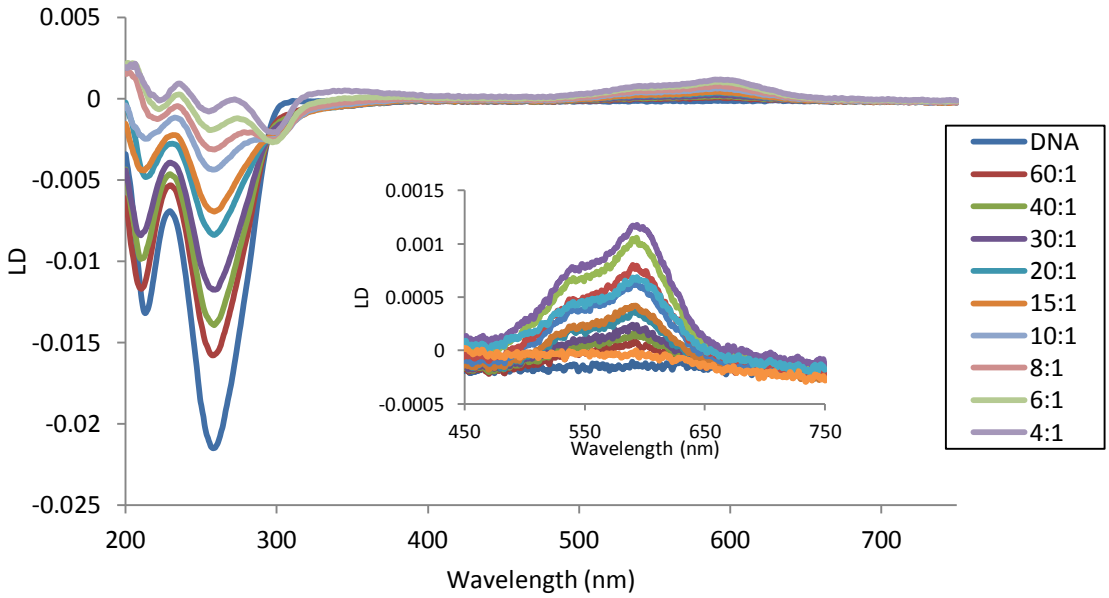

Figure 2.31 LD of 252 μM ct-DNA in 20 mM NaCl and 1 mM $Na(CH_2)_2AsO_2.3H_2O$ (pH 6.8) with increasing concentrations of complex $[Fe_2L^{TB}_3][BF_4]_4$. Inset shows expansion of MLCT region. Legend shows ct-DNA:complex ratios. 5% max. MeOH.

In the LD titration spectrum (Fig. 2.32) of the propargyl alcohol cylinder, $[Fe_2L^{PA}_3][BF_4]_4$, an ILD signal between 500-650 nm, with a maximum at 599 nm, can be observed. The magnitude of this LD signal increases as the cylinder concentration increases revealing oriented binding of the complex to the ct-DNA. At higher complex loading, with ratios of DNA:complex of 10:1 to 4:1, an induced LD signal at 310 nm can also be seen. The negative DNA LD band decreases in magnitude with increasing cylinder loading. This means that complex binding induces bending or coiling of the DNA, even at very low complex loading.

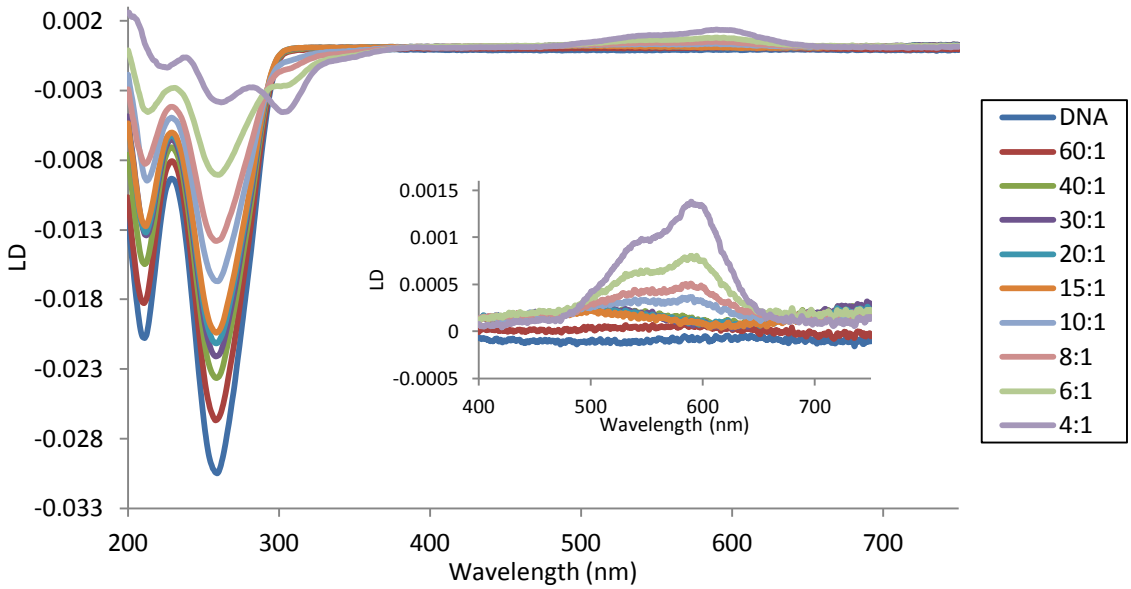

Figure 2.32 LD of 262 μM ct-DNA in 20 mM NaCl and 1 mM $Na(CH_2)_2AsO_2.3H_2O$ (pH 6.8) with increasing concentrations of complex $[Fe_2L^{PA}_3][BF_4]_4$. Inset shows expansion of MLCT region. Legend shows ct-DNA:complex ratios. 5.2% max. MeOH.

In the LD titration spectrum of $[Fe_2L^{Hex}_3][BF_4]_4$ (Fig. 2.33), an induced LD signal can be observed in the MLCT region of the complex, with a maximum at 598 nm. This ILD signal increases in intensity as the cylinder concentration is increased, indicating that the complex binds to the DNA in a specific orientation and not just randomly. Another ILD signal can be seen at 305 nm at higher complex loading. Upon increasing complex concentration, the magnitude of negative DNA LD band decreases, indicating coiling or bending of the DNA induced by the hexyn-ol functionalised cylinder.

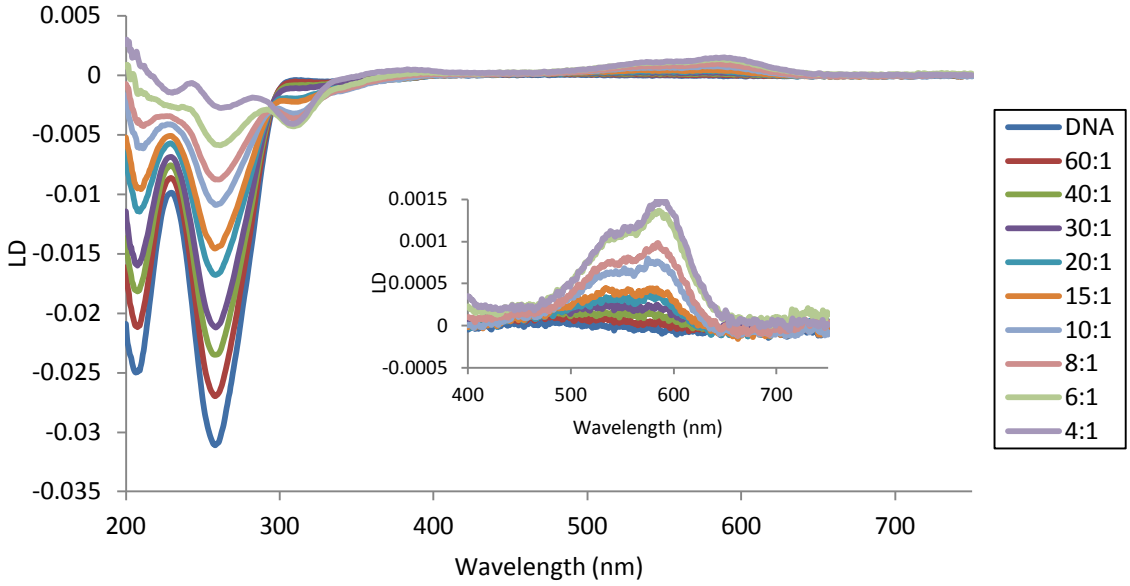

Figure 2.33 LD of 286 μM ct-DNA in 20 mM NaCl and 1 mM $Na(CH_2)_2AsO_2.3H_2O$ (pH 6.8) with increasing concentrations of complex $[Fe_2L^{Hex}{}_3][BF_4]_4$. Inset shows expansion of MLCT region. Legend shows ct-DNA:complex ratios. 5.7% max. MeOH.

There is no detectable ILD signal in the LD titration spectrum for complex $[Fe_2L^{Phen}{}_3][BF_4]_4$ (Fig. 2.34). Even at high complex loading, with a DNA:complex ratio of 4:1, no signals are observed that would suggest oriented binding of this complex. However the magnitude of the negative DNA LD band at 260 nm can be observed to decrease as the concentration of the complex is increased, even at low cylinder loading. This confirms that although no induced LD signal is apparent, the complex is binding to the DNA and causing the dramatic coiling or bending observed for other iron(II) cylinders.

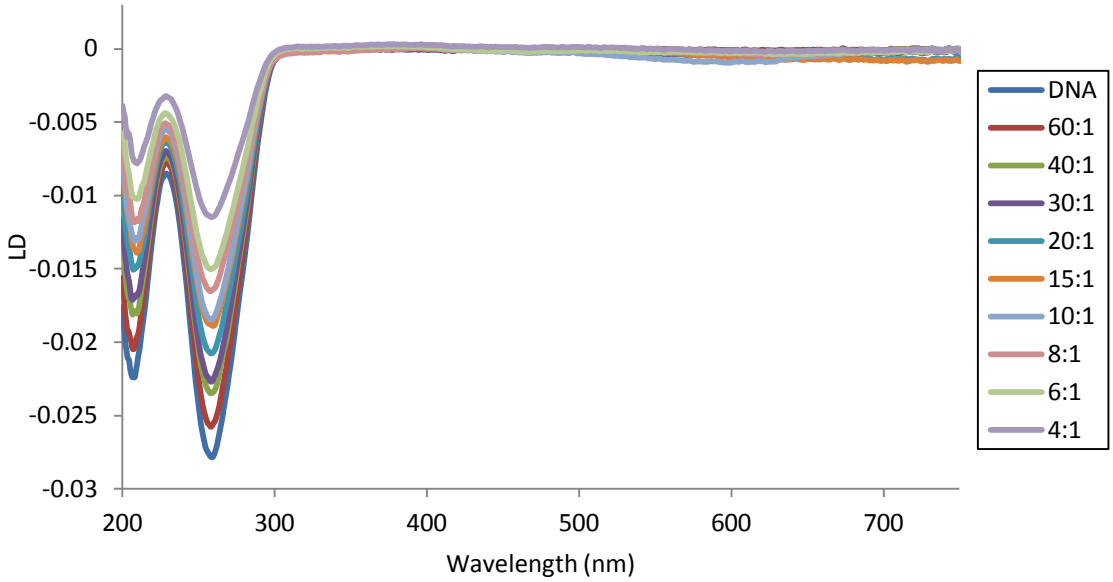

Figure 2.34 LD of 274 μM ct-DNA in 20 mM NaCl and 1 mM $Na(CH_2)_2AsO_2.3H_2O$ (pH 6.8) with increasing concentrations of complex $[Fe_2L^{Phen}{}_3][BF_4]_4$. Legend shows ct-DNA:complex ratios. 6.9% max. MeCN.

The DNA binding activities of the alkyne cylinders discussed can be compared to each other and to the parent cylinder by calculating the percentage loss of LD signal of the negative DNA band at 260 nm (Table 2.1) and also by plotting the magnitude of this LD DNA band versus complex concentration (Fig. 2.35). It can be observed that all of the complexes induce dramatic DNA coiling/bending on binding, even at low complex concentration. At the highest complex loading, corresponding to a DNA:complex ratio of 4:1, a loss of 99% of the LD signal is induced by the parent cylinder with tetrafluoroborate counterions. The complexes $[Fe_2L^{TB}{}_3][BF_4]_4$, $[Fe_2L^{PA}{}_3][BF_4]_4$ and $[Fe_2L^{Hex}{}_3][BF_4]_4$ have a similar effect, especially at high complex loading. The phenylacetylene complex induces the least coiling of the DNA, with a 59% loss of LD signal for the DNA band. This is likely due to its bulky inflexible nature which perhaps does not allow such close proximity to the DNA as the other cylinders.

DNA:complex ratio	% Loss of LD signal at 260nm upon interaction with complexes				
4:1	$[Fe_2L^{P}{}_3][BF_4]_4$	$[Fe_2L^{TB}{}_3][BF_4]_4$	$[Fe_2L^{PA}{}_3][BF_4]_4$	$[Fe_2L^{Hex}{}_3][BF_4]_4$	$[Fe_2L^{Phen}{}_3][BF_4]_4$
	99	97	87	91	59

Table 2.1 Comparison of the percentage loss of LD signal at 260 nm upon interaction with complexes at a ratio of DNA:complex 4:1.

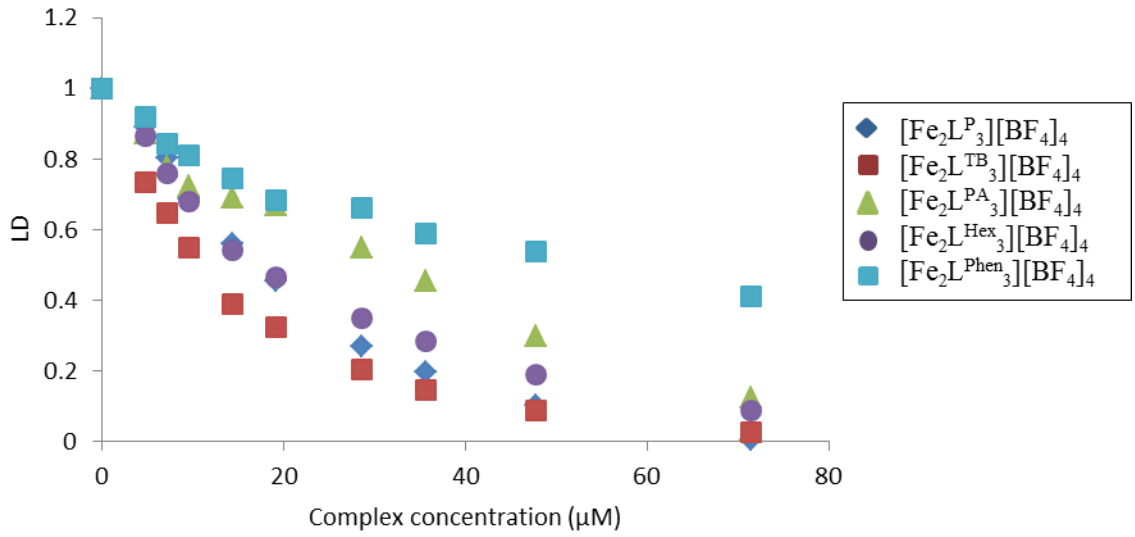

Figure 2.35 Normalised LD signal at 260 nm vs complex concentration for parent and alkyne complexes.

2.6.3 Gel electrophoresis

Agarose gel electrophoresis is a widely used technique for the separation of biomolecules, such as DNA fragments, based on their size, charge or conformation.[23] In this work, a small bacterial plasmid pBR322 is used as a model system for probing the interaction between DNA-binding drug molecules and supercoiled DNA.[24] Supercoiled DNA is found extensively in living cells, and is important in any process that requires opening of the double helix of DNA, such as replication and transcription.[25,26] The pBR322 plasmid exists as two forms in solution, supercoiled and circular (relaxed) forms. The supercoiled form is negatively supercoiled (Fig. 2.36), which means that it is under wound, as are most circular

DNA's found in nature (mitochondrial, viral and bacterial).[26] As this negatively supercoiled structure is under wound it exerts a force that helps to separate the strands of duplex DNA, assisting the processes of replication and transcription.[26]

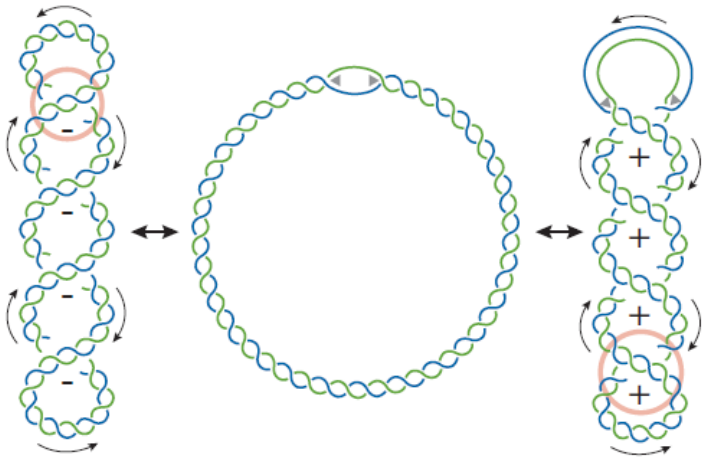

Figure 2.36 Negatively supercoiled DNA (left); Relaxed circular form; loss of supercoiling due to unwinding by DNA helicases or DNA-binding drug (middle); Positive supercoiling of relaxed form due to further strand separation (right). [Reproduced from Ref [24]]

Agarose gel electrophoresis is employed in this work to study the interaction between the metallo-helicates synthesised and supercoiled pBR322 plasmid DNA. Gel electrophoresis studies are performed by loading the agarose gel with samples of mixtures of pBR322 DNA and the metal complexes at different ratios. When an electric field is applied, the negatively charged DNA migrates through the gel towards the positive electrode separating the two forms of DNA, circular and supercoiled, due to their difference in size and therefore migration speed (Fig. 2.37).

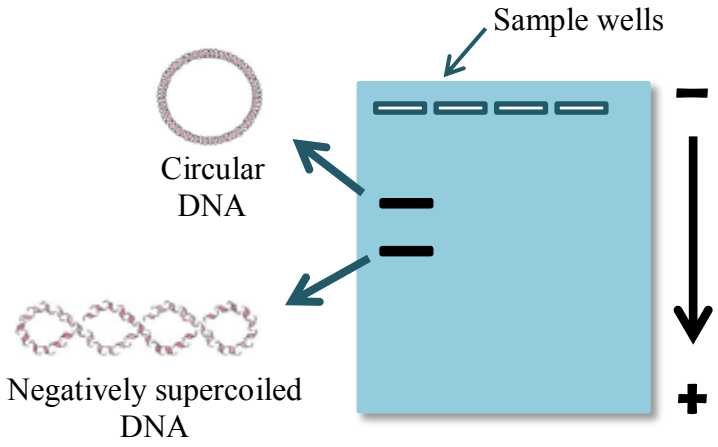

Figure 2.37 Schematic representation of an agarose gel showing different migration speeds of circular and supercoiled DNA.

The different bands in the gel corresponding to the two forms of DNA are visualised using ethidium bromide as a stain, which intercalates into the DNA and is visible under UV light.[23]

If a drug does bind to the supercoiled form of plasmid DNA, this will cause the supercoiled DNA to unwind and therefore increase in size or volume (Fig.2.36). This can be observed as a slowing down of the speed of migration of the supercoiled band through the gel, from the negative to positive electrode. Therefore if the supercoiled DNA is observed to be unwound by the metal complex, it suggests that the complex is binding to the DNA.[6]

If the circular and supercoiled bands co-migrate then the unwinding angle, Φ, defined as the number of degrees by which the DNA is unwound about its helical axis per molecule bound, can be calculated using the formula:

$$\Phi = \frac{-18\sigma}{r(c)}$$

where, Φ = DNA unwinding angle, σ = superhelicity constant and $r_{(c)}$ = ratio of DNA base:complex bound at which the circular and supercoiled bands co-migrate.

The superhelicity constants for plasmids pBR322 and pUC19, determined using cisplatin which has a known unwinding angle of 13°, were found to be -0.059 and -0.058 respectively.[6,27]

In the studies detailed in this thesis agarose gel electrophoresis was performed using DNA plasmids pUC19, for parent complex $[Fe_2L^P_3][Cl]_4$, and pBR322, for all other complexes. Solutions containing different ratios of plasmid DNA:metal complex are loaded onto a 1% agarose gel and the gel is run by applying an electric current. The DNA bands in the gel are visualised using ethidium bromide as a stain. If the bands corresponding to the circular and supercoiled forms of DNA co-migrate the unwinding angle, Φ, can be calculated.

2.6.3.1 Gel electrophoresis studies of the parent cylinder, $[Fe_2L^P_3]^{4+}$, with different counterions

In recent work, it was reported that the parent iron(II) cylinder, $[Fe_2L^P_3][Cl]_4$, was able to bind to duplex DNA and to unwind it.[6] The band corresponding to the supercoiled form of the pUC19 plasmid DNA can be observed to migrate at an increasingly slower speed through the gel as the cylinder concentration is increased (lanes 2 to 8, Fig. 2.38).[6] This shows that as the cylinder concentration increases, more and more complex is binding to the supercoiled form of DNA, unwinding it and increasing its size or volume, and therefore causing it to run at a slower speed through the gel. At a DNA:complex ratio of 26:1 all of the supercoiled form has been unwound to the circular relaxed form (lane 8, Fig. 2.38).

As the cylinder concentration is increased further, a band corresponding to positively supercoiled DNA becomes apparent, with a faster migration rate through the gel. This shows that the cylinder is continuing to bind to the relaxed circular form of DNA, winding and supercoiling it up again.

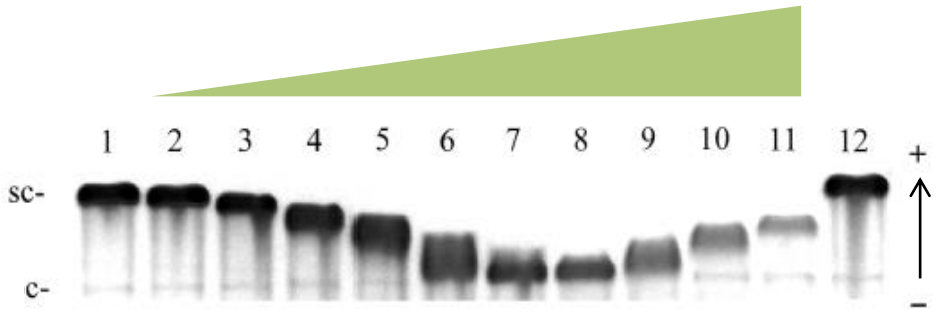

Figure 2.38 Agarose gel (1%) electrophoresis showing changes in electrophoretic mobility of circular (C) and supercoiled (SC) forms of pUC19 plasmid DNA incubated at 25°C for 30 minutes with different ratios of complex $[Fe_2L^P_3][Cl]_4$. Lanes 2-11: DNA:complex ratio = 125:1, 67:1, 44:1, 37:1, 33:1, 29:1, 26:1, 22:1, 19:1 and 16:1 respectively). Control lanes: 1 and 12 = non-modified DNA. [Reproduced from Ref [6]]

For $[Fe_2L^P_3][Cl]_4$, the supercoiled and circular forms of the plasmid DNA co-migrate at a DNA:complex ratio of 26:1.[6] Using this ratio, the unwinding angle, Φ, is calculated to be 27°±3.[6]

Gel electrophoresis was also performed using the parent cylinder with tetrafluoroborate counterions, $[Fe_2L^P_3][BF_4]_4$, so as to compare the unwinding ability of both complexes.

The gel for the $[Fe_2L^P_3][BF_4]_4$ complex (Fig. 2.39) shows that, as for $[Fe_2L^P_3][Cl]_4$, the mobility of the supercoiled DNA band decreases as the cylinder concentration increases, giving evidence for the unwinding of the supercoiled form of DNA by the cylinder. As cylinder concentration increases further, positive supercoiling of the DNA occurs.

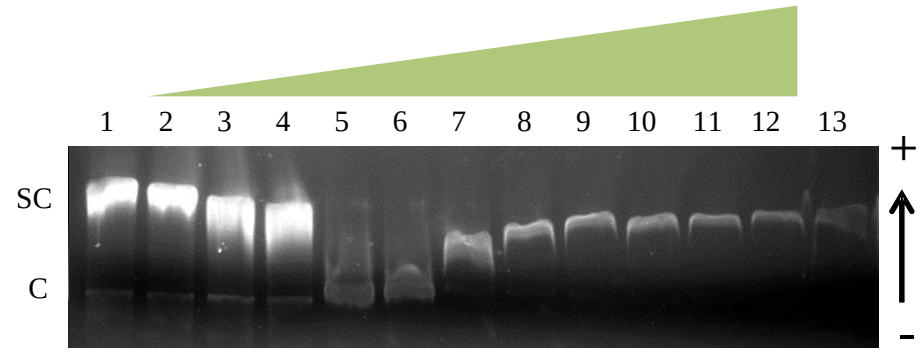

Figure 2.39 Agarose gel (1%) electrophoresis showing changes in electrophoretic mobility of C and SC forms of pBR322 plasmid DNA incubated at 20°C for 2 hours with different ratios of complex $[Fe_2L^P_3][BF_4]_4$. Lanes 2-13: DNA:complex ratio = 100:1, 50:1, 40:1, 20:1, 15:1, 10:1, 8:1, 6:1, 5:1, 4:1, 3:1 and 2:1 respectively). Control lane: 1 = non-modified DNA.

The two forms of DNA co-migrate at a DNA:complex ratio of 20:1, allowing the unwinding angle, Φ, to be calculated as 21°.

When comparing the unwinding angles of the two complexes, $[Fe_2L^P_3][Cl]_4$ and $[Fe_2L^P_3][BF_4]_4$, the different ratios of DNA:complex used when performing the experiment must be taken into account. However the unwinding angles, 27°±3 and 21° respectively, are quite similar, therefore their unwinding activities can be said to be similar and not significantly affected by the difference in counterion.

The unwinding angle of 27° observed for $[Fe_2L^P_3][Cl]_4$ shows that the parent cylinder has very good DNA unwinding activity, especially when compared to other non-intercalative compounds such as the minor groove binder Hoechst which has an unwinding angle of 1°.[6,28]

2.6.3.2 Gel electrophoresis studies of synthesised alkyne cylinders

Gel electrophoresis experiments analogous to those performed with the parent cylinder were also carried out for the alkyne cylinders synthesised. Due to the insolubility of the complexes in water, a small percentage of methanol or acetonitrile was used to dissolve the compounds. In each experiment control lanes containing samples of DNA with and without solvent were compared to ensure the solvent used had no effect on the DNA or the gel. Samples containing different plasmid DNA:complex ratios (Table 2.2) were incubated at room temperature for two hours before being run on a 1% agarose gel.

Lanes	1	2	3	4	5	6	7
DNA:complex ratio	MeOH/MeCN control	50:1	40:1	30:1	20:1	15:1	10:1
Lanes	8	9	10	11	12	13	14
DNA:complex ratio	8:1	6:1	5:1	4:1	3:1	2:1	control

Table 2.2 Ratios of plasmid DNA:complex used in gel electrophoresis experiments. Control lane 1: untreated DNA with max. percentage of solvent used. Control lane 14: untreated DNA without solvent.

The agarose gel (Fig. 2.40) for the triple bond cylinder, $[Fe_2L^{TB}_3][BF_4]_4$, indicates that the complex is binding to the supercoiled form of DNA. From a DNA:complex ratio of 10:1 the supercoiled (SC) band can be seen to be migrating at a slower pace through the gel. As the complex concentration increases, the band slows down even more. This means that the complex is binding to the DNA and unwinding it, causing an increase in the size or shape of the DNA, and so it migrates at a slower rate through the gel. At a ratio of 8:1 the circular (C) band of DNA begins to migrate at a faster speed through the gel. This is due to the complex binding to and shortening or condensing the helical form of the circular DNA. At

a 5:1 DNA:complex ratio, the supercoiled and circular bands co-migrate indicating that all of the supercoiled DNA has been unwound to the relaxed circular form. At higher complex loading, lanes 11-13, the supercoiled band has reappeared and can be seen to migrate faster through the gel as the complex concentration is increased. This indicates that the DNA has decreased in size, due to positive supercoiling of the DNA.

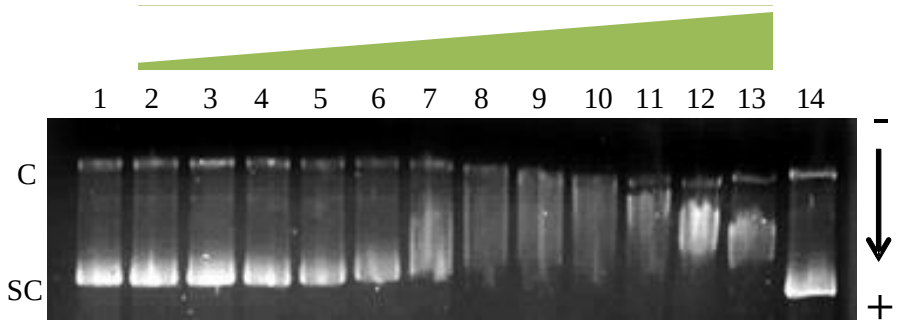

Figure 2.40 Agarose gel (1%) electrophoresis showing changes in electrophoretic mobility of C and SC forms of pBR322 plasmid DNA incubated at 20°C for 2 hours with different ratios of complex $[Fe_2L^{TB}_3][BF_4]_4$ (lanes 2-13). Control lanes (1 and 14): pBR322 plasmid DNA in absence of complex. 7% max. MeOH.

DNA binding can be seen in the agarose gel (Fig. 2.41) for the propargyl alcohol complex, $[Fe_2L^{PA}_3][BF_4]_4$. The migration of the supercoiled band is observed to slow down at a DNA:complex ratio of 15:1. This is due to the complex binding to the supercoiled plasmid and unwinding it by lengthening or stiffening it. The circular and supercoiled bands can be seen to co-migrate at a ratio of 6:1, due to all of the supercoiled DNA being unwound to the relaxed circular form. As the cylinder concentration is increased further, lanes 10-13, the supercoiled band reforms and begins to migrate faster through the gel. This indicates that the complex is causing the plasmid to wind up again, this time in a positive supercoil.

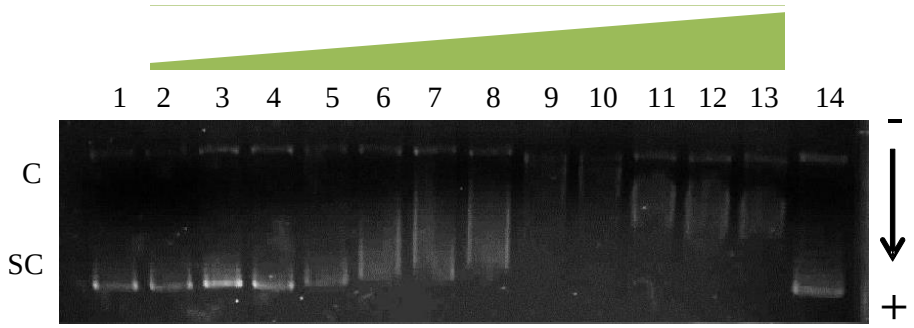

Figure 2.41 Agarose gel (1%) electrophoresis showing changes in electrophoretic mobility of C and SC forms of pBR322 plasmid DNA incubated at 20°C for 2 hours with different ratios of complex $[Fe_2L^{PA}{}_3][BF_4]_4$ (lanes 2-13). Control lanes (1 and 14): pBR322 plasmid DNA in absence of complex. 7% max. MeOH.

The agarose gel (Fig. 2.42) for the hexyn-ol cylinder, $[Fe_2L^{Hex}{}_3][BF_4]_4$, does not show any DNA unwinding. There is no change in the mobility of the plasmid bands with increasing complex concentration, showing that the cylinder has no effect. This result is surprising as the CD and LD studies show good DNA binding activity of this complex.

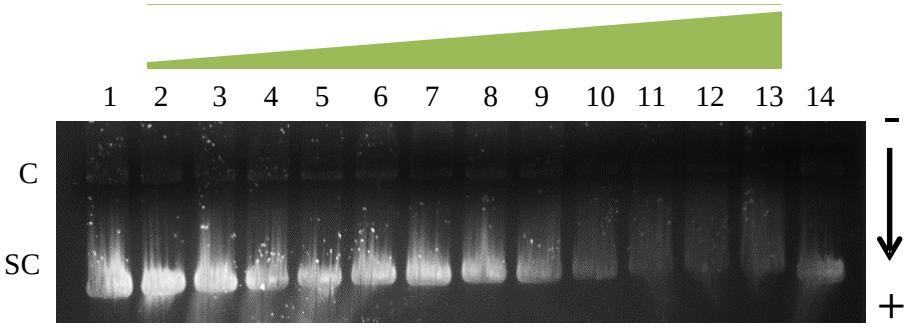

Figure 2.42 Agarose gel (1%) electrophoresis showing changes in electrophoretic mobility of C and SC forms of pBR322 plasmid DNA incubated at 20°C for 2 hours with different ratios of complex $[Fe_2L^{Hex}{}_3][BF_4]_4$ (lanes 2-13). Control lanes (1 and 14): pBR322 plasmid DNA in absence of complex. 7% max. MeOH.

DNA binding is not observed in the agarose gel for the phenylacetylene cylinder, $[Fe_2L^{Phen}{}_3][BF_4]_4$ (Fig. 2.43). No effect on the mobility of the bands can be observed even

at high complex concentration. This indicates that no DNA unwinding is observed.

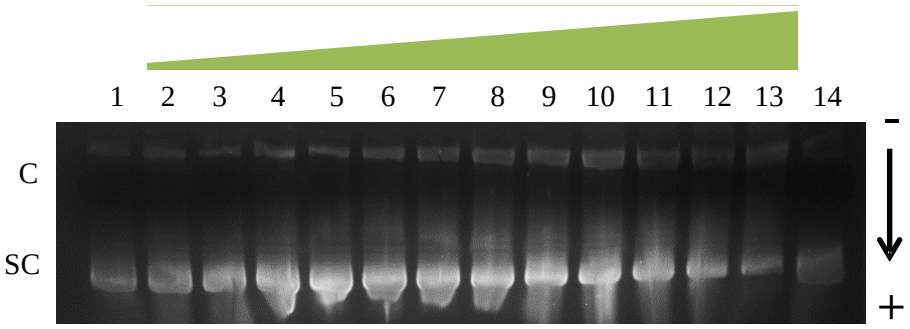

Figure 2.43 Agarose gel (1%) electrophoresis showing changes in electrophoretic mobility of C and SC forms of pBR322 plasmid DNA incubated at 20°C for 2 hours with different ratios of complex $[Fe_2L^{Phen}{}_3][BF_4]_4$ (lanes 2-13). Control lanes (1 and 14): pBR322 plasmid DNA in absence of complex. 7% max. MeCN.

As co-migration of the circular and supercoiled forms of the pBR322 plasmid was induced by the triple bond and propargyl alcohol cylinders, $[Fe_2L^{TB}{}_3][BF_4]_4$ and $[Fe_2L^{PA}{}_3][BF_4]_4$, unwinding angles could be calculated for these compounds and compared to that of the parent cylinder (Table 2.3). The triple bond cylinder is able to unwind the supercoiled DNA by 5°±1 and the propargyl alcohol complex by 6°±1. When compared to the value for the parent cylinder these values seem rather small. However compared to the unwinding value calculated for cisplatin, which is 13°,[27] these complexes do show promising DNA unwinding activity.

Complexes	$[Fe_2L^{P}{}_3][Cl]_4$	$[Fe_2L^{TB}{}_3][BF_4]_4$	$[Fe_2L^{PA}{}_3][BF_4]_4$
Φ values	27° ±3	5° ±1	6° ±1

Table 2.3 Unwinding angles (Φ) of complexes calculated from gel electrophoresis experiments.

2.6.4 PAGE studies

Polyacrylamide gel electrophoresis (PAGE) is a similar technique to that of agarose gel electrophoresis (Section 2.6.3), and is employed for the separation of smaller DNA fragments than those separated by agarose gels, due to a smaller pore size in the gel.[29] Polyacrylamide gel electrophoresis is used to separate complex mixtures of macromolecules, such as DNA fragments, by size.[30] PAGE studies are advantageous as only very low concentrations of the macromolecule to be investigated are needed, as radiolabelling allows highly sensitive detection of the bands in the gel, corresponding to the separated fragments.[31]

PAGE studies investigating the interaction between supramolecular helicates and DNA three-way junctions have recently been reported[31] and were employed herein. In these studies three oligonucleotide strands that are able to form a DNA three-way junction are employed and one of these strands is labelled with ^{32}P. Mixtures of the three oligonucleotide strands and the metallo-cylinder at different ratios are incubated and then loaded onto the polyacrylamide gel (Fig. 2.44). A control consisting of the three DNA strands with magnesium chloride is also used, as it is known that magnesium dications can stabilise three-way junctions at low to medium ionic strengths.[32] As with the agarose gels, an electric current is then applied which causes migration of the negatively charged DNA fragments through the gel towards the positive electrode. The smaller single strands have a faster migration rate through the gel than the larger three-way junction, and so the different species are separated. An autoradiogram is then obtained that allows visualisation of the bands corresponding to these different species.

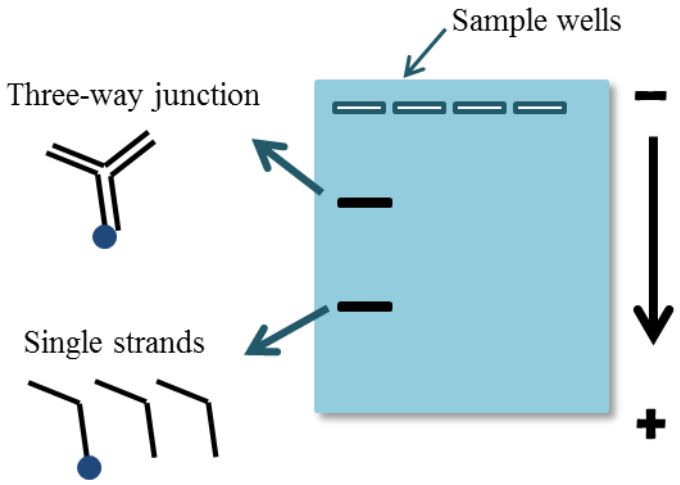

Figure 2.44 Schematic representation of a polyacrylamide gel showing different migration speeds of single strand oligonucleotides and DNA three-way junction. One strand is radiolabelled with ^{32}P (blue circle).

In the absence of cylinder, or magnesium ions, the three-way junction is not stabilised and so cannot form. Therefore, only bands corresponding to the single strands will be observed in the polyacrylamide gel. If the cylinder being investigated can promote the formation and stabilisation of the three-way junction, a band corresponding to the three-way junction will be observed.

2.6.4.1 PAGE studies of the parent cylinder, $[Fe_2L^P{}_3]^{4+}$, and bulky cylinder, $[Fe_2L^{CF3}{}_3]^{4+}$ 31

Recently, three-way junction polyacrylamide gel electrophoresis studies of the parent cylinder and a bulky substituted cylinder, $[Fe_2L^{CF3}{}_3]^{4+}$, were reported.[31] A PAGE experiment was carried out with three 14-mer non-palindromic oligonucleotide DNA strands which could form a three-way junction with arms of seven base pairs long (Fig. 2.45).[31] These three strands were incubated with $[Fe_2L^P{}_3][Cl]_4$ at different mixing ratios.[31] The autoradiogram of the gel (Fig. 2.45) shows that the three oligonucleotide strands do

not form a three-way junction structure unless in the presence of the iron(II) cylinder.[31] An increase in the concentration of the cylinder (lanes 6 and 7) did not further enhance the formation of the three-way junction.[31] Interestingly, the presence of a very high concentration of magnesium chloride did not afford stabilisation of the three-way junction under the experimental conditions used (lane 8) as would be expected, indicating the highly stabilising nature of the iron(II) cylinder to the three-way junction structure.[31]

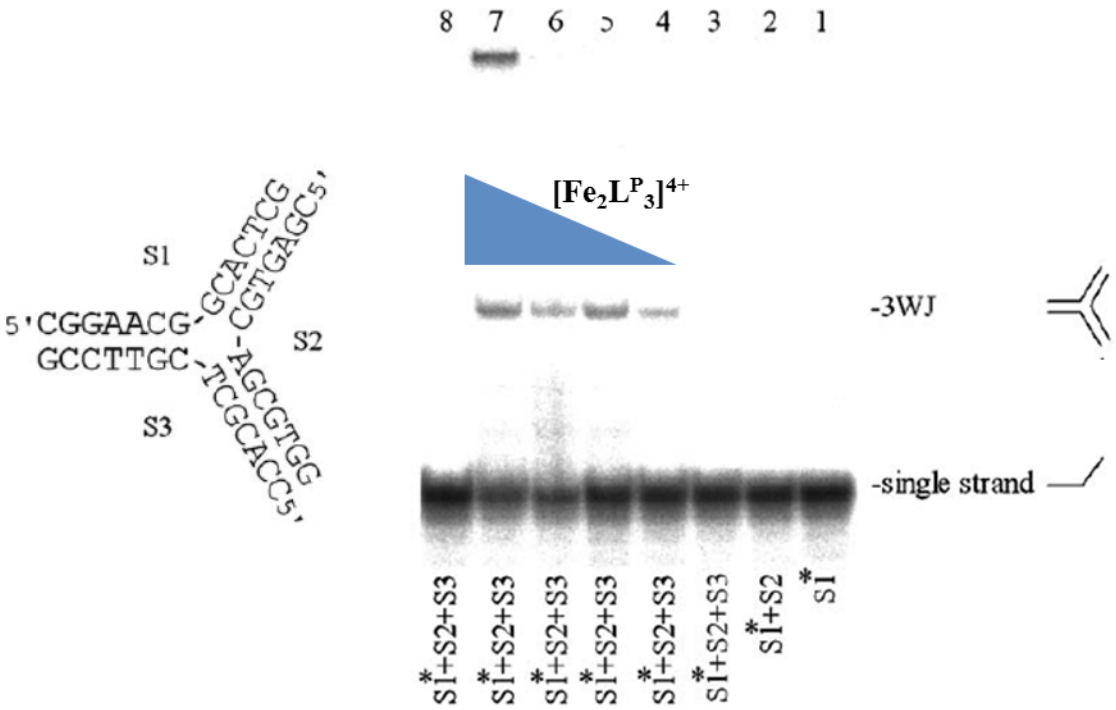

Figure 2.45 Structure of DNA three-way junction formed from three 14-mer nonpalindromic oligonucleotide strands (left); Autoradiogram of polyacrylamide gel (right) run at 25 °C. Lanes 1-3: controls containing one, two and three oligonucleotide strands. Lanes 4-7: all three strands with $[Fe_2L^P_3]^{4+}$ at mixing ratios of strand:cylinder of 6:1, 3:1, 3:2 and 3:10 respectively (blue triangle indicates increasing concentration of cylinder). Lane 8: all three strands with 10 mM $MgCl_2$. Asterisk indicates ^{32}P labelled strand. [Adapted from Ref [31]]

Further studies with different oligonucleotide sequences confirmed that this stabilisation is also apparent for other three-way junction and Y-shaped junction structures, including those with palindromic and non-palindromic sequences.[31] The M and P enantiomers of the

parent cylinder were also investigated and both were shown to promote the formation and stabilisation of DNA three-way junctions, with the M enantiomer having a greater efficacy than the P.[31]

To study the importance of the size and shape of the cylinder on its ability to stabilise DNA three-way junctions, a bulky cylinder, $[Fe_2L^{CF3}{}_3]^{4+}$, (Fig. 2.46) was also employed.[31] It was found that no three-way junction was formed, confirming the theory that the stabilisation of the three-way junction is afforded by the interactions induced by the perfect fit of the cylinder in the heart of the junction structure.[31]

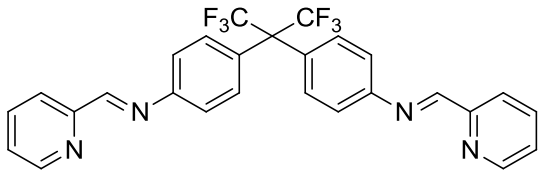

Figure 2.46 Structure of L^{CF3} ligand of bulky cylinder, $[Fe_2L^{CF3}{}_3]^{4+}$.[31]

2.6.4.2 PAGE studies of the parent cylinder, $[Fe_2L^P{}_3]^{4+}$, with different counterions and alkyne cylinders

To assess the ability of these cylinders to bind to and stabilise DNA three-way junctions, they were studied by PAGE. These studies were carried out by co-worker N. Calle Alonso from the University of Birmingham. The results are briefly described herein for completeness.

Oligonucelotide strands of the same sequence as those used for the experiments reported and discussed previously (Section 2.6.4.1) were used (Fig. 2.45).[3,31] Due to the insolubility

of the alkyne complexes in water, a small percentage of methanol or acetonitrile was used to dissolve the compounds. In each experiment control lanes containing one, two and three DNA strands and magnesium chloride were incorporated. The parent and alkyne cylinders were mixed with the three non-palindromic oligonucleotide strands to give a ratio of three-way-junction:cylinder of 1:1, incubated for one hour and run on a 15% polyacrylamide gel.

The autoradiogram of the polyacrylamide gel (Fig. 2.47, cropped image; for whole gel see Appendix) indicates that the individual oligonucleotide strands cannot form a DNA three-way junction under these experimental conditions. Only a band corresponding to the individual strands can be seen at the bottom of the gel, due to the fast migration rate of these small fragments. Magnesium chloride did not promote the formation of a three-way junction, as was observed in the previous PAGE studies with the parent cylinder (Section 2.6.4.1). However, when the oligonucleotide strands were incubated with the parent, $[Fe_2L^{P}_3][Cl]_4$ and $[Fe_2L^{P}_3][BF_4]_4$, and alkyne, $[Fe_2L^{TB}_3][BF_4]_4$, $[Fe_2L^{PA}_3][BF_4]_4$ and $[Fe_2L^{Hex}_3][BF_4]_4$, cylinders, a three-way junction was formed. A small difference in the migration rate of these bands through the gel can be seen and this is due to the molecular weight of the cylinders. The lower molecular weight cylinders, $[Fe_2L^{P}_3][Cl]_4$ and $[Fe_2L^{P}_3][BF_4]_4$, run through the gel with higher electrophoretic mobility, whereas as the molecular weight increases, from $[Fe_2L^{TB}_3][BF_4]_4$ to $[Fe_2L^{Hex}_3][BF_4]_4$, the migration rate decreases. The phenyl cylinder, $[Fe_2L^{Phen}_3][BF_4]_4$, did not promote the formation of a DNA three-way junction.

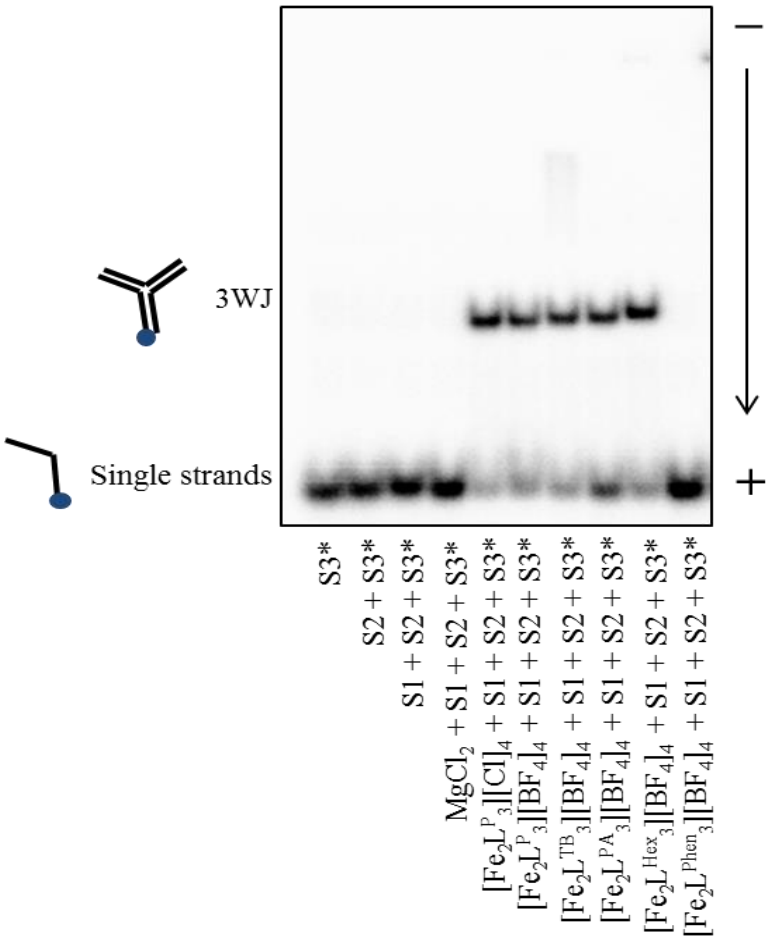

Figure 2.47 Autoradiogram of polyacrylamide gel run at 25 °C. Lanes 1-3: S3*, S3*+S2, S3*+S2+S1 respectively; Lane 4: S3*+S2+S1+$MgCl_2$; Lanes 5-10: S3*+S2+S1 with $[Fe_2L^{P}_3][Cl]_4$, $[Fe_2L^{P}_3][BF_4]_4$, $[Fe_2L^{TB}_3][BF_4]_4$, $[Fe_2L^{PA}_3][BF_4]_4$, $[Fe_2L^{Hex}_3][BF_4]_4$ and $[Fe_2L^{Phen}_3][BF_4]_4$ respectively. Ratio of three-way junction (S1+S2+S3*):complex of 1:1. Asterisk indicates ^{32}P labelled strand.

As the PAGE experiments were carried out in duplicate, only a preliminary comparison of the three-way junction promotion and stabilisation ability of the parent and functionalised cylinders can be noted. Quantification of the band in the gel corresponding to the three-way junction (Fig. 2.48) indicates that the parent cylinders with chloride and tetrafluoroborate counterions have a similar promotion and stabilisation effect.

The $[Fe_2L^{PA}_3][BF_4]_4$ cylinder appears to be less able to promote the formation of a three-way junction than the parent cylinder.

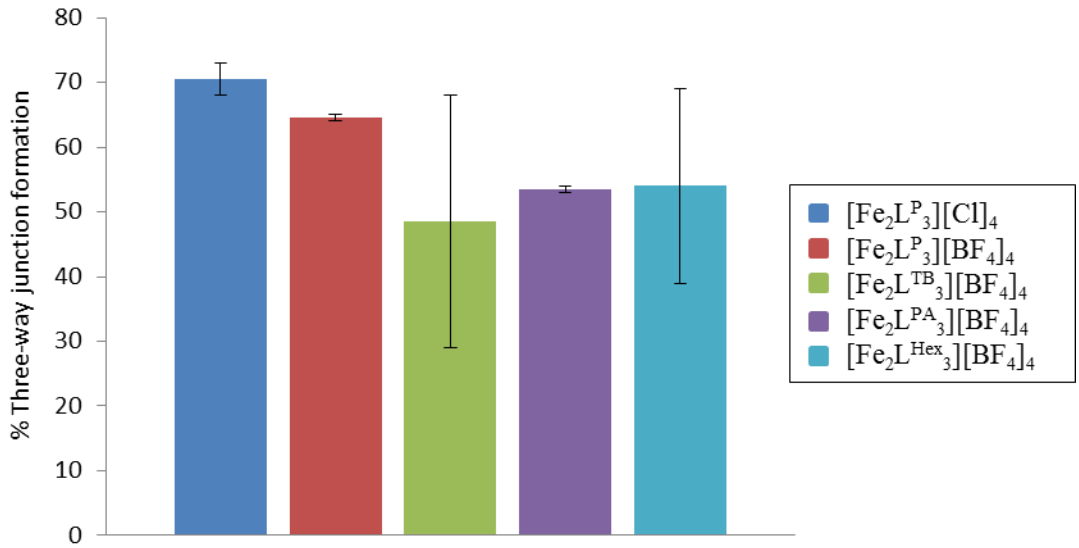

Figure 2.48 Bar graph showing percentage of three-way junction formed by complexes. Data based on two repeats; error bars shown demonstrate the two data points (not standard deviation), and the bar their average.

2.7 Conclusions

In this chapter, a novel cylinder functionalisation route has been presented which allows the easy and efficient modification of metallo-cylinders. It has been demonstrated that different groups can be attached to the edges of the cylinder via this route, in few reaction steps.

Using this synthesis route, four novel iron(II) cylinders functionalised with chemical groups have been designed and synthesised in only two or three steps with overall yields of 15-56%, with respect to the 5-bromo-2-pyridinecarboxaldehyde starting material. As the substituent attached to the cylinder gets larger and bulkier, the yield of the cylinder formation step decreases, likely due to steric hindrance.

Unfortunately these complexes are insoluble in water, however their solubility in water-miscible solvents allowed DNA binding studies to be carried out. The stability of these complexes in DNA binding experimental conditions, at room temperature in aqueous solution in the presence of DNA, was evaluated. The majority of the complexes showed very good stabilities in these conditions, however $[Fe_2L^{Phen}{}_3][BF_4]_4$ was less stable with a degradation of one third over a period of five hours.

DNA binding studies, including circular and linear dichroism with ct-DNA and gel electrophoresis with plasmid DNA, were carried out for the parent cylinder and novel functionalised cylinders. The DNA binding activity of the parent cylinder with tetrafluoroborate counterions was found to be very similar to that of the chloride version, $[Fe_2L^{P}{}_3][Cl]_4$. Both complexes were able to bind to ct-DNA, and to bend or coil it, and also to bind to and unwind supercoiled plasmid DNA. PAGE studies revealed the ability of the cylinders to promote the formation of a DNA three-way junction with similar efficiency.

The triple bond, propargyl alcohol and hexyn-ol cylinders, $[Fe_2L^{TB}{}_3][BF_4]_4$, $[Fe_2L^{PA}{}_3][BF_4]_4$ and $[Fe_2L^{Hex}{}_3][BF_4]_4$, were found to be DNA binders when evaluated using circular dichroism. In the LD titration experiments the $[Fe_2L^{TB}{}_3][BF_4]_4$, $[Fe_2L^{PA}{}_3][BF_4]_4$ and $[Fe_2L^{Hex}{}_3][BF_4]_4$ cylinders all induced significant DNA bending/coiling. Gel electrophoresis studies found the triple bond and propargyl alcohol functionalised helicates unwound supercoiled plasmid DNA with unwinding angles of 5°±1 and 6°±1 respectively. However the hexyn-ol functionalised cylinder showed no DNA unwinding. PAGE studies revealed that these three complexes could all promote the formation of a DNA three-way junction.

The phenylacteylene complex, $[Fe_2L^{Phen}{}_3][BF_4]_4$, seems to behave differently to the other three novel functionalised compounds. CD and LD studies indicated that the complex could bind to ct-DNA, however far less DNA coiling/bending was observed for this complex when compared to the other three, unwinding of supercoiled DNA by this compound was not observed in the gel electrophoresis experiment, and the complex did not promote the formation of a DNA three-way junction as observed by polyacrylamide gel electrophoresis. This is likely due to the bulky inflexible nature of the phenylacetylene moiety that is attached at the ends of this cylinder, which somehow inhibits close proximity to the DNA or possibly does not allow the complex to bind in the major groove of the DNA.

Unfortunately, *in vitro* studies could not be undertaken with these alkyne functionalised cylinders due to their insolubility in the solvent systems required.

These investigations indicate that modification of the iron(II) parent cylinder can be achieved without complete loss of its inherent DNA binding properties. However the functionalisation moiety to be attached has to be chosen carefully to avoid a significant loss of DNA affinity or water solubility; it appears that directly linked aryl groups on the alkyne may present problems.

2.8 Experimental: synthesis

2.8.1 Materials and methods

All reagents and solvents were purchased from Aldrich, Fisher, Apollo Scientific and Fluorochem and used without further purification. Deuterated NMR solvents were purchased from Goss Scientific. NMR spectra were recorded on Brüker AVIII300 and AVIII400 spectrometers and processed using standard Brüker software. Electrospray Ionisation (ESI) spectra were recorded on a Micromass LCT Time of flight mass spectrometer in positive ionisation mode. IR spectra were recorded on a PerkinElmer Spectrum 100 FT-IR spectrometer. Microanalyses data were obtained using a CE Instruments EA1110 elemental analyser. UV-Vis spectra were performed using a Varian Cary 5000 UV-Vis spectrometer. CD and LD spectra were recorded on a Jasco J-810 spectropolarimeter.

2.8.2 Synthesis of Parent cylinder, $[Fe_2L^P_3][BF_4]_4$[11]

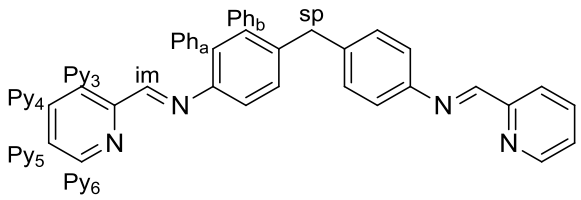

$[Fe_2(C_{25}H_{20}N_4)_3][BF_4]_4$
FW: 1588.29

To a solution of 2-pyridinecarboxaldehyde (0.021 g, 0.20 mmol) in ethanol (1 ml) was added a solution of 4,4'-methylenedianiline (0.019 g, 0.10 mmol) in ethanol (1.5 ml) dropwise. A solution of iron(II) tetrafluoroborate hexahydrate (0.022 g, 0.07 mmol) in

ethanol (0.5 ml) was then immediately added dropwise and the reaction mixture stirred overnight at room temperature. The resulting purple precipitate was collected by vacuum filtration, washed with chloroform (1 L), diethyl ether (200 ml) and dried for 12 hours over silica, yielding a light purple solid (0.042 g, 81% yield).

^{1}H NMR (300 MHz, CD_3CN): δ 8.90 (s, 2H, H_{im}), 8.55 (dd, *J* = 7.7, 0.7 Hz, 2H, H_{Py3}), 8.38 (td, *J* = 7.7, 1.2 Hz, 2H, H_{Py4}), 7.78 – 7.70 (m, 2H, H_{Py5}), 7.32 (d, *J* = 5.4 Hz, 2H, H_{Py6}), 6.95 (br s, 4H, $H_{Pha/\ Phb}$), 5.52 (br s, 4H, $H_{Pha/\ Phb}$), 4.01 (s, 2H, H_{sp}).

Mass spectrum (ESI): *m/z* = 310.5 $[Fe_2(C_{25}H_{20}N_4)_3]^{4+}$, 414.4 $[Fe_2(C_{25}H_{20}N_4)_3]^{3+}$, 621.1 $[Fe_2(C_{25}H_{20}N_4)_3]^{2+}$.

IR (ν) = 3040 (m, C-H), 2908 (m, C-H), 1614 (m, C≡C), 1585 (m, C=C), 1034 (s, br, BF_4).

UV-Vis (H_2O): λ_{max} [nm] (ε_{max}/$dm^3mol^{-1}cm^{-1}$): 236 (47,400), 277 (46,100), 324 (20,000), 525 sh (8,000), 573 (10,800).

2.8.3 Synthesis of Triple Bond cylinder, $[Fe_2L^{TB}{}_3][BF_4]_4$

2.8.3.1 Synthesis of 5-[(trimethylsily)ethynyl]-2-pyridinecarboxaldehyde (1) [12]

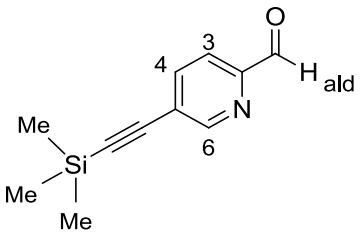

$C_{11}H_{13}NOSi$
FW: 203.32

A schlenk flask was charged with 5-bromo-2-pyridinecarboxaldehyde (0.401 g, 2.16 mmol), bis(triphenylphosphine)dichloropalladium(II) (0.058 g, 0.08 mmol), copper iodide (0.033 g, 0.17 mmol) and triphenylphosphine (0.047 g, 0.18 mmol). Anhydrous THF (8

ml), triethylamine (8 ml) and trimethylsilylacetylene (0.42 ml, 2.97 mmol) were added, and the reaction mixture stirred under an argon atmosphere with light exclusion at 80°C for 5 hours. The resulting dark brown crude mixture was evaporated to dryness *in vacuo* and purified by column chromatography on a silica column (DCM). To remove the triphenylphosphine oxide impurity, diethyl ether and 2 M HCl were added to the pale yellow solid, the layers were separated and the aqueous layer washed again with diethyl ether. The aqueous layer was neutralised with aqueous saturated $NaHCO_3$ and extracted with ethyl acetate. The ethyl acetate was dried over Na_2SO_4 and evaporated *in vacuo* yielding an off-white solid (0.399g, 91% yield).

^{1}H NMR (300 MHz, $CDCl_3$): δ 10.05 (s, 1H, H_{ald}), 8.79 (t, J = 1.4 Hz, 1H, H_6), 7.89 - 7.88 (m, 2H, H_3, H_4), 0.26 (s, 9H, H_{Me}).

HRMS (EI): *m/z* = calculated for $C_{11}H_{13}NOSi$ $[M]^+$ 203.0766; Found 203.0773.

IR (ν) = 3039 (m, C-H), 2964 (m, C-H), 2824 (m, C-H), 2158 (s, C≡C), 1709 (s, C=O), 1576 (m, C=C).

2.8.3.2 Synthesis of 5-ethynyl-2-pyridinecarboxaldehyde (2) [12]

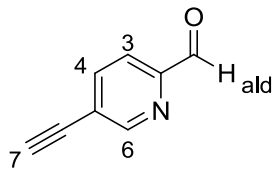

C_8H_5NO
FW: 131.13

To a solution of 5-[(trimethylsily)ethynyl]-2-pyridinecarboxaldehyde (1) (0.254 g, 0.12 mmol) in methanol (15 ml) was added potassium carbonate (0.021 g, 0.15 mmol) and the reaction mixture was stirred for 5 hours at room temperature. Ethyl acetate was added and

the solution was washed twice with water, twice with brine and dried over $MgSO_4$. After evaporation of the solvent, the crude mixture was purified by column chromatography on a silica column (DCM) yielding an off-white solid (0.102 g, 62% yield).

^{1}H NMR (300 MHz, $CDCl_3$): δ 10.04 (s, 1H, H_{ald}), 8.84 – 8.80 (m, 1H, H_6), 7.91 - 7.90 (m, 2H, H_3, H_4), 3.43 (s, 1H, H_7).

^{13}C NMR (100 MHz, $CDCl_3$): δ192.4 (C_{ald}), 153.0 (C_6), 151.4 (C_q), 140.0 ($C_{3/4}$), 120.8 ($C_{3/4}$), 84.0 (C_7), 79.7 (C_q).

HRMS (EI): *m/z* = calculated for C_8H_5NO $[M]^+$ 131.0371; Found 131.0368.

IR (ν) = 3210 (s, C≡C-H), 3086 (m, C-H), 2104 (s, C≡C), 1689 (s, C=O), 1580 (m, C=C).

Elemental analysis (%) calculated for C_8H_5NO: C: 73.3; H: 3.8; N: 10.7; Found: C: 73.1; H: 3.7; N: 10.6.

2.8.3.3 Synthesis of $[Fe_2L^{TB}_3][BF_4]_4$

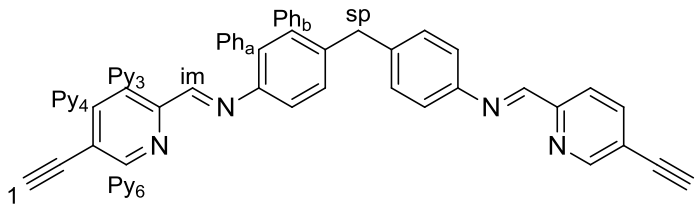

$[Fe_2(C_{29}H_{20}N_4)_3][BF_4]_4$
FW: 1732.42

To a solution of 5-ethynyl-2-pyridinecarboxaldehyde (2) (0.040 g, 0.31 mmol) in ethanol (1 ml) was added a solution of 4,4'-methylenedianiline (0.030 g, 0.15 mmol) in ethanol (1.5 ml) dropwise. A solution of iron(II) tetrafluoroborate hexahydrate (0.034 g, 0.10 mmol) in ethanol (0.5 ml) was then immediately added dropwise and the reaction mixture stirred overnight at room temperature. The resulting purple precipitate was collected by

vacuum filtration, washed with chloroform (1 L), diethyl ether (200 ml) and dried for 12 hours over silica, yielding a light purple solid (0.064 g, 73% yield).

^{1}H NMR (300 MHz, CD_3CN): δ 9.13 (s, 2H, H_{im}), 8.61 (d, *J* = 7.9 Hz, 2H, H_{Py3}), 8.44 (d, *J* = 7.9 Hz, 2H, H_{Py4}), 7.57 (s, 2H, H_{Py6}), 6.94 (br s, 4H, $H_{Pha/\ Phb}$), 5.50 (br s, 4H, $H_{Pha/\ Phb}$), 4.05 (s, 2H, H_{sp}), 3.98 (s, 2H, H_1).

Mass spectrum (ESI): *m/z* = 346.2 $[Fe_2(C_{29}H_{20}N_4)_3]^{4+}$, 461.9 $[Fe_2(C_{29}H_{20}N_4)_3]^{3+}$.

IR (ν) = 3041 (w, C-H), 2116 (s, C≡C), 1597 (m, C=C), 1546 (m, C=C), 1051 (s, br, BF_4).

UV-Vis (MeOH): λ_{max} [nm] (ε_{max}/$dm^3mol^{-1}cm^{-1}$): 276 sh (51,900), 302 (78,000), 533 sh (10,200), 591 (14,400).

2.8.4 Synthesis of Propargyl Alcohol cylinder, $[Fe_2L^{PA}{}_3][BF_4]_4$

2.8.4.1 Synthesis of 5-(3-hydroxyprop-1-ynyl)-2-pyridinecarboxaldehyde (3)

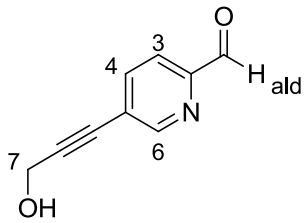

$C_9H_7NO_2$
FW: 161.16

A schlenk flask was charged with 5-bromo-2-pyridinecarboxaldehyde (0.801 g, 4.31 mmol), bis(triphenylphosphine)dichloropalladium(II) (0.115 g, 0.16 mmol), copper iodide (0.061 g, 0.32 mmol) and triphenylphosphine (0.085 g, 0.32 mmol). Anhydrous THF (11 ml), triethylamine (16 ml) and propargyl alcohol (0.29 ml, 4.98 mmol) were added, and the reaction mixture stirred under an argon atmosphere with light exclusion at 80°C for 5 hours. The resulting dark brown crude mixture was evaporated to dryness *in vacuo* and

purified by column chromatography on a silica column (MeOH:DCM 5:95). To remove the triphenylphosphine oxide impurity, diethyl ether and 2 M HCl were added to the pale yellow solid obtained, the layers were separated and the aqueous layer washed again with diethyl ether. The aqueous layer was neutralised with aqueous saturated $NaHCO_3$ and extracted with ethyl acetate. The ethyl acetate was dried over Na_2SO_4 and evaporated *in vacuo* yielding an off-white solid (0.404 g, 58% yield).

^{1}H NMR (300 MHz, $CDCl_3$): δ 10.05 (s, 1H, H_{ald}), 8.82 - 8.81 (m, 1H, H_6), 7.92 – 7.85 (m, 2H, H_3, H_4), 4.55 (s, 2H, H_7).

^{13}C NMR (100 MHz, $CDCl_3$): δ192.2 (C_{ald}), 152.4 (C_6), 139.6 ($C_{3/4}$), 121.1 ($C_{3/4}$), 51.2 (C_7).

HRMS (EI): *m/z* = calculated for $C_9H_7NO_2$ $[M]^+$ 161.0477; Found 161.0472.

IR (ν) = 3229 (br, OH), 2854 (m, C-H), 2242 (s, C≡C), 1707 (s, C=O), 1582 (m, C=C).

2.8.4.2 Synthesis of $[Fe_2L^{PA}{}_3][BF_4]_4$

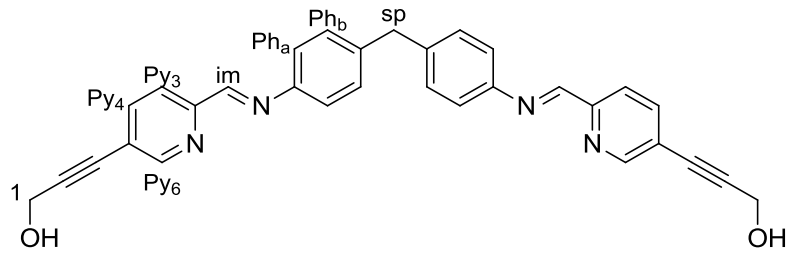

$[Fe_2(C_{31}H_{24}N_4O_2)_3][BF_4]_4$
FW: 1912.58

To a solution of 5-(3-hydroxyprop-1-ynyl)-2-pyridinecarboxaldehyde (3) (0.030 g, 0.19 mmol) in ethanol (1 ml) was added a solution of 4,4'-methylenedianiline (0.018 g, 0.09

mmol) in ethanol (1.5 ml) dropwise. A solution of iron(II) tetrafluoroborate hexahydrate (0.021 g, 0.06 mmol) in ethanol (0.5 ml) was then immediately added dropwise and the reaction mixture stirred overnight at room temperature. The resulting purple precipitate was collected by vacuum filtration, washed with chloroform (1 L), diethyl ether (200 ml) and dried for 12 hours over silica, yielding a light purple solid (0.057 g, 96% yield).

^{1}H NMR (300 MHz, CD_3CN): δ 9.00 (s, 2H, H_{im}), 8.55 (d, *J* = 7.9 Hz, 2H, H_{Py3}), 8.37 (d, *J* = 7.9 Hz, 2H, H_{Py4}), 7.48 (s, 2H, H_{Py6}), 6.94 (br s, 4H, $H_{Pha/\ Phb}$), 5.49 (br s, 4H, $H_{Pha/\ Phb}$), 4.40 (d, *J* = 5.5 Hz, 4H, H_1), 4.03 (s, 2H, H_{sp}).

Mass spectrum (ESI): *m/z* = 391.4 $[Fe_2(C_{31}H_{24}N_4O_2)_3]^{4+}$, 521.5 $[Fe_2(C_{31}H_{24}N_4O_2)_3]^{3+}$, 781.8 $[Fe_2(C_{31}H_{24}N_4O_2)_3]^{2+}$.

IR (ν) = 3322 (br, OH), 2221 (s, C≡C), 1594 (m, C=C), 1543 (m, C=C), 1016 (s, br, BF_4).

UV-Vis (MeOH): λ_{max} [nm] (ε_{max}/$dm^3mol^{-1}cm^{-1}$): 235 (56,500), 277 sh (39,000), 311 (55,600), 538 sh (4,700), 591(6,300).

2.8.5 Synthesis of Hexyn-ol Cylinder, $[Fe_2L^{Hex}_3][BF_4]_4$

2.8.5.1 Synthesis of 5-(hex-5-yn-1-ol)-2-pyridinecarboxaldehyde (4)

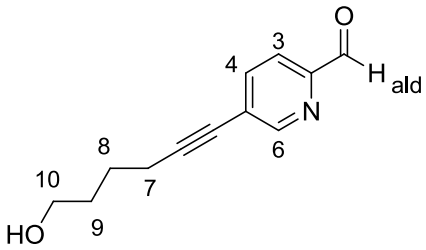

$C_{12}H_{13}NO_2$
FW: 203.24

A schlenk flask was charged with 5-bromo-2-pyridinecarboxaldehyde (0.200 g, 1.08 mmol), bis(triphenylphosphine)dichloropalladium(II) (0.030 g, 0.04 mmol) and copper iodide (0.017 g, 0.09 mmol). 5-Hexyn-1-ol (0.11 ml, 1.00 mmol), anhydrous THF (35 ml) and diisopropylamine (0.63 ml) were added, and the reaction mixture stirred under an argon atmosphere with light exclusion, at room temperature, for 72 hours. The resulting dark brown crude mixture was evaporated to dryness *in vacuo* and purified by column chromatography on a silica column (MeOH:DCM 2:98). The resulting off-white solid was dissolved in diethyl ether and purified by column chromatography on a short silica column (diethyl ether) to remove the triphenylphosphine oxide impurity. Evaporation of the solvent yielded an off-white solid (0.092 g, 42% yield).

^{1}H NMR (300 MHz, $CDCl_3$): δ10.04 (s, 1H, H_{ald}), 8.74 - 8.73 (m, 1H, H_6), 7.89 – 7.79 (m, 2H, H_3, H_4), 3.73 – 3.69 (m, 2H, H_{10}), 2.54 – 2.48 (m, 2H, H_7), 1.76 – 1.71 (m, 4H, H_8, H_9).

^{13}C NMR (100 MHz, $CDCl_3$): δ 192.6 (C_{ald}), 152.5 (C_6), 139.5 (C_3), 120.7 (C_4), 61.8 (C_7), 31.7 ($C_{8/9}$), 24.6 ($C_{8/9}$), 19.4 (C_{10}).

HRMS (EI): *m/z* = calculated for $C_{12}H_{13}NO_2$ $[M]^+$ 203.0946; Found 203.0945.

IR (ν) = 3164 (br, OH), 2945 (m, C-H), 2861 (m, C-H), 2222 (s, C≡C), 1710 (s, C=O), 1580 (m, C=C).

2.8.5.2 Synthesis of $[Fe_2L^{Hex}{}_3][BF_4]_4$

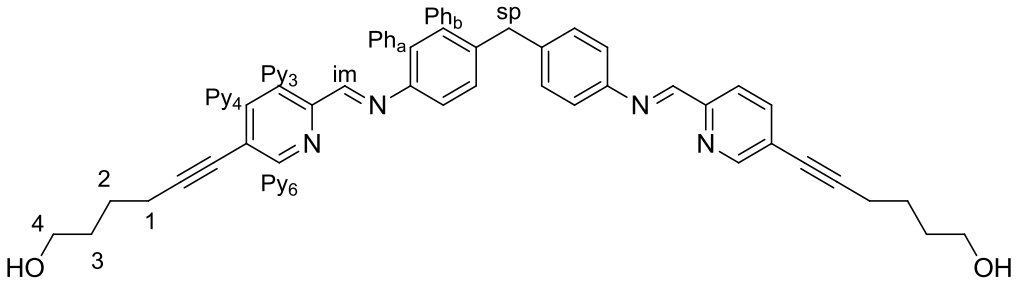

$[Fe_2(C_{37}H_{36}N_4O_2)_3][BF_4]_4$
FW: 2165.06

To a solution of 5-(hex-5-yn-1-ol)-2-pyridinecarboxaldehyde (4) (0.138 g, 0.68 mmol) in ethanol (2.5 ml) was added a solution of 4,4'-methylenedianiline (0.068 g, 0.34 mmol) in ethanol (4 ml) dropwise. A solution of iron(II) tetrafluoroborate hexahydrate (0.076 g, 0.23 mmol) in ethanol (1.5 ml) was then immediately added dropwise and the reaction mixture stirred overnight at room temperature. The resulting purple precipitate was collected by vacuum filtration, washed with chloroform (1.5 L), diethyl ether (200 ml) and dried for 12 hours over silica, yielding a dark purple solid (0.143 g, 58% yield).

^{1}H NMR (300 MHz, CD_3CN): δ 8.95 (s, 2H, H_{im}), 8.50 (d, *J* = 7.9 Hz, 2H, H_{Py3}), 8.30 (d, *J* = 7.9 Hz, 2H, H_{Py4}), 7.34 (s, 2H, H_{Py6}), 6.92 (br s, 4H, $H_{Pha/Phb}$), 5.50 (br s, 4H, $H_{Pha/Phb}$), 4.02 (s, 2H, H_{sp}), 3.54 – 3.52 (m, 4H, H_4), 2.68 (s, 2H, H_{OH}), 2.49 (t, *J* = 6.2 Hz, 4H, H_1), 1.63 – 1.61 (m, 8H, H_2, H_3).

Mass spectrum (ESI): *m/z* = 454.6 $[Fe_2(C_{37}H_{36}N_4O_2)_3]^{4+}$, 605.8 $[Fe_2(C_{37}H_{36}N_4O_2)_3]^{3+}$, 908.2 $[Fe_2(C_{37}H_{36}N_4O_2)_3]^{2+}$.

IR (ν) = 3365 (br, OH), 2934 (w, C-H), 2225 (s, C≡C), 1594 (m, C=C), 1542 (m, C=C), 1016 (s, br, BF_4).

UV-Vis (MeOH): λ_{max} [nm] (ε_{max}/$dm^3mol^{-1}cm^{-1}$): 237 (121,800), 276 sh (53,700), 318 (116,200), 534 sh (11,400), 589 (16,500).

2.8.6 Synthesis of Phenyl Cylinder, $[Fe_2L^{Phen}{}_3][BF_4]_4$

2.8.6.1 Synthesis of 5-(ethynylphenyl)-2-pyridinecarboxaldehyde (5)

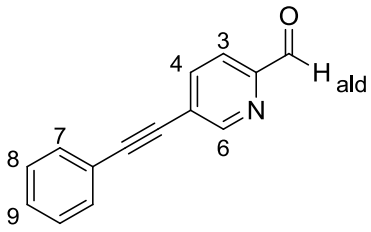

$C_{14}H_9NO$
FW: 207.23

A schlenk flask was charged with 5-bromo-2-pyridinecarboxaldehyde (0.201 g, 1.08 mmol), bis(triphenylphosphine)dichloropalladium(II) (0.031 g, 0.04 mmol) and copper iodide (0.016 g, 0.08 mmol). Phenylacetylene (0.12 ml, 1.06 mmol), anhydrous THF (35 ml) and diisopropylamine (0.63 ml) were added, and the reaction mixture stirred under an argon atmosphere with light exclusion, at room temperature, for 72 hours. The resulting dark brown crude mixture was evaporated to dryness *in vacuo* and purified by column chromatography on a silica column (DCM). The resulting pale brown solid was dissolved in diethyl ether and purified by column chromatography on a short silica column (diethyl ether) to remove the triphenylphosphine oxide impurity. Evaporation of the solvent yielded an off-white solid (0.161 g, 72% yield).

^{1}H NMR (300 MHz, $CDCl_3$): δ 10.1 (s, 1H, H_{ald}), 8.91 – 8.87 (m, 1H, H_6), 7.96 – 7.95 (m, 2H, H_3, H_4), 7.59 – 7.56 (m, 2H, H_7), 7.43 – 7.36 (m, 3H, H_8, H_9).

^{13}C NMR (100 MHz, $CDCl_3$): δ 192.5 (C_{ald}), 152.4 (C_6), 139.2 ($C_{3/4}$), 131.8 (C_7), 129.4 ($C_{8/9}$), 128.5 ($C_{8/9}$), 120.9 ($C_{3/4}$).

HRMS (EI): *m/z* = calculated for $C_{14}H_9NO$ $[M]^+$ 207.0684; Found 207.0673.

IR (ν) = 3000 (w, C-H), 2821 (w, C-H), 2215 (s, C≡C), 1703 (s, C=O), 1576 (m, C=C).

2.8.6.2 Synthesis of $[Fe_2L^{Phen}{}_3][BF_4]_4$

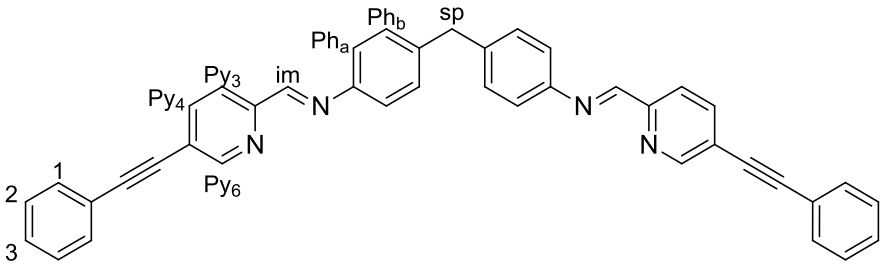

$[Fe_2(C_{41}H_{28}N_4)_3][BF_4]_4$
FW: 2189.00

To a solution of 5-(ethynylphenyl)-2-pyridinecarboxaldehyde (5) (0.107 g, 0.52 mmol) in ethanol (3 ml) was added a solution of 4,4'-methylenedianiline (0.051 g, 0.26 mmol) in ethanol (2 ml) dropwise. A solution of iron(II) tetrafluoroborate hexahydrate (0.058 g, 0.17 mmol) in ethanol (2 ml) was then immediately added dropwise and the reaction mixture stirred overnight at room temperature. The resulting purple precipitate was collected by vacuum filtration, washed with chloroform (1 L), diethyl ether (200 ml) and dried for 12 hours over silica, yielding a dark purple solid (0.039 g, 21% yield).

^{1}H NMR (300 MHz, CD_3CN): δ 9.07 (s, 2H, H_{im}), 8.62 (d, *J* = 7.9 Hz, 2H, H_{Py3}), 8.49 (d, *J* = 7.9 Hz, 2H H_{Py4}), 7.67 (s, 2H, H_{Py6}), 7.57 (d, *J* = 6.8 Hz, 4H, H_1), 7.50 – 7.47 (m, 6H, H_2, H_3), 6.97 (br s, 4H, $H_{Pha/\ Phb}$), 5.55 (br s, 4H, $H_{Pha/\ Phb}$), 4.06 (s, 2H, H_{sp}).

Mass spectrum (ESI): *m/z* = 460.3 $[Fe_2(C_{41}H_{28}N_4)_3]^{4+}$.

IR (ν) = 3035 (w, C-H), 2219 (s, C≡C), 1597 (m, C=C), 1545 (m, C=C), 1056 (s, br, BF_4).

UV-Vis (MeCN): λ_{max} [nm] (ε_{max}/$dm^3mol^{-1}cm^{-1}$): 231 (106,700), 261 sh (107,000), 354 (148,100), 596 (17,400).

2.9 Experimental: DNA binding studies

2.9.1 Materials and methods

All DNA binding studies were carried out using Ultrapure water (18.2 MΩ) purchased from Fisher Scientific. Calf thymus (ct-) DNA, highly polymerised, was purchased from Sigma Aldrich and pBR322 plasmid DNA was purchased from New England Biolabs. Both were used without further purification and kept frozen. Tris-acetate-EDTA buffer was purchased from Fisher and agarose from USB Corporation.

2.9.2 Circular and Linear Dichroism Experiments

CD and LD measurements were recorded using a Jasco J-810 spectropolarimeter. CD measurements were carried out in quartz cuvettes of 1cm (750-200 nm) or 0.1 cm (450-200 nm) pathlength. LD experiments were recorded in a flow couette cell (Krometek) with a 0.1 cm pathlength.

Stock solutions of ct-DNA (3000 μM) in water were prepared and kept frozen until the day of the experiment. Sodium chloride (1 M) and sodium cacodylate ($Na(CH_2)_2AsO_2.3H_2O$) (100 mM) buffer stock solutions were used to prepare final ct-DNA solutions of 300 μM with 20 mM NaCl and 1 mM sodium cacodylate (pH 6.8). DNA concentrations were determined by UV-Vis measurements using the known molar extinction coefficient of ε_{258} = 6600 $mol^{-1}dm^3cm^{-1}$ per DNA base.

CD and LD titrations were carried out using three solutions; solution A (a 300 μM ct-DNA solution, containing NaCl (20 mM) and sodium cacodylate (1 mM)); solution B (a 500 μM complex solution) and solution C (a 600 μM ct-DNA solution, containing 40 mM NaCl and sodium cacodylate (2 mM)). Firstly solution A was recorded, then equal aliquots of solutions B and C were added, keeping the concentration of ct-DNA constant throughout the titration. The titration was carried out to obtain an initial ct-DNA:complex ratio of 60:1 decreasing to 4:1. The stock solution of complex was stored in ice during the experiment.

2.9.3 Agarose Gel Electrophoresis

Agarose gels were prepared by warming agarose (2 g) in 1x Tris-acetate-EDTA buffer which was then poured into a gel tray (210 x 150 mm) fitted with a 15 toothed comb, to produce sample wells. The gel was left to set for 40 minutes. Sample solutions (16 μl) were prepared containing 96.3 μM pBR322 plasmid DNA and different concentrations of complexes (from 60 μM stock solution in water and up to 7% MeOH or MeCN) to obtain plasmid:complex ratios ranging from 100:1 to 2:1. These sample solutions were incubated for 2 hours at room temperature. Before loading , 4 μl loading buffer (30% glycerol, 0.25%

bromophenol blue) was added, the samples were mixed and then 16 µl of the samples loaded into the gel wells. The gel was run for 2.5 hours in an Amersham Biosciences HE99X Maxi submarine kit with an electrophoresis Power Supply-EPS 301 system, at a constant voltage of 120 V and 400 mA, in 1x Tris-acetate-EDTA running buffer. The gel was then stained with an ethidium bromide solution (0.5 $mg.ml^{-1}$) in 200 ml of water for 20 minutes and visualised using a UVtec–uvipro platinum 2.0 system (UVidoc, Cambridge, UK) at 312 nm.

2.9.4 Polyacrylamide Gel Electrophoresis (PAGE)

Procedure provided by S. Phongtongpasuk [3] and carried out by N. Calle Alonso, both of the Hannon group, University of Birmingham.

2.9.4.1 Radioactive labelling

Oligonucleotides (sequences S1: CGGAACGGCACTCG, S2: CGAGTGCAGCGTGG, S3: CCACGCTCGTTCCG) were purchased from MWG Eurofin. One strand was labelled with ^{32}P at the 5' terminus using T4 polynucleotide kinase (New England Biolabs) and [γ-^{32}P] adenosine 5'-triphosphate (Perkin Elmer). First ultrapure water (4.8 µl), 10x bacteriophage T4 polynucleotide kinase buffer (1 µl), oligonucleotide S3 (1.2 µl of 100 µM), bacteriophage T4 polynucleotide kinase (1 µl) (New England Biolabs) and γ-^{32}P ATP (2 µl of 6000 Ci/mmol) (Perkin Elmer) were incubated in an eppendorf at 37°C for 40 minutes. To deactivate the polynucleotide kinase, the solution was then heated to 80°C for 3 minutes.

To purify the radioactive-labelled DNA fragments from any unreacted ATP a QIAquick

nucleotide removal kit (QIAGEN) was employed. 10 volumes of PN buffer were added to 1 volume of reaction sample and this solution was loaded onto a QIAquick spin column with a 2ml collection tube, centrifuged for 1 minute at 6000 rpm and the flow through discarded. A new collection tube was then fitted to the column, PE buffer (500 µl) was added and this solution was centrifuged for 1 minute at 6000 rpm and the flow through discarded. Again, PE buffer (500 µl) was added and the solution was centrifuged at 13000 rpm for 1 minute to remove residual buffer. The column was then put into a fresh eppendorf, ultrapure water (30 µl) was added to the column and this was left for 5 minutes. After centrifuging at 13000 rpm for 2 minutes a radiolabelled DNA stock solution (8 µM) was obtained.

2.9.4.2 Polyacrylamide gel preparation

A 15% native polyacrylamide gel was prepared by mixing 52.5 ml of ultra pure water, 10 ml of 10x TB buffer (890 mM tris(hydroxymethy)amino methane and 890 mM boric acid) (pH 8.3), 37.5 ml of 40% acrylamide (29:1) (Geneflow), 500 µl of 10% (w/v) ammonium persulfate and 75 µl tetramethylenediamine (TEMED). This was then poured onto a set of glass plates and left to set for 40 minutes. The wells of the polymerised gel were washed with running buffer (TB buffer) and the gel was pre-run at 200 V for 5 minutes before sample loading.

2.9.4.3 PAGE electrophoresis experiment

Sample solutions were prepared by mixing solutions of the complexes with stoichiometric amounts of oligonucleotides in TBN buffer (89 mM tris(hydroxymethy)amino methane, 89

mM of boric acid and 100 µM NaCl) (pH 8.3) to give final concentrations of 0.4 µM for each single strand (1.2 µM total concentration of DNA) and 0.4 µM of complex. This gives a three-way junction:complex ratio of 1:1. The sample solutions were incubated for 1 hour at room temperature and then in ice for 15 minutes. To prepare the samples for loading, 5 µl of 30% glycerol was added to each eppendorf. 13 µl of each sample was then loaded onto the 15% polyacrylamide gel. The gel was run for 4 hours at 120 V using Gel System equipment (Thermo Scientific UK). It was then exposed on a phosphor imaging plate for 1-16 hours depending on how fresh the radioactive ATP used was. A radiogel image was obtained using a Molecular Imager FX (Bio-Rad) and the gel was quantified using Quantity One software.

2.10 References

(1) Hannon, M. J.; Painting, C. L.; Jackson, A.; Hablin, J.; Errington, W., *Chem. Commun.* **1997**, 1807.

(2) Hotze, A. C.; Hodges, N. J.; Hayden, R. E.; Sanchez-Cano, C.; Paines, C.; Male, N.; Tse, M. K.; Bunce, C. M.; Chipman, J. K.; Hannon, M. J., *Chem. Biol.* **2008**, *15*, 1258.

(3) Phongtongpasuk, S., Investigating the Interaction of a Metallosupramolecular Cylinder With Nucleic Acids, *PhD Thesis, University of Birmingham* **2011**.

(4) Oleksi, A.; Blanco, A. G.; Boer, R.; Usón, I.; Aymamí, J.; Rodger, A.; Hannon, M. J.; Coll, M., *Angew. Chem. Int. Ed.* **2006**, *45*, 1227.

(5) Hannon, M. J.; Moreno, V.; Prieto, M. J.; Moldrheim, E.; Sletten, E.; Meistermann, I.; Isaac, C. J.; Sanders, K. J.; Rodger, A., *Angew. Chem. Int. Ed.* **2001**, *40*, 879.

(6) Malina, J.; Hannon, M. J.; Brabec, V., *Nucleic Acids Res.* **2008**, *36*, 3630.

(7) Cardo, L.; Hannon, M. J., *Inorg. Chim. Acta* **2009**, *362*, 784.

(8) Sonogashira, K.; Tohda, Y.; Hagihara, N., *Tetrahedron Lett.* **1975**, *16*, 4467.

(9) Li, J. J., Name Reactions for Homologation Part 1, *Wiley* **2009**.

(10) Peberdy, J. C.; Malina, J.; Khalid, S.; Hannon, M. J.; Rodger, A., *J. Inorg. Biochem.* **2007**, *101*, 1937.

(11) Pearmund, C. R., Metallo-supramolecular Cylinders as Chemical Nucleases, *PhD Thesis, University of Warwick* **2006**.

(12) Rajadurai, C.; Enkelmann, V.; Zopellaro, G.; Baumgarten, M., *J. Phys. Chem. B* **2007**, *111*, 4327.

(13) Twyman, L. J.; Beezer, A. E.; Esfand, R.; Hardy, M. J.; Mitchell, J. C., *Tetrahedron Lett.* **1999**, *40*, 1743.

(14) Torchilin, V. P., *J. Controlled Release* **2001**, *73*, 137.

(15) Timerbaev, A. R.; Hartinger, C. G.; Keppler, B. K., *TrAC, Trends Anal. Chem.* **2006**, *25*, 868.

(16) Cardo, L., Metallo-supramolecular Cylinders and their Peptide Conjugates. Synthesis, dynamics and DNA recognition, *PhD Thesis, University of Birmingham* **2010**.

(17) Ivanov, V. I.; Minchenkova, L. E.; Schyolkina, A. K.; Poletayev, A. I., *Biopolymers* **1973**, *12*, 89.

(18) Bulheller, B. M.; Rodger, A.; Hirst, J. D., *Phys. Chem. Chem. Phys.* **2007**, *9*, 2020.

(19) Rodger, A.; Norden, B., Circular Dichroism and Linear Dichroism, *Oxford University Press* **1997**.

(20) Warnke, I.; Furche, F., *WIREs: Comput. Mol. Sci.* **2012**, *2*, 150.

(21) Meistermann, I., DNA Major Groove Recognition by Supramolecular Helicates, *PhD Thesis, University of Warwick* **2001**.

(22) Rodger, A.; Marrington, R.; Geeves, M. A.; Hicks, M.; de Alwis, L.; Halsall, D. J.; Dafforn, T. R., *Phys. Chem. Chem. Phys.* **2006**, *8*, 3161.

(23) Wink, M., An Introduction to Molecular Biotechnology. Molecular Fundamentals, Methods and Applications in Modern Biotechnology, *Wiley-VCH* **2006**.

(24) Schvartzman, J. B.; Stasiak, A., *EMBO Rep.* **2004**, *5*, 256.

(25) Kanaar, R.; Cozzarelli, N. R., *Curr. Opin. Struct. Biol.* **1992**, *2*, 369.

(26) Karp, G., Cell and Molecular Biology: Concepts and Experiments, *Wiley* **2009.**

(27) Bellon, S. F.; Coleman, J. H.; Lippard, S. J., *Biochemistry* **1991**, *30*, 8026.

(28) Utsuno, K.; Maeda, Y.; Tsuboi, M., *Chem. Pharm. Bull.* **1999**, *47*, 1363.

(29) Wilson, K.; Walker, J., Principles and Techniques of Biochemistry and Molecular Biology**,** *Cambridge University Press* **2010**.

(30) Rosenberg, I. M., Protein Analysis and Purification: Benchtop Techniques, *Birkhauser* **2005**.

(31) Malina, J.; Hannon, M. J.; Brabec, V., *Chem. Eur. J.* **2007**, *13*, 3871.

(32) Leontis, N. B.; Kwok, W.; Newman, J. S., *Nucleic Acids Res.* **1991**, *19*, 759.

Chapter 3: Steroid Functionalised Metallo-Cylinders

3.1 Introduction and aims

In chapter 2, a novel cylinder functionalisation route was developed which allows the easy and efficient modification of iron(II) cylinders. Several complexes functionalised with simple chemical groups were synthesised and the DNA binding studies of these proved that functionalisation at the ends of the cylinder does not result in a significant loss of DNA binding affinity.

Although the parent and the majority of the second generation cylinders described show DNA binding activity, they all have an inherent disadvantage; their activity and cytotoxicity is not specific to cancerous tissue. *In vitro* studies with the iron(II) parent cylinder and the immortalised non-tumour cell line MRC5 indicated no sensitivity to cancerous tissue, and cytotoxicity to normal cells.[1] It is well known that the anticancer agent cisplatin causes severe side effects such as nephrotoxicity, neurotoxicity, nausea and vomiting.[2] These side effects are due to the non-targeting nature of cisplatin which leads to non-cancerous cells and tissues being damaged.[2] Therefore it can be supposed that if these metallo-cylinders were to be used therapeutically in the clinic, they would also cause side-effects due to their non-specific nature. To overcome this problem the specificity of metallo-cylinders to tumour cells must be improved.

3.1.1 Drug targeting strategies

Many strategies have been developed to target therapeutic drugs to cancerous tissues. Passive targeting is common, with the development of drugs bound to polymers, liposomes, dendrimers or other macromolecular carriers to allow concentration and retention of the drug in tumour tissue.[3] Receptor mediated targeting is another strategy, in which receptors that are overexpressed can be used to deliver drugs to specific cancerous tissues and organs.[3] Known biomolecules with receptors overexpressed by cancerous cells include folic acid, oncofoetal proteins, peptides, carbohydrates and steroids (Fig. 3.1).[3,4] Drug-biomolecule conjugates that retain a high affinity for the corresponding receptor will be preferentially delivered and accumulated into the cells that overexpress this receptor, by endocytosis.[4]

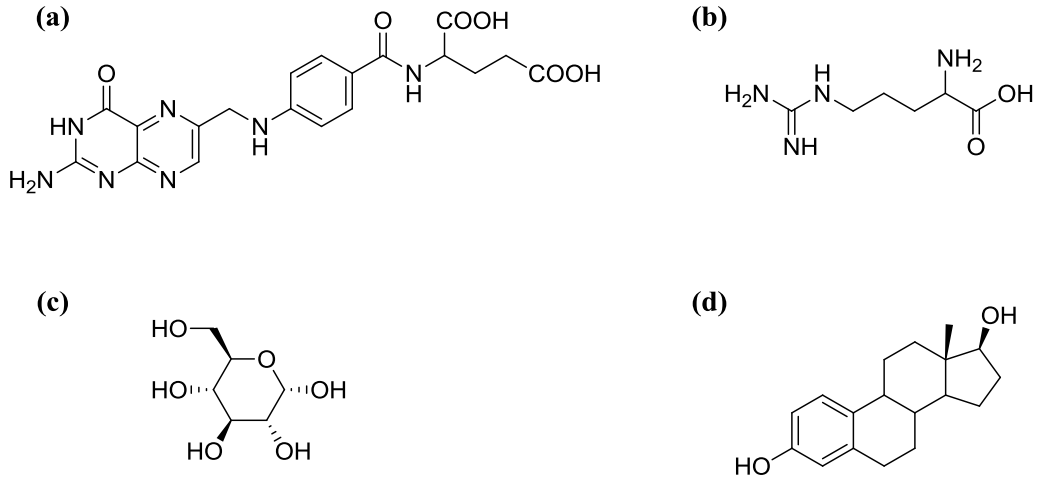

Figure 3.1 Structure of (a) folic acid; (b) arginine; (c) D-glucose; (d) estrogen.

3.1.1.1 Biomolecule conjugated supramolecular cylinders

Peptides are one type of biomolecule that can be used in the targeted delivery of drugs. Cell-penetrating peptides are short sequences of peptides that can cross the plasma

membrane and cell-targeting peptides have specificity to certain cell lines and enter the cell via receptor mediated endocytosis.[5]

Several metallo-cylinders conjugated to short peptide fragments have been developed by Cardo of the Hannon group.[6,7] These cylinders were designed to have enhanced cellular uptake and increased specificity towards certain DNA base sequences.[6,7] The first peptide conjugated cylinders to be developed were functionalised with a glycine-glycine-serine tripeptide sequence (Fig. 3.2).[6] Both the iron(II) cylinder, $[Fe_2L^a_3]^{4+}$, and the copper(I) cylinder, $[Cu_2L^a_2]^{2+}$, showed that the inherent DNA binding activity of the cylinder had been retained.[6]

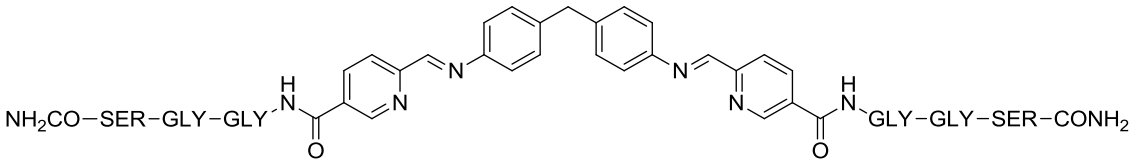

Figure 3.2 Structure of L^a ligand of complex $[Fe_2L^a_3]^{4+}$.[6]

An iron(II) cylinder conjugated to arginine, $[Fe_2L^b_3]^{4+}$ (Fig. 3.3), was also developed and was found to have good DNA binding activity and could stabilise DNA three-way junctions.[7] The complex was also shown to have potent cytotoxicity in an ovarian cancer cell line.[7]

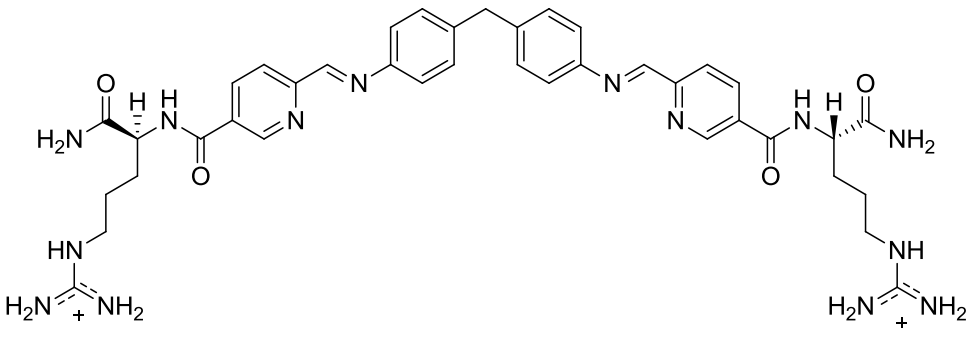

Figure 3.3 Structure of L^b ligand of complex $[Fe_2L^b_3]^{4+}$.[7]

These peptide functionalised helicates show promising DNA binding activity and the arginine conjugate shows potent cytotoxicity, however the synthesis of these complexes has many reaction steps and the iron(II) cylinders possess very poor stability, with the $[Fe_2L^a_3]^{4+}$ complex only being stable for two hours.[6]

Steroid hormones can also be used to facilitate the delivery of cytotoxic drugs, as many hormone-dependant cancers overexpress steroid receptors, and these can be targeted by steroid-drug conjugates. The estrogen receptor (ER) is overexpressed in 60-75% of breast cancer tumours[8] and the androgen receptor, for testosterone conjugates, is overexpressed in approximately 80% of breast[9,10,11], 74-90% of ovarian[12,13,14] and in all prostate tumours.[15,16,17]

Steroid functionalised anticancer agents have previously been reported by the Hannon group.[18,19] Examples include an estrogen-functionalised platinum(II) terpyridine complex and a platinum(II)-testosterone conjugate (Fig. 3.4).[18,19] Cellular uptake and cytotoxicity studies showed that the steroid conjugates retained their receptor binding affinities and were delivered across the cell membrane into tumour cells with the corresponding steroid receptor.[18,19] The uptake of these complexes was much higher than their non-steroidal analogues. 80-100% of the estrogen-Pt(II)-terpyridine complex was taken up by cells displaying the estrogen receptor (ERα+) compared to only 25% for the non-steroidal analogue.[18,19] Both complexes showed potent cytotoxicity against ovarian and breast cancer cell lines, with the platinum(II)-testosterone conjugate showing better activity than its non-steroidal analogue.[18,19]

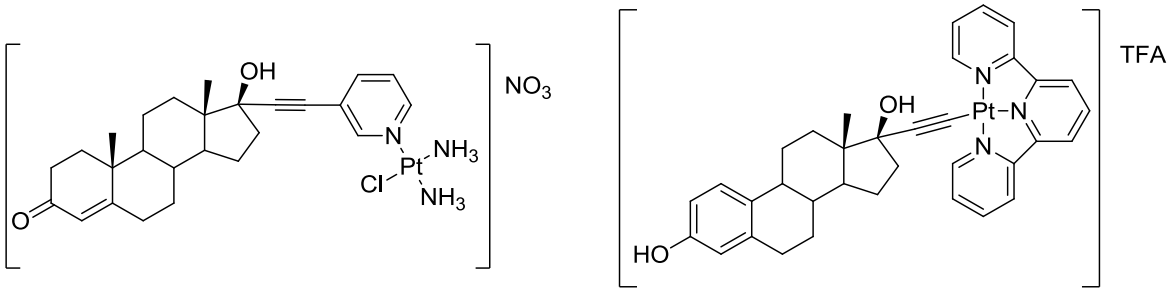

Figure 3.4 Structure of platinum(II)-testosterone conjugate (left) and estrogen-functionalised platinum(II) terpyridine complex (right).[18,19]

3.1.2 Conjugation of chiral substituents and biomolecules

As previously mentioned (Section 1.5.2, Chapter 1), the introduction of chiral substituents onto helicate ligands can force the stereoselectivity of the helicate, known as chiral induction.[20,21] Many biomolecules have stereogenic centres and so functionalisation with these moieties might lead to enantiopure helicates.

The inducement of chirality to these iron(II) helicates by chiral substituents has previously been observed in the development of Cardo's peptide-conjugated cylinders (Section 3.1.1.1).[6,7] The conjugation of L-arginine (Fig. 3.5) to the cylinder resulted in the formation of a diastereoisomerically pure helicate of the P configuration and the conjugation of D-arginine resulted in a diastereoisomerically pure helicate of the M configuration.[7]

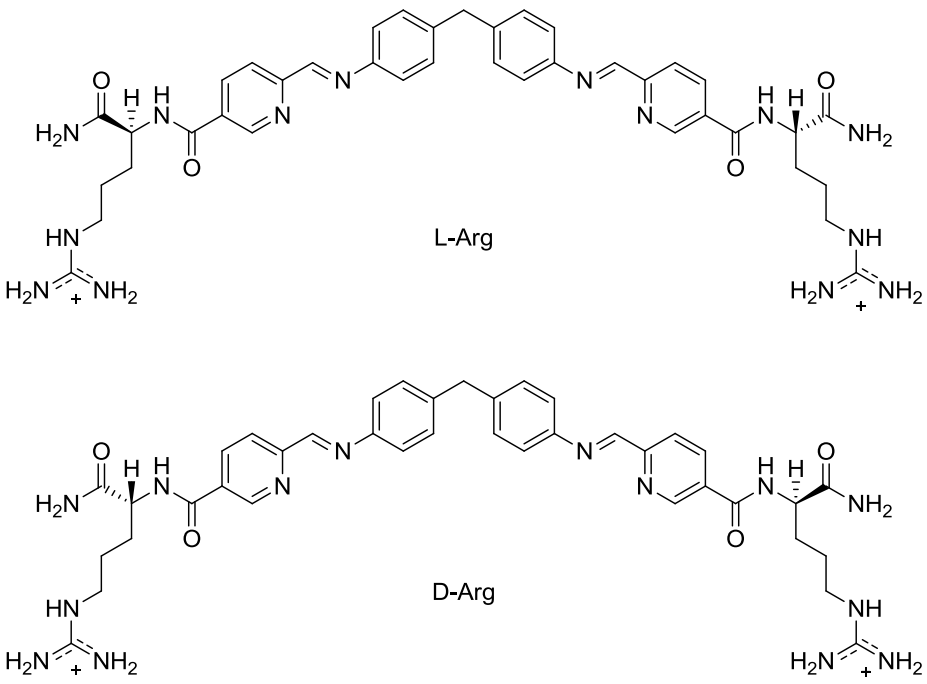

Figure 3.5 Structure of ligands conjugated to L-arginine (top) and D-arginine (bottom).[7]

The chirality of a DNA-binding agent will influence its ability to bind to DNA, as DNA is also chiral. This was observed with the peptide cylinders, as both diastereoisomers were found to bind to and stabilise DNA three-way junctions more than the parent cylinder, and the D-arginine conjugate (M helical isomer) showed stronger binding than the L-arginine conjugate (P helical isomer).[7]

3.2 Molecular design

As the steroid hormone-platinum(II) conjugates described previously (Section 3.1.1.1) showed good activity and selectivity, it was thought that a supramolecular cylinder functionalised with steroid hormones may also possess the same properties. To synthesise these biomolecule-conjugated cylinders the novel functionalisation route, detailed and

employed in chapter 2, offers a straightforward synthesis route with few reaction steps. As estrogen and testosterone steroid hormones conjugated with alkyne groups, estradiol and ethisterone respectively, are already commercially available, the synthesis route will have fewer steps. Two iron(II) cylinders were designed that were functionalised with testosterone and estrogen hormones, $[Fe_2L^{Test}{}_3]^{4+}$ and $[Fe_2L^{Estro}{}_3]^{4+}$ respectively (Fig. 3.6). The 5-position of the pyridine ring was chosen as the modification site, as for the functionalised cylinders developed in Chapter 2, so as not to effect the cylinder formation or significantly reduce the DNA affinity of the synthesised cylinders. By positioning the hormones at the ends of the cylinder, and attaching them at the 17α position, it was hoped that the hormone-receptor binding affinity would be retained, allowing delivery of the conjugates across the cell membrane.

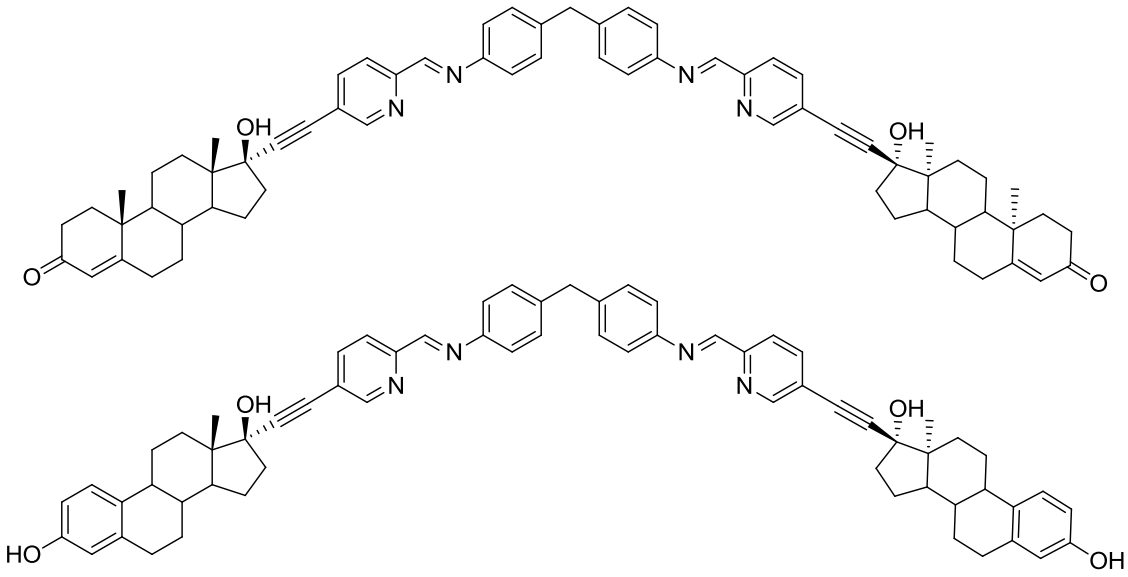

Figure 3.6 Structure of ligands L^{Test} (top) and L^{Estro} (bottom).

As these steroid hormones have multiple stereogenic centres, their effect on the chirality of the cylinder when conjugated must be considered. Once synthesised, the chirality of the

designed steroid-functionalised cylinders will be investigated to see whether any chiral induction is observed.

3.3 Synthesis

3.3.1 Synthesis of testosterone cylinder, $[Fe_2L^{Test}_3][BF_4]_4$

3.3.1.1 Synthesis of 17α-[(2-pyridinecarboxaldehyde)-5-ethynyl]ethisterone (6)

As 17α-[(2-pyridinecarboxaldehyde)-5-ethynyl]ethisterone (6) is not commercially available it was synthesised, with the synthesis based on a literature procedure.[22] Sonogashira coupling was employed to couple 5-bromo-2-pyridinecarboxaldehyde to 17α-ethynyltestosterone using the catalysts copper iodide and bis(triphenylphosphine)dichloropalladium(II) (Scheme 3.1). Basic conditions were used and the reaction mixture was stirred under an argon atmosphere at room temperature for seventy two hours. The crude product was then purified by removal of the triphenylphosphine oxide impurity, with use of a short silica column with diethyl ether as eluent, and removal of unreacted starting materials using column chromatography on silica. A pale brown solid was produced in 44% yield.

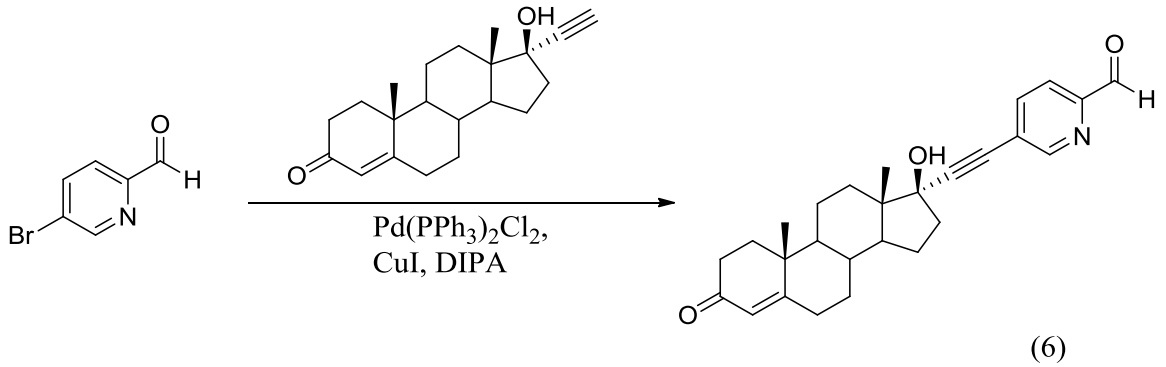

(6)

Scheme 3.1 Synthetic route for preparation of 17α-[(2-pyridinecarboxaldehyde)-5-ethynyl]ethisterone (6).

The product was characterised using high resolution EI mass spectrometry and elemental analysis, which both confirmed the formation of the desired product, 17α-[(2-pyridinecarboxaldehyde)-5-ethynyl]ethisterone (6) of formula [$C_{27}H_{31}NO_3$]. Characteristic peaks in the ^{1}H NMR spectrum (Fig. 3.7), assigned using a 2D-COSY (see Appendix), corresponding to the steroid $H_{4'}$ and methyl ($H_{18'}$ and $H_{19'}$) protons and the pyridine-carboxaldehyde aldehyde proton (H_{ald}) at the expected integration confirm the product has been formed.

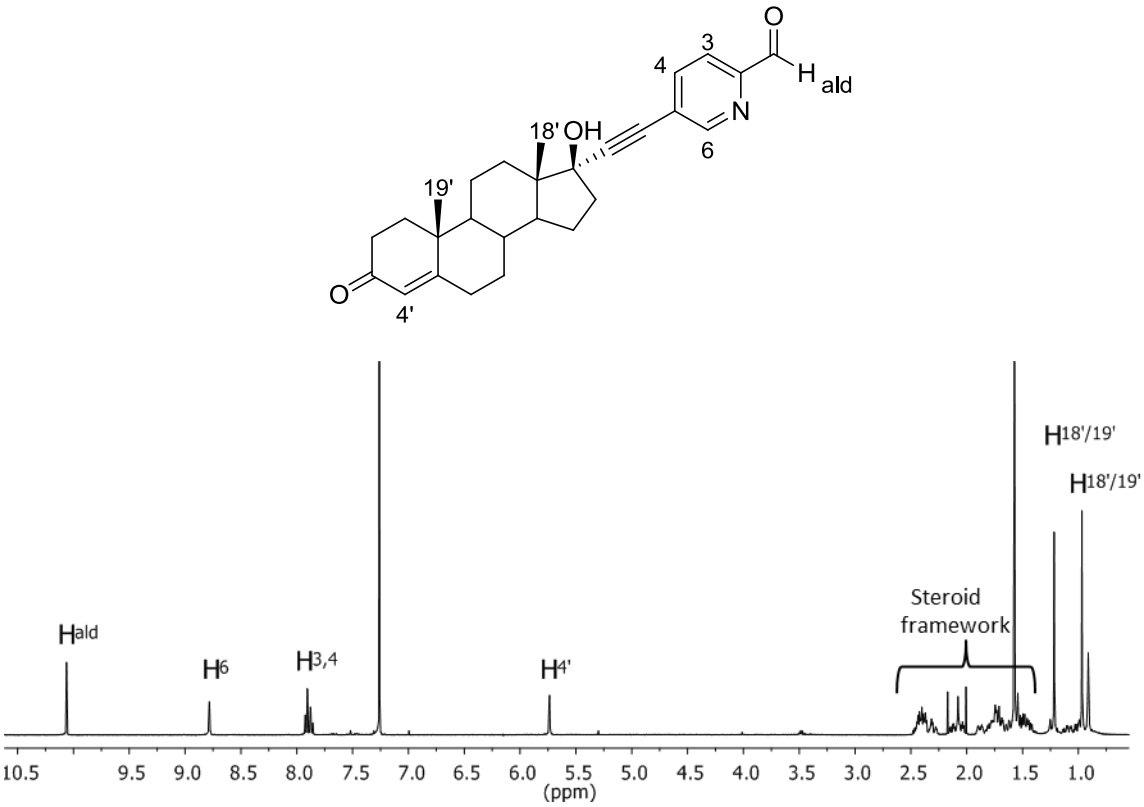

Figure 3.7 ^{1}H NMR (300 MHz, $CDCl_3$, 298 K) of 17α-[(2-pyridinecarboxaldehyde)-5-ethynyl]ethisterone (6).

3.3.1.2 Synthesis of $[Fe_2L^{Test}{}_3][BF_4]_4$

The testosterone cylinder, $[Fe_2L^{Test}{}_3][BF_4]_4$, was synthesised using a one-pot procedure with six equivalents of the testosterone aldehyde (6), three equivalents of the spacer, 4,4'-

methylenedianiline, and two equivalents of the metal salt, iron(II) tetrafluoroborate hexahydrate, added sequentially and dropwise, in ethanol (Scheme 3.2). An immediate dark purple precipitate formed on addition of the reactants suggesting the formation of an iron(II) cylinder. The product was isolated simply by filtration and washed with copious amounts of chloroform, in a yield of 29%.

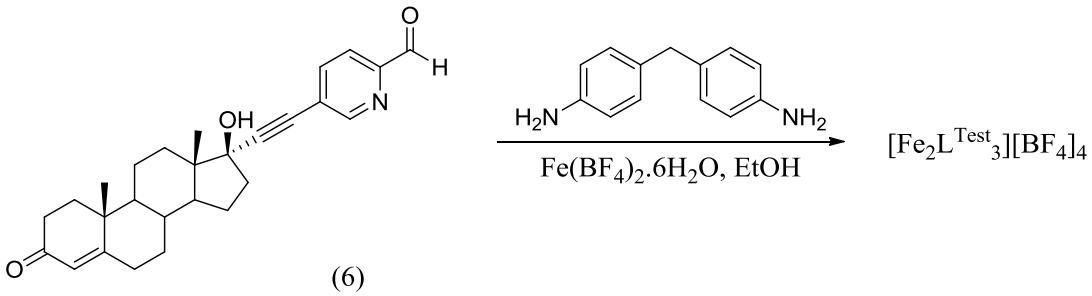

L^{Test} =

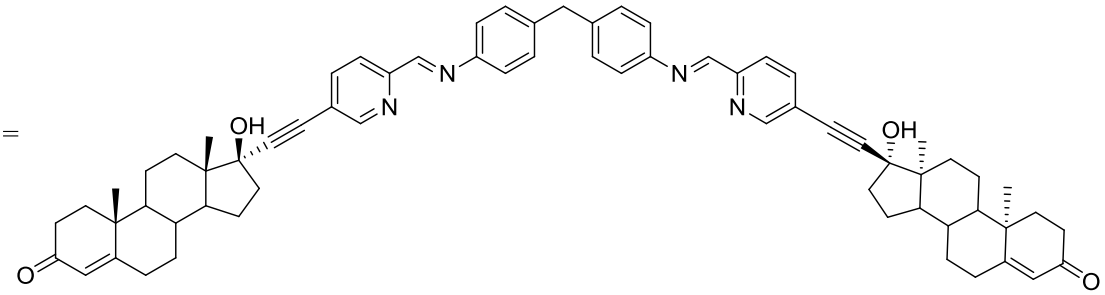

Scheme 3.2 Synthetic route for preparation of $[Fe_2L^{Test}{}_3][BF_4]_4$.

The light purple solid was confirmed to be the desired product, $[Fe_2L^{Test}{}_3][BF_4]_4$, by characterisation with ESI mass spectrometry and NMR spectroscopy. Several multiply charged peaks in the mass spectrum can be attributed to the species $[Fe_2(C_{67}H_{72}N_4O_4)_3]^{4+}$ and $[Fe_2(C_{67}H_{72}N_4O_4)_3]^{3+}$ (see Appendix). Peaks in the ^1H NMR spectrum (Fig. 3.8), assigned using 2D-COSY (see Appendix), corresponding to the characteristic imine (H_{im}), spacer (H_{sp}) and phenyl protons ($Ph_{a/b}$) as well as peaks originating from the steroid, H_{18} and H_{19}, at the correct integration suggest the formation of the product. When analysing the spectrum it became clear that some of the peaks appeared to be more split than expected,

with some that should be singlet peaks with an integration of two actually being observed as two separate peaks with an integration of one each, for example H_4 and $H_{4'}$. This is due to the formation of two diastereoisomers as will be discussed in greater depth in the next section (Section 3.4.1).

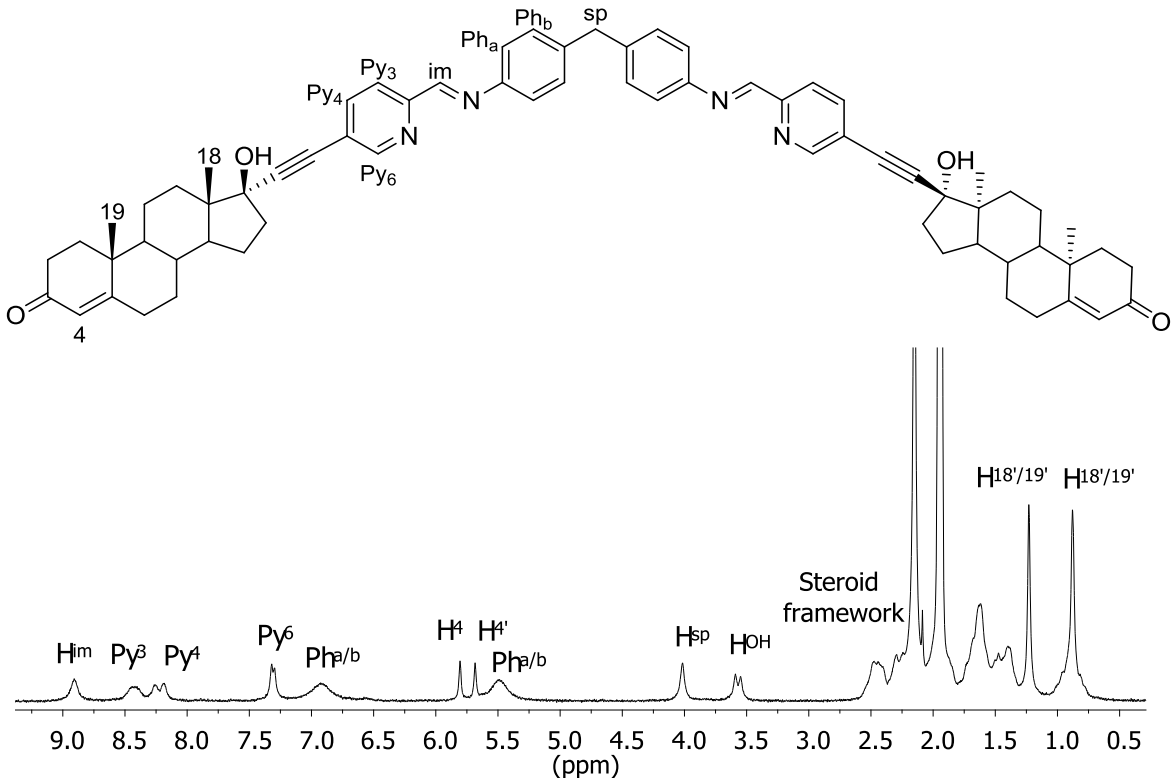

Figure 3.8 ^{1}H NMR (300 MHz, CD_3CN, 298 K) of $[Fe_2L^{Test}{}_3][BF_4]_4$.

An overall yield of 13%, with respect to the 5-bromo-2-pyridinecarboxaldehyde starting material, was obtained for the synthesis of the testosterone cylinder, $[Fe_2L^{Test}{}_3][BF_4]_4$.

3.3.2 Synthesis of estrogen cylinder, $[Fe_2L^{Estro}_3][BF_4]_4$

3.3.2.1 Synthesis of 17α-[(2-pyridinecarboxaldehyde)-5-ethynyl]estradiol (7)

As 17α-[(2-pyridinecarboxaldehyde)-5-ethynyl]estradiol (7) is not commercially available it was synthesised, with the synthesis based on a literature procedure.[22] A Sonogashira coupling reaction was employed to couple 5-bromo-2-pyridinecarboxaldehyde to 17α-ethynylestradiol, at room temperature under an inert atmosphere for seventy two hours (Scheme 3.3). Catalysts, copper iodide and bis(triphenylphosphine)dichloropalladium(II), were employed. The resulting crude mixture was purified using a short silica column with diethyl ether as eluent to remove the triphenylphosphine oxide impurity afforded by the palladium catalyst, and any unreacted starting materials were removed by column chromatography. A pale brown solid was produced in 49% yield.

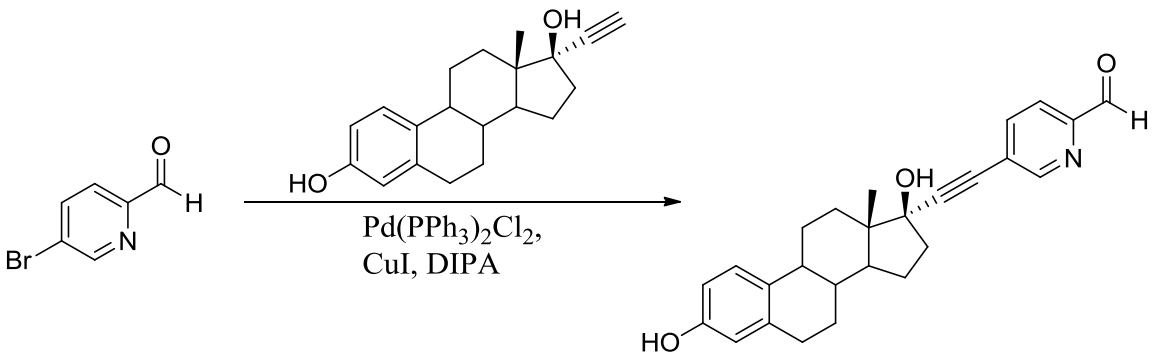

(7)

Scheme 3.3 Synthetic route for preparation of 17α-[(2-pyridinecarboxaldehyde)-5-ethynyl]estradiol (7).

The product, 17α-[(2-pyridinecarboxaldehyde)-5-ethynyl]estradiol (7), was characterised by high resolution EI mass spectrometry, with one peak corresponding to the molecular ion plus sodium being observed. ^{1}H NMR spectroscopy revealed a spectrum (Fig. 3.9) containing peaks corresponding to the steroid and pyridine-carboxaldehyde moieties of the

desired product at the expected ratios, confirming its formation. The aromatic ring of the estrogen steroid, protons $H_{1'}$, $H_{2'}$ and $H_{4'}$, can be seen at high chemical shift with the pyridine protons, H_3, H_4 and H_6. One singlet peak corresponding to the methyl group of the steroid (H_{Me}) can be observed.

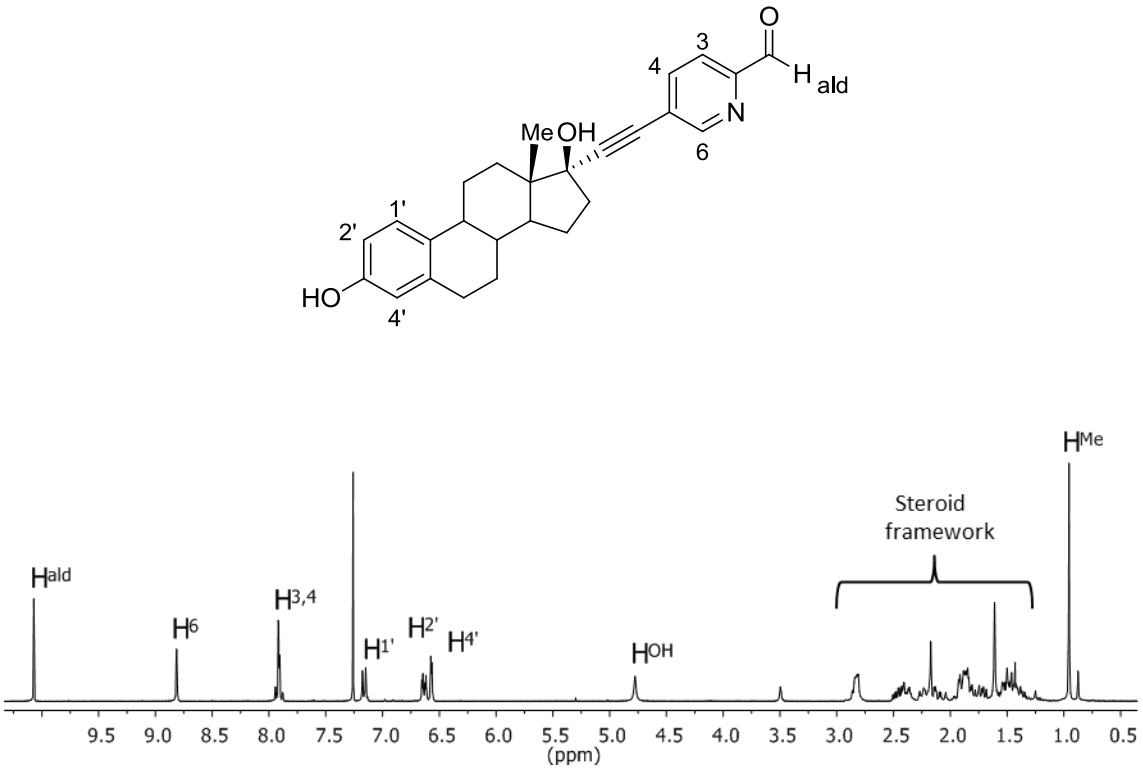

Figure 3.9 ^{1}H NMR (300 MHz, $CDCl_3$, 298 K) of 17α-[(2-pyridinecarboxaldehyde)-5-ethynyl]estradiol (7).

3.3.2.2 Synthesis of $[Fe_2L^{Estro}{}_3][BF_4]_4$

The estrogen cylinder was synthesised using a one-pot method, with the starting materials 17α-[(2-pyridinecarboxaldehyde)-5-ethynyl]estradiol (7), 4,4'-methylenedianiline and iron(II) tetrafluoroborate hexahydrate being mixed together, sequentially and dropwise, in ethanol in a 6:3:2 ratio (Scheme 3.4). Immediate colour change from pale yellow to deep purple, indicative of the formation of the desired cylinder, was observed. The purple precipitate was collected by filtration and purified by washing with a large volume of

chloroform. The resulting light purple solid was obtained in 25% yield.

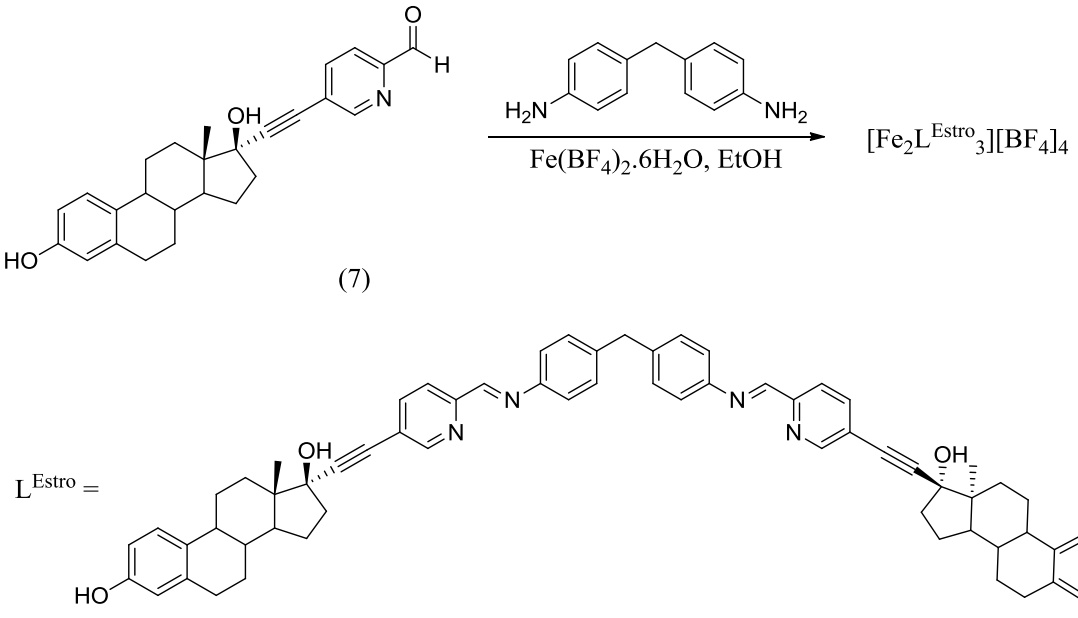

Scheme 3.4 Synthetic route for preparation of $[Fe_2L^{Estro}{}_3][BF_4]_4$.

The estrogen cylinder $[Fe_2L^{Estro}{}_3][BF_4]_4$ was characterised by ESI mass spectrometry, in which several multiply charged species corresponding to $[Fe_2(C_{65}H_{64}N_4O_4)_3]^{4+}$, $[Fe_2(C_{65}H_{64}N_4O_4)_3]^{3+}$, $[Fe_2(C_{65}H_{64}N_4O_4)_3][BF_4]^{3+}$ and $[Fe_2(C_{65}H_{64}N_4O_4)_3]^{2+}$ could be identified with the expected isotopic pattern (see Appendix). A ^{1}H NMR spectrum (Fig. 3.10), assigned using 2D-COSY (see Appendix), was employed to characterise the cylinder further. The characteristic peak corresponding to the newly formed cylinder, the imine peak (H_{im}), could be observed and peaks originating from the steroid were also evident. However most of the peaks observed did not have the splitting or integration expected, including the imine and steroid peaks discussed. This is due to a mixture of two diastereoisomers, as with the testosterone steroid cylinder, and will be discussed in greater depth in the next section (Section 3.4.1).

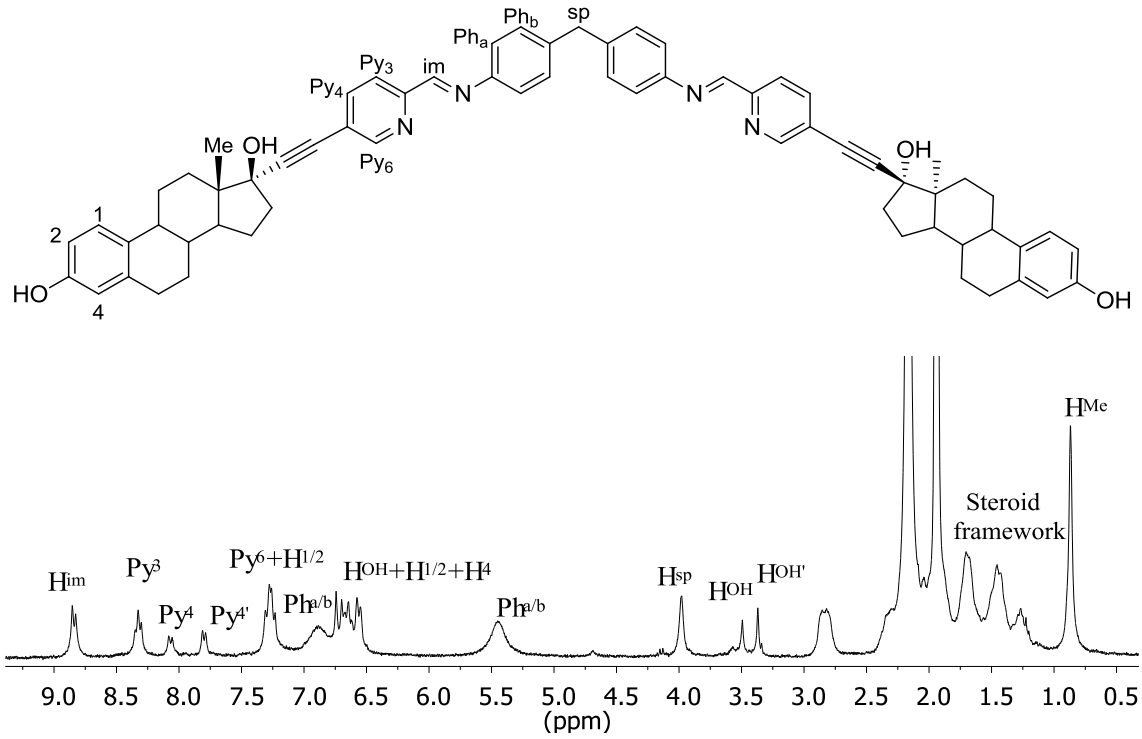

Figure 3.10 ^{1}H NMR (300 MHz, CD_3CN, 298 K) of $[Fe_2L^{Estro}{}_3][BF_4]_4$.

An overall yield of 12%, with respect to the 5-bromo-2-pyridinecarboxaldehyde starting material, was obtained for the synthesis of the estrogen cylinder, $[Fe_2L^{Estro}{}_3][BF_4]_4$.

3.4 Properties of synthesised steroid cylinders

3.4.1 Chirality of synthesised helicates, as investigated by ^{1}H NMR studies with Δ-TRISPHAT

The tetrabutylammonium salt of Δ-TRISPHAT, or tris(tetrachlorobenzenediolato)-phosphate(V) (Fig. 3.11), is a commercially available chiral NMR shift reagent developed by Lacour and co-workers.[23]

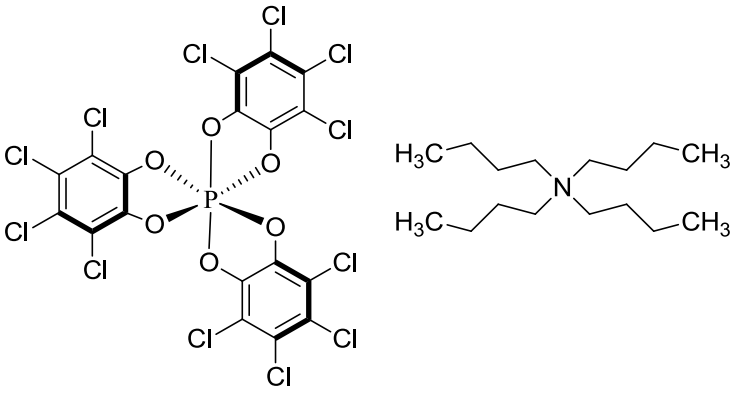

Figure 3.11 Tetrabutylammonium salt of Δ-TRISPHAT.[23]

Herein, Δ-TRISPHAT was used in order to elucidate the enantiomeric purity of the synthesised steroid functionalised helicates.

3.4.1.1 ^{1}H NMR Δ-TRISPHAT studies with the parent cylinder

^{1}H NMR Δ-TRISPHAT studies have previously been carried out in the Hannon group, exploring the effect of Δ-TRISPHAT on racemic and enantiopure solutions of the parent cylinder, $[Fe_2L^{P}_3][PF_6]_4$.[7,24,25] When Δ-TRISPHAT was added to a solution of racemic $[Fe_2L^{P}_3][PF_6]_4$, splitting of some of the resonances was observed in the ^{1}H NMR spectrum (Fig. 3.12) indicating that Δ-TRISPHAT is able to interact with the M and P enantiomers differently.[24]

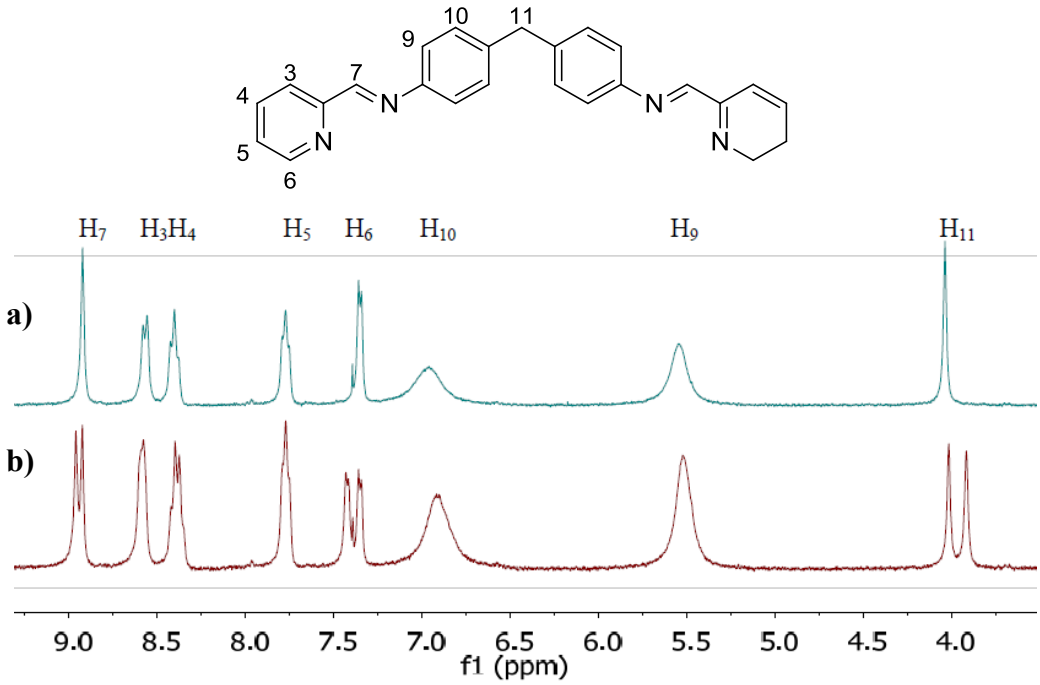

Figure 3.12 ^{1}H NMR (300 MHz, CD_3CN, 298 K) of a) a solution of rac-$[Fe_2L^{P}_3][PF_6]_4$; b) the same solution with 2 equivalents of Δ-TRISPHAT. [Reproduced from Ref [24]]

To determine whether one or both enantiomers can interact with Δ-TRISPHAT, an enantiopure solution of the M enantiomer was "doped" with 10% of enantiopure P and then two equivalents of Δ-TRISPHAT were added.[24] In the ^{1}H NMR spectrum (Fig. 3.13) it can be observed that the spacer protons (H_{11}) of the M enantiomer are shifted on addition of Δ-TRISPHAT, whereas it is the imine (H_7) and H_6 protons of the P enantiomer that are shifted.[24] This suggests that Δ-TRISPHAT interacts in the area of the central spacer for the M enantiomer and at the metal coordination site of the P enantiomer.[24]

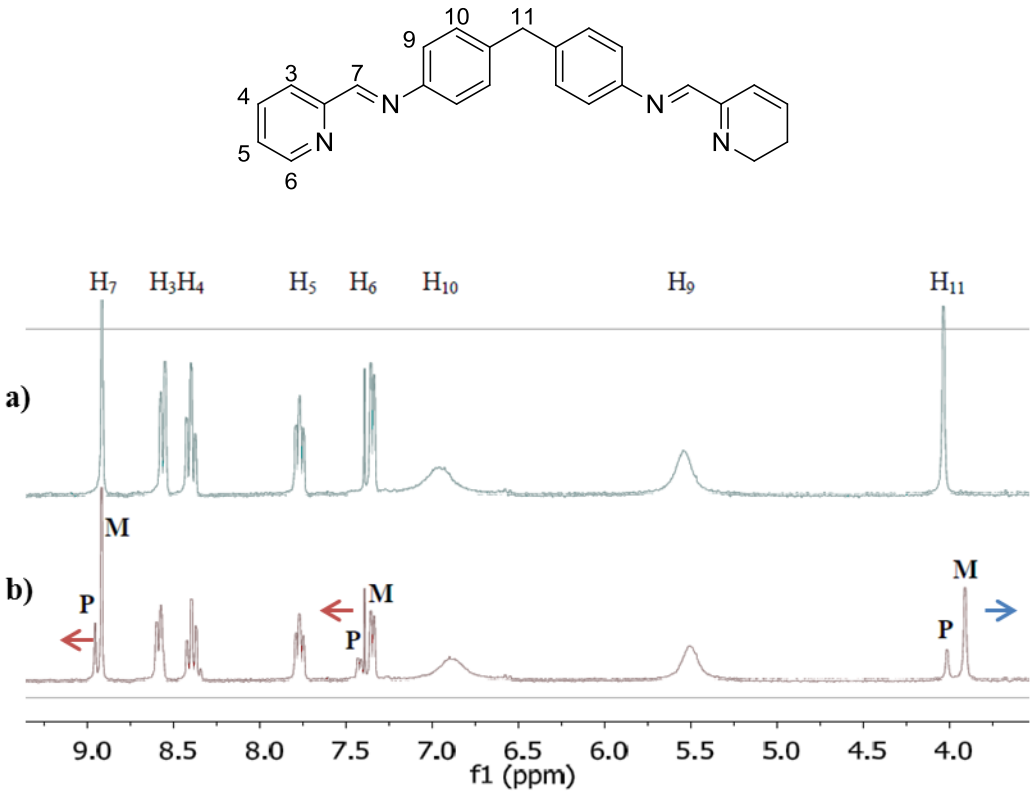

Figure 3.13 ^{1}H NMR (300 MHz, CD_3CN, 298 K of a) a solution of $[Fe_2L^{P}_3][PF_6]_4$ (ratio of enantiomers, M:P = 9:1); b) the same solution with 2 equivalents of Δ-TRISPHAT. [Reproduced from Ref [24]]

3.4.1.2 ^{1}H NMR Δ-TRISPHAT studies with peptide cylinders

Δ-TRISPHAT has also been employed to determine the enantiomeric purity of Cardo's peptide conjugated iron(II) cylinders mentioned previously (Section 3.1.2).[7] Cylinders conjugated to L- or D-arginine form seemingly diastereoisomerically pure isomers (P and M respectively) as indicated by ^{1}H NMR and CD experiments. This observation was further investigated using Δ-TRISPHAT (Fig. 3.14).[7] When two equivalents of Δ-TRISPHAT were added to solutions of the L- and D-arginine conjugated cylinders ($[Fe_2L^{L\text{-}Arg}_3][PF_6]_{10}$ and $[Fe_2L^{D\text{-}Arg}_3][PF_6]_{10}$ respectively) only one set of resonances was observed for each conjugated cylinder confirming that they are diastereoisomerically pure.[7] For the L-arginine conjugate, $[Fe_2L^{L\text{-}Arg}_3][PF_6]_{10}$, the imine ($H_7$) and H_6 protons are shifted

whereas for the D-arginine conjugate, $[Fe_2L^{D\text{-}Arg}{}_3][PF_6]_{10}$, the spacer protons ($H_{11}$) are shifted.[7] These results are in agreement with those for the parent cylinder and confirm the theory that the L-arginine conjugate is in fact the P helical isomer and the D-arginine conjugate is the M helical isomer.[7]

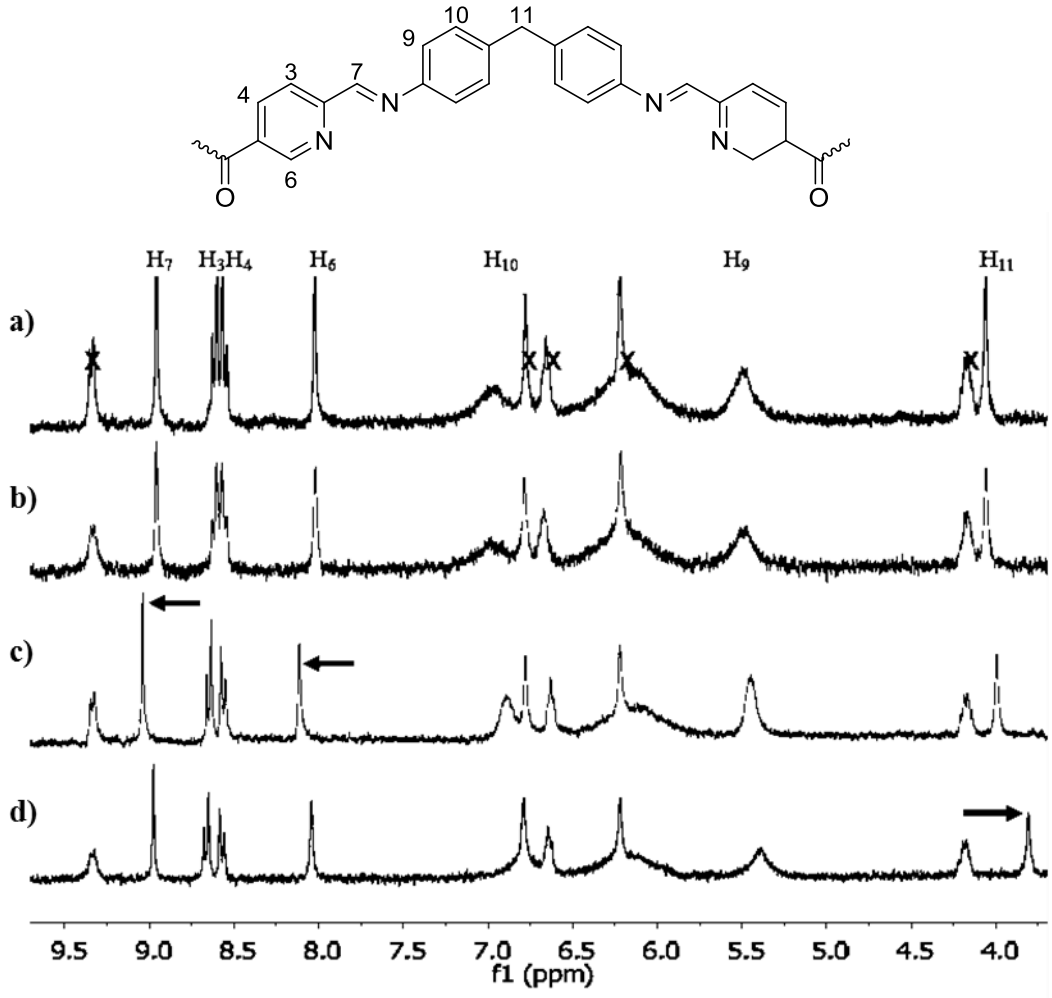

Figure 3.14 ^{1}H NMR (300 MHz, CD_3CN, 298 K) of a) a solution of $[Fe_2L^{L\text{-}Arg}{}_3][PF_6]_{10}$; b) a solution of $[Fe_2L^{D\text{-}Arg}{}_3][PF_6]_{10}$; c) a solution of $[Fe_2L^{L\text{-}Arg}{}_3][PF_6]_{10}$ with 2 equivalents of Δ-TRISPHAT; d) a solution of $[Fe_2L^{D\text{-}Arg}{}_3][PF_6]_{10}$ with 2 equivalents of Δ-TRISPHAT. Peaks with crosses correspond to arginine protons. [Reproduced from Ref [7]]

3.4.1.3 ^{1}H NMR Δ-TRISPHAT studies with novel steroid cylinders

As the ^{1}H NMR characterisation of the steroid cylinders detailed in this chapter was ambiguous, Δ-TRISPHAT studies were undertaken to investigate the possible mixture of diastereoisomers formed in the steroid cylinder synthesis. To a solution of the steroid cylinders, $[Fe_2L^{Test}_3][BF_4]_4$ and $[Fe_2L^{Estro}_3][BF_4]_4$, was added increasing equivalents of the tetrabutylammonium salt of Δ-TRISPHAT.

The ^{1}H NMR spectrum (Fig. 3.15) of the testosterone cylinder alone reveals that some of the peaks are already split, for example the H_4 peak of the steroid. After the addition of one equivalent of Δ-TRISPHAT, the peaks are split into two clear sets of resonances. Upon addition of another equivalent of Δ-TRISPHAT the peaks are further split. The ratio of the peaks of the two sets of resonances is 1:0.85 providing evidence that the solution of $[Fe_2L^{Test}_3][BF_4]_4$ is an unequal mixture of the two helical isomers, M and P.

As with the parent and peptide cylinders, the resonances that are particularly shifted are those corresponding to the imine (H_{im}), spacer (H_{sp}) and H_{Py6} protons. For the parent and peptide cylinders, the spacer proton (H_{sp}) of the M enantiomer is shifted, whereas the imine (H_{im}) and H_6 protons are shifted for the P enantiomer. This is due to the Δ-TRISPHAT anion interacting in different areas of the cylinder for each enantiomer. However for the testosterone cylinder the peaks that have shifted are all peaks of lower integration. No conclusions may be drawn as to which set of peaks corresponds to which helical isomer and therefore it is not known which helical isomer is more abundant.

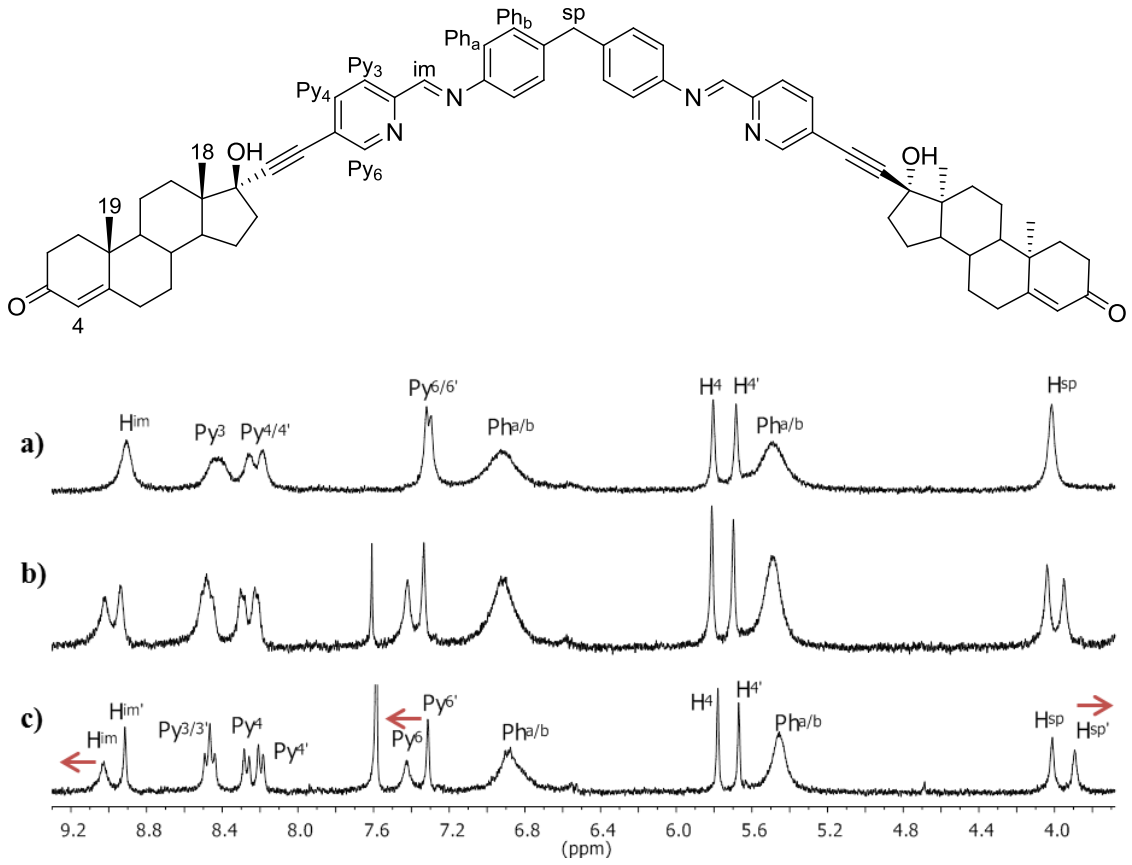

Figure 3.15 ^{1}H NMR (300 MHz, CD_3CN, 298 K) of a) a solution of $[Fe_2L^{Test}{}_3][BF_4]_4$; b) same solution with 1 equivalent of Δ-TRISPHAT; c) same solution with 2 equivalents of Δ-TRISPHAT.

^{1}H NMR Δ-TRISPHAT studies were then carried out with the estrogen cylinder, $[Fe_2L^{Estro}{}_3][BF_4]_4$. As for the testosterone cylinder, the spectrum of the cylinder alone (Fig. 3.16) reveals that some peaks are already split, including the imine (H_{im}) and H_{Py4} protons. It was observed that after the addition of one equivalent of Δ-TRISPHAT, the majority of peaks split into two sets of resonances. This splitting is increased upon the addition of further equivalents of Δ-TRISPHAT. These observations provide evidence for the solution being a mixture of M and P helical isomers. The two helical isomers present in solution are not in a 1:1 ratio; a ratio of 1:0.72 is observed for the integration of the two sets of peaks. As was observed with the other iron(II) cylinders characterised using this method, the peaks corresponding to the imine (H_{im}), spacer (H_{sp}) and pyridine (Py_3 and Py_6) protons are

split the most by the addition of Δ-TRISPHAT. It is difficult to assign the two sets of resonances from these spectra. It would be expected that the spacer proton would be shifted for the M helical isomer, and that the pyridine and imine protons would be shifted for the P helical isomer as previously observed. However all of the peaks that are shifted are of lower integration. Therefore conclusions as to the more abundant helical isomer cannot be drawn.

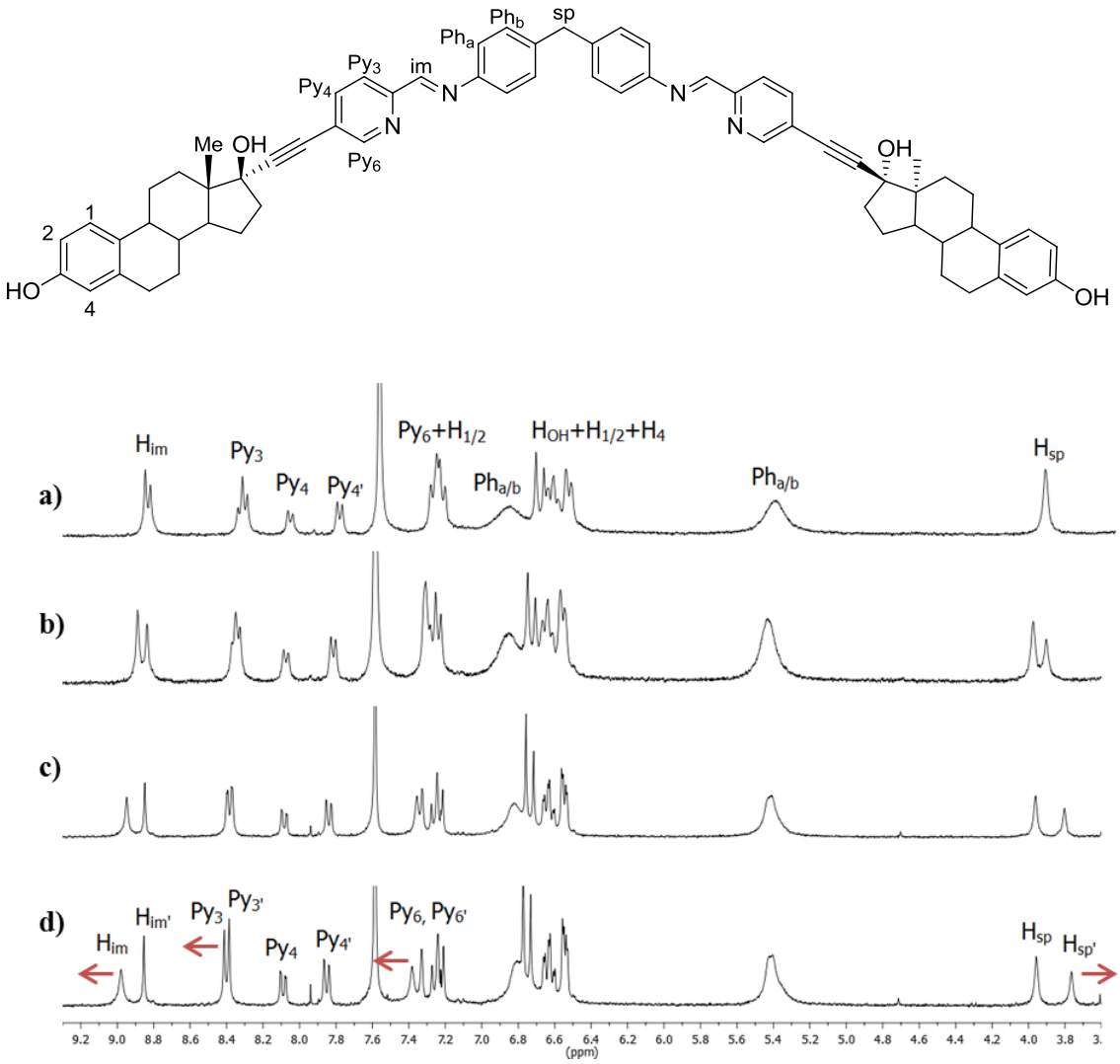

Figure 3.16 ^{1}H NMR (300 MHz, CD_3CN, 298 K) of a) a solution of $[Fe_2L^{Estro}{}_3][BF_4]_4$; b) same solution with 1 equivalent of Δ-TRISPHAT; c) same solution with 2 equivalents of Δ-TRISPHAT; d) same solution with 3 equivalents of Δ-TRISPHAT.

As the ^{1}H NMR Δ-TRISPHAT studies do not reveal the more abundant helical isomer for the two steroid cylinders, it was hoped that circular dichroism studies may provide an answer.

3.4.2 Chirality of helicates, as investigated by circular dichroism

Circular dichroism can be used to identify the chirality of iron(II) cylinders, as the CD signals arising in the visible region are due to the helicate core. CD spectra of enantiopure solutions of the M and P enantiomers of the parent cylinder, $[Fe_2L^{P}_3]^{4+}$, reveal identical but opposite CD signals (Fig. 3.17). This is also true of the peptide conjugated cylinders. When solutions of the diastereoisomerically pure L-arginine and D-arginine conjugated cylinders, P and M helical isomers respectively, are analysed by CD, the spectra looks remarkably similar to that of the parent cylinder.[7]

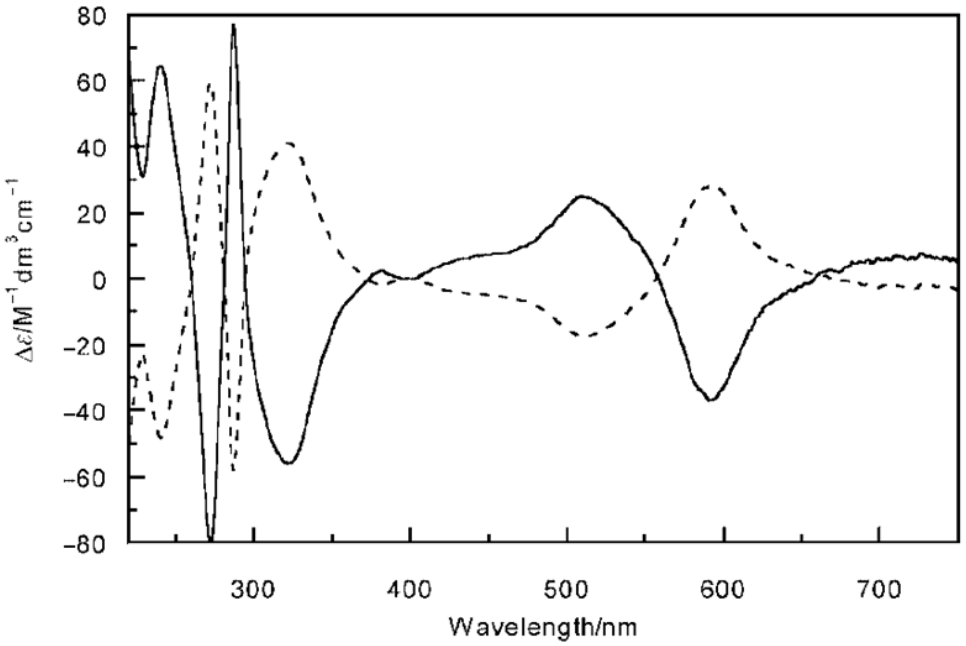

Figure 3.17 CD spectra of M (solid line) and P (dashed line) enantiomers of $[Fe_2L^{P}_3]^{4+}$. [Reproduced from Ref [26]]

CD spectra of the steroid cylinders, $[Fe_2L^{Test}{}_3][BF_4]_4$ and $[Fe_2L^{Estro}{}_3][BF_4]_4$, were recorded to see if they could give any information about the chirality of the complexes (Fig. 3.18). It is known that both cylinders are a mixture of diastereoisomers, and that these are not in an equal ratio. Comparison of the CD spectra obtained with that of the parent cylinder suggests that both the $[Fe_2L^{Test}{}_3][BF_4]_4$ and $[Fe_2L^{Estro}{}_3][BF_4]_4$ cylinders have a slightly higher ratio of the P helical isomer compared to the M helical isomer, due to the observation of the characteristic P shape in the visible region of the CD signal.

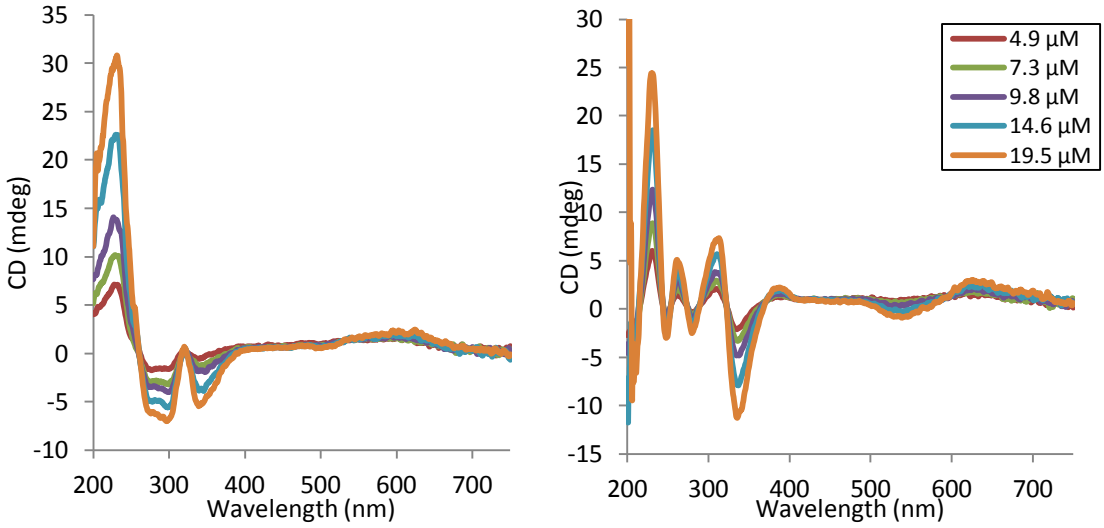

Figure 3.18 CD spectra of increasing concentrations of complexes: (left) $[Fe_2L^{Test}{}_3][BF_4]_4$; (right) $[Fe_2L^{Estro}{}_3][BF_4]_4$. Legend shows complex concentration. 5.9% max. MeOH.

3.4.3 Complex counterions

The steroid functionalised cylinders, $[Fe_2L^{Test}{}_3][BF_4]_4$ and $[Fe_2L^{Estro}{}_3][BF_4]_4$, synthesised herein have tetrafluoroborate as counterions. As discussed previously (Section 2.5.1, Chapter 2) the preferred counterion would be chloride for these complexes, as the majority of the parent and later generation iron(II) cylinders have chloride counterions.

However attempts to synthesise these steroid cylinders with chloride as counterion, to form $[Fe_2L^{Test}{}_3][Cl]_4$ and $[Fe_2L^{Estro}{}_3][Cl]_4$, were unsuccessful. Addition of iron(II) chloride tetrahydrate, instead of iron(II) tetrafluoroborate hexahydrate, into the one-pot synthesis of both steroid cylinders resulted in an immediate green precipitate which could not be identified by mass spectrometry or NMR spectroscopy. Ion exchange using tetrabutylammonium chloride induced a degradation of the steroid cylinder, as did the addition of a sodium chloride solution. It is concluded from these studies, and those performed with the simple alkyne cylinders, that these iron(II) cylinders are in some way destabilised by chloride counterions. As these cylinders all contain an alkyne linking group, it is possible that this group is somehow interacting unfavourably with the counterions, causing the complexes to be unstable. Alternatively, the effect of the alkyne on the electronic properties of the pyridylimine is to weaken the binding to the iron centre.

3.4.4 Solubility of steroid functionalised cylinders

As previously discussed (Section 2.5.2, Chapter 2), water solubility is an advantageous property of potential anti-cancer drugs[27] and DNA binding studies should be carried out in aqueous solutions. Unfortunately the steroid functionalised cylinders synthesised in this chapter are not water soluble. However they do possess very good solubility in methanol and so can be dissolved in water, with the assistance of a small percentage of methanol. This allows the DNA binding, though not the cytotoxicity, of these complexes to be studied.

3.4.5 UV-Vis stability studies

As previously discussed (Section 2.5.3, chapter 2) the stability of any drug that is to be administered into the body is an important consideration. More importantly for this work, the stability of these steroid functionalised cylinders must be established in order to fully understand the results of the DNA binding studies carried out.

Steroid cylinder stabilities in the absence and presence of ct-DNA were established using UV-Vis spectroscopy experiments analogous to those carried out in Chapter 2 (Section 2.5.3). Aqueous solutions of the steroid cylinders containing a small percentage of methanol were used due to solubility issues.

For both complexes, $[Fe_2L^{Test}{}_3][BF_4]_4$ and $[Fe_2L^{Estro}{}_3][BF_4]_4$, the λ_{max} of the MLCT band decreases with time, indicating some degradation. The stability of both complexes is very similar, with losses of absorbance of 31% and 33% for the testosterone and estrogen cylinders respectively over the twelve hour period (Fig. 3.19). In the presence of ct-DNA both complexes are more stable. The degradation of $[Fe_2L^{Test}{}_3][BF_4]_4$ and $[Fe_2L^{Estro}{}_3][BF_4]_4$ in the presence of DNA is slower with an absorbance loss of 20% for both complexes over 12 hours. Over a five hour period, the maximum experimental time of the DNA binding studies carried out herein, the testosterone functionalised cylinder loses 13% of its original absorbance and the estrogen cylinder loses 5%. Although degradation of these complexes is observed, it is thought that this should not significantly affect any conclusions drawn from the DNA binding studies carried out.

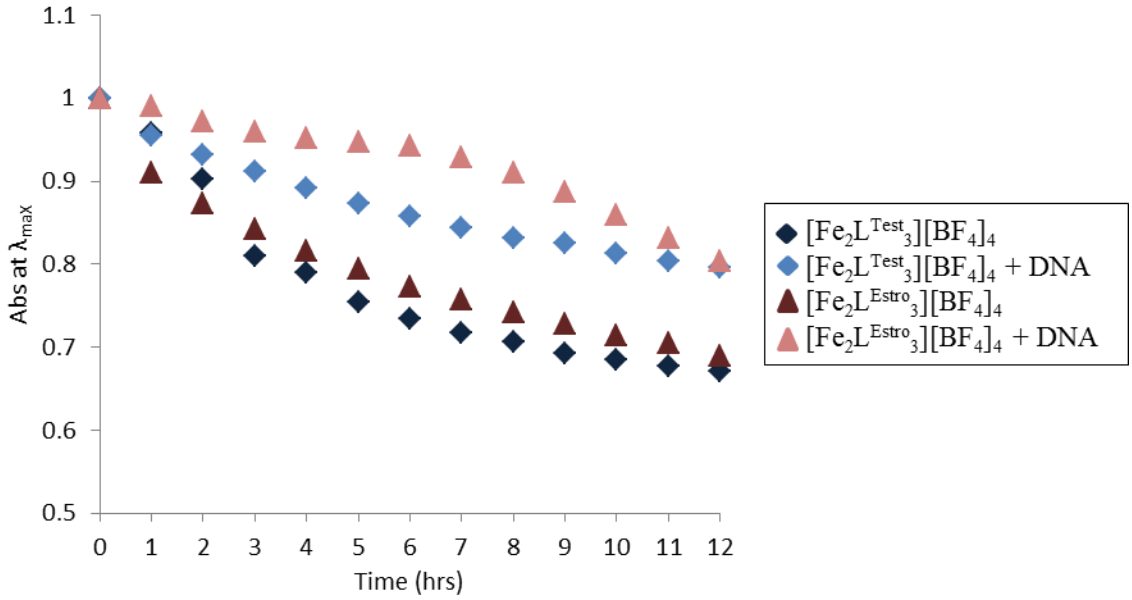

Figure 3.19 Normalised UV-Vis stability studies of complexes $[Fe_2L^{Test}{}_3][BF_4]_4$ and $[Fe_2L^{Estro}{}_3][BF_4]_4$ at room temperature (5 μM, 1.5% MeOH:water) and in presence of ct-DNA in 6.7 mM NaCl and 0.33 mM $Na(CH_2)_2AsO_2.3H_2O$ (pH 6.8) (ratio 6:1 ct-DNA:complex, 1.9% MeOH:water). λ_{max} 593 nm.

As observed for the alkyne cylinders detailed previously (Chapter 2) and other analogous iron(II) supramolecular cylinders,[24] the presence of ct-DNA appears to have a stabilising effect. One possible explanation for this may be that as these types of iron(II) cylinders bind in the major groove of DNA,[28] this environment protects them in some way from solvent attack and so they degrade more slowly.

These steroid functionalised cylinders are less stable than the $[Fe_2L^{TB}{}_3][BF_4]_4$, $[Fe_2L^{PA}{}_3][BF_4]_4$ and $[Fe_2L^{Hex}{}_3][BF_4]_4$ cylinders (Section 2.5.3, Chapter 2).

3.5 DNA binding studies

Two novel iron(II) supramolecular cylinders functionalised with steroid hormones have been synthesised and characterised. The DNA binding properties of these novel cylinders

were investigated by several techniques.

3.5.1 Circular dichroism binding studies

CD titrations were carried out for the steroid functionalised cylinders, $[Fe_2L^{Test}{}_3][BF_4]_4$ and $[Fe_2L^{Estro}{}_3][BF_4]_4$ analogous to those described in chapter 2 (Section 2.6.1). These complexes had to be dissolved in a methanol-water solvent mix as they are not water soluble. As for the CD titration experiments with the alkyne cylinders, two equal titrations were carried out in 1 cm and 0.1 cm pathlength cuvettes.

As the two steroid cylinders, $[Fe_2L^{Test}{}_3][BF_4]_4$ and $[Fe_2L^{Estro}{}_3][BF_4]_4$, are chiral they have their own intrinsic CD signal (Fig. 3.20). This must be subtracted from the ct-DNA CD titration spectrum so as to see only the ICD signal arising from the interaction with DNA. This was achieved by first performing the titration with water instead of DNA solutions and subtracting these titration spectra from those of the titration with ct-DNA.

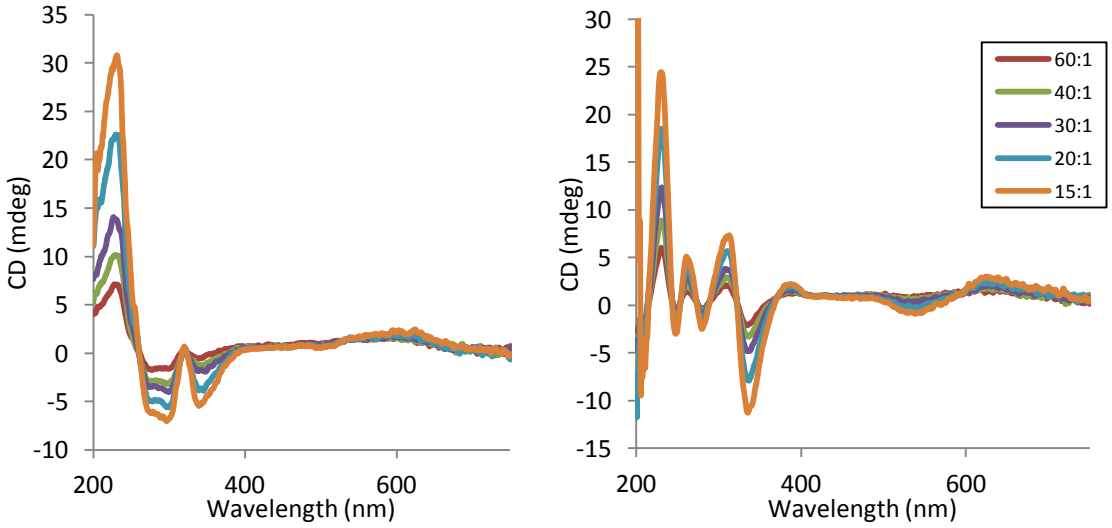

Figure 3.20 CD of control titrations of $[Fe_2L^{Test}{}_3][BF_4]_4$ (left) and $[Fe_2L^{Estro}{}_3][BF_4]_4$ (right). Water with increasing concentrations of complexes. Legend shows corresponding ct-DNA:complex ratios for titration with ct-DNA. 5.9% max. MeOH.

The CD titration spectra of the testosterone functionalised cylinder, $[Fe_2L^{Test}_3][BF_4]_4$, (Fig. 3.21) reveal an ICD signal at 346 nm. This indicates that the cylinder is binding to ct-DNA. The B-conformation of DNA is retained upon cylinder binding. However at higher complex loading, with a ratio of DNA:complex of 4:1 (0.1 cm pathlength spectrum), there is a change in the DNA signature in the region between 200-250 nm, most likely due to overlapping complex in-ligand spectroscopy.

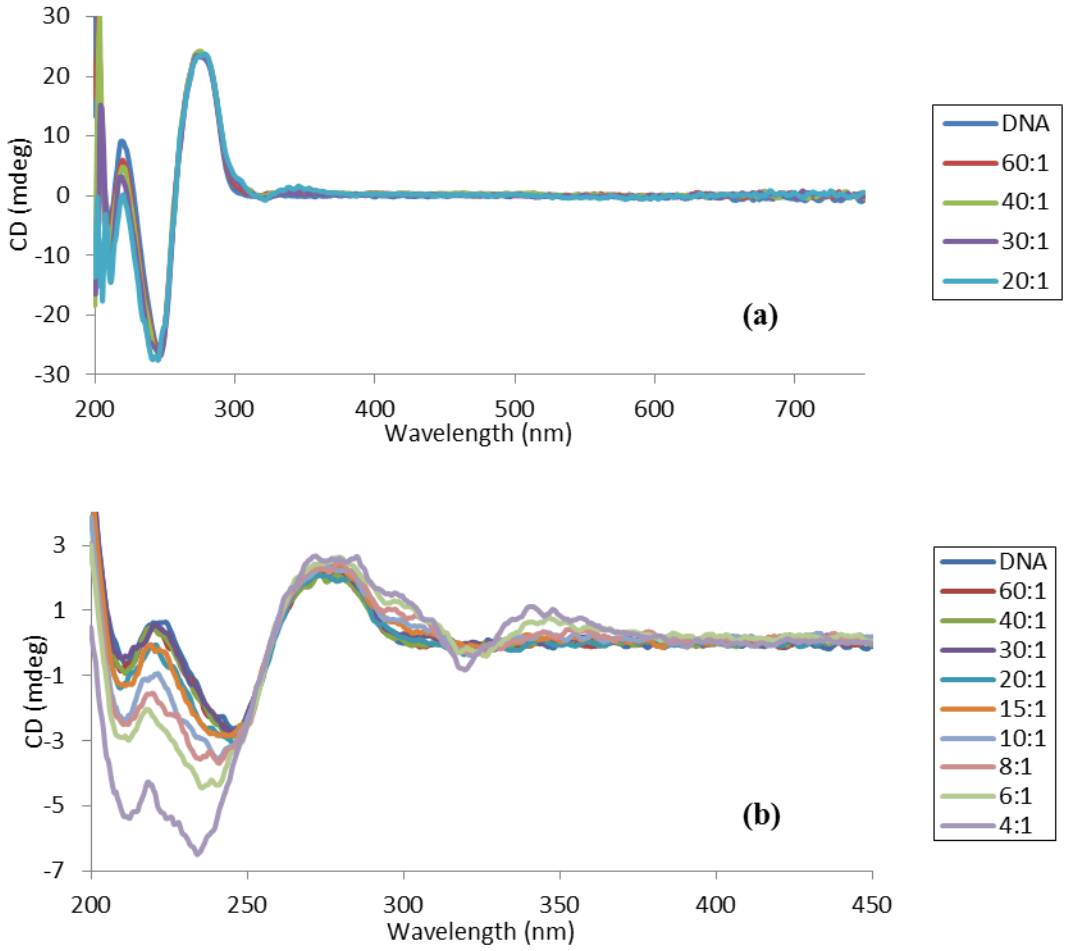

Figure 3.21 CD of 286 μM ct-DNA in 20 mM NaCl and 1 mM $Na(CH_2)_2AsO_2.3H_2O$ (pH 6.8) with increasing concentrations of complex $[Fe_2L^{Test}_3][BF_4]_4$. Legend shows ct-DNA:complex ratios. 5.7% max. MeOH. Analysed in 1cm (a) and 0.1cm (b) cuvettes.

ICD signals at 338 nm in the CD titration spectra (Fig. 3.22) of the estrogen functionalised cylinder, $[Fe_2L^{Estro}_3][BF_4]_4$, indicates DNA binding. The characteristic signal of the B-form

of DNA is observed throughout the titration, showing that cylinder binding does not affect DNA conformation. However at higher complex loading, with ratios of DNA:complex of 8:1 to 4:1 (0.1 cm pathlength spectrum), the formation of a peak at 233 nm overlaps the DNA bands. This new peak is most likely due to the complex in-ligand spectroscopy.

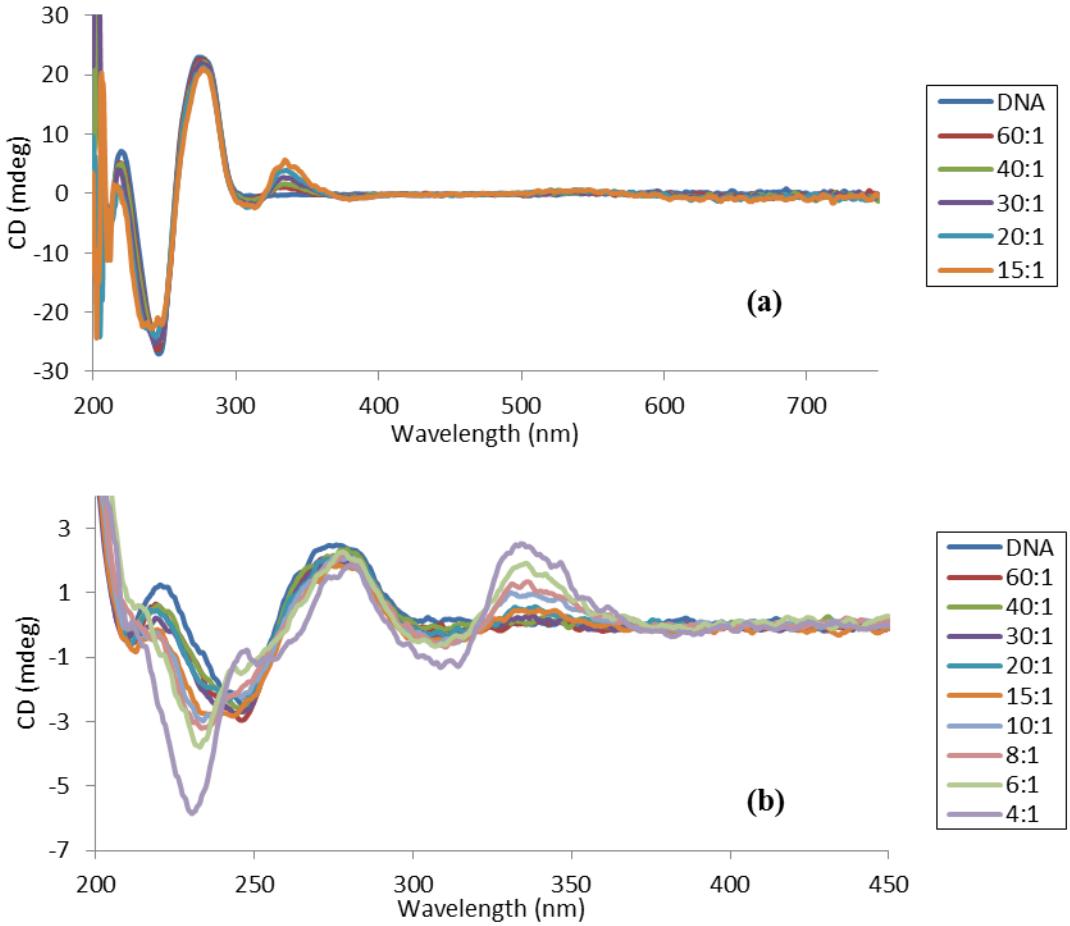

Figure 3.22 CD of 293 μM ct-DNA in 20 mM NaCl and 1 mM $Na(CH_2)_2AsO_2.3H_2O$ (pH 6.8) with increasing concentrations of complex $[Fe_2L^{Estro}{}_3][BF_4]_4$. Legend shows ct-DNA:complex ratios. 5.9% max. MeOH. Analysed in 1cm (a) and 0.1cm (b) cuvettes.

3.5.2 Linear dichroism binding studies

Linear dichroism titrations analogous to those performed with the parent and alkyne cylinders (Section 2.6.2, Chapter 2) were carried out for the steroid functionalised

complexes synthesised in this chapter. Due to poor aqueous solubility, the steroid cylinders were dissolved in a methanol/water solution.

These steroid cylinders are too small to be oriented by viscous drag and so do not have any intrinsic LD signal. Consequently any ILD signal observed must come from interaction between the complex and ct-DNA.

The LD titration spectrum (Fig. 3.23) for the testosterone functionalised cylinder, $[Fe_2L^{Test}{}_3][BF_4]_4$, shows no detectable ILD signals in the complex region. Although oriented DNA binding cannot be confirmed by the presence of ILD signals in the spectrum, there is evidence of DNA binding. The magnitude of the negative LD band at 260 nm, corresponding to DNA transitions, decreases as the complex concentration increases. This indicates that the cylinder is binding to DNA and coiling or bending it so as to induce a loss of DNA orientation, even at low cylinder loading.

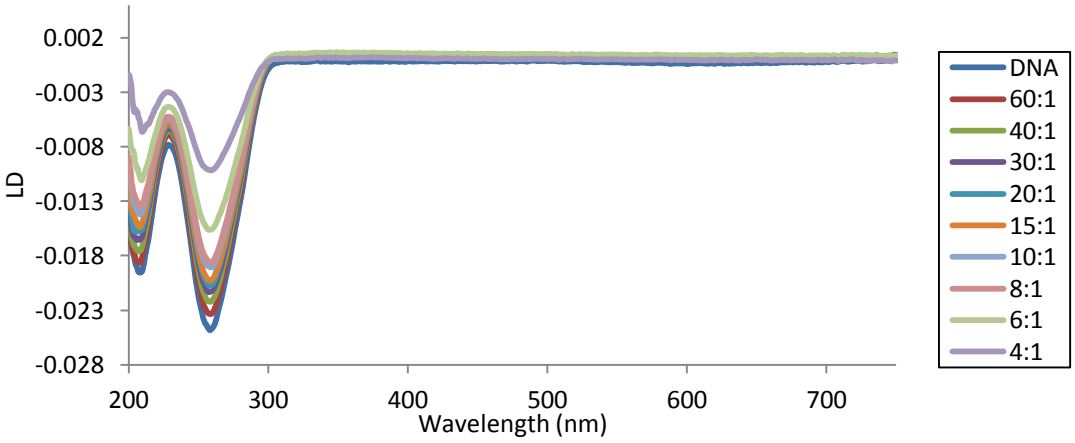

Figure 3.23 LD of 296 μM ct-DNA in 20 mM NaCl and 1 mM $Na(CH_2)_2AsO_2.3H_2O$ (pH 6.8) with increasing concentrations of complex $[Fe_2L^{Test}{}_3][BF_4]_4$. Legend shows ct-DNA:complex ratios. 5.7% max. MeOH.

The LD titration spectrum (Fig. 3.24) of the estrogen functionalised cylinder shows no induced LD signal, even at high concentrations of the metal complex. Consequently, oriented binding of the complex to DNA cannot be confirmed. DNA binding is occurring, however, as observed by the reduced magnitude of the negative LD band at 260 nm corresponding to the transitions of the DNA. This shows that the orientation of the DNA is being affected by the cylinder. The complex is causing the DNA to coil or bend by binding to the DNA and this occurs at low complex loading, and increases with higher concentrations of cylinder.

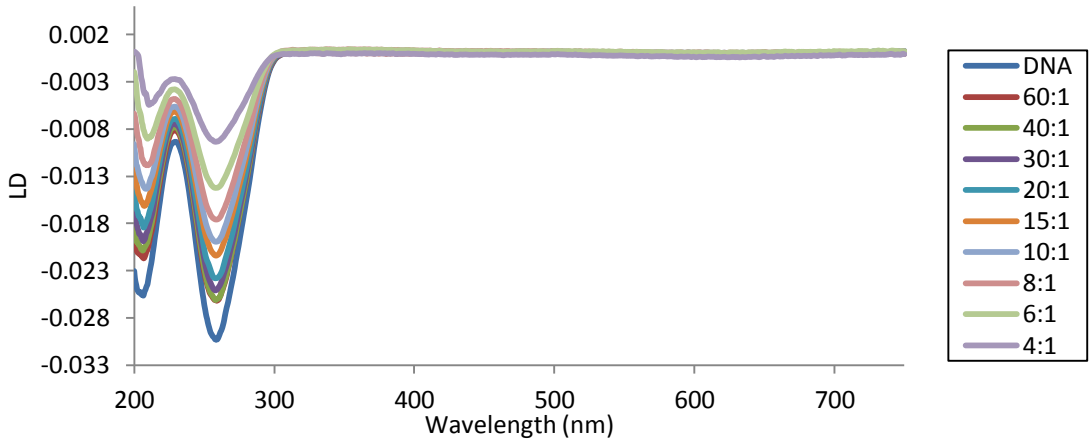

Figure 3.24 LD of 296 μM ct-DNA in 20 mM NaCl and 1 mM $Na(CH_2)_2AsO_2.3H_2O$ (pH 6.8) with increasing concentrations of complex $[Fe_2L^{Estro}{}_3][BF_4]_4$. Legend shows ct-DNA:complex ratios. 6% max. MeOH.

Comparison of the DNA bending activity of the two steroid functionalised cylinders, $[Fe_2L^{Test}{}_3][BF_4]_4$ and $[Fe_2L^{Estro}{}_3][BF_4]_4$, with that of the parent and alkyne-functionalised cylinders (Table 3.1 and Fig. 3.25) show that the steroid functionalised complexes induce less coiling/bending of the DNA. However, the steroid cylinders show a similar bending/coiling activity to that of the phenylacetylene cylinder, $[Fe_2L^{Phen}{}_3][BF_4]_4$, which has a much smaller substituent compared to the bulky steroid moieties, and so the DNA

coiling ability of the testosterone and estrogen functionalised cylinders is surprisingly pronounced.

DNA:complex ratio	% Loss of LD signal at 260nm upon interaction with complexes		
4:1	$[Fe_2L^{P}{}_3][BF_4]_4$	$[Fe_2L^{Test}{}_3][BF_4]_4$	$[Fe_2L^{Estro}{}_3][BF_4]_4$
	99	59	70

Table 3.1 Comparison of the percentage loss of LD signal at 260 nm upon interaction with complexes at a ratio of DNA:complex 4:1.

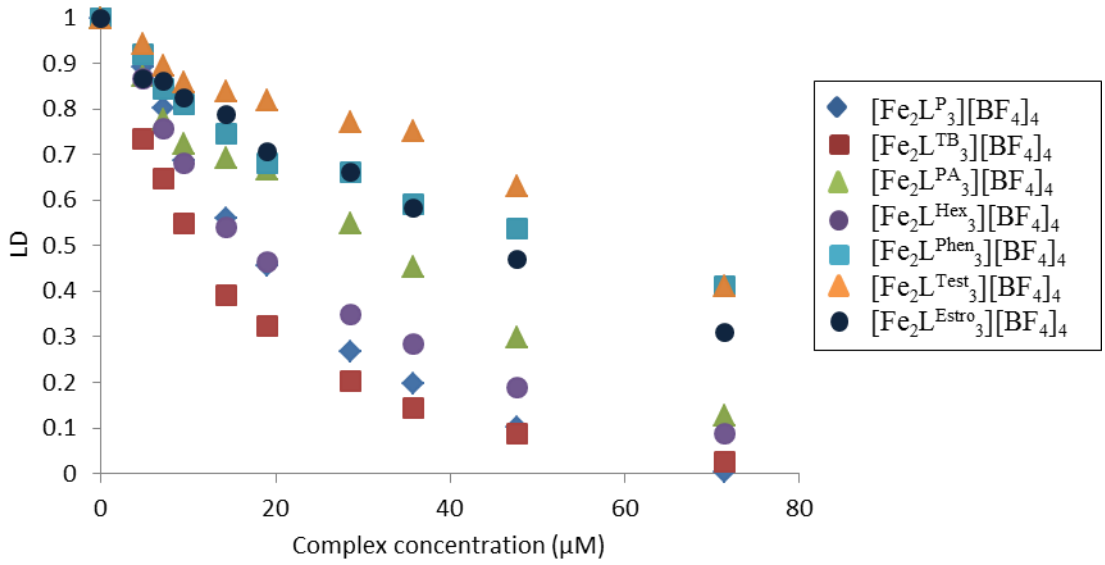

Figure 3.25 Normalised LD signal at 260 nm vs complex concentration for parent, alkyne-functionalised and steroid-functionalised complexes.

3.5.3 Gel electrophoresis studies

Gel electrophoresis experiments analogous to those performed with the parent cylinder and alkyne cylinders (Section 2.6.3, Chapter 2) were carried out for the steroid cylinders, $[Fe_2L^{Test}{}_3][BF_4]_4$ and $[Fe_2L^{Estro}{}_3][BF_4]_4$. A small percentage of methanol was used to dissolve the compounds. Samples containing different plasmid DNA:complex ratios (Table

3.2) were incubated at room temperature for two hours before being run on a 1% agarose gel.

Lanes	1	2	3	4	5	6	7
DNA:complex ratio	MeOH control	50:1	40:1	30:1	20:1	15:1	10:1
Lanes	8	9	10	11	12	13	14
DNA:complex ratio	8:1	6:1	5:1	4:1	3:1	2:1	DNA control

Table 3.2 Ratios of plasmid DNA:complex used in gel electrophoresis experiments.

The agarose gel (Fig. 3.26) for complex $[Fe_2L^{Test}{}_3][BF_4]_4$ shows that the circular and supercoiled forms of the pBR322 plasmid are not altered by addition of the complex, even at high concentrations. The experiment was repeated with a longer sample incubation time of four hours, as it was thought that the bulky steroid cylinder may take longer to correctly orient itself with the DNA to allow binding. However this made no difference to the result.

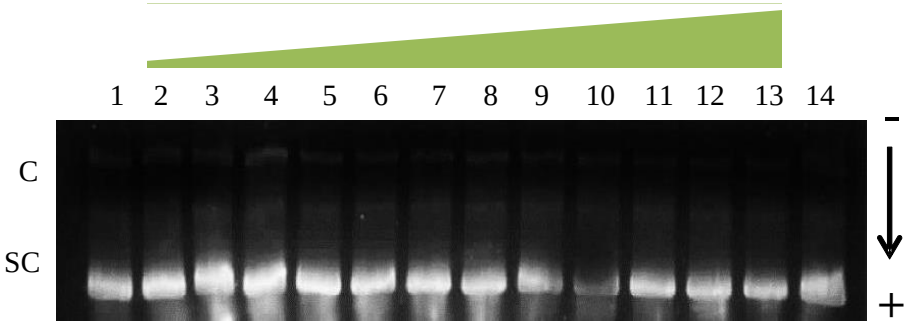

Figure 3.26 Agarose gel (1%) electrophoresis showing changes in electrophoretic mobility of circular (C) and supercoiled (SC) forms of pBR322 plasmid DNA incubated at 20°C for 2 hours with different ratios of complex $[Fe_2L^{Test}{}_3][BF_4]_4$ (lanes 2-13). Control lanes (1 and 14): pBR322 plasmid DNA in absence of complex. 7% max. MeOH.

Similarly, no change in the mobility of either the circular or supercoiled forms of the plasmid DNA can be seen in the agarose gel (Fig. 3.27) for complex $[Fe_2L^{Estro}{}_3][BF_4]_4$. As

for the testosterone version of the cylinder, a longer sample incubation time did not improve the DNA binding or unwinding for this complex.

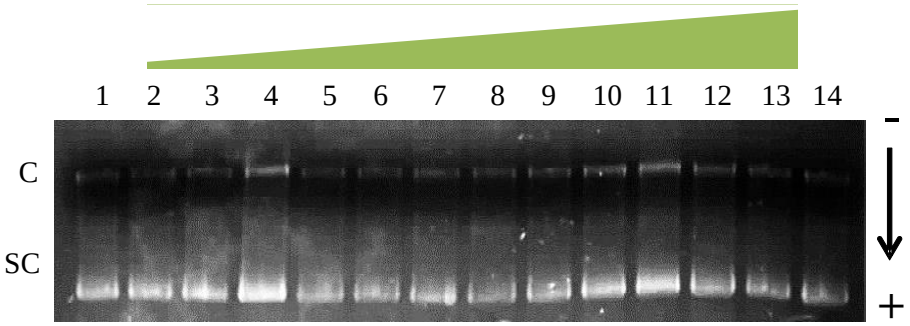

Figure 3.27 Agarose gel (1%) electrophoresis showing changes in electrophoretic mobility of C and SC forms of pBR322 plasmid DNA incubated at 20°C for 2 hours with different ratios of complex $[Fe_2L^{Estro}{}_3][BF_4]_4$ (lanes 2-13). Control lanes (1 and 14): pBR322 plasmid DNA in absence of complex. 7% max. MeOH.

The results of the gel electrophoresis assays for the steroid cylinders show that the two complexes do not unwind supercoiled plasmid DNA, even at high complex concentration.

3.5.4 PAGE studies

Three-way junction polyacrylamide gel electrophoresis studies analogous to those performed with the parent and alkyne cylinders (Section 2.6.4, Chapter 2) were carried out for the steroid cylinders, by co-worker N. Calle Alonso from the University of Birmingham, and are briefly described herein for completeness. Due to the insolubility of the steroid complexes in water, a small percentage of methanol was used to dissolve the compounds. In each experiment control lanes containing one, two and three DNA strands and magnesium chloride were incorporated. The steroid cylinders were mixed with the three non-palindromic oligonucleotide strands to give a ratio of three-way-junction:cylinder of 1:1, incubated for one hour and run on a 15% polyacrylamide gel.

The autoradiogram of the polyacrylamide gel (Fig. 3.28, cropped image; for whole gel see Appendix) shows that no three-way junction is formed by the three oligonucleotide strands on their own, as expected. It is also apparent that the steroid functionalised cylinders, $[Fe_2L^{Test}{}_3][BF_4]_4$ and $[Fe_2L^{Estro}{}_3][BF_4]_4$, do not promote the formation of a DNA three-way junction. This may be due to the size and shape of the steroid substituents and their consequent destabilising interaction with the junction structure, which possibly prevents its formation. A small amount of precipitated DNA can be observed in the sample wells at the top of the gel, indicating some interaction between the single DNA strands and the complexes.

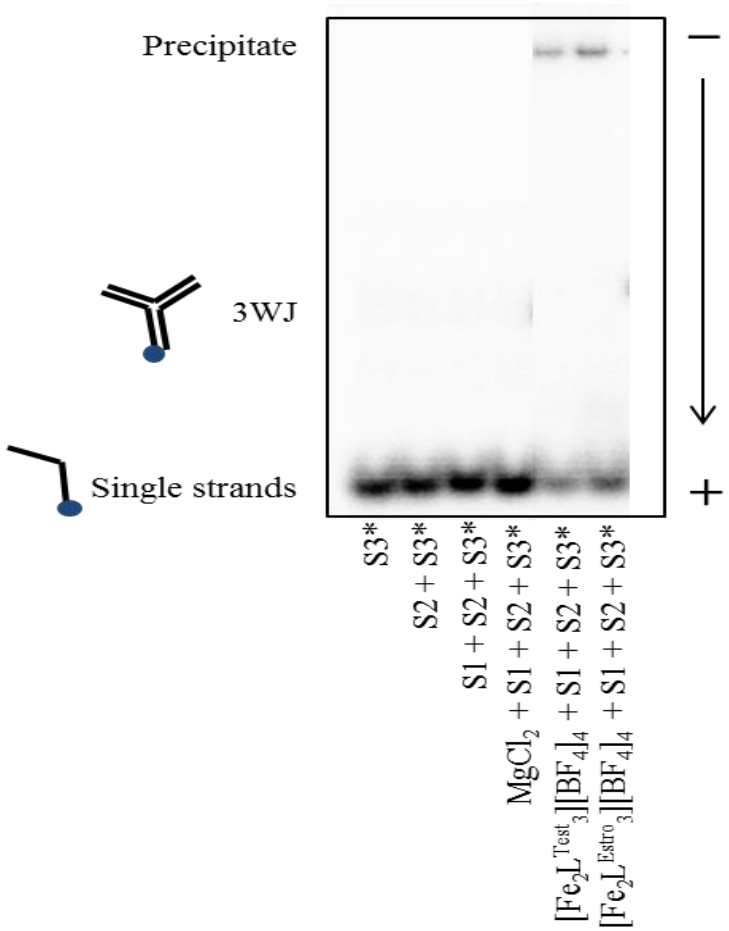

Figure 3.28 Autoradiogram of polyacrylamide gel run at 25 °C. Lanes 1-3: S3*, S3*+S2, S3*+S2+S1 respectively; Lane 4: S3*+S2+S1+$MgCl_2$; Lanes 5-6: S3*+S2+S1 with $[Fe_2L^{Test}{}_3][BF_4]4$ and $[Fe_2L^{Estro}{}_3][BF_4]_4$ respectively. Ratio of three-way junction (S1+S2+S3*):complex of 1:1. Asterisk indicates ^{32}P labelled strand.

3.6 Conclusions

In this chapter, the novel cylinder functionalisation route detailed in chapter 2 was employed to synthesise supramolecular helicates end-functionalised with tumour targeting vectors. Iron(II) cylinders conjugated to the steroid hormones testosterone and estrogen were synthesised in only two reaction steps with overall yields of 12-13%. These complexes were found to be a mixture of diastereoisomers, due to the stereogenic centres of the steroid moieties attached, as demonstrated by ^{1}H NMR Δ-TRISPHAT and circular dichroism studies.

Unfortunately these complexes are insoluble in water, however their solubility in a methanol-water solvent mix allowed DNA binding studies to be carried out. Evaluation of the stability of these complexes in the experimental conditions used for DNA binding studies indicated that they were stable enough to investigate.

Comparison of the stability of these steroid functionalised cylinders with that of Cardo's peptide cylinders (with half-lives of 2.5-4 hours [6,24]) indicates that the bioconjugates developed herein are significantly more stable. This may be due to the way in which the biomolecules are conjugated to the cylinder. The peptide moieties are linked via amide bonds whereas the steroid hormones are linked via alkyne bonds. It may be that the amide bonds are more susceptible to hydrolysis, rendering the conjugates less stable in aqueous solutions.

DNA binding studies were carried out for the $[Fe_2L^{Test}{}_3][BF_4]_4$ and $[Fe_2L^{Estro}{}_3][BF_4]_4$ cylinders. Circular dichroism titrations with ct-DNA revealed that both complexes are able

to bind to DNA. The two steroid functionalised complexes could also bend/coil DNA although less bending/coiling was observed compared to the $[Fe_2L^{TB}_3][BF_4]_4$, $[Fe_2L^{PA}_3][BF_4]_4$ and $[Fe_2L^{Hex}_3][BF_4]_4$ complexes that have smaller functional groups attached. However these compounds were not able to unwind supercoiled plasmid DNA, as investigated by agarose gel electrophoresis experiments, or able to promote the formation of a DNA three way junction, as investigated by PAGE studies.

Unfortunately, as with the alkyne helicates presented in chapter 2, *in vitro* studies could not be undertaken with these steroid functionalised cylinders due to their insolubility in the solvent systems required.

The investigations undertaken indicate that iron(II) supramolecular cylinders can be functionalised with a large biomolecule without complete loss of their inherent DNA binding properties. However, the biomolecule that is conjugated must to be able to impart water solubility to these complexes, as this is a desired and important property of anticancer agents.

3.7 Experimental: synthesis

3.7.1 Materials and methods

All reagents and solvents were purchased from Aldrich, Fisher, Apollo Scientific and Fluorochem and used without further purification. Deuterated NMR solvents were purchased from Goss Scientific. NMR spectra were recorded on Brüker AVIII300 and AVIII400 spectrometers and processed using standard Brüker software. Electrospray Ionisation (ESI) spectra were recorded on a Micromass LCT Time of flight mass spectrometer in positive ionisation mode. IR spectra were recorded on a PerkinElmer Spectrum 100 FT-IR spectrometer. Microanalyses data were obtained using a CE Instruments EA1110 elemental analyser. UV-Vis spectra were performed using a Varian Cary 5000 UV-Vis spectrometer. CD and LD spectra were recorded on a Jasco J-810 spectropolarimeter.

3.7.2 Synthesis of Testosterone cylinder, $[Fe_2L^{Test}_3][BF_4]_4$

3.7.2.1 Synthesis of 17α-[(2-pyridinecarboxaldehyde)-5-ethynyl]ethisterone (6)

Synthesis based on literature procedure.[22]

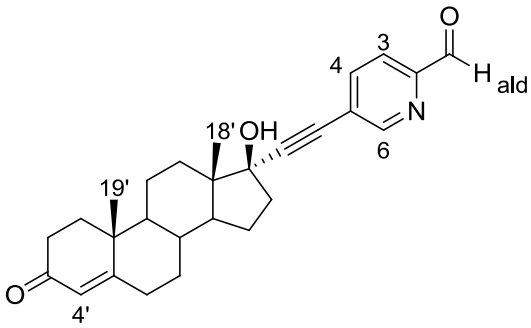

$C_{27}H_{31}NO_3$
FW: 417.55

A schlenk flask was charged with 5-bromo-2-pyridinecarboxaldehyde (0.375 g, 2.02 mmol), bis(triphenylphosphine)dichloropalladium(II) (0.058 g, 0.08 mmol), copper iodide (0.033 g, 0.17 mmol) and 17α-ethynyltestosterone (0.600 g, 1.92 mmol). Anhydrous THF (85 ml) and diisopropylamine (1.19 ml) were added, and the reaction mixture stirred under an argon atmosphere with light exclusion at room temperature for 72 hours. The resulting dark brown crude mixture was evaporated to dryness *in vacuo* and purified by column chromatography on a silica column (MeOH:DCM 2:98). The resulting pale brown solid was dissolved in diethyl ether and purified by column chromatography on a short silica column (diethyl ether) to remove the triphenylphosphine oxide impurity. Evaporation of the solvent yielded a pale brown solid (0.368 g, 44% yield).

^{1}H NMR (300 MHz, $CDCl_3$): δ 10.06 (s, 1H, H_{ald}), 8.79 – 8.78 (m, 1H, H_6), 7.94 – 7.84 (m, 2H, H_3, H_4), 5.74 (s, 1H, $H_{4'}$), 2.48-1.42 (m, 18H, $H_{testosterone}$), 1.22 (s, 3H, $H_{18'/19'}$), 1.13-1.00 (m, 1H, $H_{testosterone}$), 0.97 (s, 3H, H $H_{18'/19'}$).

^{13}C NMR (100 MHz, $CDCl_3$): δ 192.5 (C_{ald}), 152.5 (C_6), 139.5 ($C_{3/4}$), 124.0 ($C_{4'}$), 120.9 ($C_{3/4}$), 53.5 ($C_{testost}$), 50.5 ($C_{testost}$), 39.1 ($C_{testost}$), 36.3 ($C_{testost}$), 35.7 ($C_{testost}$), 33.9 ($C_{testost}$), 32.9 ($C_{testost}$), 32.7 ($C_{testost}$), 31.5 ($C_{testost}$), 23.3 ($C_{testost}$), 20.8 ($C_{testost}$), 17.4 ($C_{18/19}$), 12.9 ($C_{18/19}$).

HRMS (EI): *m/z* = calculated for $C_{27}H_{32}NO_3$ $[M+H]^+$ 418.2382; Found 418.2377.

IR (ν) = 3287 (br, OH), 2937 (m, C-H), 2858 (m, C-H), 2816 (m, C-H), 2217 (s, C≡C), 1713 (s, C=O), 1669 (s, C=O), 1616 (m, C=C), 1582 (m, C=C).

Elemental analysis (%) calculated for $C_{27}H_{31}NO_3$: C: 77.4; H: 7.2; N: 3.7; Found: C: 77.6; H: 7.5; N: 3.6.

3.7.2.2 Synthesis of $[Fe_2L^{Test}_3][BF_4]_4$

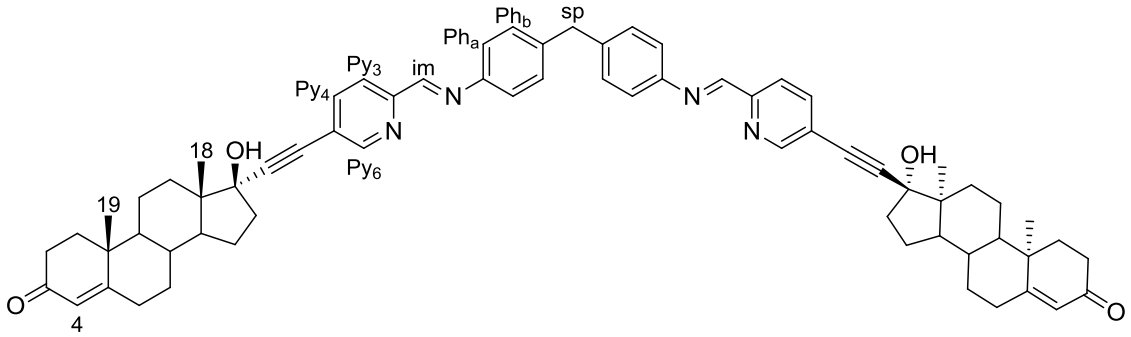

$[Fe_2(C_{67}H_{72}N_4O_4)_3][BF_4]_4$
FW: 3450.90

To a solution of 17α-[(2-pyridinecarboxaldehyde)-5-ethynyl]ethisterone (6) (0.060 g, 0.14 mmol) in ethanol (2 ml) was added a solution of 4,4'-methylenedianiline (0.014 g, 0.07 mmol) in ethanol (3 ml) dropwise. A solution of iron(II) tetrafluoroborate hexahydrate (0.016 g, 0.05 mmol) in ethanol (1 ml) was then immediately added dropwise and the reaction mixture stirred overnight at room temperature. The resulting purple precipitate

was collected by vacuum filtration, washed with chloroform (2 L), diethyl ether (200 ml) and dried for 12 hours over silica, yielding a light purple solid (0.024 g, 29% yield).

^{1}H NMR (300 MHz, CD_3CN): δ 8.91 (s, 2H, H_{im}), 8.47 – 8.39 (m, 2H, H_{Py3}), 8.27 – 8.17 (m, 2H, H_{Py4}), 7.32 – 7.30 (m, 2H, H_{Py6}), 6.91 (br s, 4H, $H_{Pha/\ Phb}$), 5.80 (s, 1H, H_4), 5.68 (s, 1H, $H_{4'}$), 5.50 (br s, 4H, $H_{Pha/\ Phb}$), 4.02 (s, 2H, H_{sp}), 3.60 – 3.56 (m, 2H, H_{OH}), 2.49 – 1.38 (m, 38H, $H_{testosterone}$ + 43H, solvent), 1.23 (s, 6H, $H_{18/19}$), 0.88 (s, 6H, $H_{18/19}$).

Mass spectrum (ESI): *m/z* = 775.8 $[Fe_2(C_{67}H_{72}N_4O_4)_3]^{4+}$, 1034.1 $[Fe_2(C_{67}H_{72}N_4O_4)_3]^{3+}$.

IR (ν) = 3384 (br, OH), 2941 (w, C-H), 2218 (s, C≡C), 1655 (s, C=O), 1543 (m, C=C), 1054 (s, br, BF_4).

UV-Vis (MeOH): λ_{max} [nm] (ε_{max}/$dm^3mol^{-1}cm^{-1}$): 240 (148,500), 319 (91,200), 534 sh (8,900), 593 (13,700).

3.7.3 Synthesis of Estrogen cylinder, $[Fe_2L^{Estro}{}_3][BF_4]_4$

3.7.3.1 Synthesis of 17α-[(2-pyridinecarboxaldehyde)-5-ethynyl]estradiol (7)

Synthesis based on literature procedure.[22]

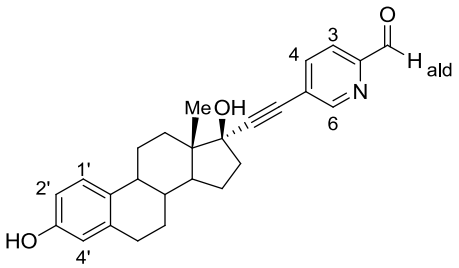

$C_{26}H_{27}NO_3$
FW: 401.50

A schlenk flask was charged with 5-bromo-2-pyridinecarboxaldehyde (0.300 g, 1.61 mmol), bis(triphenylphosphine)dichloropalladium(II) (0.024 g, 0.03 mmol), copper iodide

(0.020 g, 0.11 mmol) and 17α-ethynylestradiol (0.486 g, 1.64 mmol). Anhydrous THF (24 ml) and diisopropylamine (10 ml) were added, and the reaction mixture stirred under an argon atmosphere with light exclusion at room temperature for 72 hours. The resulting dark brown crude mixture was evaporated to dryness *in vacuo* and purified by column chromatography on a silica column (MeOH:DCM 2:98). The resulting pale brown solid was dissolved in diethyl ether and purified by column chromatography on a short silica column (diethyl ether) to remove the triphenylphosphine oxide impurity. Evaporation of the solvent yielded a pale brown solid (0.317 g, 49% yield).

^{1}H NMR (300 MHz, $CDCl_3$): δ 10.07 (s, 1H, H_{ald}), 8.82 – 8.81 (m, 1H, H_6), 7.92 – 7.90 (m, 2H, H_3, H_4), 7.16 (d, *J* = 8.5, 1.0 Hz, 1H, $H_{1'}$), 6.72 – 6.52 (m, 1H, $H_{2'}$), 6.57 (d, *J* = 2.8 Hz, 1H, $H_{4'}$), 4.78 (s, 1H, H_{OH}), 2.86 – 2.81 (m, 2H, $H_{estrogen}$), 2.51-1.25 (m, 13H, $H_{estrogen}$), 0.96 (s, 3H, H_{Me}).

^{13}C NMR (100 MHz, $CDCl_3$): δ 192.5 (C_{ald}), 152.4 (C_6), 139.5 ($C_{3/4}$), 126.5 ($C_{1'}$), 120.9 ($C_{3/4}$), 115.2 ($C_{4'}$), 112.7 ($C_{2'}$), 50.0 ($C_{estrogen}$), 43.6 ($C_{estrogen}$), 39.4 ($C_{estrogen}$), 39.1 ($C_{estrogen}$), 33.2 ($C_{estrogen}$), 29.6 ($C_{estrogen}$), 27.2 ($C_{estrogen}$), 26.4 ($C_{estrogen}$), 22.9 ($C_{estrogen}$), 12.8 (C_{Me}).

HRMS (EI): *m/z* = calculated for $C_{26}H_{27}NO_3Na$ $[M+Na]^+$ 424.1889; Found 424.1890.

IR (ν) = 3316 (br, OH), 2928 (m, C-H), 2867 (m, C-H), 2224 (s, C≡C), 1707 (s, C=O), 1611 (m, C=C), 1581 (m, C=C).

3.7.3.2 Synthesis of $[Fe_2L^{Estro}{}_3][BF_4]_4$

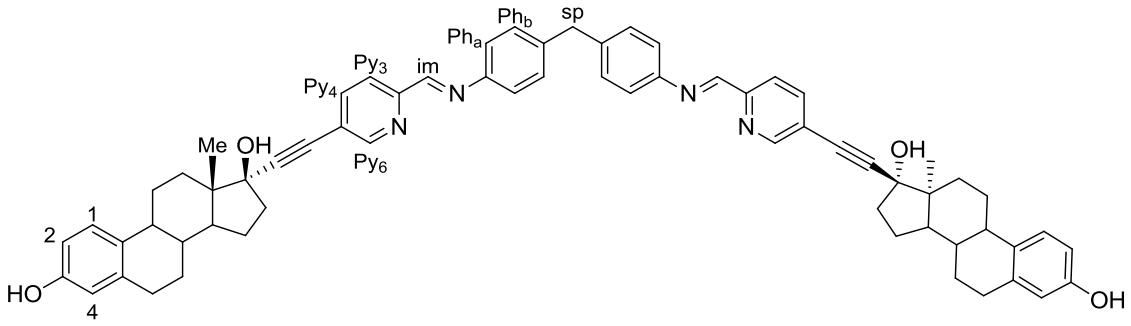

$[Fe_2(C_{65}H_{64}N_4O_4)_3][BF_4]_4$
FW: 3354.64

To a solution of 17α-[(2-pyridinecarboxaldehyde)-5-ethynyl]estradiol (7) (0.060 g, 0.15 mmol) in ethanol (2 ml) was added a solution of 4,4'-methylenedianiline (0.015 g, 0.08 mmol) in ethanol (3 ml) dropwise. A solution of iron(II) tetrafluoroborate hexahydrate (0.017 g, 0.05 mmol) in ethanol (1 ml) was then immediately added dropwise and the reaction mixture stirred overnight at room temperature. The resulting purple precipitate was collected by vacuum filtration, washed with chloroform (1 L), diethyl ether (200 ml) and dried for 12 hours over silica, yielding a light purple solid (0.021 g, 25% yield).

^{1}H NMR (300 MHz, CD_3CN): δ 8.85 – 8.83 (m, 2H, H_{im}), 8.35 – 8.30 (m, 2H, H_{Py3}), 8.07 (d, *J* = 7.5 Hz, 1H, H_{Py4}), 7.81 (d, *J* = 7.5 Hz, 1H, $H_{Py4'}$), 7.31 – 7.23 (m, 4H, $H_{Py6,}$ $H_{1/2}$), 6.89 (br s, 4H, $H_{Pha/b}$), 6.74 – 6.52 (m, 6H, $H_{estrogen\text{-}OH}$/$H_{1/2,}$ H_4), 5.45 (br s, 4H, $H_{Pha/b}$), 3.98 (s, 2H, H_{sp}), 3.48 (s, 1H, H_{OH}), 3.36 (s, 1H, H_{OH}), 2.88 – 2.79 (m, 4H, $H_{estrogen}$), 2.35 – 1.20 (m, 26H, $H_{estrogen}$ + 95H, solvent), 0.87 (s, 6H, H_{Me}).

Mass spectrum (ESI): *m/z* = 751.9 $[Fe_2(C_{65}H_{64}N_4O_4)_3]^{4+}$, 1002.2 $[Fe_2(C_{65}H_{64}N_4O_4)_3]^{3+}$, 1031.6 $[Fe_2(C_{65}H_{64}N_4O_4)_3][BF_4]^{3+}$, 1502.9 $[Fe_2(C_{65}H_{64}N_4O_4)_3]^{2+}$.

IR (ν) = 3449 (br, OH), 2928 (m, C-H), 2869 (m, C-H), 2221 (s, C≡C), 1610 (m, C=C), 1587 (m, C=C), 1543 (m, C=C), 1056 (s, br, BF_4).

UV-Vis (MeOH): λ_{max} [nm] (ε_{max}/$dm^3mol^{-1}cm^{-1}$): 230 sh (117,500), 279 sh (60,200), 321 (106,000), 542 sh (11,500), 593 (15,500).

3.8 Experimental: DNA binding studies

3.8.1 Materials and methods

All DNA binding studies were carried out using Ultrapure water (18.2 MΩ) purchased from Fisher Scientific. Calf thymus (ct) DNA, highly polymerised, was purchased from Sigma Aldrich and pBR322 plasmid DNA was purchased from New England Biolabs. Both were used without further purification and kept frozen. Tris-acetate-EDTA buffer was purchased from Fisher and agrose from USB Corporation.

3.8.2 Circular and Linear Dichroism Experiments

CD and LD measurements were recorded using a Jasco J-810 spectropolarimeter. CD measurements were carried out in quartz cuvettes of 1 cm (750-200 nm) or 0.1 cm (450-200 nm) pathlength. LD experiments were recorded in a flow couette cell (Krometek) with a 0.1 cm pathlength.

Stock solutions of ct-DNA (3000 μM) in water were prepared and kept frozen until the day of the experiment. Sodium chloride (1 M) and sodium cacodylate ($Na(CH_2)_2AsO_2.3H_2O$) (100 mM) buffer stock solutions were used to prepare final ct-DNA solutions of 300 μM

with 20 mM NaCl and sodium cacodylate (1 mM) (pH 6.8). DNA concentrations were determined by UV-Vis measurements using the known molar extinction coefficient of ε_{258} = 6600 $mol^{-1}dm^3cm^{-1}$ per DNA base.

CD and LD titrations were carried out using three solutions; solution A (a 300 μM ct-DNA solution, containing NaCl (20 mM) and sodium cacodylate (1 mM)); solution B (a 500 μM complex solution) and solution C (a 600 μM ct-DNA solution, containing 40 mM NaCl and sodium cacodylate (2 mM)). Firstly solution A was recorded, then equal aliquots of solutions B and C were added, keeping the concentration of ct-DNA constant throughout the titration. The titration was carried out to obtain an initial ct-DNA:complex ratio of 60:1 decreasing to 4:1. The stock solution of complex was stored in ice during the experiment.

3.8.3 Agarose gel electrophoresis

Agarose gels were prepared by warming agarose (2 g) in 1x Tris-acetate-EDTA buffer which was then poured into a gel tray (210 x 150 mm) fitted with a 15 toothed comb, to produce sample wells. The gel was left to set for 40 minutes. Sample solutions (16 μl) were prepared containing 96.3 μM pBR322 plasmid DNA and different concentrations of complexes (from 60 μM stock solution in water and up to 7% MeOH) to obtain plasmid:complex ratios ranging from 100:1 to 2:1. Theses sample solutions were incubated for 2 hours at room temperature. Before loading , 4 μl loading buffer (30% glycerol, 0.25% bromophenol blue) was added, the samples were mixed and then 16 μl of the samples loaded into the gel wells. The gel was run for 2.5 hours in an Amersham Biosciences HE99X Maxi submarine kit with an electrophoresis Power Supply-EPS 301 system, at a

constant voltage of 120 V and 400 mA, in 1x Tris-acetate-EDTA running buffer. The gel was then stained with an ethidium bromide solution (0.5 $mg.ml^{-1}$) in 200 ml of water for 20 minutes and visualised using a UVtec–uvipro platinum 2.0 system (UVidoc, Cambridge, UK) at 312 nm.

3.8.4 Polyacrylamide Gel Electrophoresis (PAGE)

Procedure provided by S. Phongtongpasuk [29] and carried out by N. Calle Alonso, both of the Hannon group, University of Birmingham.

3.8.4.1 Radioactive labelling

Oligonucleotides (sequences S1: CGGAACGGCACTCG, S2: CGAGTGCAGCGTGG, S3: CCACGCTCGTTCCG) were purchased from MWG Eurofin. One strand was labelled with P^{32} at the 5' terminus using T4 polynucleotide kinase (New England Biolabs) and [γ-^{32}P] adenosine 5'-triphosphate (Perkin Elmer). First ultrapure water (4.8 µl), 10x bacteriophage T4 polynucleotide kinase buffer (1 µl), oligonucleotide S3 (1.2 µl of 100 µM), bacteriophage T4 polynucleotide kinase (1 µl) (New England Biolabs) and γ-^{32}P ATP (2 µl of 6000 Ci/mmol) (Perkin Elmer) were incubated in an eppendorf at 37°C for 40 minutes. To deactivate the polynucleotide kinase, the solution was then heated to 80°C for 3 minutes.

To purify the radioactive-labelled DNA fragments from any unreacted ATP a QIAquick nucleotide removal kit (QIAGEN) was employed. 10 volumes of PN buffer were added to 1 volume of reaction sample and this solution was loaded onto a QIAquick spin column

with a 2 ml collection tube, centrifuged for 1 minute at 6000 rpm and the flow through discarded. A new collection tube was then fitted to the column, PE buffer (500 µl) was added and this solution was centrifuged for 1 minute at 6000 rpm and the flow through discarded. Again, PE buffer (500 µl) was added and the solution was centrifuged at 13000 rpm for 1 minute to remove residual buffer. The column was then put into a fresh eppendorf, ultrapure water (30 µl) was added to the column and this was left for 5 minutes. After centrifuging at 13000 rpm for 2 minutes a radiolabelled DNA stock solution (8 µM) was obtained.

3.8.4.2 Polyacrylamide gel preparation

A 15% native polyacrylamide gel was prepared by mixing 52.5 ml of ultra pure water, 10 ml of 10x TB buffer (890 mM tris(hydroxymethy)amino methane and 890 mM boric acid) (pH 8.3), 37.5 ml of 40% acrylamide (29:1) (Geneflow), 500 µl of 10% (w/v) ammonium persulfate and 75 µl tetramethylenediamine (TEMED). This was then poured onto a set of glass plates and left to set for 40 minutes. The wells of the polymerised gel were washed with running buffer (TB buffer) and the gel was pre-run at 200 V for 5 minutes before sample loading.

3.8.4.3 PAGE electrophoresis experiment

Sample solutions were prepared by mixing solutions of the complexes with stoichiometric amounts of oligonucleotides in TBN buffer (89 mM tris(hydroxymethy)amino methane, 89 mM of boric acid and 100 µM NaCl) (pH 8.3) to give final concentrations of 0.4 µM for each single strand (1.2 µM total concentration of DNA) and 0.4 µM of complex. This gives

a three-way junction:complex ratio of 1:1. The sample solutions were incubated for 1 hour at room temperature and then in ice for 15 minutes. To prepare the samples for loading, 5 µl of 30% glycerol was added to each eppendorf. 13 µl of each sample was then loaded onto the 15% polyacrylamide gel. The gel was run for 4 hours at 120 V using Gel System equipment (Thermo Scientific UK). It was then exposed on a phosphor imaging plate for 1-16 hours depending on how fresh the radioactive ATP used was. A radiogel image was obtained using a Molecular Imager FX (Bio-Rad) and the gel was quantified using Quantity One software.

3.9 References

(1) Hotze, A. C.; Hodges, N. J.; Hayden, R. E.; Sanchez-Cano, C.; Paines, C.; Male, N.; Tse, M. K.; Bunce, C. M.; Chipman, J. K.; Hannon, M. J., *Chem. Biol.* **2008**, *15*, 1258.

(2) Wong, E.; Giandomenico, C. M., *Chem. Rev.* **1999**, *99*, 2451.

(3) Zutphen, S. v.; Reedijk, J., *Coord. Chem. Rev.* **2005**, *249*, 2845.

(4) Sinha, R.; Kim, G. J.; Nie, S.; Shin, D. M., *Mol. Cancer Ther.* **2006**, *5*, 1909.

(5) Vivès, E.; Schmidt, J.; Pèlegrin, A., *BBA - Rev. Cancer* **2008**, *1786*, 126.

(6) Cardo, L.; Hannon, M. J., *Inorg. Chim. Acta* **2009**, *362*, 784.

(7) Cardo, L.; Sadovnikova, V.; Phongtongpasuk, S.; Hodges, N. J.; Hannon, M. J., *Chem. Commun.* **2011**, *47*, 6575.

(8) Borgquist, S.; Holm, C.; Stendahl, M.; Anagnostaki, L.; Landberg, G.; Jirström, K., *J. Clin. Pathol.* **2008**, *61*, 197.

(9) Isola, J. J., *J. Pathol.* **1993**, *170*, 31.

(10) Kuenen-Boumeester, V.; van der Kwast, T. H.; van Putten, W. L. J.; Claassen, C.; van Ooijen, B.; Henzen-Logmans, S. C., *Int. J. Cancer* **1992**, *52*, 581.

(11) Lea, O. A.; Kvinnsland, S.; Thorsen, T., *Cancer Res.* **1989**, *49*, 7162.

(12) Cardillo, M. R.; Petrangeli, E.; Aliotta, N.; Salvatori, L.; Ravenna, L.; Chang, C.; Castagna, G., *J. Exp. Clin. Cancer Res.* **1998**, *17*, 231.

(13) Kühnel, R.; de Graapf, J.; Rao, B. R.; Stolk, J. G., *J. Steroid Biochem.* **1987**, *26*, 393.

(14) Ilekis, J. V.; Connor, J. P.; Prins, G. S.; Ferrer, K.; Niederberger, C.; Scoccia, B., *Gynecologic Oncology* **1997**, *66*, 250.

(15) Leav, I.; Lau, K.-M.; Adams, J. Y.; McNeal, J. E.; Taplin, M.-E.; Wang, J.; Singh, H.; Ho, S.-M., *Am. J. Pathol.* **2001**, *159*, 79.

(16) Hobisch, A.; Culig, Z.; Radmayr, C.; Bartsch, G.; Klocker, H.; Hittmair, A., *Cancer Res.* **1995**, *55*, 3068.

(17) Ruizeveld de Winter, J. A.; Janssen, P. J.; Sleddens, H. M.; Verleun-Mooijman, M. C.; Trapman, J.; Brinkmann, A. O.; Santerse, A. B.; Schröder, F. H.; van der Kwast, T. H., *Am. J. Pathol.* **1994**, *144*, 735.

(18) Sanchez-Cano, C.; Hannon, M. J., *Dalton Trans.* **2009**, 10765.

(19) Huxley, M.; Sanchez-Cano, C.; Browning, M. J.; Navarro-Ranninger, C.; Quiroga, A. G.; Rodger, A.; Hannon, M. J., *Dalton Trans.* **2010**, *39*, 11353.

(20) Jodry, J. J.; Lacour, J., *Chem. Eur. J.* **2000**, *6*, 4297.

(21) Albrecht, M., *Chem. Eur. J.* **2000**, *6*, 3485.

(22) Browning, M., Estrogen Steroid Derived Metallo-drugs, *PhD Thesis, University of Warwick* **2006**.

(23) Lacour, J.; Ginglinger, C.; Grivet, C.; Bernardinelli, G., *Angew. Chem. Int. Ed. Engl.* **1997**, *36*, 608.

(24) Cardo, L., Metallo-supramolecular Cylinders and their Peptide Conjugates. Synthesis, dynamics and DNA recognition, *PhD Thesis, University of Birmingham* **2010**.

(25) Pearmund, C. R., Metallo-supramolecular Cylinders as Chemical Nucleases, *PhD Thesis, University of Warwick* **2006**.

(26) Hannon, M. J.; Meistermann, I.; Isaac, C. J.; Blomme, C.; Aldrich-Wright, J. R.; Rodger, A., *Chem. Commun.* **2001**, 1078.

(27) Twyman, L. J.; Beezer, A. E.; Esfand, R.; Hardy, M. J.; Mitchell, J. C., *Tetrahedron Lett.* **1999**, *40*, 1743.

(28) Hannon, M. J.; Moreno, V.; Prieto, M. J.; Moldrheim, E.; Sletten, E.; Meistermann, I.; Isaac, C. J.; Sanders, K. J.; Rodger, A., *Angew. Chem. Int. Ed.* **2001**, *40*, 879.

(29) Phongtongpasuk, S., Investigating the Interaction of a Metallosupramolecular Cylinder With Nucleic Acids, *PhD Thesis, University of Birmingham* **2011**.

Chapter 4: Sugar Functionalised Metallo-Cylinders

4.1 Introduction and aims

In chapter 3, the design and synthesis of two supramolecular helicates end-functionalised with tumour targeting vectors, testosterone and estrogen, were described. The DNA binding studies carried out for these compounds showed that aspects of the inherent DNA binding of the parent cylinder had been retained, with both complexes binding to DNA and causing intramolecular coiling of the DNA. Unfortunately, *in vitro* studies could not be undertaken with these compounds due to their insolubility in water.

These studies show that functionalisation of the cylinder with a biomolecule via an alkyne linker can produce relatively stable complexes that retain some of the DNA binding properties of the unmodified parent cylinder. Reasoning that attaching a highly water soluble biomolecule to the cylinder might produce a water-soluble targeted helicate, with enhanced or specific delivery to cancerous tissues, this chapter details the design and DNA binding of sugar functionalised cylinders.

4.1.1 Sugar functionalisation

As previously discussed (Section 3.1.1, Chapter 3), one of the strategies for the delivery of anticancer drugs to cancerous tissue is receptor mediated targeting. This involves the exploitation of cell surface receptors that are overexpressed by tumour cells to deliver biomolecule-drug conjugates across the cell membrane.[1]

Carbohydrates make up one category of biomolecules that can be used in this strategy.[1,2] Conjugation of sugars to therapeutic drugs can lead to increased water solubility, membrane permeability, molecular targeting and can also introduce chirality.[3,4] The carbohydrate can interact with carbohydrate transporters and metabolic pathways in the body if attached to the drug by some kind of linker.[4] A large and varied range of tissues and cells highly express carbohydrate receptors that can be targeted by sugar-conjugates.[5] For example, mannose receptors are present on macrophages and so can be targeted to treat bacterial infectious diseases, inflammatory diseases and genetic metabolic diseases, and galactose and lactose receptors are abundant in a variety of tumour types.[5]

There are many examples of cisplatin and cisplatin derivatives conjugated to sugar moieties, for improved cellular targeting. An oxaliplatin analogue functionalised with a glucose derivative (Fig. 4.1) was designed to take advantage of the increased glycolytic activity observed in all primary and metastatic cancers, and the upregulation of glucose transporters.[6] The complex was found to be cytotoxic in cervical and colon cancer cell lines, however enhanced uptake due to the sugar moiety was not proven.[6] Another cisplatin analogue conjugated to glucose (Fig. 4.1) was found to be cytotoxic to human ovarian and melanoma cancer cell lines with potency similar to that of cisplatin, and was found to have improved water solubility.[7]

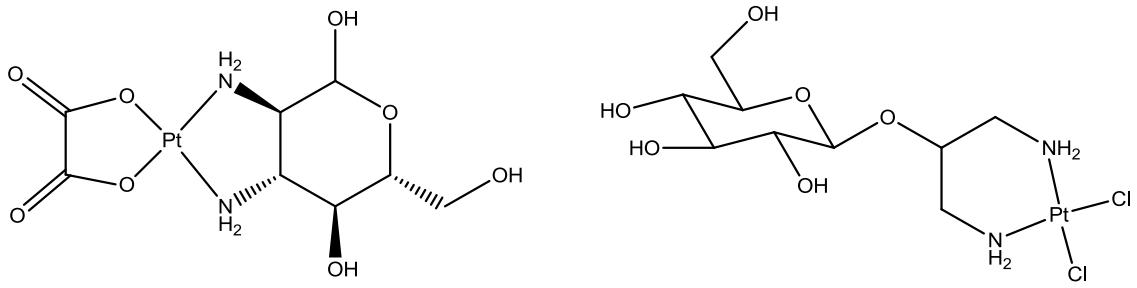

Figure 4.1 Structure of sugar functionalised oxaliplatin analogue (left) and cisplatin analogue conjugated to a glucose derivative (right).[6,7]

Carbohydrates are also employed to target radiopharmaceuticals such as a ^{99m}Tc-ethylenedicysteine-deoxyglucose complex (Fig. 4.2).[8] The tumour imaging agent was found to have a significantly higher cellular uptake compared with its non-sugar analogue, thought to be mediated by a glucose receptor.[8] The agent was observed to accumulate in proliferating tumour tissue due to the increased carbohydrate metabolism of these cells.[8]

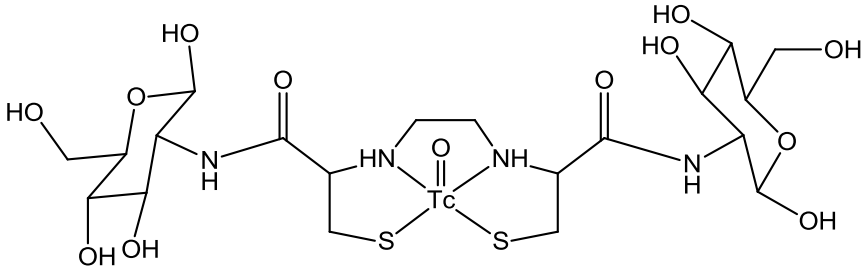

Figure 4.2 Structure of ^{99m}Tc-ethylenedicysteine-deoxyglucose complex.[8]

A metallo-intercalator designed as a luminescent biological probe was conjugated to several different sugars including a β-D-glucosaminide (Fig. 4.3).[9] The water soluble complex binds to DNA by intercalation and has similar cytotoxic potency to that of cisplatin in brain, breast and epithelial carcinoma cancer cell lines.[9] Unfortunately the complex was not luminescent.[9]

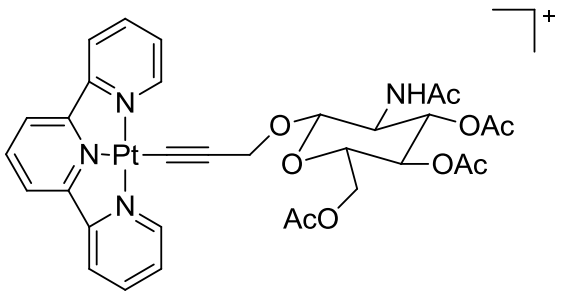

Figure 4.3 Structure of metallo-intercalator conjugated to a β-D-glucosaminide sugar.[9]

4.2 Molecular design

As drug-sugar conjugates show promising targeting activity, helicates functionalised with sugars will be developed. The conjugation of a sugar moiety can be achieved using the novel functionalisation route described in chapter 2, and may lead to increased water solubility of the complexes. The acetyl and hydroxyl analogues of β-D-glucosaminide will be conjugated to the ends of the cylinder, at the 5-position of the pyridine-carboxaldehyde (Fig. 4.4).

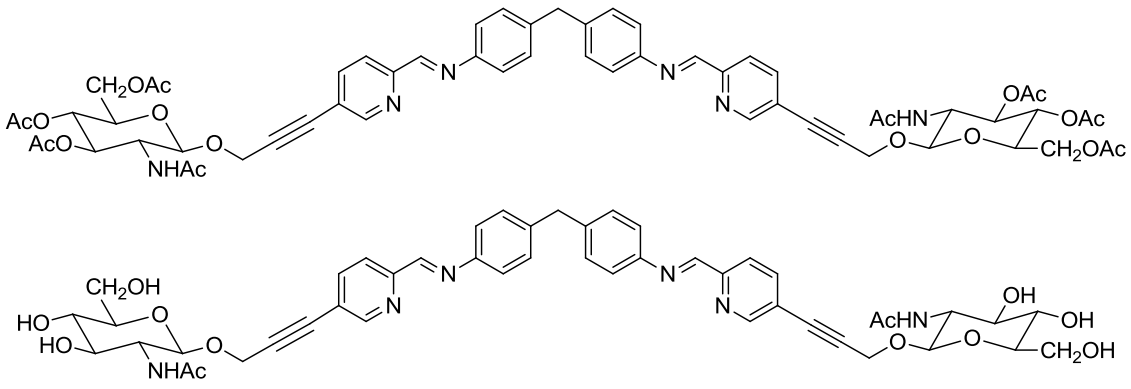

Figure 4.4 Structures of ligands functionalised with acetyl β-D-glucosaminide (top) and hydroxyl β-D-glucosaminide (bottom).

As these sugars have multiple stereogenic centres, their effect on the chirality of the

cylinder when conjugated must be considered. This will be investigated to see whether any chiral induction is observed.

4.3 Synthesis

4.3.1 Synthesis of acetyl sugar cylinder, $[Fe_2L^{OAcSug}{}_3][BF_4]_4$

4.3.1.1 Synthesis of 5-(2-N-acetyl-3,4,6-tri-O-acetyl-1-(2'-propargyl)-β-D-glucosaminide)-2-pyridinecarboxaldehyde (9)

As 5-(2-N-acetyl-3,4,6-tri-O-acetyl-1-(2'-propargyl)-β-D-glucosaminide)-2-pyridinecarboxaldehyde (9) is not commercially available it was synthesised in two steps (Scheme 4.1). The first step, to synthesise 2-N-acetyl-3,4,6-tri-O-acetyl-1-(2'-propargyl)-β-D-glucosaminide (8), was carried out according to a literature procedure.[9] The sugar starting material was coupled to propargyl alcohol using silver trifluoromethane sulfonate at low temperature. A Sonogashira coupling, based on literature procedure,[10] was then used to couple this alkyne sugar to 5-bromo-2-pyridinecarboxaldehyde, with bis(triphenylphosphine)dichloropalladium(II) and copper iodide as catalysts. After reaction for seventy two hours under an argon atmosphere, the triphenylphosphine impurity was removed by protonating the product with hydrochloric acid, partitioning the product and impurity in immiscible solvents, neutralising the acidic solution and extraction of the product with ethyl acetate. After further purification by column chromatography on silica, a white solid was obtained in 40% yield.

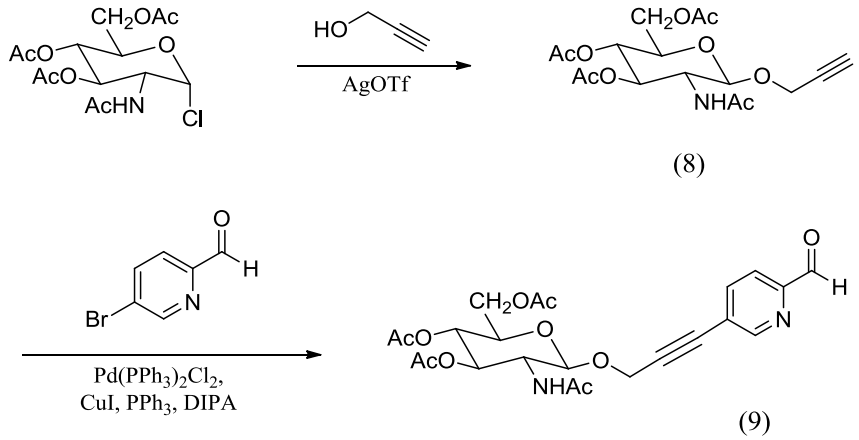

Scheme 4.1 Synthetic route for preparation of 5-(2-N-acetyl-3,4,6-tri-O-acetyl-1-(2'-propargyl)-β-D-glucosaminide)-2-pyridinecarboxaldehyde (9).

The product (9) was characterised by high resolution EI mass spectrometry and elemental analysis, both of which confirmed the formation of the desired product. Peaks in the ^{1}H NMR spectrum (Fig. 4.5), assigned using a 2D-COSY (see Appendix), corresponding to the sugar and pyridine-carboxaldehyde moieties at equal integration gives evidence for the formation of the product. The acetyl methyl groups of the sugar can be seen at low chemical shift.

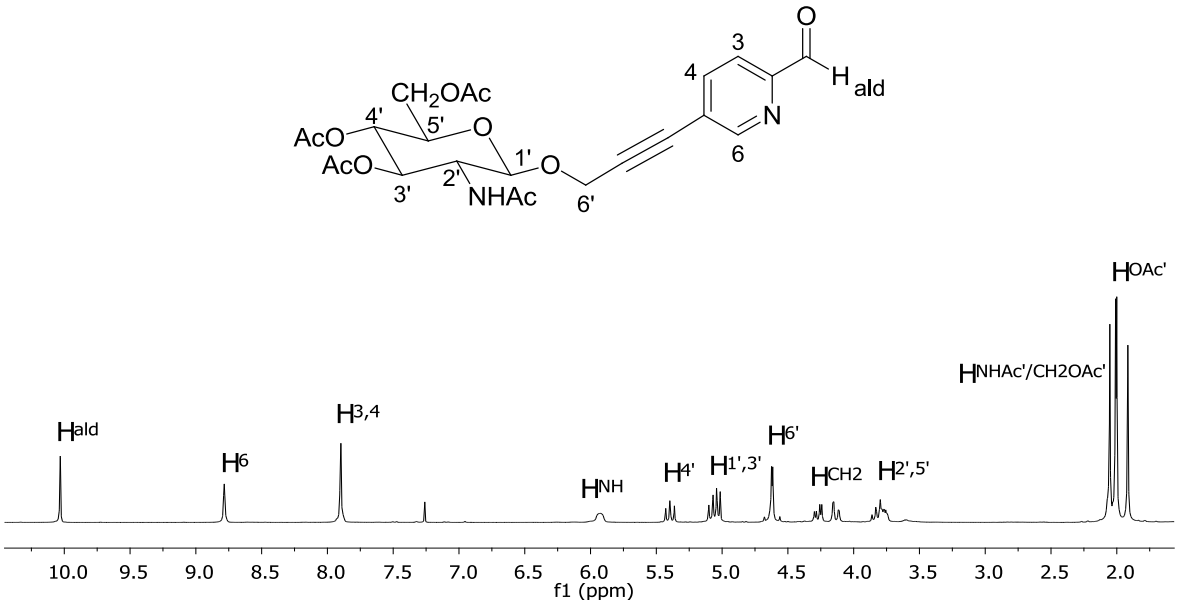

Figure 4.5 ^{1}H NMR (300 MHz, $CDCl_3$, 298 K) of 5-(2-N-acetyl-3,4,6-tri-O-acetyl-1-(2'-propargyl)-β-D-glucosaminide)-2-pyridinecarboxaldehyde (9).

4.3.1.2 Synthesis of $[Fe_2L^{OAcSug}{}_3][BF_4]_4$

The acetyl sugar cylinder, $[Fe_2L^{OAcSug}{}_3][BF_4]_4$, was synthesised using a one-pot procedure with six equivalents of 5-(2-N-acetyl-3,4,6-tri-O-acetyl-1-(2'-propargyl)-β-D-glucosaminide)-2-pyridinecarboxaldehyde (9), three equivalents of the spacer, 4,4'-methylenedianiline, and two equivalents of the metal salt, iron(II) tetrafluoroborate hexahydrate, added sequentially and dropwise, in ethanol (Scheme 4.2). An immediate dark purple precipitate formed on addition of the reactants, suggesting the formation of an iron(II) cylinder. The product was isolated by filtration and washed with copious amounts of ethanol yielding a purple solid in 31% yield.

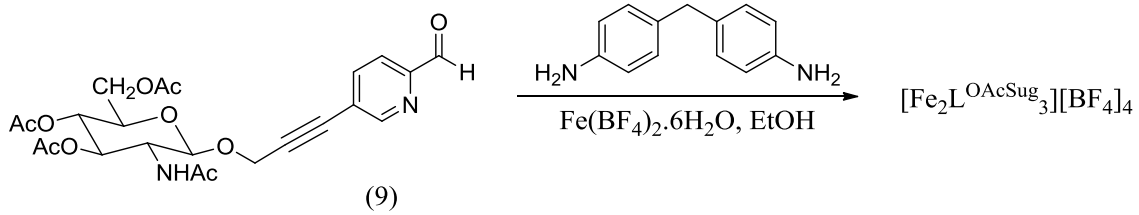

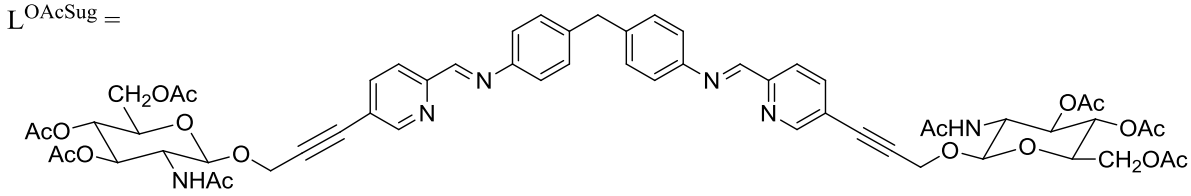

Scheme 4.2 Synthetic route for preparation of $[Fe_2L^{OAcSug}{}_3][BF_4]_4$.

The light purple solid was confirmed to be the desired product, $[Fe_2L^{OAcSug}{}_3][BF_4]_4$, by characterisation with ESI mass spectrometry and NMR spectroscopy. One multiply charged peak in the ESI mass spectrum can be attributed to the species $[Fe_2(C_{59}H_{62}N_6O_{18})_3]^{4+}$ (see Appendix). The characteristic imine peak (H_{im}) of the cylinder observed in the ^1H NMR spectrum (Fig. 4.6), assigned using 2D-COSY (see Appendix),

shows formation of the product. Peaks corresponding to the spacer (H_{sp}) and phenyl protons ($Ph_{a/b}$) and the protons of the sugar moiety can also be observed. The formation of the cylinder has not altered the chemical shift of the sugar protons much, most likely due to the metal coordination site being quite a distance from the sugar moiety. The peaks of the acetyl methyl protons are partially obscured by the deuterated acetonitrile solvent peak and corresponding water peak, however they are observed and at the correct integration (Fig. 4.7).

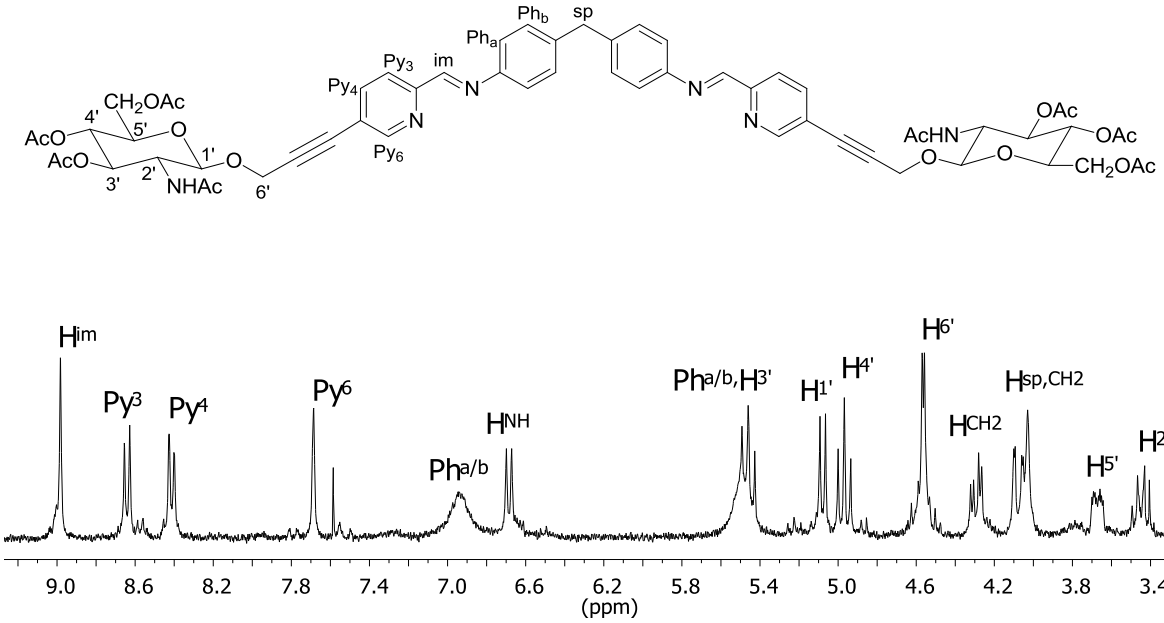

Figure 4.6 ^{1}H NMR (300 MHz, CD_3CN, 298 K) of $[Fe_2L^{OAcSug}{}_3][BF_4]_4$.

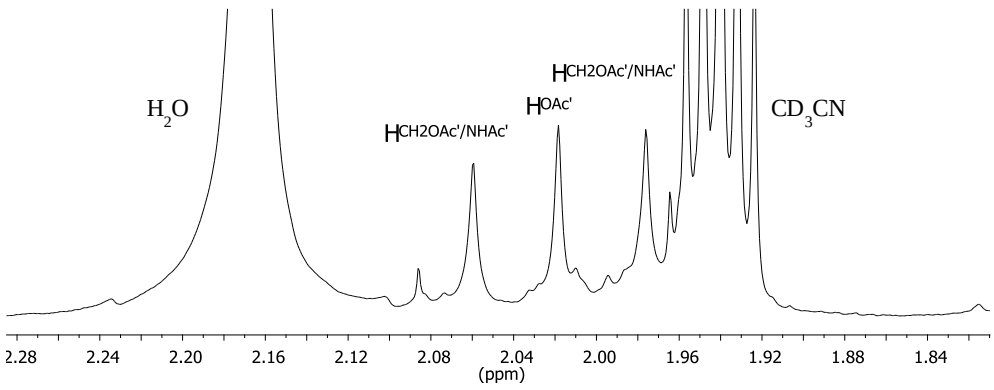

Figure 4.7 ^{1}H NMR (300 MHz, CD_3CN, 298 K) of $[Fe_2L^{OAcSug}{}_3][BF_4]_4$; low chemical shift region.

An overall yield of 4%, with respect to the sugar starting material, was obtained for the synthesis of the acetyl-sugar cylinder, $[Fe_2L^{OAcSug_3}][BF_4]_4$.

4.3.2 Attempted synthesis of hydroxyl sugar cylinder, $[Fe_2L^{OHSug_3}][BF_4]_4$

4.3.2.1 Synthesis of 5-(2-N-acetyl-1-O-(2'-propargyl)-β-D-glucosaminide)-2-pyridinecarboxaldehyde (10)

The acetyl protected aldehyde, 5-(2-N-acetyl-3,4,6-tri-O-acetyl-1-(2'-propargyl)-β-D-glucosaminide)-2-pyridinecarboxaldehyde (9) (Section 4.3.1.1), was deprotected with sodium methoxide (Scheme 4.3), based on literature procedure.[11] The starting material was stirred with sodium methoxide at room temperature for two hours and then the crude product was purified by column chromatography, yielding a white solid in 60% yield.

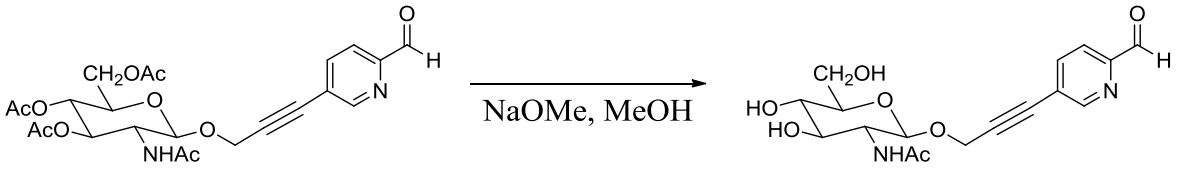

(9) (10)

Scheme 4.3 Synthetic route for preparation of 5-(2-N-acetyl-1-O-(2'-propargyl)-β-D-glucosaminide)-2-pyridinecarboxaldehyde (10).

High resolution EI mass spectrometry and NMR spectroscopy were used to confirm the formation of the desired product (10). It appears that two species are present in the ^1H NMR spectrum (Fig. 4.8), assigned using a 2D-COSY (see Appendix), due to the aldehyde group being in equilibrium with the hydrate form in deuterated water. As such, resonances corresponding to the aldehyde pyridine and hydrate pyridine protons can be observed, and the resonances of the sugar moiety have contributions from both species and so the

integration of these peaks is doubled.

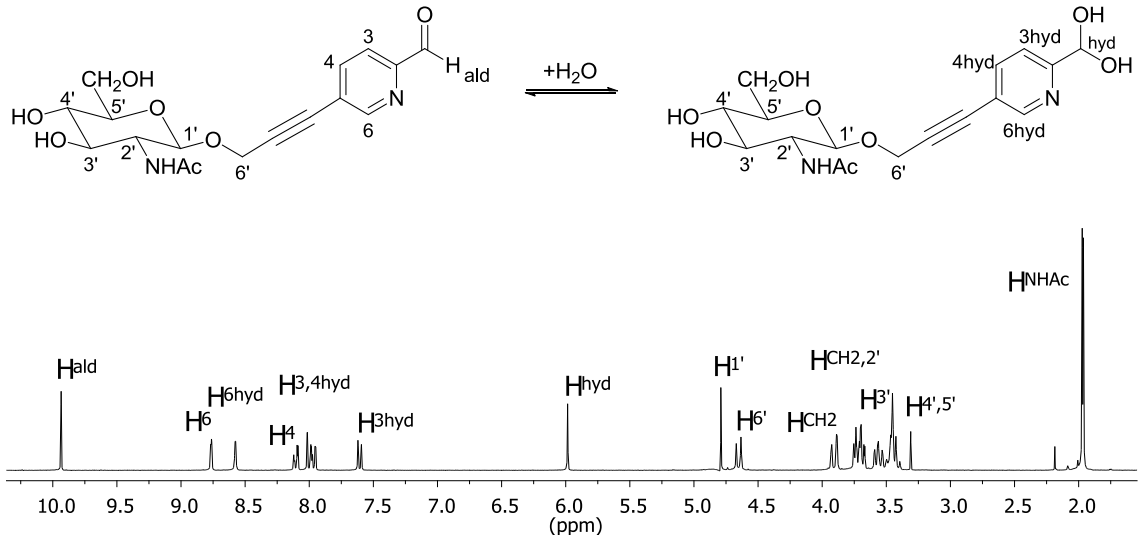

Figure 4.8 ^{1}H NMR (300 MHz, D_2O, 298 K) of 5-(2-N-acetyl-1-O-(2'-propargyl)-β-D-glucosaminide)-2-pyridinecarboxaldehyde (10).

4.3.2.2 Attempted synthesis of $[Fe_2L^{OHSug}{}_3][BF_4]_4$

The hydroxyl sugar cylinder, $[Fe_2L^{OHSug}{}_3][BF_4]_4$, was synthesised using a one-pot procedure with the aldehyde 5-(2-N-acetyl-1-O-(2'-propargyl)-β-D-glucosaminide)-2-pyridinecarboxaldehyde (10), 4,4'-methylenedianiline and iron(II) tetrafluoroborate, in a 6:3:2 stoichiometry, added sequentially and dropwise, in a methanol-ethanol solvent mix (Scheme 4.4).

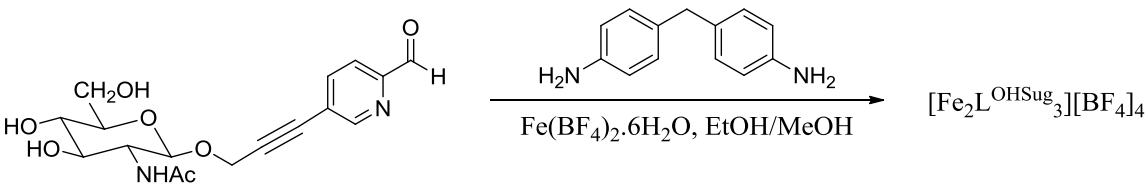

(10)

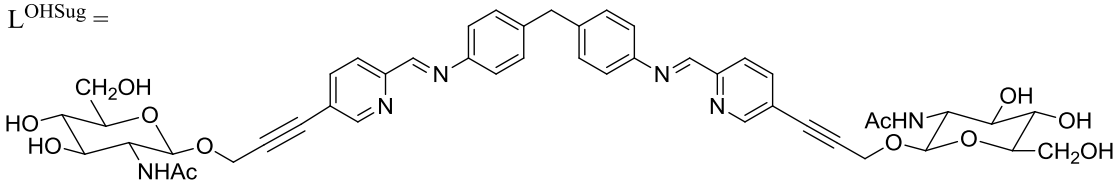

Scheme 4.4 Synthetic route for preparation of $[Fe_2L^{OHSug}{}_3][BF_4]_4$.

Immediately after addition of the iron salt, a dark purple precipitate formed, indicating formation of the iron(II) cylinder. The isolated purple solid was washed with a large volume of methanol and diethyl ether and dried overnight. Excitingly it was found that the solid was soluble in water, and in fact only water, however when preparing an NMR sample in deuterated water it was observed that the hydroxy-sugar cylinder was extremely unstable. Immediately after dissolution of the solid, obvious degradation was seen with the formation of a pale precipitate, which could not be identified by NMR spectroscopy or mass spectrometry. Further problems with stability were encountered when the solution was freeze-dried, which gave a dark grey solid that was completely insoluble in water and all other solvents. Addition of other solvents to a solution of the cylinder in water caused almost immediate degradation of the cylinder, with the deep purple/blue solution turning a pale yellow colour.

Although the hydroxyl-sugar cylinder was soluble in water, it was difficult to obtain a clear ^{1}H NMR spectrum due to the degradation of the complex. Only broad peaks can be

observed in the NMR spectrum (Fig. 4.9), that were difficult to integrate with no observable splitting patterns. However, the overall appearance of the spectrum can be compared to that of the other iron(II) cylinders synthesised herein and shows the characteristic imine peak (H_{im}) confirming that the cylinder has been formed. There are no peaks corresponding to the 5-(2-N-acetyl-1-O-(2'-propargyl)-β-D-glucosaminide)-2-pyridinecarboxaldehyde (10), or 4,4'-methylenedianiline spacer starting materials. The resonances of the sugar moiety (between 3-5 ppm and at 2 ppm) are very broad and partly obscured by solvent peaks, as is the peak of the spacer (H_{sp}).

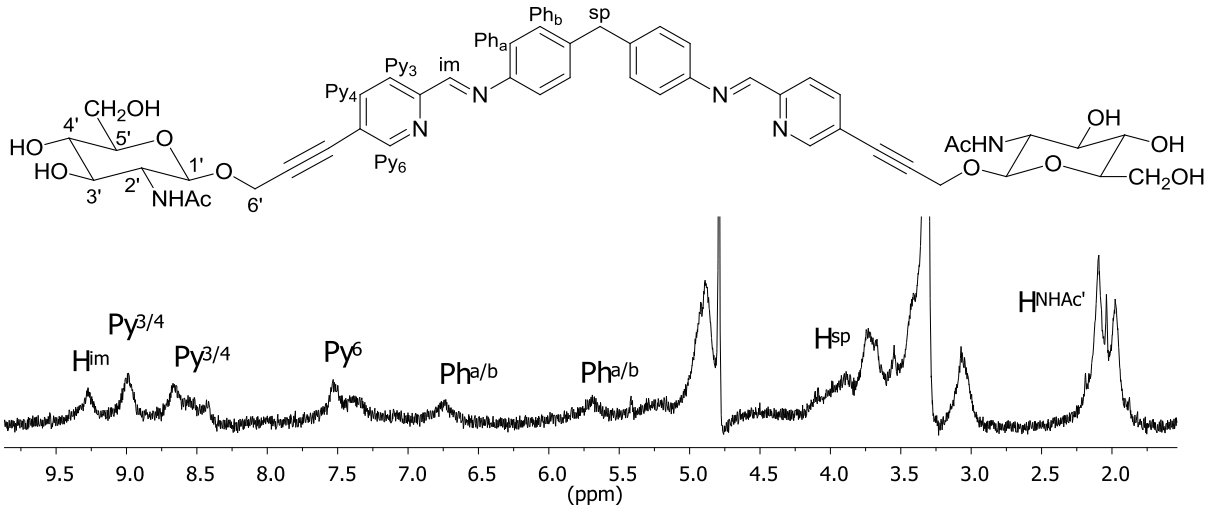

Figure 4.9 ^{1}H NMR (300 MHz, D_2O, 298 K) of $[Fe_2L^{OHSug}{}_3][BF_4]_4$.

Characterisation by ESI mass spectrometry revealed multiply charged peaks corresponding to the species $[Fe_2(C_{47}H_{50}N_6O_{12})_3]^{4+}$ and $[Fe_2(C_{47}H_{50}N_6O_{12})_3][BF_4]^{3+}$ (see Appendix). Although purity of the hydroxyl-sugar cylinder could not be confirmed by this characterisation, it was thought that preliminary DNA binding studies could be employed to assess the DNA binding activity of the complex.

4.4 Properties of synthesised sugar cylinders

4.4.1 Chirality of synthesised helicates, as investigated by ^{1}H NMR Δ-TRISPHAT studies

As detailed previously (Section 3.4.1, Chapter 3), Δ-TRISPHAT is a commercially available chiral NMR shift reagent. It has been used to investigate the enantiopurity of the parent and peptide conjugated iron(II) cylinders[12,13] and also to study the chirality of the steroid functionalised cylinders presented in this work.

The $[Fe_2L^{OAcSug}{}_3][BF_4]_4$ and $[Fe_2L^{OHSug}{}_3][BF_4]_4$ cylinders synthesised herein are functionalised with chiral sugar moieties. Therefore, they may be a mixture of diastereoisomers, as was observed for the steroid functionalised cylinders (Chapter 3), or only one, pure diastereoisomer may have formed due to chiral induction, as was seen previously for the peptide cylinders.[14] As the NMR spectrum of the acetyl-sugar cylinder has only one set of resonances this implies that the cylinder may be diastereoisomerically pure. To investigate the chirality of the sugar complexes ^{1}H NMR Δ-TRISPHAT studies were carried out. The chiral NMR shift reagent was added to a solution of the acetyl-sugar functionalised cylinder in deuterated acetonitrile. As Δ-TRISPHAT is not soluble in water, and the hydroxyl-sugar cylinder is only soluble in water, a solution of Δ-TRISPHAT in deuterated acetonitrile was added to a solution of the hydroxyl-sugar cylinder in deuterated water.

The ^{1}H NMR spectrum (Fig. 4.10) observed for the acetyl-sugar cylinder, $[Fe_2L^{OAcSug}{}_3][BF_4]_4$, after addition of one equivalent of Δ-TRISPHAT, shows small changes in the chemical shifts of some of the peaks. Upon addition of further equivalents

of Δ-TRISPHAT, the peaks corresponding to the imine (H_{im}), and two of the pyridine protons (H_{Py3} and H_{Py6}) can be seen to shift. A shift of the peaks nearest to the metal coordination site indicates that the complex has the M helical configuration, as was observed for the isomerically pure parent and peptide functionalised cylinders (Section 3.4.1, Chapter 3).

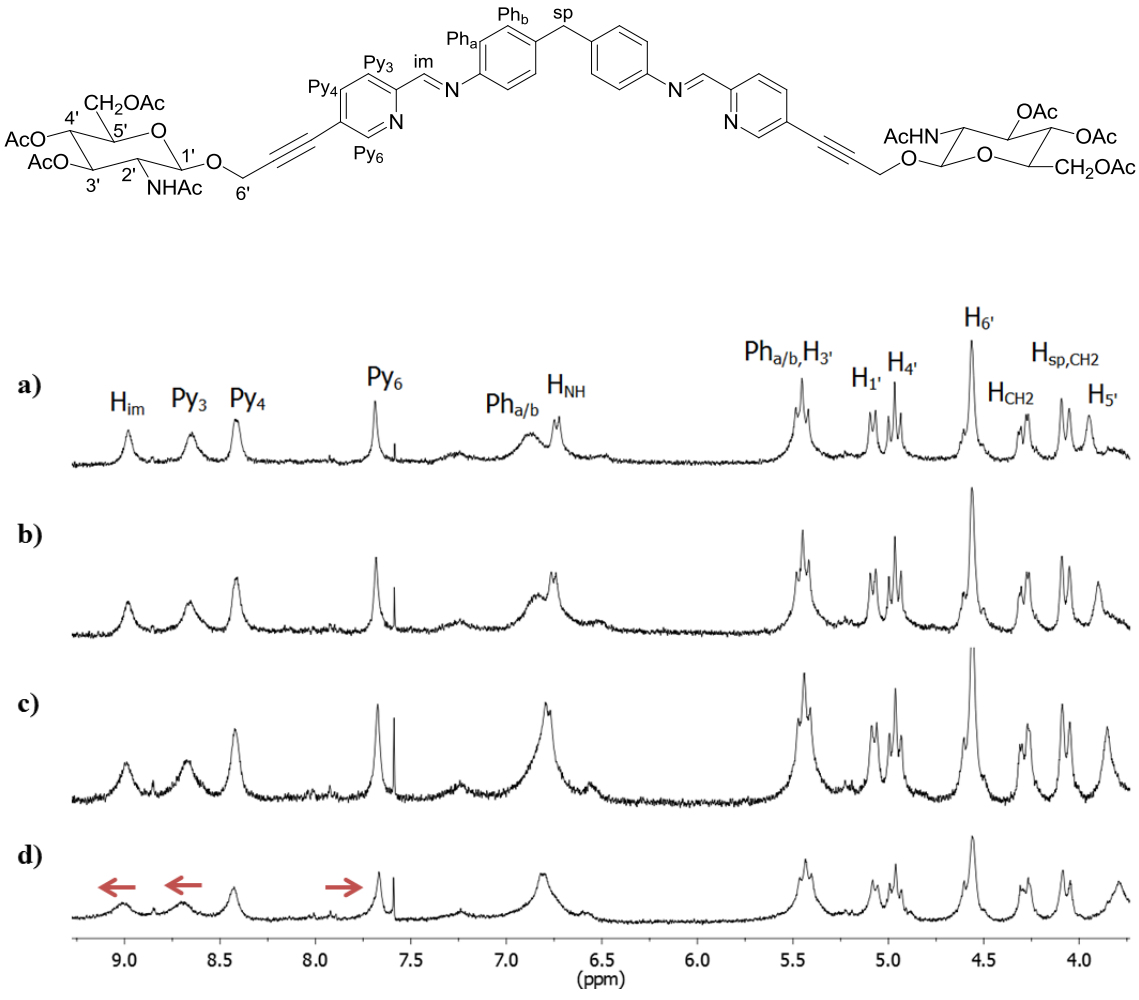

Figure 4.10 ^{1}H NMR (300 MHz, CD_3CN, 298 K) of a) a solution of $[Fe_2L^{OAcSug}{}_3][BF_4]_4$; b) same solution with 1 equivalent of Δ-TRISPHAT; c) same solution with 2 equivalents of Δ-TRISPHAT; d) same solution with 4 equivalents of Δ-TRISPHAT.

The ^{1}H NMR spectra (Fig. 4.11) from the preliminary Δ-TRISPHAT experiment with the hydroxyl-sugar cylinder, $[Fe_2L^{OHSug}{}_3][BF_4]_4$, are very difficult to interpret due to the low

concentration of complex that could be obtained in solution. After addition of the Δ-TRISPHAT chiral shift reagent, some changes can be seen in the resonances although this may be due to changes in concentration or precipitation of the complex, and so no conclusions may be drawn. Also, the Δ-TRISPHAT had to be added to the cylinder solution in acetonitrile, which although is miscible with water may affect its ability to interact with the complex in some way.

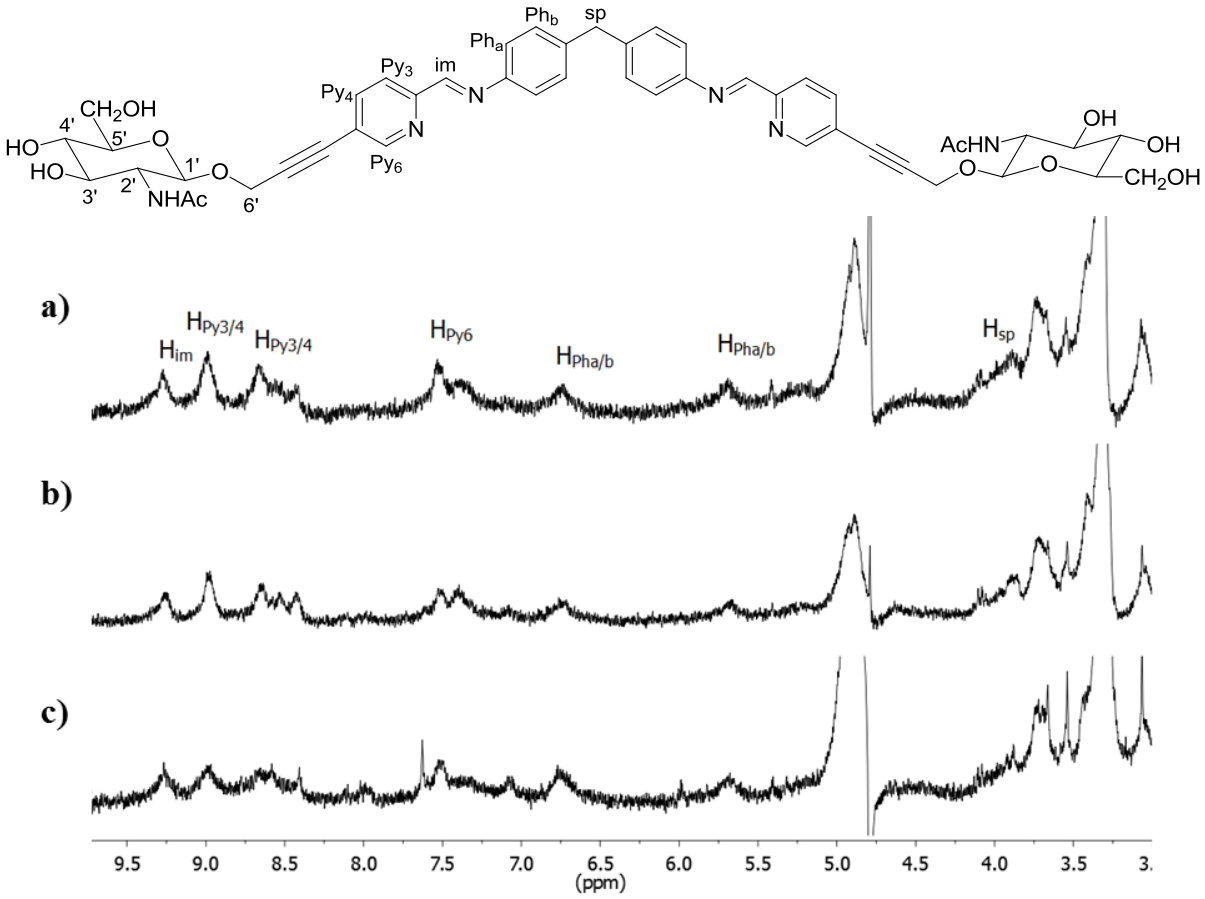

Figure 4.11 ^{1}H NMR (300 MHz, D_2O/CD_3CN, 298 K) of a) a solution of $[Fe_2L^{OHSug}{}_3][BF_4]_4$; b) same solution with 1 equivalent of Δ-TRISPHAT; c) same solution with 2 equivalents of Δ-TRISPHAT.

Circular dichroism studies were undertaken to gain more information about the chirality of the sugar functionalised cylinders developed.

4.4.2 Chirality of helicates, as investigated by circular dichroism

As previously detailed (Section 3.4.2, Chapter 3), circular dichroism can be used to identify the chirality of iron(II) cylinders. CD spectra of enantiopure solutions of the M and P enantiomers of the parent cylinder, $[Fe_2L^P_3]^{4+}$, reveal identical but opposite CD signals (Fig. 4.12).

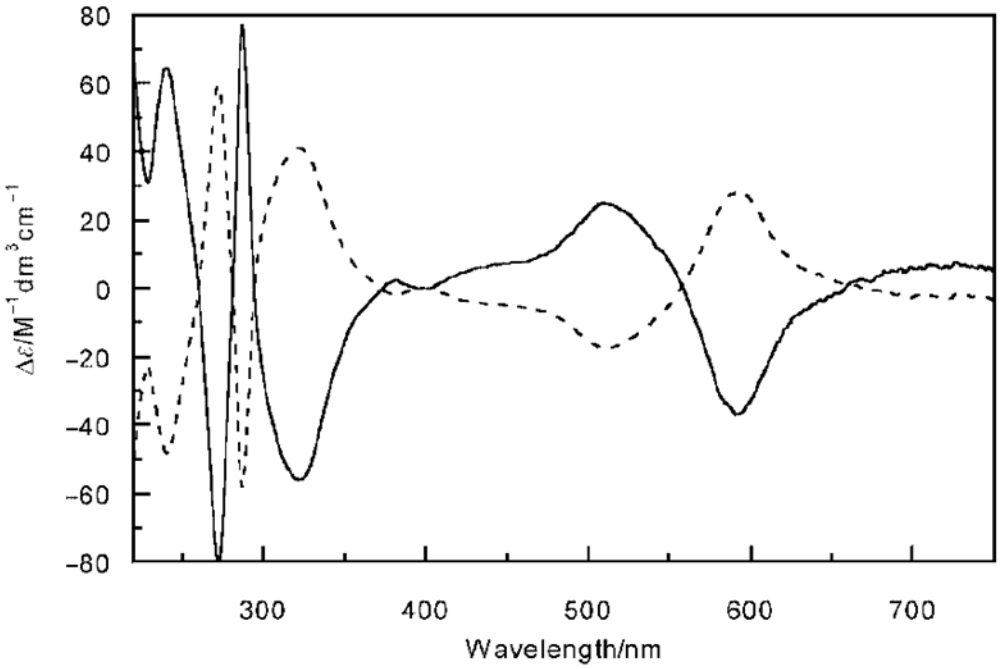

Figure 4.12 CD spectra of M (solid line) and P (dashed line) enantiomers of $[Fe_2L^P_3]^{4+}$. [Reproduced from Ref [15]]

CD spectra of the sugar cylinders, $[Fe_2L^{OAcSug}_3][BF_4]_4$ and $[Fe_2L^{OHSug}_3][BF_4]_4$, were recorded (Fig. 4.13), and compared to those of the parent cylinder. As the purity of the hydroxyl-sugar cylinder cannot be confirmed, solutions of component parts of the complex were also measured and were found to have no inherent CD signal. The spectra of the sugar cylinders reveal that the complexes are chiral, as they have a strong CD signal. The pattern of the CD signals of the sugar cylinders is almost the exact opposite of that of the

estrogen steroid cylinder (Section 3.4.2, Chapter 3), which is thought to be a mixture of diastereoisomers with a larger proportion of the P helical isomer. Comparison of the spectra of the sugar cylinders with those of the M and P enantiomers of the parent cylinder (Fig. 4.12) reveals that the sugar complexes have the characteristic CD signal of the M helical isomer. Therefore it can be concluded that the acetyl-sugar complex, $[Fe_2L^{OAcSug}{}_3][BF_4]_4$, is diastereoisomerically pure, from the ^{1}H NMR Δ-TRISPHAT studies, and is of the M helical configuration, as shown by the CD studies. Investigation of the hydroxyl-sugar cylinder, $[Fe_2L^{OHSug}{}_3][BF_4]_4$, by ^{1}H NMR Δ-TRISPHAT studies was more ambiguous, however by CD the cylinder is chiral and either has a higher proportion of the M helical isomer than the P helical isomer, or is diastereoisomerically pure and of the M helical configuration.

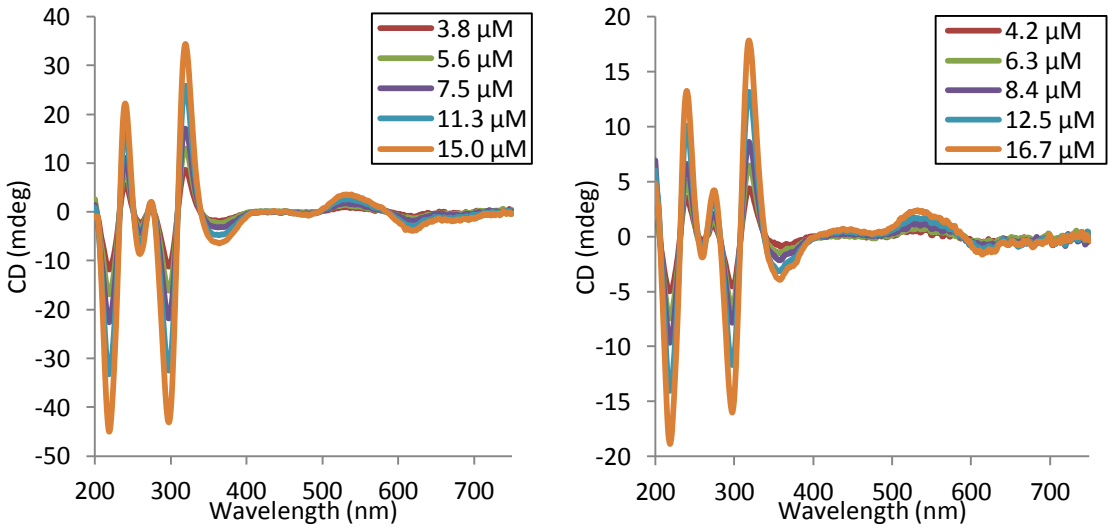

Figure 4.13 CD spectra of increasing concentrations of complexes: (left) $[Fe_2L^{OAcSug}{}_3][BF_4]_4$ (1.2% max. MeOH); (right) $[Fe_2L^{OHSug}{}_3][BF_4]_4$. Legend shows complex concentration.

4.4.3 Solubility of sugar functionalised cylinders

Water solubility is an advantageous property for potential anti-cancer drugs [16] and DNA binding studies are carried out in aqueous solutions. With this in mind, the iron(II) helicates synthesised in this chapter were functionalised with sugars which are known for their solubilising properties in aqueous medium.[4] The acetyl-sugar cylinder, $[Fe_2L^{OAcSug}{}_3][BF_4]_4$, is unfortunately not soluble in water, which is not surprising as it is the hydroxyl groups of the sugar that give aqueous solubility, proven by the observation that the hydroxyl-sugar functionalised cylinder is soluble in water. However, the acetyl-sugar complex is soluble in water miscible methanol, which allows DNA binding studies to be carried out.

Although the purity of the hydroxyl-sugar cylinder cannot be confirmed and it is relatively unstable in water, this aqueous solubility is exciting as it demonstrates that cylinders functionalised via alkyne bonds can be water soluble, if a suitable moiety is attached. Poor aqueous stability was observed for the peptide-conjugated cylinders developed by Cardo, with the tripeptide complex being stable for only two hours.[17] The stability of the sugar cylinders was further investigated by UV-Vis studies, detailed in the next section.

4.4.4 UV-Vis stability studies

Studies were carried out with $[Fe_2L^{OAcSug}{}_3][BF_4]_4$ and $[Fe_2L^{OHSug}{}_3][BF_4]_4$ to determine their stability in aqueous solvents. Stabilities in the absence and presence of ct-DNA were established using UV-Vis spectroscopy. The acetyl-sugar complex was dissolved in a small amount of methanol as it was not soluble in water alone. Solutions containing

complex and ct-DNA in a 6:1 ratio were also monitored.

As the hydroxyl-sugar complex cannot be confirmed as pure and degrades quickly in solution, only a preliminary stability study was carried out. As it is the MLCT region of the complex that is monitored in this experiment, any component parts of the complex present due to degradation would not affect the results.

For both complexes, $[Fe_2L^{OAcSug}{}_3][BF_4]_4$ and $[Fe_2L^{OHSug}{}_3][BF_4]_4$, the λ_{max} of the MLCT band decreases with time, indicating complex degradation (Fig. 4.14). The acetyl-sugar cylinder is quite stable with a loss of only 12% of its original absorbance over a period of twelve hours. In the presence of ct-DNA there is a great improvement in the stability of the complex with only a 4% loss of the original absorbance after twelve hours and a 2% loss over a five hour period, the longest duration of the DNA binding experiments carried out with the complex. This sugar functionalised cylinder is more stable than the steroid functionalised cylinders on their own and in the presence of DNA. Although there is some degradation of the complex, it is not expected to significantly affect the DNA binding studies.

The hydroxyl-sugar cylinder is much less stable, with a loss of almost one quarter of the original absorbance over a five hour period. However there are significant improvements to the stability of the complex in the presence of ct-DNA, with a 9% loss of original absorbance. This degradation must be taken into account when performing the DNA binding experiments and analysing the results.

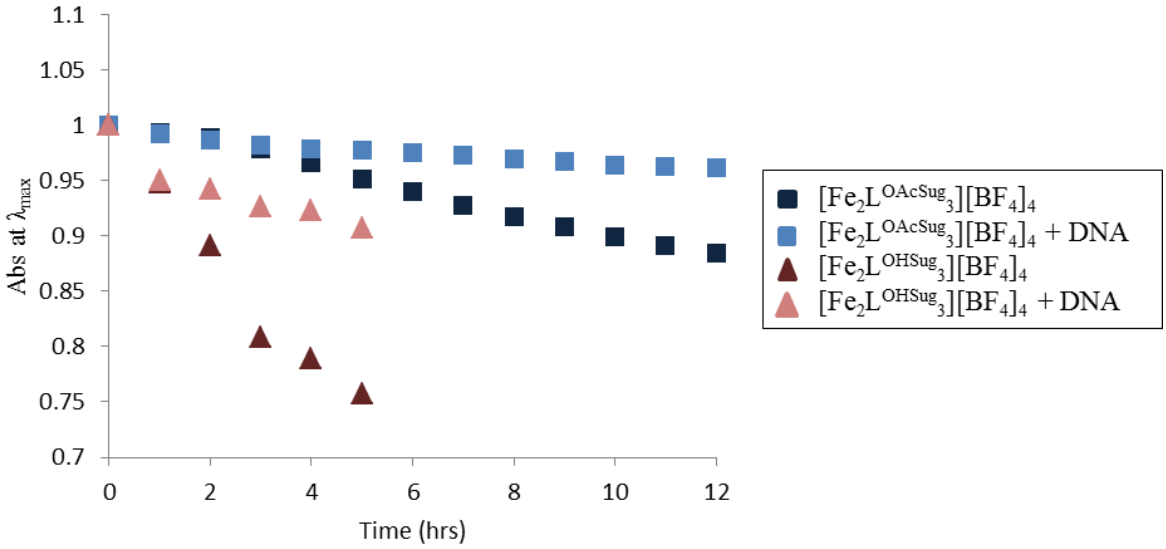

Figure 4.14 Normalised UV-Vis stability studies of complexes $[Fe_2L^{OAcSug_3}][BF_4]_4$ and $[Fe_2L^{OHSug_3}][BF_4]_4$ at room temperature (5 μM, 2.5% MeOH:water and 8 μM, water respectively) and in presence of ct-DNA in 6.7 mM NaCl and 0.33 mM $Na(CH_2)_2AsO_2.3H_2O$ (pH 6.8) (ratio 6:1 ct-DNA:complex) (1.9% MeOH:water and water respectively). λ_{max} = 591 nm and 595 nm respectively.

4.5 DNA binding studies

Novel sugar-functionalised iron(II) supramolecular cylinders have been synthesised and characterised herein. The DNA binding properties of these novel cylinders were investigated by several techniques including circular dichroism, linear dichroism and gel electrophoresis.

4.5.1 Circular dichroism binding studies

CD titrations were carried out for the sugar functionalised cylinders, $[Fe_2L^{OAcSug_3}][BF_4]_4$ and $[Fe_2L^{OHSug_3}][BF_4]_4$ analogous to those described in chapter 2 (Section 2.6.1). The acetyl-sugar cylinder was dissolved in a methanol-water solvent mix due to being insoluble in water. Due to the instability of the hydroxyl-sugar complex, aliquots of the solution to be used in the experiment were kept frozen until the time of addition. It was hoped that the

cylinder would degrade more slowly once added to the DNA solution as the presence of ct-DNA has been found to stabilise the complex. Control experiments were also carried out for the components of the cylinder, and these were found to have no inherent CD signal, induced CD signal or effect on the DNA.

As the sugar-functionalised cylinders are chiral, their own intrinsic CD signal (Fig. 4.15) must be subtracted from the CD titration with DNA so as to only see the induced CD signal arising from the interaction between the complex and the DNA.

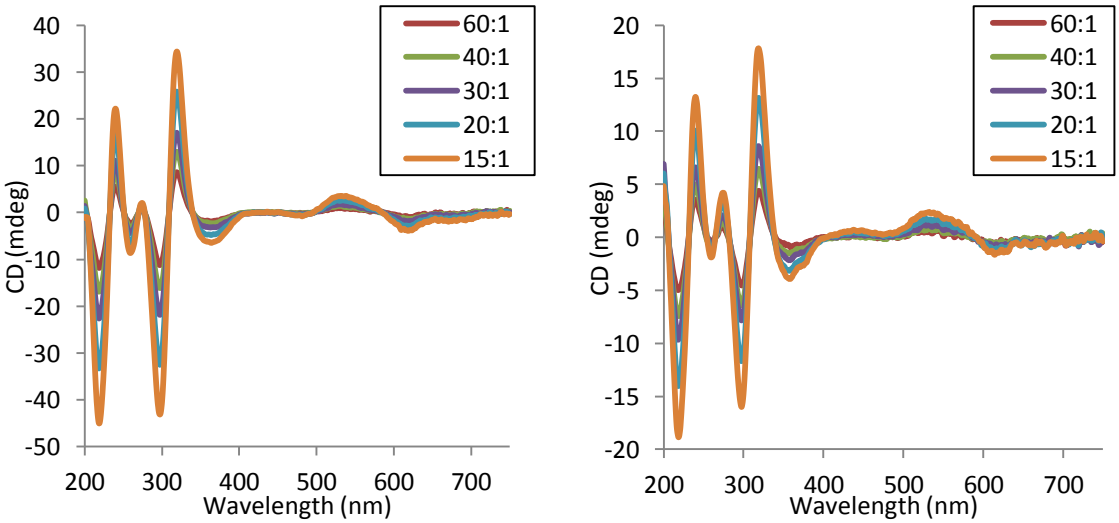

Figure 4.15 CD of control titrations of $[Fe_2L^{OAcSug}{}_3][BF_4]_4$ (1.2% max. MeOH) (left) and $[Fe_2L^{OHSug}{}_3][BF_4]_4$ (right). Water with increasing concentrations of complexes. Legend shows corresponding ct-DNA:complex ratios for titration with ct-DNA.

The CD titration spectrum of the acetyl-sugar functionalised cylinder, $[Fe_2L^{OAcSug}{}_3][BF_4]_4$, (Fig. 4.16) reveals negative ICD signals at 316 and 354 nm. This indicates that the cylinder is binding to ct-DNA. The B-conformation of DNA is retained upon cylinder binding.

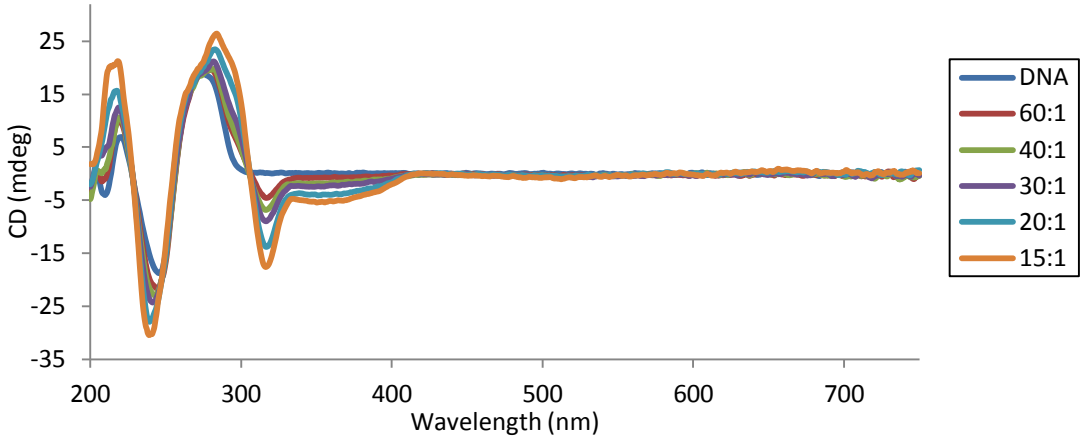

Figure 4.16 CD of 226 μM ct-DNA in 20 mM NaCl and 1 mM $Na(CH_2)_2AsO_2.3H_2O$ (pH 6.8) with increasing concentrations of complex $[Fe_2L^{OAcSug}{}_3][BF_4]_4$. Legend shows ct-DNA:complex ratios. 1.2% max. MeOH. Analysed in 1cm pathlength cuvette.

In the preliminary CD titration spectrum of the hydroxyl-sugar functionalised cylinder, $[Fe_2L^{OHSug}{}_3][BF_4]_4$, (Fig. 4.17) similar ICD signals at 316 and 354 nm are also observed indicating DNA binding. The induced CD signals are very similar to those of the acetyl-sugar cylinder. The DNA conformation is unperturbed by this DNA binding as the B-conformation is retained.

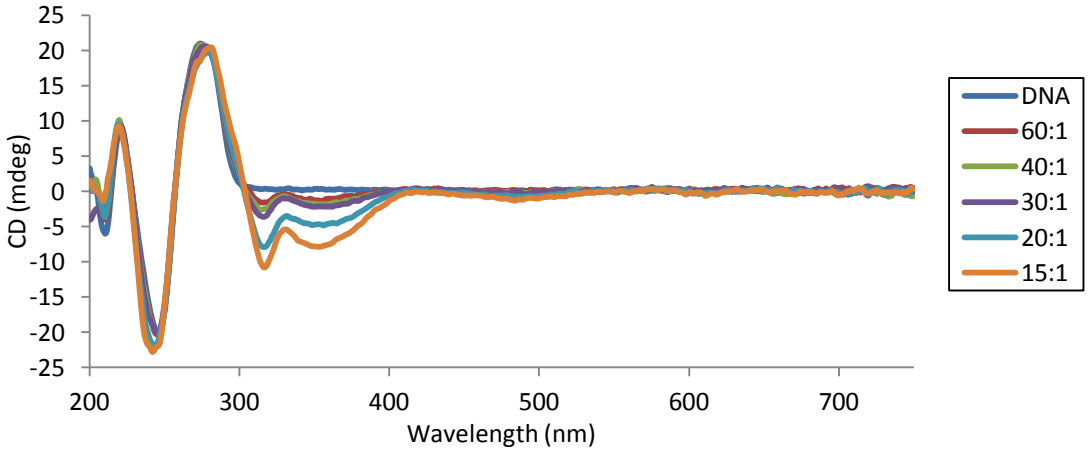

Figure 4.17 CD of 251 μM ct-DNA in 20 mM NaCl and 1 mM $Na(CH_2)_2AsO_2.3H_2O$ (pH 6.8) with increasing concentrations of complex $[Fe_2L^{OHSug}{}_3][BF_4]_4$. Legend shows ct-DNA:complex ratios. Analysed in 1cm pathlength cuvette.

Comparison of the ICD signals of the two complexes with ct-DNA allows the response to DNA to be compared (Fig. 4.18). Both complexes have an immediate effect on the DNA, with DNA binding at low complex loading. At high complex loading the hydroxyl-sugar cylinder has a slightly stronger binding response than the acetyl-sugar version.

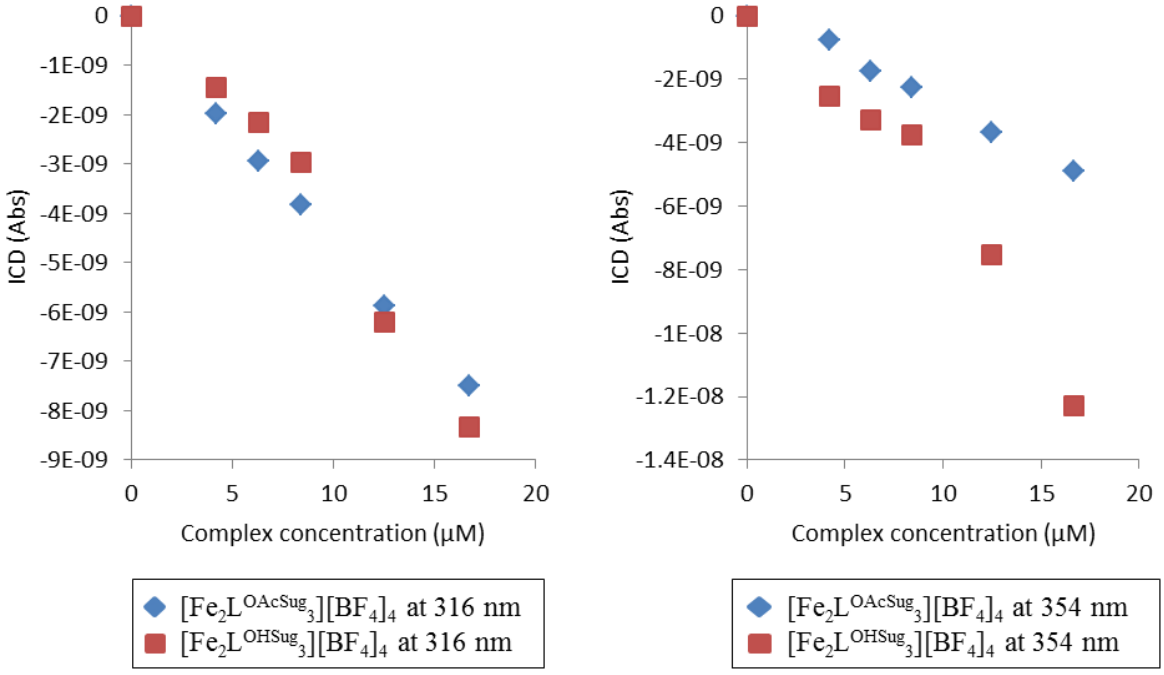

Figure 4.18 Normalised ICD signal vs complex concentration for complexes $[Fe_2L^{OAcSug}{}_3][BF_4]_4$ and $[Fe_2L^{OHSug}{}_3][BF_4]_4$.

4.5.2 Linear dichroism binding studies

Linear dichroism titrations were also performed with the sugar-functionalised cylinders, analogous to those carried out in Chapter 2 (Section 2.6.2). As the hydroxyl-sugar cylinder is significantly unstable over the duration of the LD experiment, aliquots of the solution were frozen and defrosted immediately before each titration. As the cylinder is known to be more stable in the presence of ct-DNA, it was thought that degradation of the complex would slow down once added to the DNA solution. Control experiments indicated that the

component parts of the cylinder did not induce any LD signal. The acetyl-sugar cylinder was dissolved in a methanol-water solvent mix due to being insoluble in water. As the sugar functionalised cylinders are too small to be oriented by viscous drag they do not have any intrinsic LD signal, and so any ILD signal observed must come from the interaction between the complex and ct-DNA.

The LD titration spectrum (Fig. 4.19) for the acetyl-sugar functionalised cylinder, $[Fe_2L^{OAcSug}{}_3][BF_4]_4$, shows no detectable ILD signals in the complex region. DNA binding of the complex is evident, although oriented DNA binding cannot be confirmed. The magnitude of the negative LD band at 260 nm, corresponding to DNA transitions, decreases as the complex concentration increases. This indicates that the cylinder is binding to DNA and coiling or bending it so as to induce a loss of orientation. This occurs even at low cylinder loading.

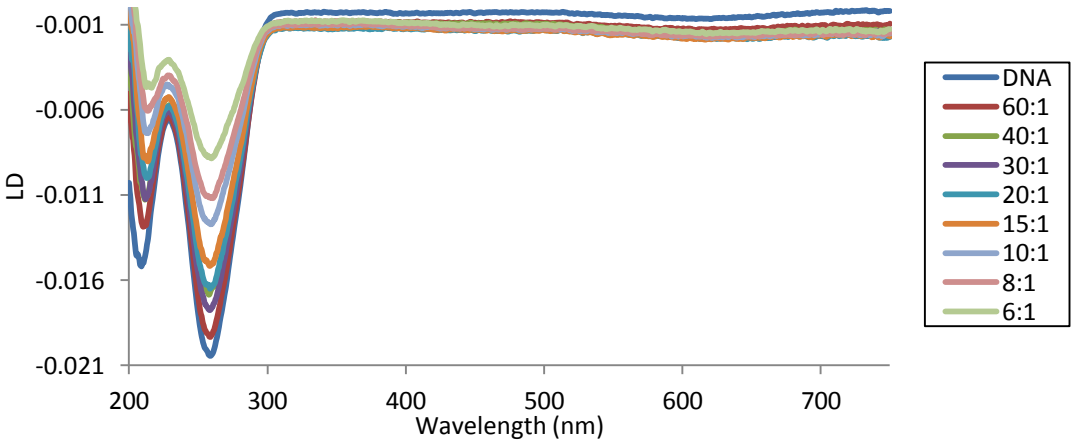

Figure 4.19 LD of 273 μM ct-DNA in 20 mM NaCl and 1 mM $Na(CH_2)_2AsO_2.3H_2O$ (pH 6.8) with increasing concentrations of complex $[Fe_2L^{OAcSug}{}_3][BF_4]_4$. Legend shows ct-DNA:complex ratios. 4.5% max. MeOH.

The preliminary LD titration spectrum (Fig. 4.20) for the hydroxyl-sugar functionalised

cylinder, $[Fe_2L^{OHSug}{}_3][BF_4]_4$, shows an ILD signal at 322 nm, at higher complex loading, indicating oriented DNA binding. DNA binding is also proven by a loss in the magnitude of the negative LD band at 260 nm, with increasing concentration of cylinder. This indicates loss of orientation of the DNA due to the complex coiling or bending it and occurs immediately upon addition of the complex at low cylinder loading.

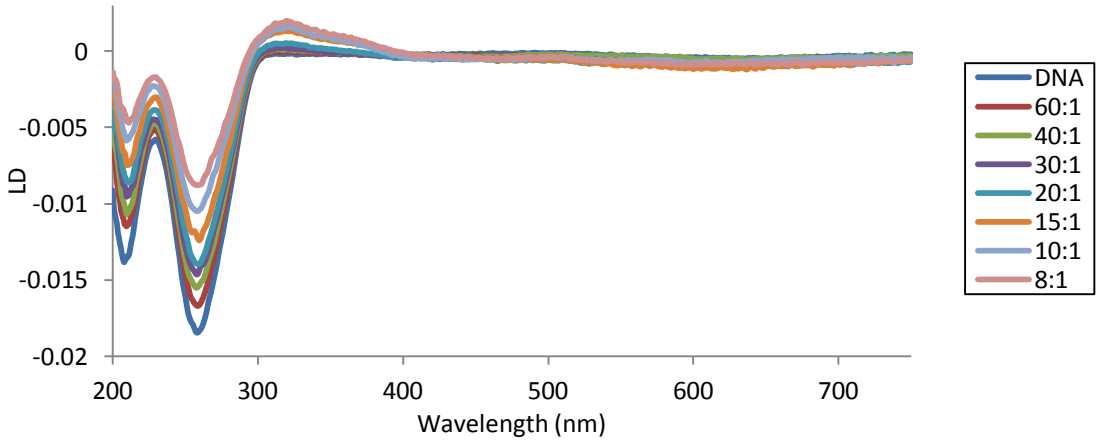

Figure 4.20 LD of 232 μM ct-DNA in 20 mM NaCl and 1 mM $Na(CH_2)_2AsO_2.3H_2O$ (pH 6.8) with increasing concentrations of complex $[Fe_2L^{OHSug}{}_3][BF_4]_4$. Legend shows ct-DNA:complex ratios.

Comparison of the DNA bending/coiling activity of the sugar functionalised cylinders with that of the parent, alkyne and steroid functionalised cylinders (Table 4.1 and Fig. 4.21) reveals that the $[Fe_2L^{OAcSug}{}_3][BF_4]_4$ and $[Fe_2L^{OHSug}{}_3][BF_4]_4$ complexes have similar activity. It is apparent that at low complex loading, the bending activity of all of the cylinders is very similar. At high complex concentration it can be observed that the sugar functionalised cylinders have a slightly greater activity than the steroid functionalised cylinders and a similar activity to the $[Fe_2L^{TB}{}_3][BF_4]_4$, $[Fe_2L^{PA}{}_3][BF_4]_4$ and $[Fe_2L^{Hex}{}_3][BF_4]_4$ complexes. This may be due to the size differences of the substituents functionalising the cylinders.

DNA:complex ratio	% Loss of LD signal at 260 nm upon interaction with complexes		
8:1	$[Fe_2L^{P}{}_3][BF_4]_4$	$[Fe_2L^{OAcSug}{}_3][BF_4]_4$	$[Fe_2L^{OHSug}{}_3][BF_4]_4$
	80	63	52

Table 4.1 Comparison of the percentage loss of LD signal at 260 nm upon interaction with complexes at a ratio of DNA:complex 8:1.

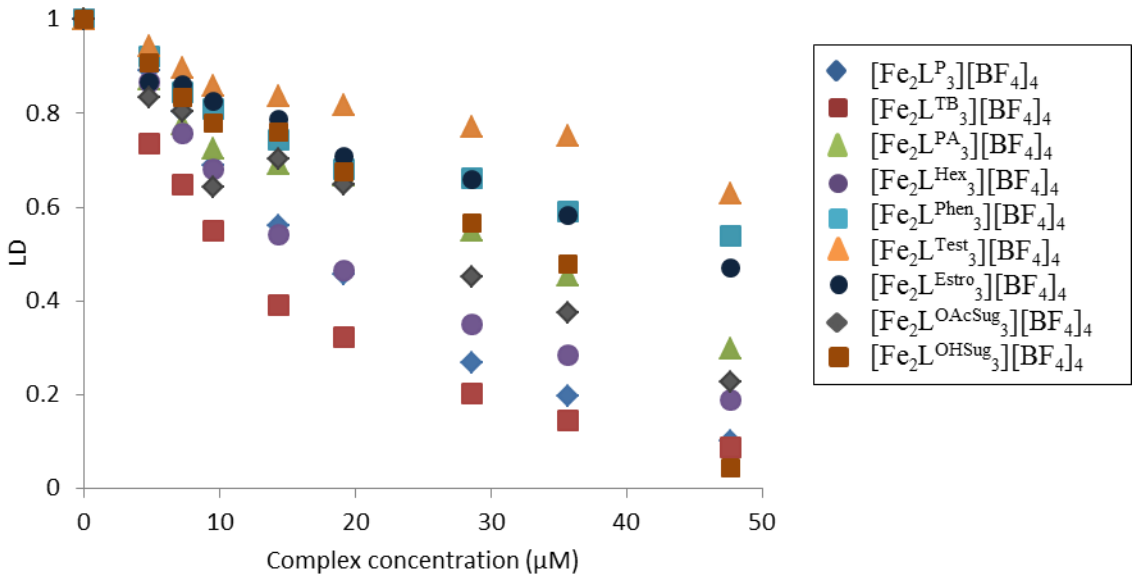

Figure 4.21 Normalised LD signal at 260 nm vs complex concentration for parent and alkyne, steroid and sugar functionalised complexes.

4.5.3 Gel electrophoresis studies

The DNA unwinding activity of the sugar-functionalised cylinders $[Fe_2L^{OAcSug}{}_3][BF_4]_4$ and $[Fe_2L^{OHSug}{}_3][BF_4]_4$ was investigated by agarose gel electrophoresis analogous to those carried out in chapter 2 (Section 2.6.3). As the acetyl-sugar complex is not soluble in water alone, a small percentage of methanol was used to dissolve the compound. As the hydroxyl-sugar complex is fairly unstable, control gel electrophoresis experiments were carried out with the component parts of the complex and these were found to have no

effect. Samples containing different plasmid DNA:complex ratios (Table 4.2) were incubated at room temperature for two hours before being run on a 1% agarose gel.

Lanes	1	2	3	4	5	6	7
DNA:complex ratio	MeOH or DNA control	50:1	40:1	30:1	20:1	15:1	10:1
Lanes	8	9	10	11	12	13	14
DNA:complex ratio	8:1	6:1	5:1	4:1	3:1	2:1	DNA control

Table 4.2 Ratios of plasmid DNA:complex used in gel electrophoresis experiments.

The agarose gel (Fig. 4.22) for complex $[Fe_2L^{OAcSug}{}_3][BF_4]_4$ shows that the circular and supercoiled forms of the pBR322 plasmid are not altered by addition of the complex, even at high concentrations. At a ratio of plasmid DNA:complex of 2:1 no bands can be seen corresponding to either forms of plasmid DNA, due to difficulties with ethidium bromide staining.

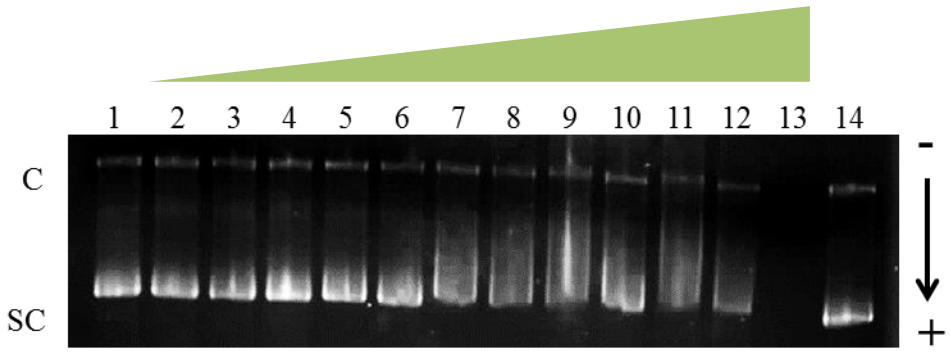

Figure 4.22 Agarose gel (1%) electrophoresis showing changes in electrophoretic mobility of circular (C) and supercoiled (SC) forms of pBR322 plasmid DNA incubated at 20°C for 2 hours with different ratios of complex $[Fe_2L^{OAcSug}{}_3][BF_4]_4$ (lanes 2-13). Control lanes (1 and 14): pBR322 plasmid DNA in absence of complex. 8% max. MeOH.

The preliminary agarose gel (Fig. 4.23) for the hydroxyl-sugar cylinder, $[Fe_2L^{OHSug}{}_3][BF_4]_4$, indicates that the complex is binding to the supercoiled form of DNA.

From a DNA:complex ratio of 30:1 the band corresponding to the supercoiled DNA can be seen to be migrating at a slower pace through the gel. As the complex concentration increases, the migration rate slows even more indicating unwinding of the supercoiled DNA. At a 6:1 DNA:complex ratio the supercoiled and circular band co-migrate, indicating that all of the supercoiled DNA has been unwound to the relaxed circular form. At higher complex loading, lanes 10-13, the absence of the supercoiled band indicates that the sugar cylinder does not positively supercoil the DNA, as has been observed for some of the cylinders developed, such as the triple bond complex.

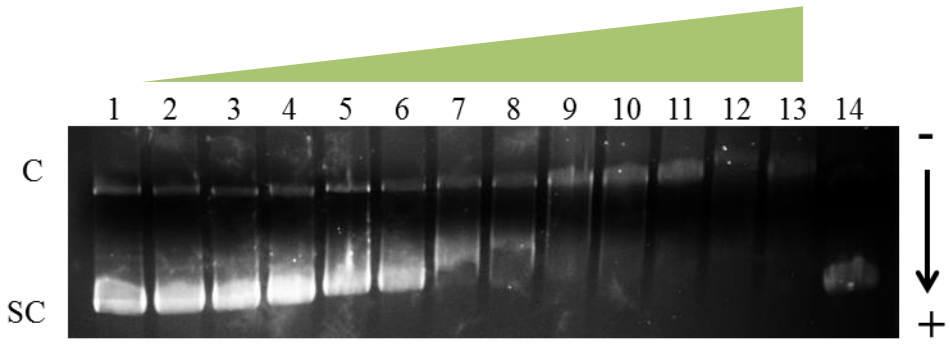

Figure 4.23 Agarose gel (1%) electrophoresis showing changes in electrophoretic mobility of C and SC forms of pBR322 plasmid DNA incubated at 20°C for 2 hours with different ratios of complex $[Fe_2L^{OHSug}{}_3][BF_4]_4$ (lanes 2-13). Control lanes (1 and 14): pBR322 plasmid DNA in absence of complex.

If the circular and supercoiled forms of the pBR322 plasmid co-migrate in the gel, unwinding angles can be calculated. The unwinding angle, Φ, is a measure of the number of degrees by which the DNA is unwound about its helical axis per molecule bound. Comparison of the unwinding angles of the parent, $[Fe_2L^{TB}{}_3][BF_4]_4$ and $[Fe_2L^{PA}{}_3][BF_4]_4$ cylinders with the preliminary unwinding angle of the hydroxyl-sugar cylinder (Table 4.3), shows that $[Fe_2L^{OHSug}{}_3][BF_4]_4$ is less able to unwind the supercoiled plasmid DNA than the parent cylinder. However, it has the same or similar activity as the $[Fe_2L^{TB}{}_3][BF_4]_4$ and

$[Fe_2L^{PA}{}_3][BF_4]_4$ functionalised cylinders. The unwinding angle is similar to that of cisplatin, which is 13°,[18] therefore this complex does show some promising DNA unwinding activity.

Complexes	$[Fe_2L^{P}{}_3][Cl]_4$	$[Fe_2L^{TB}{}_3][BF_4]_4$	$[Fe_2L^{PA}{}_3][BF_4]_4$	$[Fe_2L^{OHSug}{}_3][BF_4]_4$
Φ values	27° ±3	5° ±1	6° ±1	6° ±1

Table 4.3 Unwinding angles (Φ) of complexes calculated from gel electrophoresis experiments.

4.5.4 PAGE studies

Three-way junction polyacrylamide gel electrophoresis studies analogous to those performed with the alkyne cylinders (Section 2.6.4, Chapter 2) were carried out for $[Fe_2L^{OAcSug}{}_3][BF_4]_4$, by co-worker N. Calle Alonso from the University of Birmingham, and are briefly described herein for completeness. Due to the insolubility of the complex in water, a small percentage of methanol was used to dissolve the compound. $[Fe_2L^{OAcSug}{}_3][BF_4]_4$ was mixed with the three non-palindromic oligonucleotide strands to give a ratio of three-way-junction:cylinder of 1:1, incubated for one hour and run on a 15% polyacrylamide gel.

The autoradiogram of the polyacrylamide gel (Fig. 4.24, cropped image; for whole gel see Appendix) indicates that the acetyl-sugar cylinder, $[Fe_2L^{OAcSug}{}_3][BF_4]_4$, can promote the formation of a DNA three-way junction. Some precipitation of DNA can be seen in the loading wells, indicating binding of the complex to the single strands of DNA.

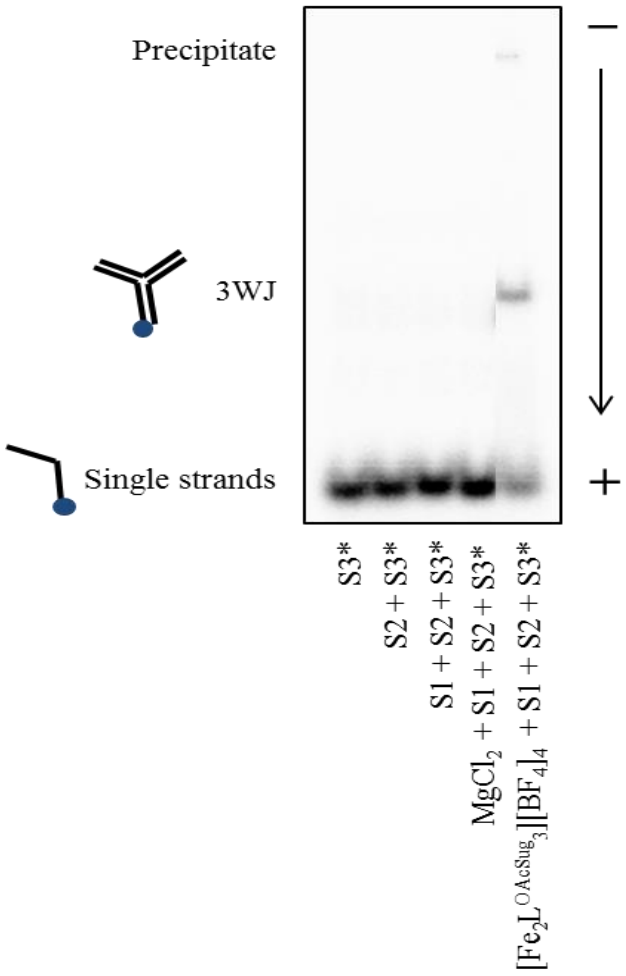

Figure 4.24 Autoradiogram of polyacrylamide gel run at 25 °C. Lanes 1-3: S3*, S3*+S2, S3*+S2+S1 respectively; Lane 4: S3*+S2+S1+$MgCl_2$; Lane 5: S3*+S2+S1 with $[Fe_2L^{OAcSug}{}_3][BF_4]_4$. Ratio of three-way junction(S1+S2+S3*):complex of 1:1. Asterisk indicates ^{32}P labelled strand.

As the PAGE experiments were carried out in duplicate, only a preliminary comparison of the three-way junction promotion and stabilisation ability of the cylinders can be noted (Fig. 4.25). It is apparent that the $[Fe_2L^{OAcSug}{}_3][BF_4]_4$ cylinder is less effective at stabilising the junction structure than the parent complexes, which may be due to the increased size of the functionalised cylinder.

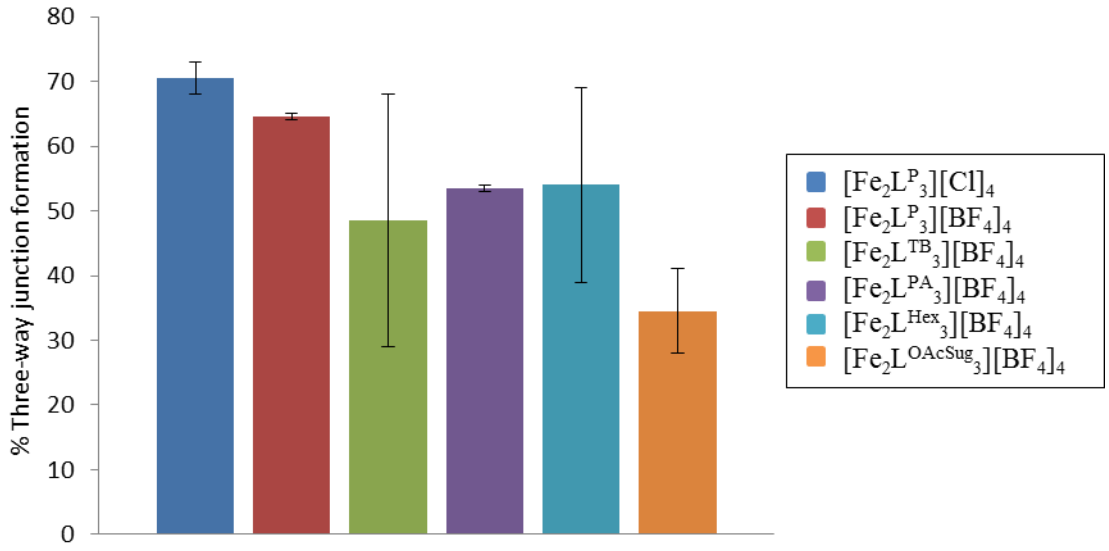

Figure 4.25 Bar graph showing percentage of three-way junction formed by complexes. Data based on two repeats; error bars shown demonstrate the two data points (not standard deviation), and the bar their average.

4.6 Conclusions

In this chapter, the synthesis of an acetyl-sugar functionalised cylinder, $[Fe_2L^{OAcSug}{}_3][BF_4]_4$, and the attempted synthesis of an hydroxyl-sugar functionalised cylinder, $[Fe_2L^{OHSug}{}_3][BF_4]_4$, have been reported. These functionalised cylinders were designed in order to improve the targeting of these types of complexes to tumour cells with highly or overexpressed carbohydrate receptors. These two complexes were synthesised via the novel functionalisation route detailed in chapter 2, over three or four reaction steps, with a poor yield of 4% for $[Fe_2L^{OAcSug}{}_3][BF_4]_4$.

The acetyl-sugar was unfortunately not water soluble, however it was soluble in water-miscible solvent and so could be further investigated. Excitingly, the hydroxyl-sugar cylinder was found to be water soluble, an important and desirable property for therapeutic agents. Unfortunately, it was very unstable in aqueous solution and so was very difficult to

work with and characterise. Although full characterisation could not be achieved, preliminary characterisation and DNA binding studies were performed to assess whether further work in this area would be beneficial.

By attaching chiral sugar moieties to the edges of the cylinder it was thought that induction of chirality may be achieved and this was investigated by ^{1}H NMR Δ-TRISPHAT and circular dichroism studies. These studies revealed that the acetyl-sugar cylinder was in fact diastereoisomerically pure and was of the M helical configuration. Chiral induction was previously observed in the development of peptide conjugated cylinders, where conjugation of L- or D-arginine induced the formation of pure diastereoisomers of the M and P helical configuration respectively.[14,17] Induction of chirality is usually achieved by attaching chiral substituents to the spacer groups of helicates,[19,20] whereas induction by substituents placed further from the helicate core is less common and quite exciting.[14] The chirality of the hydroxyl-sugar cylinder was also investigated. ^{1}H NMR Δ-TRISPHAT studies were inconclusive, with the spectra too weak and broad to allow proper analysis. However, the circular dichroism spectrum confirmed that the complex was chiral and a strong signal characteristic of the M helical isomer was observed.

DNA binding studies were carried out for the $[Fe_2L^{OAcSug}{}_3][BF_4]_4$ and $[Fe_2L^{OHSug}{}_3][BF_4]_4$ cylinders. Circular dichroism titrations with ct-DNA revealed that the complexes were able to bind to DNA. In the LD experiments, an induced LD signal was observed for the hydroxyl-sugar helicate indicating oriented binding to the DNA. Both complexes were found to coil/bend ct-DNA, even at low complex loading. At high complex concentration the sugar functionalised cylinders showed DNA bending/coiling comparable to

$[Fe_2L^{TB}{}_3][BF_4]_4$, $[Fe_2L^{PA}{}_3][BF_4]_4$ and $[Fe_2L^{Hex}{}_3][BF_4]_4$ and greater than that of the steroid functionalised cylinders. The hydroxyl-sugar cylinder also showed promising DNA unwinding activity in a preliminary gel electrophoresis study, with an unwinding angle of 6°. The acetyl-sugar cylinder showed no DNA unwinding ability. These results may be due to the relative size of the two complexes, with the hydroxyl-sugar cylinder having a slightly reduced size. This may be due to the smaller cylinder being able to fit better into its DNA binding site, giving a closer proximity to the DNA and therefore allowing stronger contacts between the cylinder and the DNA. However, the acetyl-sugar was able to promote and stabilise the formation of a DNA three-way junction, as investigated by polyacrylamide gel electrophoresis.

Unfortunately, as with the alkyne and steroid helicates presented in chapters 2 and 3, *in vitro* studies could not be undertaken with these sugar functionalised cylinders due to their insolubility or instability in the solvent systems required. Cytotoxicity assays, such as the MTT assay, are necessary to investigate the anti-tumour effect of the developed anti-cancer agent. The tumour targeting ability of the functionalised drug can also be assessed by comparing the cellular uptake and cytotoxicity in cells that display the targeted receptor and those that do not.

In summary, iron(II) cylinders functionalised with sugars have been developed that retain some of the inherent DNA binding activity of the parent cylinder. It has been shown that by conjugating water solubilising groups, these alkyne functionalised cylinders can be

water soluble, however further investigation as to the effects on the stability of these complexes is needed.

4.7 Experimental: synthesis

4.7.1 Materials and methods

All reagents and solvents were purchased from Aldrich, Fisher, Apollo Scientific and Fluorochem and used without further purification. Deuterated NMR solvents were purchased from Goss Scientific. NMR spectra were recorded on Brüker AVIII300 and AVIII400 spectrometers and processed using standard Brüker software. Electrospray Ionisation (ESI) spectra were recorded on a Micromass LCT Time of flight mass spectrometer in positive ionisation mode. IR spectra were recorded on a PerkinElmer Spectrum 100 FT-IR spectrometer. UV-Vis spectra were performed using a Varian Cary 5000 UV-Vis spectrometer. CD and LD spectra were recorded on a Jasco J-810 spectropolarimeter.

4.7.2 Synthesis of Acetyl Sugar, $[Fe_2L^{OAcSug}{}_3][BF_4]_4$

4.7.2.1 Synthesis of 2-N-acetyl-3,4,6-tri-O-acetyl-1-(2'-propargyl)-β-D-glucosaminide (8)[9]

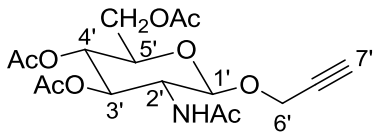

$C_{17}H_{23}NO_9$
FW: 385.37

A solution of 2-acetimido-2-deoxy-α-D-glucopyranosyl chloride 3,4,6 triacetate (0.400 g, 1.09 mmol) and propargyl alcohol (0.12 ml, 2.06 mmol) in anhydrous DCM (8 ml) was stirred at -10°C for 15 minutes. Silver trifluoromethanesulfonate (0.312 g, 1.21 mmol) was added and the reaction mixture was stirred overnight at room temperature. The mixture

was then neutralised with aqueous saturated $NaHCO_3$, filtered and the filter cake washed with DCM. The solution was separated and the organic layer washed with brine and evaporated to dryness *in vacuo*. The crude material was purified by column chromatography on a silica column (EtOAc:hexane 3:1) yielding a white solid (0.134 g, 32% yield).

^{1}H NMR (300 MHz, $CDCl_3$): δ 6.04 (d, *J* = 9.0 Hz, 1H, $H_{NH'}$), 5.27 (t, *J* = 10.0 Hz, 1H, $H_{3'}$), 5.04 (t, *J* = 12.9 Hz, 1H, $H_{4'}$), 4.84 (d, *J* = 8.3 Hz, 1H, $H_{1'}$), 4.34 – 4.33 (m, 2H, $H_{6'}$), 4.28 – 4.19 (m, 1H, $H_{\underline{CH2}OAc'}$), 4.12 - 4.08 (m, 1H, $H_{\underline{CH2}OAc'}$), 3.98 – 4.88 (m, 1H, $H_{2'}$), 3.74 – 3.70 (m, 1H, $H_{5'}$), 2.47 (s, 1H, $H_{7'}$), 2.05 (s, 3H, $H_{NH\underline{Ac}'/CH2O\underline{Ac}'}$), 1.99 (d, *J* = 2.8 Hz, 6H, $H_{OAc'}$), 1.92 (s, 3H, $H_{NH\underline{Ac}'/CH2O\underline{Ac}'}$).

^{13}C NMR (100 MHz, $CDCl_3$): δ100.1 ($C_{1'}$), 74.2 ($C_{3'}$), 73.6 ($C_{5'}$), 70.3 ($C_{4'}$), 63.7 ($C_{\underline{CH2}OAc'}$), 63.5 ($C_{\underline{CH2}OAc'}$), 57.6 ($C_{6'}$), 57.1 ($C_{6'}$), 55.9 ($C_{2'}$), 25.0 ($C_{NH\underline{Ac}'/CH2O\underline{Ac}'}$), 22.5 ($C_{NH\underline{Ac}'/CH2O\underline{Ac}'}$), 22.4 ($C_{O\underline{Ac}'}$), 22.3 ($C_{OAc'}$).

HRMS (EI): *m/z* = calculated for $C_{17}H_{23}NO_9Na$ $[M+Na]^+$ 408.1271; Found 408.1278.

IR (ν) = 3267 (m, C≡C-H), 3091 (w, C-H), 2116 (m, C≡C), 1739 (s, C=O), 1655 (s, C=O), 1566 (m, C=C).

4.7.2.2 Synthesis of 5-(2-N-acetyl-3,4,6-tri-O-acetyl-1-(2'-propargyl)-β-D-glucosaminide)-2-pyridinecarboxaldehyde (9)

Synthesis based on literature procedure.[10]

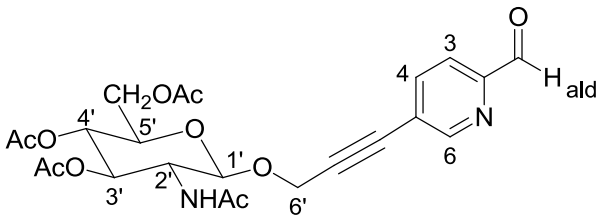

$C_{23}H_{26}N_2O_{10}$
FW: 490.47

A schlenk flask was charged with 2-N-acetyl-3,4,6-tri-O-acetyl-1-(2'-propargyl)-β-D-glucosaminide (8) (0.392 g, 1.02 mmol), 5-bromo-2-pyridinecarboxaldehyde (0.227 g, 1.22 mmol), bis(triphenylphosphine)dichloropalladium(II) (0.032 g, 0.05 mmol) and copper iodide (0.020 g, 0.11 mmol). Anhydrous THF (28 ml) and diisopropylamine (0.91 ml) were added, and the reaction mixture stirred under an argon atmosphere with light exclusion at room temperature for 72 hours. The resulting dark brown crude mixture was evaporated to dryness *in vacuo* and purified by column chromatography on a silica column (EtOAc). To remove the triphenylphosphine oxide impurity diethyl ether and 2 M HCl were added to the pale yellow solid obtained, the layers were separated and the aqueous layer washed again with diethyl ether. The aqueous layer was neutralised with aqueous saturated $NaHCO_3$ and extracted with ethyl acetate. The ethyl acetate was dried over Na_2SO_4 and evaporated *in vacuo* yielding a white solid (0.197 g, 40% yield).

^{1}H NMR (300 MHz, $CDCl_3$): δ 10.03 (s, 1H, H_{ald}), 8.78 (s, 1H, H_6), 7.92 – 7.90 (m, 2H, H_3, H_4), 5.93 (s, 1H, H_{NH}), 5.46 – 5.32 (m, 1H, $H_{4'}$), 5.10 – 5.01 (m, 2H, $H_{1'}$, $H_{3'}$), 4.62 (d, *J* = 2.8 Hz, 2H, $H_{6'}$), 4.30 - 4.24 (m, 1H, $H_{\underline{CH2}OAc'}$), 4.16 – 4.11 (m, 1H, $H_{\underline{CH2}OAc'}$), 3.87 –

3.72 (m, 2H, $H_{2'}$, $H_{5'}$), 2.05 (s, 3H, $H_{NHAc'/CH2OAc'}$), 2.01 (d, *J* = 2.6 Hz, 6H, $H_{OAc'}$), 1.92 (s, 3H, $H_{NHAc'/CH2OAc'}$).

^{13}C NMR (100 MHz, $CDCl_3$): δ 192.4 (C_{ald}), 152.5 (C_6), 139.6 ($C_{3/4}$), 120.9 ($C_{3/4}$), 98.4 ($C_{1'/3'}$), 74.1($C_{4'}$), 71.9 ($C_{2'/5'}$), 68.5 ($C_{1'/3'}$), 61.9 ($C_{CH2OAc'}$), 56.3 ($C_{6'}$), 54.7 ($C_{2'/5'}$), 23.2 ($C_{NHAc'/CH2OAc'}$), 20.6 ($C_{NHAc'/CH2OAc'}$), 20.5 ($C_{OAc'}$), 20.4 ($C_{OAc'}$).

HRMS (EI): *m/z* = calculated for $C_{23}H_{26}N_2O_{10}Na$ $[M+Na]^+$ 513.1485; Found 513.1487.

IR (ν) = 3306 (m, N-H), 2867 (w, C-H), 2163 (m, C≡C), 1739 (s, C=O), 1714 (s, C=O), 1666 (m, C=C), 1546 (m, C=C).

Elemental analysis (%) calculated for : C: 56.3; H: 5.7; N: 5.3; Found: C: 56.6; H: 5.6; N: 5.7.

4.7.2.3 Synthesis of $[Fe_2L^{OAcSug_3}][BF_4]_4$

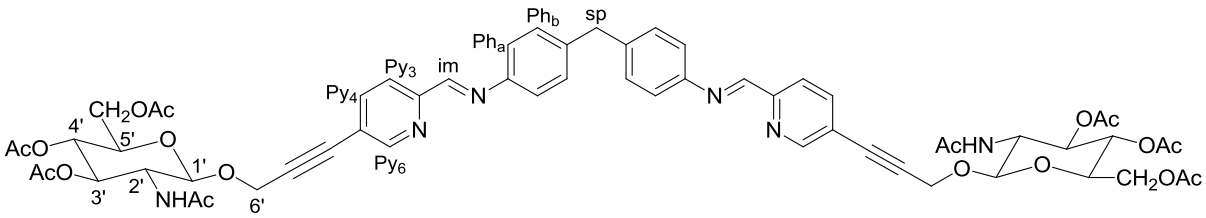

$[Fe_2(C_{59}H_{62}N_6O_{18})_3][BF_4]_4$
FW: 3888.41

To a solution of 5-(2-N-acetyl-3,4,6-tri-O-acetyl-1-(2'-propargyl)-β-D-glucosaminide)-2-pyridinecarboxaldehyde (9) (0.080 g, 0.16 mmol) in ethanol (3 ml) was added a solution of 4,4'-methylenedianiline (0.016 g, 0.08 mmol) in ethanol (2 ml) dropwise. A solution of iron(II) tetrafluoroborate hexahydrate (0.018 g, 0.06 mmol) in ethanol (2 ml) was then immediately added dropwise and the reaction mixture stirred overnight at room temperature. The resulting purple precipitate was collected by vacuum filtration, washed

with ethanol (1 L), diethyl ether (200 ml) and dried for 12 hours over silica, yielding a dark purple solid (0.032 g, 31% yield).

^{1}H NMR (300 MHz, CD_3CN) δ 8.98 (s, 2H, H_{im}), 8.64 (d, *J* = 8.1 Hz, 2H, H_{Py3}), 8.41 (d, *J* = 8.1 Hz, 2H, H_{Py4}), 7.69 (s, 2H, H_{Py6}), 6.94 (br s, 4H, $H_{Pha/Phb}$), 6.69 (d, *J* = 8.1 Hz, 2H, H_{NH}), 5.56 – 5.40 (br m, 6H, $H_{Pha/Phb}$, $H_{3'}$), 5.08 (d, *J* = 8.1 Hz, 2H, $H_{1'}$), 4.97 (t, *J* = 9.7 Hz, 2H, $H_{4'}$), 4.56 (d, *J* = 3.5 Hz, 4H, $H_{6'}$), 4.32 – 4.26 (m, 2H, $H_{\underline{CH2}OAc'}$), 4.13 – 3.99 (m, 4H, $H_{\underline{CH2}OAc'}$, H_{sp}), 3.70 – 3.64 (m, 2H, $H_{5'}$), 3.49 – 3.41 (m, 2H, $H_{2'}$), 2.06 – 1.92 (m, 24H, $H_{CH2O\underline{Ac}'}$, $H_{NHAc'}$, $H_{OAc'}$ + 39H, solvent).

Mass spectrum (ESI): *m/z* = 885.6 $[Fe_2(C_{59}H_{62}N_6O_{18})_3]^{4+}$.

IR (ν) = 2942 (w, C-H), 2232 (m, C≡C), 1739 (s, C=O), 1668 (s, C=O), 1544 (m, C=C), 1035 (s, br, BF_4).

UV-Vis (1% MeOH:H_2O): λ_{max} [nm] (ε_{max}/$dm^3mol^{-1}cm^{-1}$): 231 (90,800), 266 (60,400), 308 (7,500), 540 (7,300), 596 (10,400).

4.7.3 Attempted synthesis of $[Fe_2L^{OHSug}{}_3][BF_4]_4$

4.7.3.1 Synthesis of 5-(2-N-acetyl-1-O-(2'-propargyl)-β-D-glucosaminide)-2-pyridinecarboxaldehyde (10)

Synthesis based on literature procedure.[11]

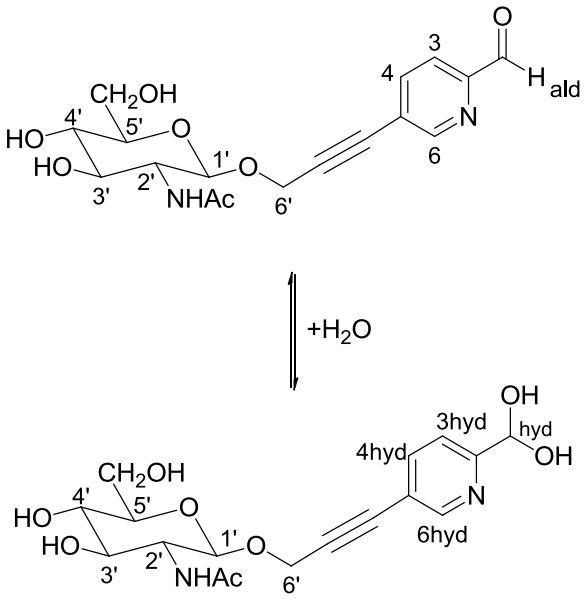

$C_{17}H_{20}N_2O_7$
FW: 364.35

To a solution of 5-(2-N-acetyl-3,4,6-tri-O-acetyl-1-(2'-propargyl)-β-D-glucosaminide)-2-pyridinecarboxaldehyde (9) (0.591 g, 1.20 mmol) in anhydrous MeOH (10 ml) was added sodium methoxide (0.071 g, 1.31 mmol) and the reaction mixture was stirred at room temperature for 2 hours. Dowex (50W x8, H^+ form) (1.6 g) was then added until pH 5 was reached. The reaction mixture was then filtered, the Dowex washed with MeOH (30 ml), and the filtrate evaporated to dryness *in vacuo*. The off-white crude solid was purified by column chromatography on a silica column (MeOH:DCM 15:85) yielding a white solid (0.263 g, 60% yield).

^{1}H NMR (300 MHz, D_2O) δ 9.97 (s, 1H, H_{ald}), 8.80 (d, *J* = 1.2 Hz, 1H, H_6), 8.61 (d, *J* = 1.2 Hz, 1H, H_{6hyd}), 8.14 (dd, *J* = 8.1, 1.7 Hz, 1H, H_4), 8.02 – 7.93 (m, 2H, H_3, H_{4hyd}), 7.64 (d, *J* = 8.2 Hz, 1H, H_{3hyd}), 6.02 (s, 1H, H_{hyd}), 4.78 – 4.76 (m, 2H, $H_{1'}$), 4.68 (d, *J* = 11.0 Hz,

4H, $H_{6'}$), 3.93 – 3.89 (m, 2H, $H_{\underline{CH2}OH'}$), 3.75 – 3.67 (m, 4H, $H_{\underline{CH2}OH'}$, $H_{2'}$), 3.60 – 3.53 (m, 2H, $H_{3'}$), 3.50 – 3.40 (m, 4H, $H_{4'}$, $H_{5'}$), 2.00 (d, J = 3.7 Hz, 6H, $H_{NH\underline{Ac}}$).

^{13}C NMR (100 MHz, D_2O): δ193.8 (C_{ald}), 152.3 (C_{6hyd}), 151.0 (C_6), 141.1 ($C_{4,4hyd}$), 123.8 (C_3), 120.0 (C_{3hyd}), 99.9 ($C_{1'}$), 89.7 (C_{hyd}), 76.0 ($C_{4'/5'}$), 73.6 ($C_{3'}$), 69.8 ($C_{4'/5'}$), 60.7 ($C_{\underline{CH2}OH}$), 57.3 ($C_{6'}$), 55.5 ($C_{2'}$), 22.2 ($C_{NH\underline{Ac}'}$).

HRMS (EI): *m/z* = calculated for $C_{17}H_{20}N_2O_7Na$ $[M+Na]^+$ 387.1168; Found 387.1173.

IR (ν) = 3263 (m, N-H), 3100 (w, C-H), 2210 (m, C≡C), 1710 (s, C=O), 1646 (s, C=O), 1563 (m, C=C).

4.7.3.2 Attempted synthesis of $[Fe_2L^{OHSug}{}_3][BF_4]_4$

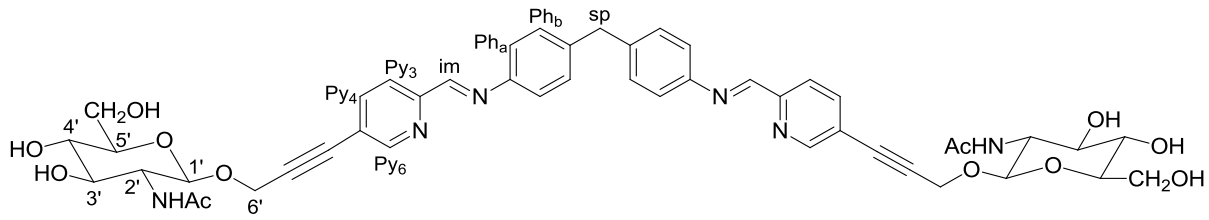

$[Fe_2(C_{47}H_{50}N_6O_{12})_3][BF_4]_4$
FW: 3131.74

To a solution of 5-(2-N-acetyl-1-O-(2'-propargyl)-β-D-glucosaminide)-2-pyridinecarboxaldehyde (10) (0.066 g, 0.18 mmol) in methanol (3 ml) was added a solution of 4,4'-methylenedianiline (0.018 g, 0.09 mmol) in ethanol (2 ml) dropwise. A solution of iron(II) tetrafluoroborate hexahydrate (0.021 g, 0.06 mmol) in ethanol (2 ml) was then immediately added dropwise and the reaction mixture stirred overnight at room temperature. The resulting purple precipitate was collected by vacuum filtration, washed with methanol (1 L), diethyl ether (200 ml) and dried for 12 hours over silica, yielding a dark purple solid (0.033 g, 35% yield).

^{1}H NMR (300 MHz, D_2O) δ 9.35 – 9.18 (br m, 2H, H_{im}), 8.99 (br s, 2H, $H_{Py3/4}$), 8.67 (br s, 2H, $H_{Py3/4}$), 7.53 (br s, 2H, H_{Py6}), 6.73 (br s, 4H, $H_{Pha/Phb}$), 5.69 (br s, 4H, $H_{Pha/Phb}$), 3.96 – 3.86 (br m, 2H, H_{sp}), 2.09 (br s, 6H, $H_{NH\underline{Ac}'}$).

Mass spectrum (ESI): *m/z* = 696.4 $[Fe_2(C_{47}H_{50}N_6O_{12})_3]^{4+}$, 956.2 $[Fe_2(C_{47}H_{50}N_6O_{12})_3][BF_4]^{3+}$.

IR (ν) = 3270 (m, OH), 2926 (w, C-H), 2165 (m, C≡C), 1646 (s, C=O), 1545 (m, C=C), 1028 (s, br, BF_4).

UV-Vis (H_2O): λ_{max} [nm] (ε_{max}/$dm^3mol^{-1}cm^{-1}$): 233 (36,600), 269 (55,800), 303 (45,900), 539 sh (4,400), 594 (5,800).

4.8 Experimental: DNA binding studies

4.8.1 Materials and methods

All DNA binding studies were carried out using Ultrapure water (18.2 MΩ) purchased from Fisher Scientific. Calf thymus (ct) DNA, highly polymerised, was purchased from Sigma Aldrich and pBR322 plasmid DNA was purchased from New England Biolabs. Both were used without further purification and kept frozen. Tris-acetate-EDTA buffer was purchased from Fisher and agrose from USB Corporation.

4.8.2 Circular and Linear Dichroism Experiments

CD and LD measurements were recorded using a Jasco J-810 spectropolarimeter. CD measurements were carried out in quartz cuvettes of 1 cm (750-200 nm) or 0.1 cm (450-

200 nm) pathlength. LD experiments were recorded in a flow couette cell (Krometek) with a 0.1 cm pathlength.

Stock solutions of ct-DNA (3000 μM) in water were prepared and kept frozen until the day of the experiment. Sodium chloride (1 M) and sodium cacodylate ($Na(CH_2)_2AsO_2.3H_2O$) (100 mM) buffer stock solutions were used to prepare final ct-DNA solutions of 300 μM with 20 mM NaCl and sodium cacodylate (1 mM) (pH 6.8). DNA concentrations were determined by UV-Vis measurements using the known molar extinction coefficient of ε_{258} = 6600 $mol^{-1}dm^3cm^{-1}$ per DNA base.

CD and LD titrations were carried out using three solutions; solution A (a 300 μM ct-DNA solution, containing NaCl (20 mM) and sodium cacodylate (1 mM)); solution B (a 500 μM complex solution) and solution C (a 600 μM ct-DNA solution, containing 40 mM NaCl and sodium cacodylate (2 mM)). Firstly solution A was recorded, then equal aliquots of solutions B and C were added, keeping the concentration of ct-DNA constant throughout the titration. The titration was carried out to obtain an initial ct-DNA:complex ratio of 60:1 decreasing to 4:1. The stock solution of complex was stored in ice during the experiment.

4.8.3 Agarose Gel Electrophoresis

Agarose gels were prepared by warming agarose (2 g) in 1x Tris-acetate-EDTA buffer which was then poured into a gel tray (210 x 150 mm) fitted with a 15 toothed comb, to produce sample wells. The gel was left to set for 40 minutes. Sample solutions (16 μl) were prepared containing 96.3 μM pBR322 plasmid DNA and different concentrations of

complexes (from 60 µM stock solution in water and up to 7% MeOH) to obtain plasmid:complex ratios ranging from 100:1 to 2:1. Theses sample solutions were incubated for 2 hours at room temperature. Before loading , 4 µl loading buffer (30% glycerol, 0.25% bromophenol blue) was added, the samples were mixed and then 16 µl of the samples loaded into the gel wells. The gel was run for 2.5 hours in an Amersham Biosciences HE99X Maxi submarine kit with an electrophoresis Power Supply-EPS 301 system, at a constant voltage of 120 V and 400 mA, in 1x Tris-acetate-EDTA running buffer. The gel was then stained with an ethidium bromide solution (0.5 $mg.ml^{-1}$) in 200 ml of water for 20 minutes and visualised using a UVtec–uvipro platinum 2.0 system (UVidoc, Cambridge, UK) at 312 nm.

4.8.4 Polyacrylamide Gel Electrophoresis (PAGE)

Procedure provided by S. Phongtongpasuk [21] and carried out by N. Calle Alonso, both of the Hannon group, University of Birmingham.

4.8.4.1 Radioactive labelling

Oligonucleotides (sequences S1: CGGAACGGCACTCG, S2: CGAGTGCAGCGTGG, S3: CCACGCTCGTTCCG) were purchased from MWG Eurofin. One strand was labelled with P^{32} at the 5' terminus using T4 polynucleotide kinase (New England Biolabs) and [γ-^{32}P] adenosine 5'-triphosphate (Perkin Elmer). First ultrapure water (4.8 µl), 10x bacteriophage T4 poynucleotide kinase buffer (1 µl), oligonucleotide S3 (1.2 µl of 100 µM), bacteriophage T4 poynucleotide kinase (1 µl) (New England Biolabs) and γ-^{32}P ATP (2 µl of 6000 Ci/mmol) (Perkin Elmer) were incubated in an eppendorf at 37°C for 40

minutes. To deactivate the polynucleotide kinase, the solution was then heated to 80°C for 3 minutes.

To purify the radioactive-labelled DNA fragments from any unreacted ATP a QIAquick nucleotide removal kit (QIAGEN) was employed. 10 volumes of PN buffer were added to 1 volume of reaction sample and this solution was loaded onto a QIAquick spin column with a 2 ml collection tube, centrifuged for 1 minute at 6000 rpm and the flow through discarded. A new collection tube was then fitted to the column, PE buffer (500 µl) was added and this solution was centrifuged for 1 minute at 6000 rpm and the flow through discarded. Again, PE buffer (500 µl) was added and the solution was centrifuged at 13000 rpm for 1 minute to remove residual buffer. The column was then put into a fresh eppendorf, ultrapure water (30 µl) was added to the column and this was left for 5 minutes. After centrifuging at 13000 rpm for 2 minutes a radiolabelled DNA stock solution (8 µM) was obtained.

4.8.4.2 Polyacrylamide gel preparation

A 15% native polyacrylamide gel was prepared by mixing 52.5 ml of ultra pure water, 10 ml of 10x TB buffer (890 mM tris(hydroxymethy)amino methane and 890 mM boric acid) (pH 8.3), 37.5 ml of 40% acrylamide (29:1) (Geneflow), 500 µl of 10% (w/v) ammonium persulfate and 75 µl tetramethylenediamine (TEMED). This was then poured onto a set of glass plates and left to set for 40 minutes. The wells of the polymerised gel were washed with running buffer (TB buffer) and the gel was pre-run at 200 V for 5 minutes before sample loading.

4.8.4.3 PAGE electrophoresis experiment

Sample solutions were prepared by mixing solutions of the complexes with stoichiometric amounts of oligonucleotides in TBN buffer (89 mM tris(hydroxymethy)amino methane, 89 mM of boric acid and 100 µM NaCl) (pH 8.3) to give final concentrations of 0.4 µM for each single strand (1.2 µM total concentration of DNA) and 0.4 µM of complex. This gives a three-way junction:complex ratio of 1:1. The sample solutions were incubated for 1 hour at room temperature and then in ice for 15 minutes. To prepare the samples for loading, 5 µl of 30% glycerol was added to each eppendorf. 13 µl of each sample was then loaded onto the 15% polyacrylamide gel. The gel was run for 4 hours at 120 V using Gel System equipment (Thermo Scientific UK). It was then exposed on a phosphor imaging plate for 1-16 hours depending on how fresh the radioactive ATP used was. A radiogel image was obtained using a Molecular Imager FX (Bio-Rad) and the gel was quantified using Quantity One software.

4.9 References

(1) Zutphen, S. v.; Reedijk, J., *Coord. Chem. Rev.* **2005**, *249*, 2845.

(2) Sinha, R.; Kim, G. J.; Nie, S.; Shin, D. M., *Mol. Cancer Ther.* **2006**, *5*, 1909.

(3) Mikata, Y.; Shinohara, Y.; Yoneda, K.; Nakamura, Y.; Brudziñska, I.; Tanase, T.; Kitayama, T.; Takagi, R.; Okamoto, T.; Kinoshita, I.; Doe, M.; Orvig, C.; Yano, S., *Bioorg. Med. Chem. Lett.* **2001**, *11*, 3045.

(4) Storr, T.; Thompson, K. H.; Orvig, C., *Chem. Soc. Rev.* **2006**, *35*, 534.

(5) Freichels, H.; Jérôme, R.; Jérôme, C., *Carbohydr. Polym.* **2011**, *86*, 1093.

(6) Berger, I.; Nazarov, A. A.; Hartinger, C. G.; Groessl, M.; Valiahdi, S. M.; Jakupec, M. A.; Keppler, B. K., *ChemMedChem* **2007**, *2*, 505.

(7) Chen, Y.; Heeg, M. J.; Braunschweiger, P. G.; Xie, W.; Wang, P. G., *Angew. Chem. Int. Ed.* **1999**, *38*, 1768.

(8) Yang, D. J.; Kim, C.-G.; Schechter, N. R.; Azhdarinia, A.; Yu, D.-F.; Oh, C.-S.; Bryant, J. L.; Won, J.-J.; Kim, E. E.; Podoloff, D. A., *Radiology* **2003**, *226*, 465.

(9) Ma, D.-L.; Shum, T. Y.-T.; Zhang, F.; Che, C.-M.; Yang, M., *Chem. Commun.* **2005**, 4675.

(10) Browning, M., Estrogen Steroid Derived Metallo-drugs, *PhD Thesis, University of Warwick* **2006**.

(11) Rowan, A. S.; Nicely, N. I.; Cochrane, N.; Wlassoff, W. A.; Claiborne, A.; Hamilton, C. J., *Org. Biomol. Chem.* **2009**, *7*, 4029.

(12) Pearmund, C. R., Metallo-supramolecular Cylinders as Chemical Nucleases, *PhD Thesis, University of Warwick* **2006**.

(13) Cardo, L., Metallo-supramolecular Cylinders and their Peptide Conjugates. Synthesis, dynamics and DNA recognition, *PhD Thesis, University of Birmingham* **2010**.

(14) Cardo, L.; Sadovnikova, V.; Phongtongpasuk, S.; Hodges, N. J.; Hannon, M. J., *Chem. Commun.* **2011**, *47*, 6575.

(15) Hannon, M. J.; Meistermann, I.; Isaac, C. J.; Blomme, C.; Aldrich-Wright, J. R.; Rodger, A., *Chem. Commun.* **2001**, 1078.

(16) Twyman, L. J.; Beezer, A. E.; Esfand, R.; Hardy, M. J.; Mitchell, J. C., *Tetrahedron Lett.* **1999**, *40*, 1743.

(17) Cardo, L.; Hannon, M. J., *Inorg. Chim. Acta* **2009**, *362*, 784.

(18) Bellon, S. F.; Coleman, J. H.; Lippard, S. J., *Biochemistry* **1991**, *30*, 8026.

(19) Jodry, J. J.; Lacour, J., *Chem. Eur. J.* **2000**, *6*, 4297.

(20) Albrecht, M., *Chem. Eur. J.* **2000**, *6*, 3485.

(21) Phongtongpasuk, S., Investigating the Interaction of a Metallosupramolecular Cylinder With Nucleic Acids, *PhD Thesis, University of Birmingham* **2011**.

Chapter 5: Conclusions and Future Work

5.1 Conclusions

Due to the successes of supramolecular metallo-cylinders developed in the Hannon group, the aim of the work described herein was to design and synthesise iron(II) cylinders functionalised with a range of chemical groups and biomolecules. It was hoped that these novel cylinders could be employed to further probe and advance the DNA and cellular recognition of metallo-cylinders. A novel functionalisation route was developed (Chapter 2) to allow the easy and varied modification of these metallo-cylinders by attachment of a vast array of functional moieties.

Several cylinders functionalised with simple chemical groups, such as hydroxyl and phenyl groups, were synthesised in few reaction steps with good yields, using this novel synthesis route. DNA binding studies carried out with these complexes demonstrated the importance of the size and shape of these cylinders to their DNA recognition. A better understanding has been gained of the type of functionalisation that can be tolerated by these complexes while still retaining their DNA binding activity.

The triple bond, propargyl alcohol and hexyn-ol cylinders, $[Fe_2L^{TB}{}_3][BF_4]_4$, $[Fe_2L^{PA}{}_3][BF_4]_4$ and $[Fe_2L^{Hex}{}_3][BF_4]_4$, were all found to be effective DNA binders when evaluated by CD and LD DNA binding studies. Gel electrophoresis studies found the triple bond and propargyl alcohol functionalised helicates to unwind supercoiled plasmid DNA

with unwinding angles of 5° and 6° respectively. However the hexyn-ol functionalised cylinder showed no DNA unwinding in this experiment. PAGE studies revealed all three complexes were able to promote the formation of a DNA three-way junction.

The phenylacteylene complex, $[Fe_2L^{Phen}{}_3][BF_4]_4$, exhibited the lowest DNA binding activity of the four novel compounds, as investigated by linear dichroism and agarose and polyacrylamide gel electrophoresis studies, likely due to the bulky and hydrophobic nature of the phenylacetylene moiety that is attached at the ends of this cylinder. The main disadvantage of these novel iron(II) cylinders is their lack of solubility in water, preventing further investigation of their anti-cancer properties using *in vitro* studies.

The aim of the work detailed in chapter 3 was to try to improve the targeting of these supramolecular helicates to cancerous tissue, by the conjugation of biomolecule vectors. Iron(II) cylinders conjugated to the steroid hormones testosterone and estrogen were synthesised in only two reaction steps, with moderate yields. Chirality studies revealed that these complexes were a mixture of M and P helical isomers, with a slightly higher proportion of the P configuration. DNA binding studies demonstrated that these compounds could bind to ct-DNA and induce intramolecular coiling of the DNA. These compounds showed no ability to unwind supercoiled plasmid DNA or induce the formation of a DNA three-way junction, which is likely due to their bulky size and shape. As with the functionalised cylinders, detailed in Chapter 2, the main disadvantage of these novel steroid conjugated cylinders is their lack of solubility in water, preventing further *in vitro* studies and investigation of their possible targeting abilities.

In chapter 4, supramolecular cylinders were functionalised with sugars with the aim of targeting them to cancerous tissue expressing carbohydrate receptors and to increase their water solubility. Iron(II) complexes with acetyl and hydroxyl β-D-glucosaminide sugar moieties were designed and synthesised over three or four reaction steps. Unfortunately the yield of these syntheses was poor. The hydroxyl-sugar cylinder was found to be very unstable and therefore difficult to fully characterise. However, DNA binding studies were carried out to investigate the potential of the complex. The acetyl-sugar cylinder, $[Fe_2L^{OAcSug}{}_3][BF_4]_4$, was found to be diastereoisomerically pure and of the M helical configuration. Chiral characterisation of the hydroxyl-sugar cylinder was ambiguous, however the complex is chiral and is predominantly of the M configuration.

DNA binding studies were undertaken with the acetyl-sugar complex and revealed that the cylinder could bind to ct-DNA, induce intramolecular coiling and promote the formation of a DNA three-way junction. However the complex did not unwind supercoiled DNA. Preliminary DNA binding studies were also carried out with the hydroxyl-sugar cylinder and revealed a strong DNA binding ability. The helicate could bind to ct-DNA in an oriented manner, causing intramolecular coiling of the DNA helix. It was also able to unwind supercoiled plasmid DNA. Unfortunately further *in vitro* studies could not be undertaken due to the lack of solubility or stability of the sugar functionalised cylinders, and so the targeting ability of these sugar cylinders could not be investigated.

The work detailed herein shows that cylinders with a range of functionalisation groups, including biomolecules, conjugated via alkyne linkers can be synthesised and that the

inherent DNA binding activity of the parent cylinder is not lost due to this functionalisation.

5.2 Future work

Several supramolecular cylinders functionalised with biomolecules such as steroids and sugars have been described herein. However, there are many other biomolecules that could be explored to target the cylinder to specific tissues, organs or cancers; such as other sugars, folic acid or biotin. Another type of interesting functionalisation would be to conjugate a fluorescent probe to the cylinder, to allow cellular localisation studies to be performed.

Another route to functionalised cylinders with enhanced properties would be to synthesise the ruthenium(II) analogues. The ruthenium(II) parent cylinder has enhanced stability compared to the analogous iron(II) complex, is luminescent and can bind and photocleave DNA in a sequence specific manner.[1,2]

One of the main problems encountered during this work was the lack of water solubility of a number of the novel cylinders synthesised. This is a major disadvantage as *in vitro* studies, such as cellular uptake experiments and cytotoxicity assays, cannot be performed. One possible solution would be to attach the functional moiety to the ends of the cylinder via a linker that imparts water solubility, such as polyethylene glycol (PEG).[3] If the aqueous solubility of the biomolecule-functionalised cylinders presented in this work could be improved, the possible targeting effect of these cylinders could be investigated using *in*

vitro studies. There are many known cancer cell lines that display estrogen or androgen (for testosterone conjugates) receptors and cellular studies with these would indicate whether some enhancement of cellular uptake has been imparted to the cylinder by the steroid functionalisation.

Another interesting idea that could improve the functionalisation, solubility and DNA affinity of these compounds, would be to cap the ends of the cylinder (Fig. 5.1). This cap could be formed of three 'arms' that would be attached to the three ligands, with a chemical unit that would allow conjugation of a biomolecule. This would allow functionalisation of the cylinder without having to attach three bulky moieties to each end and may be more stable. The affinity for DNA may also be improved by this design as the cylinder would be more compact overall and so may fit better into the DNA major groove or Y-shaped junction. If relatively hydrophobic functional groups are to be attached, the difference in number may improve the solubility of the cylinder.

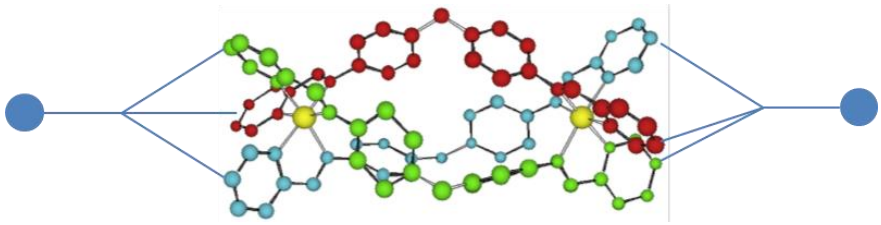

Figure 5.1 Capped cylinder with functionalisation (blue spheres). [Adapted from Ref [4]]

5.3 References

(1) Pascu, G. I.; Hotze, A. C.; Sanchez-Cano, C.; Kariuki, B. M.; Hannon, M. J., *Angew. Chem. Int. Ed. Engl.* **2007**, *46*, 4374.

(2) Malina, J.; Hannon, M. J.; Brabec, V., *Chem. Eur. J.* **2008**, *14*, 10408.

(3) Alcantar, N. A.; Aydil, E. S.; Israelachvili, J. N., *J. Biomed. Mater. Res.* **2000**, *51*, 343.

(4) Hotze, A. C.; Hodges, N. J.; Hayden, R. E.; Sanchez-Cano, C.; Paines, C.; Male, N.; Tse, M. K.; Bunce, C. M.; Chipman, J. K.; Hannon, M. J., *Chem. Biol.* **2008**, *15*, 1258.

Appendix

A.1 2D-NMR (COSY) of $[Fe_2L^P_3][BF_4]_4$

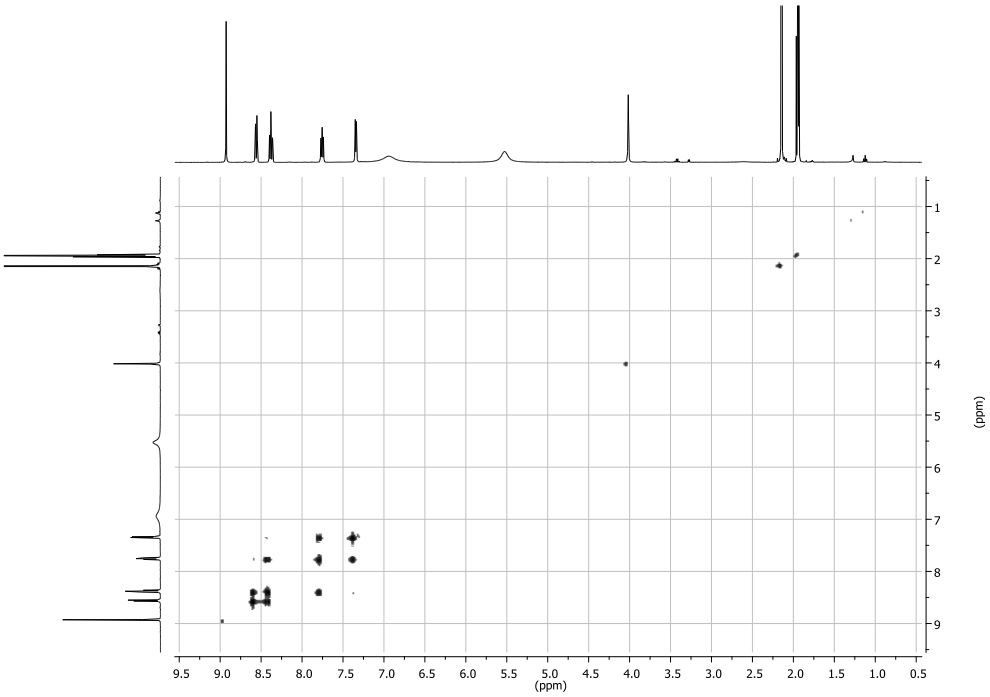

^{1}H-^{1}H COSY NMR (400 MHz, CD_3CN, 298 K)

A.2 2D-NMR (COSY) of 5-ethynyl-2-pyridinecarboxaldehyde (2)

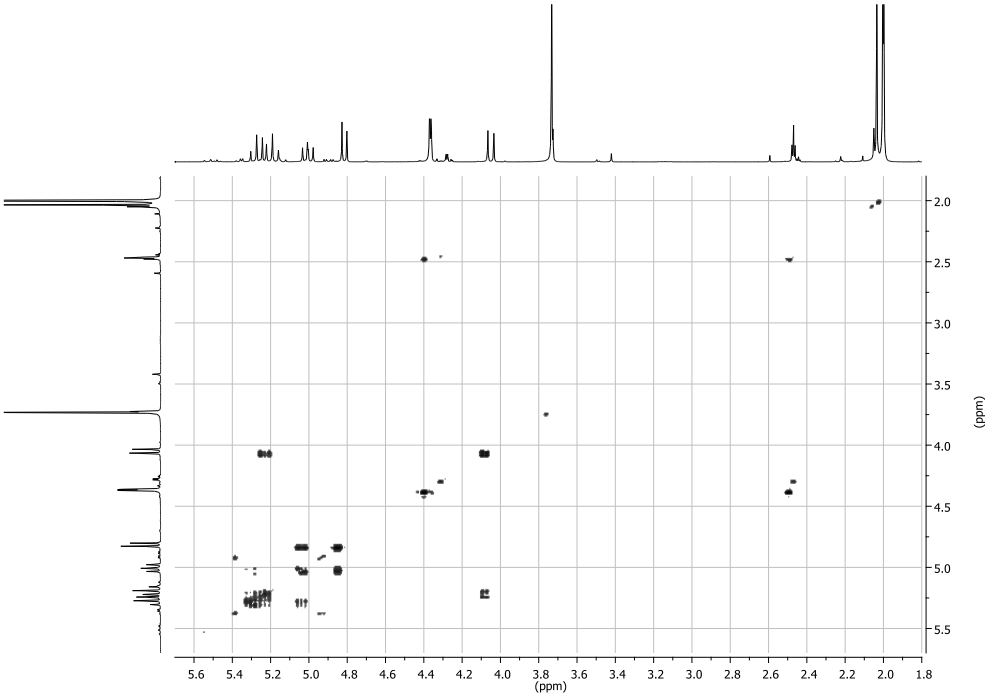

^{1}H-^{1}H COSY NMR (400 MHz, $CDCl_3$, 298 K)

A.3 2D-NMR (COSY) of $[Fe_2L^{TB}_3][BF_4]_4$

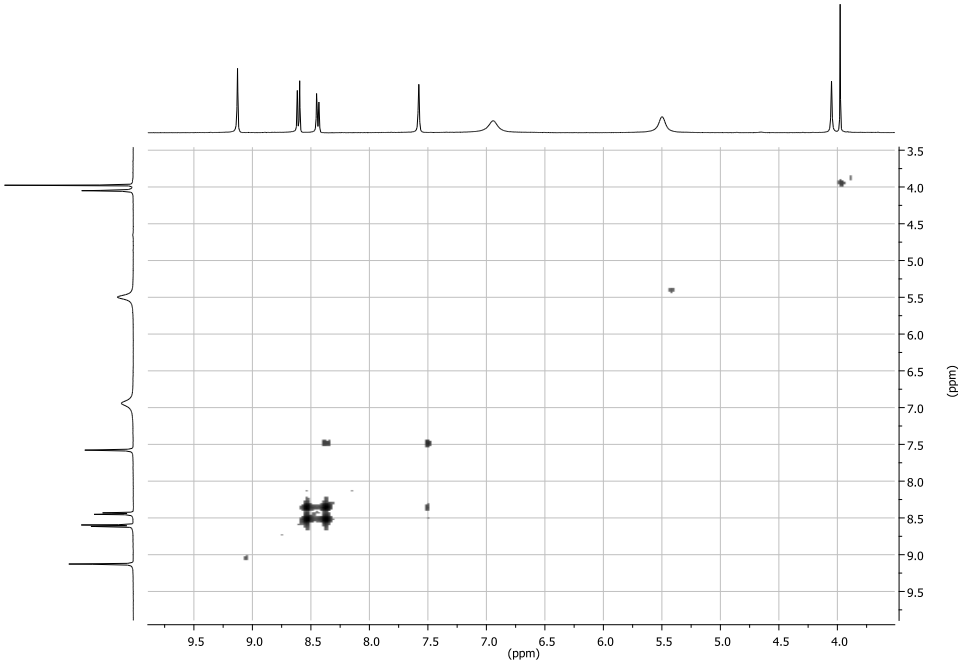

^{1}H-^{1}H COSY NMR (400 MHz, CD_3CN, 298 K)

A.4 2D-NMR (COSY) of 5-(3-hydroxyprop-1-ynyl)-2-pyridinecarboxaldehyde (3)

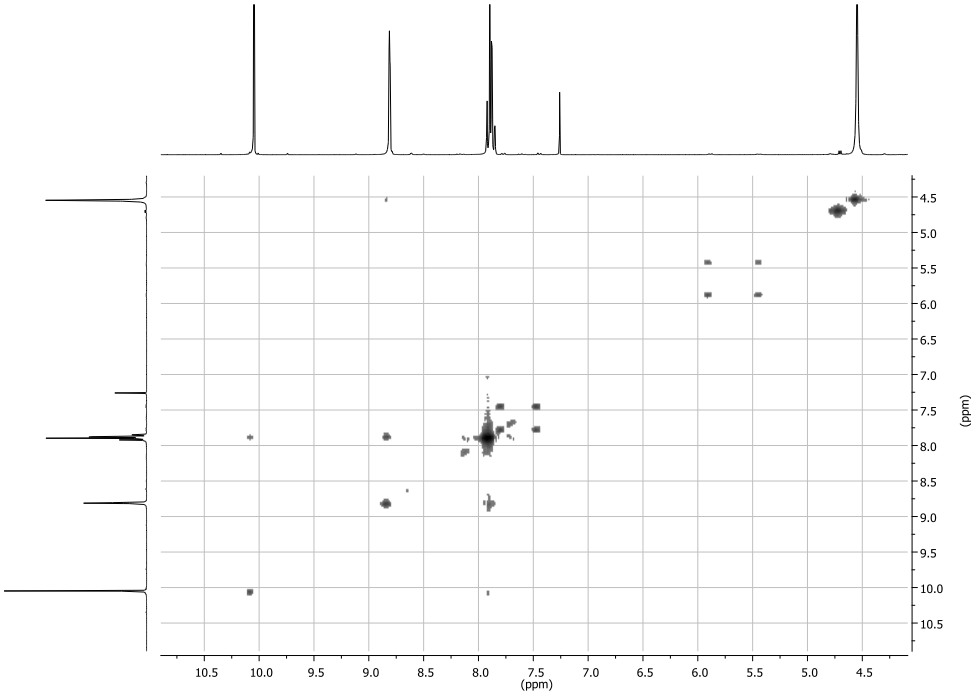

^{1}H-^{1}H COSY NMR (400 MHz, $CDCl_3$, 298 K)

A.5 2D-NMR (COSY) of $[Fe_2L^{PA}_3][BF_4]_4$

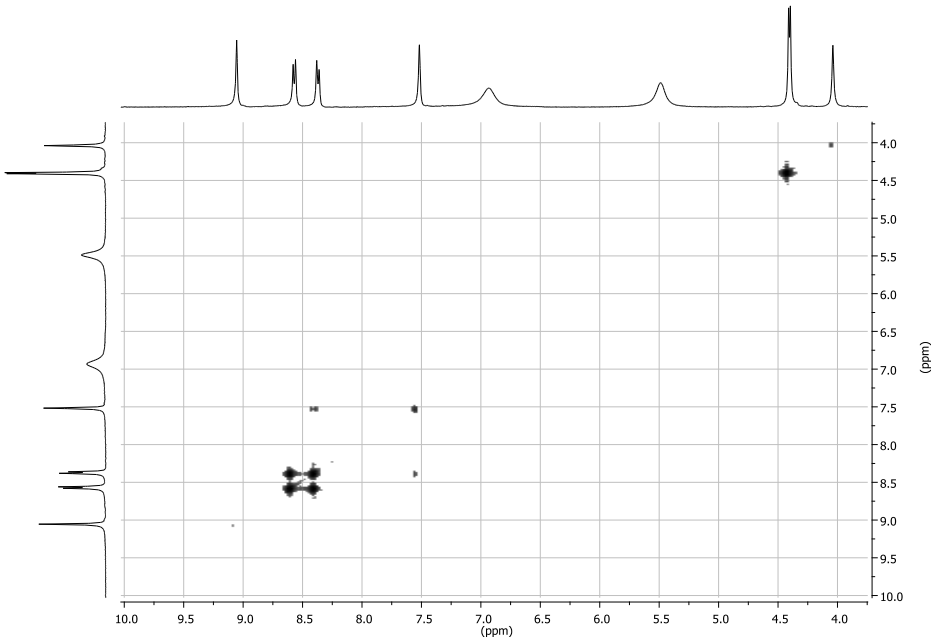

^{1}H-^{1}H COSY NMR (400 MHz, CD_3CN, 298 K)

A.6 2D-NMR (COSY) of 5-(hex-5-yn-1-ol)-2-pyridinecarboxaldehyde (4)

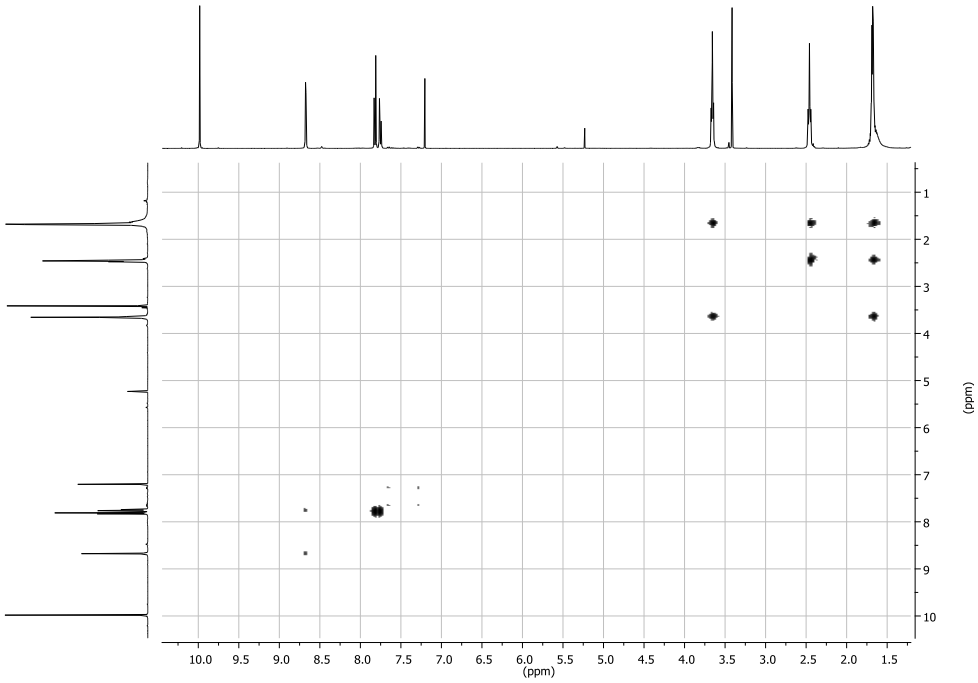

^{1}H-^{1}H COSY NMR (400 MHz, $CDCl_3$, 298 K)

A.7 2D-NMR (COSY) of $[Fe_2L^{Hex}{}_3][BF_4]_4$

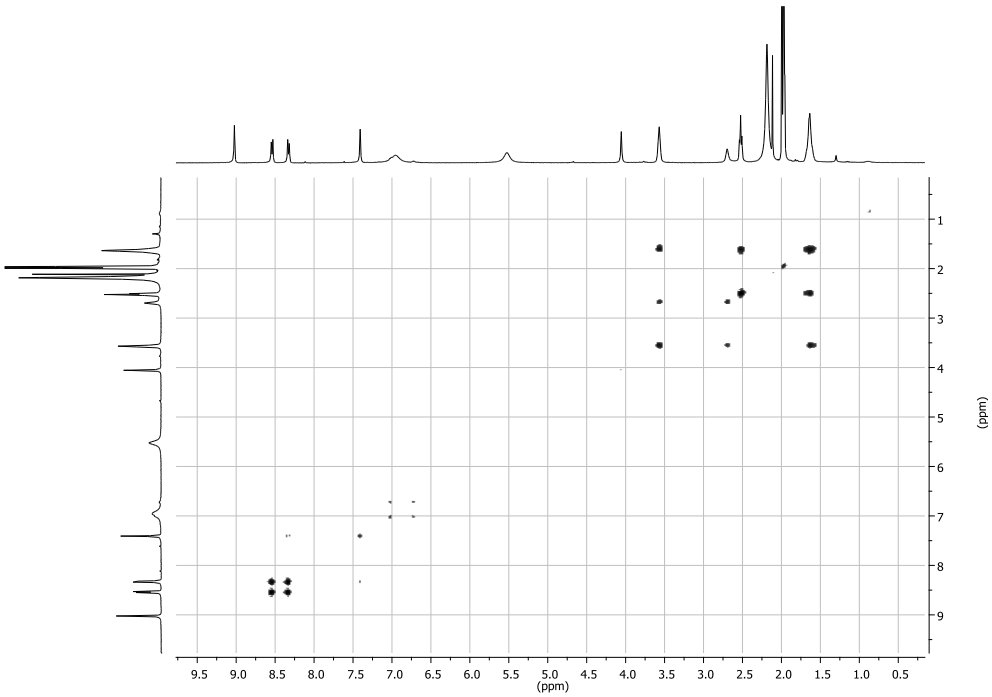

^{1}H-^{1}H COSY NMR (400 MHz, CD_3CN, 298 K)

A.8 2D-NMR (COSY) of 5-(ethynylphenyl)-2-pyridinecarboxaldehyde (5)

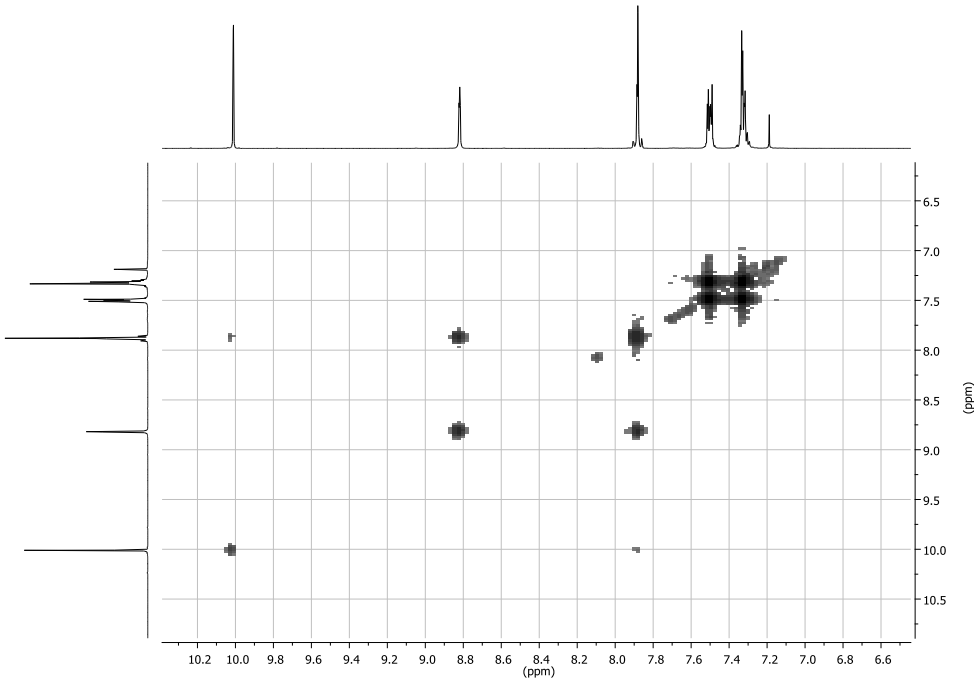

^{1}H-^{1}H COSY NMR (400 MHz, $CDCl_3$, 298 K)

A.9 2D-NMR (COSY) of $[Fe_2L^{Phen}_3][BF_4]_4$

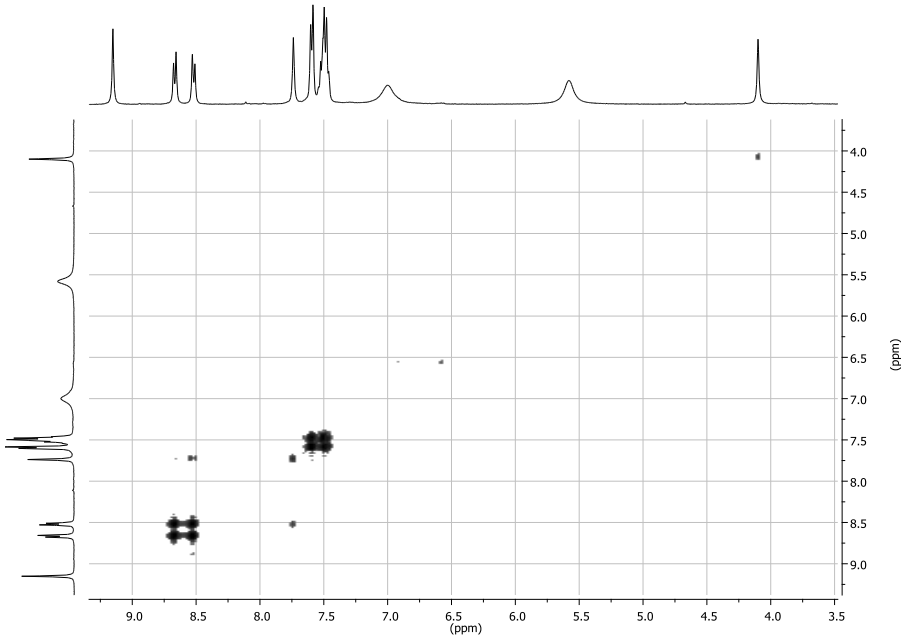

^{1}H-^{1}H COSY NMR (400 MHz, CD_3CN, 298 K)

A.10 2D-NMR (COSY) of 17α-[(2-pyridinecarboxaldehyde)-5-ethynyl]ethisterone (6)

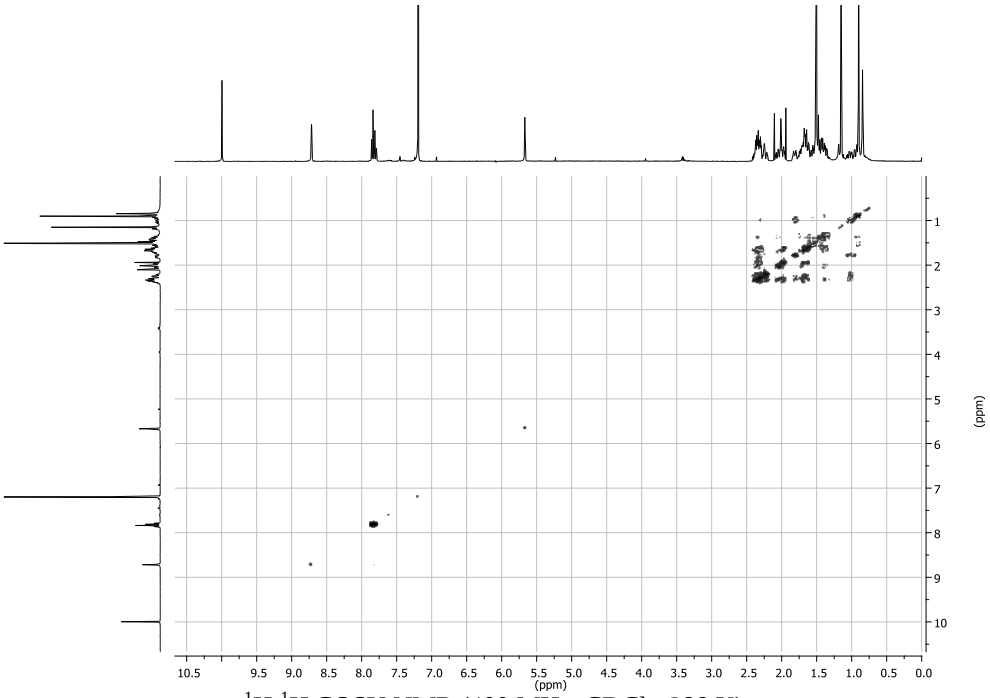

^{1}H-^{1}H COSY NMR (400 MHz, $CDCl_3$, 298 K)

A.11 2D-NMR (COSY) of $[Fe_2L^{Test}_3][BF_4]_4$

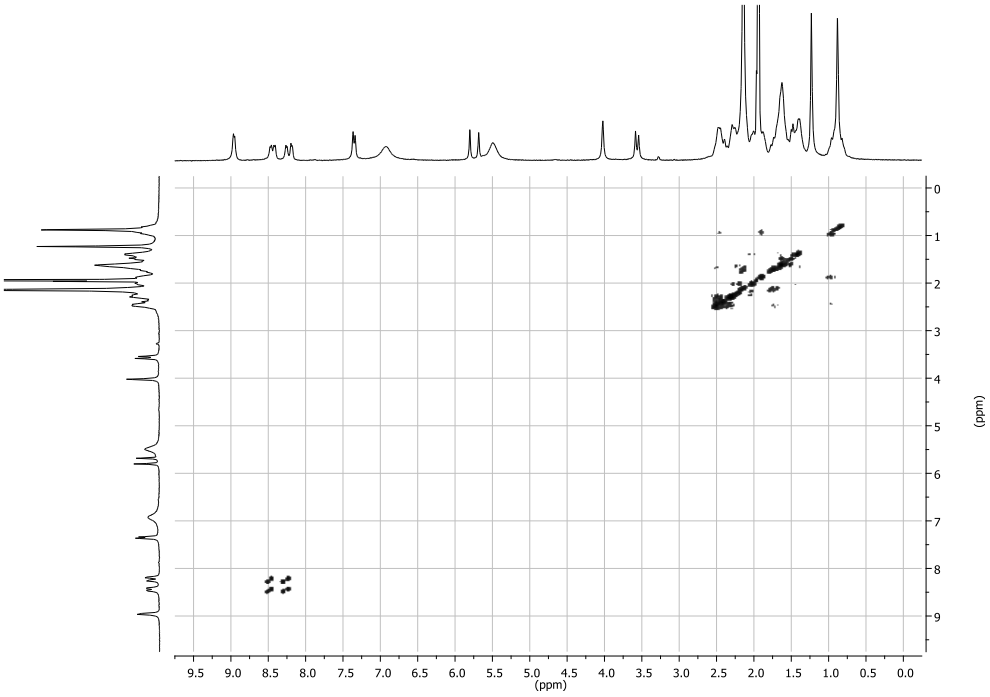

^{1}H-^{1}H COSY NMR (400 MHz, CD_3CN, 298 K)

A.12 2D-NMR (COSY) of 17α-[(2-pyridinecarboxaldehyde)-5-ethynyl]estradiol (7)

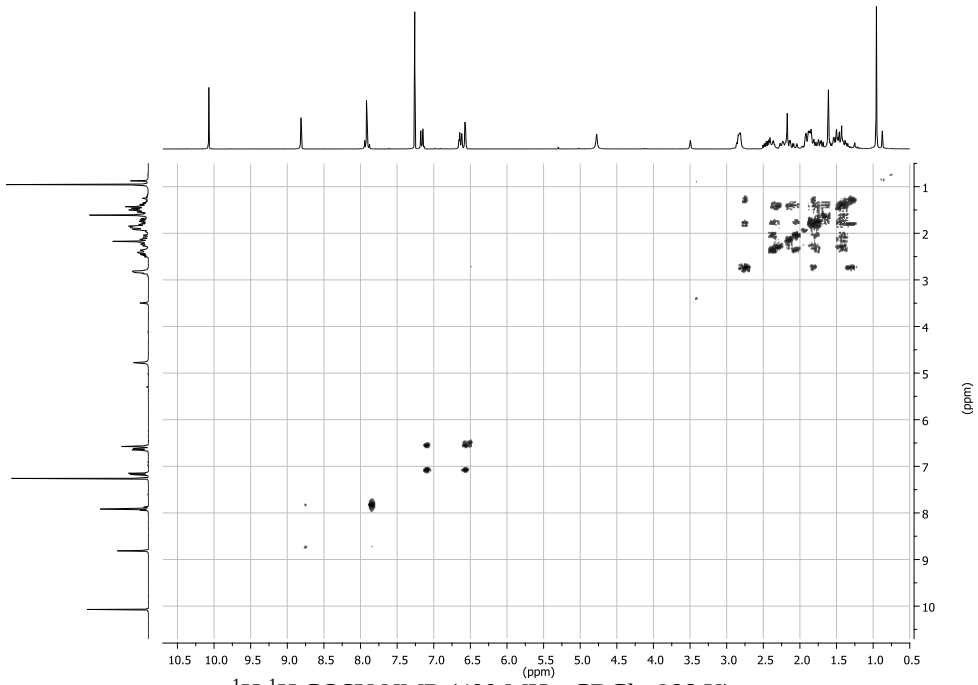

^{1}H-^{1}H COSY NMR (400 MHz, $CDCl_3$, 298 K)

A.13 2D-NMR (COSY) of $[Fe_2L^{Estro}{}_3][BF_4]_4$

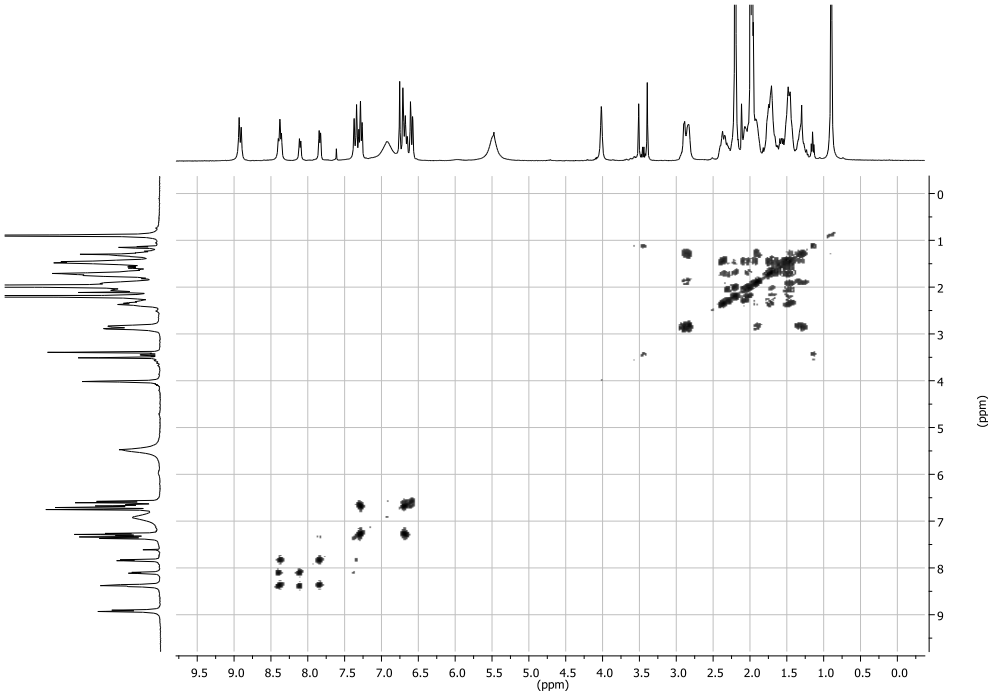

^{1}H-^{1}H COSY NMR (400 MHz, CD_3CN, 298 K)

A.14 2D-NMR (COSY) of 5-(2-N-acetyl-3,4,6-tri-O-acetyl-1-(2'-propargyl)-β-D-glucosaminide)-2-pyridinecarboxaldehyde (9)

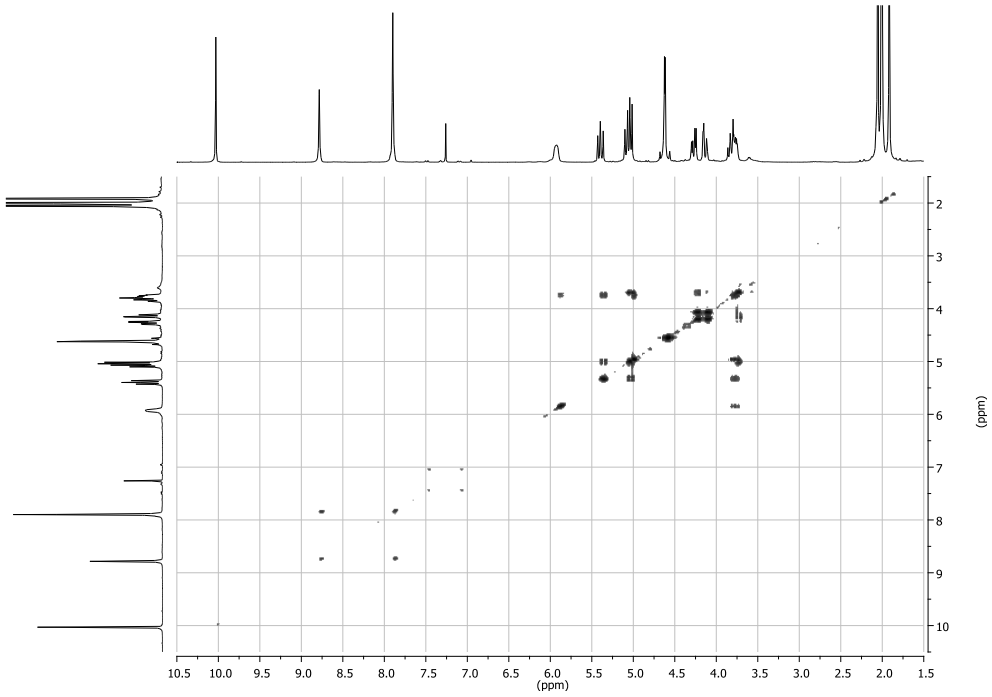

^{1}H-^{1}H COSY NMR (400 MHz, $CDCl_3$, 298 K)

A.15 2D-NMR (COSY) of $[Fe_2L^{OAcSug}{}_3][BF_4]_4$

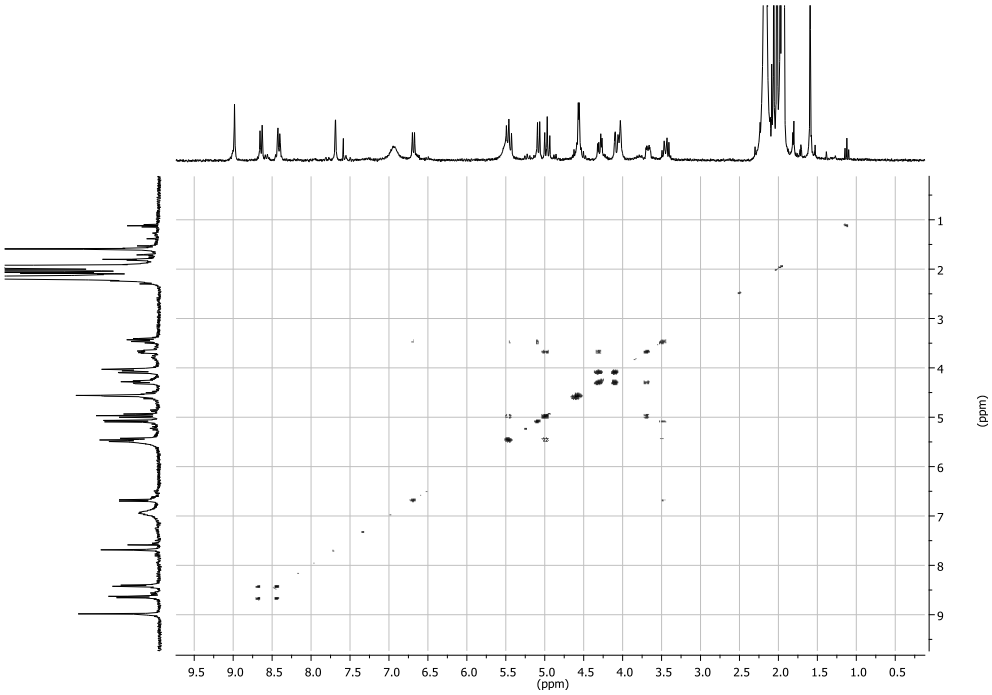

^{1}H-^{1}H COSY NMR (400 MHz, CD_3CN, 298 K)

A.16 2D-NMR (COSY) of 5-(2-N-acetyl-1-O-(2'-propargyl)-β-D-glucosaminide)-2-pyridinecarboxaldehyde (10)

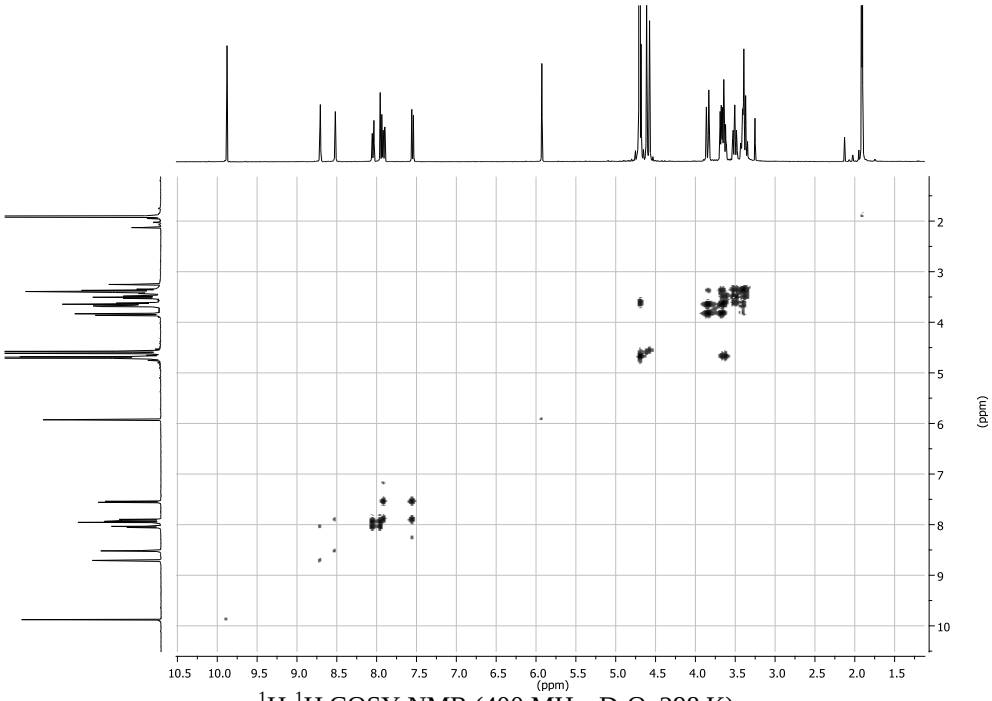

^{1}H-^{1}H COSY NMR (400 MHz, D_2O, 298 K)

A.17 ESI mass spectrum of $[Fe_2L^P_3][BF_4]_4$

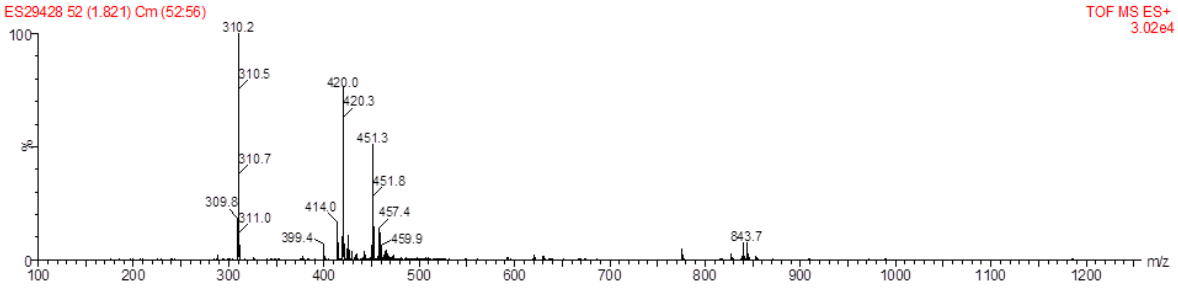

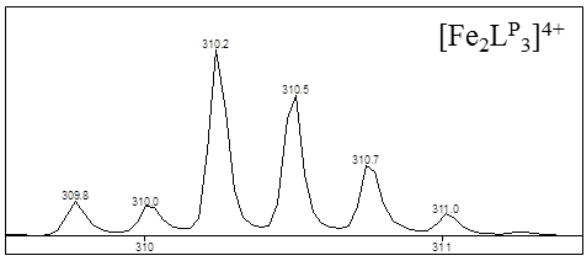

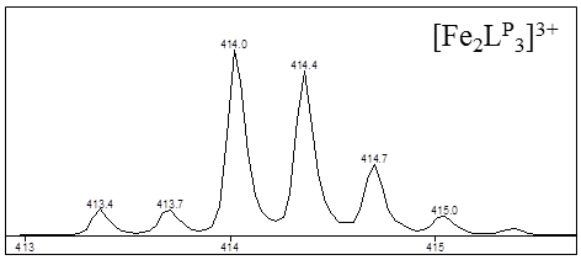

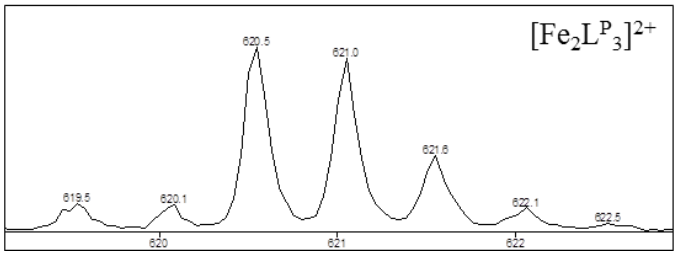

A.18 ESI mass spectrum of $[Fe_2L^{TB}_3][BF_4]_4$

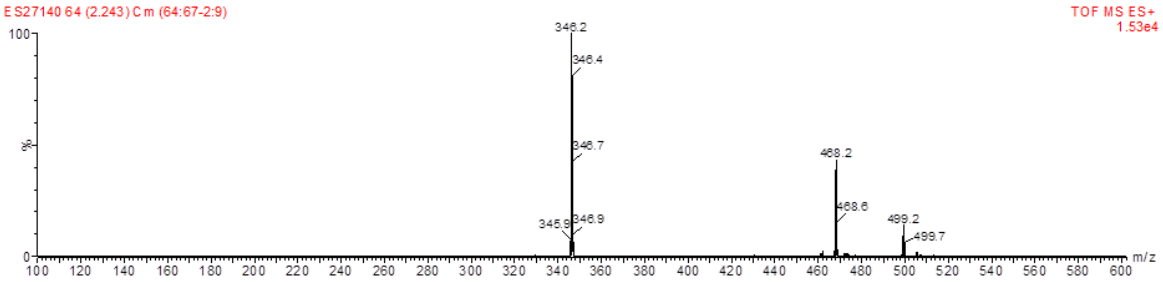

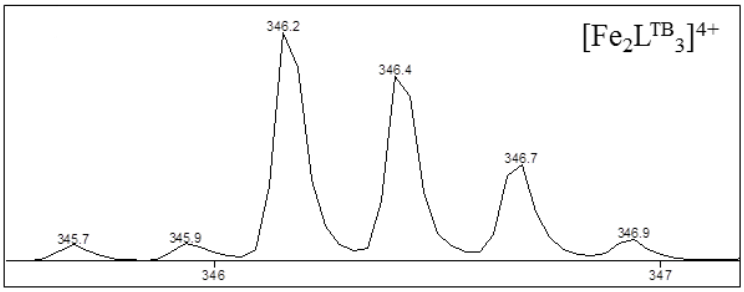

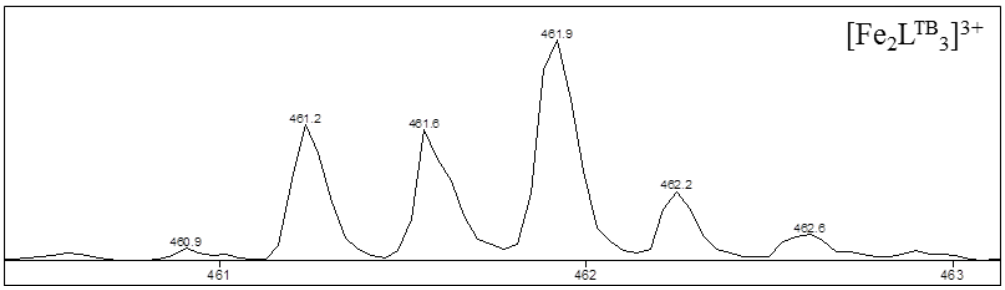

A.19 ESI mass spectrum of $[Fe_2L^{PA}{}_3][BF_4]_4$

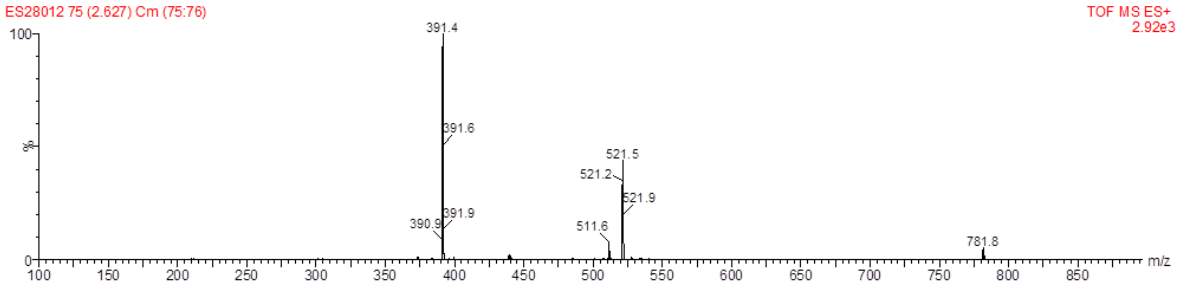

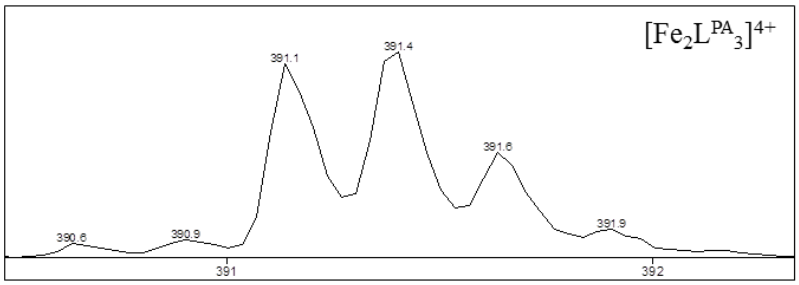

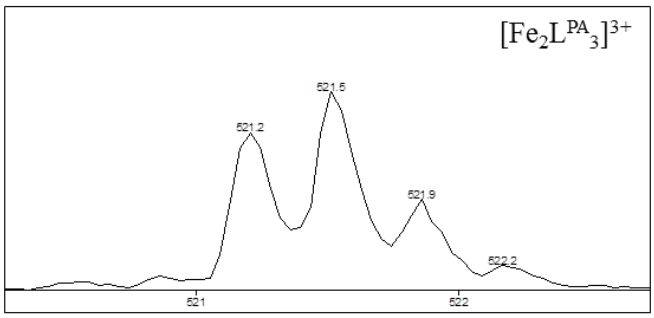

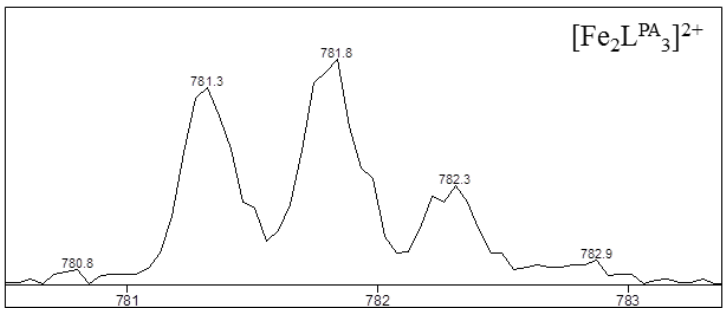

A.20 ESI mass spectra of $[Fe_2L^{Hex}_3][BF_4]_4$

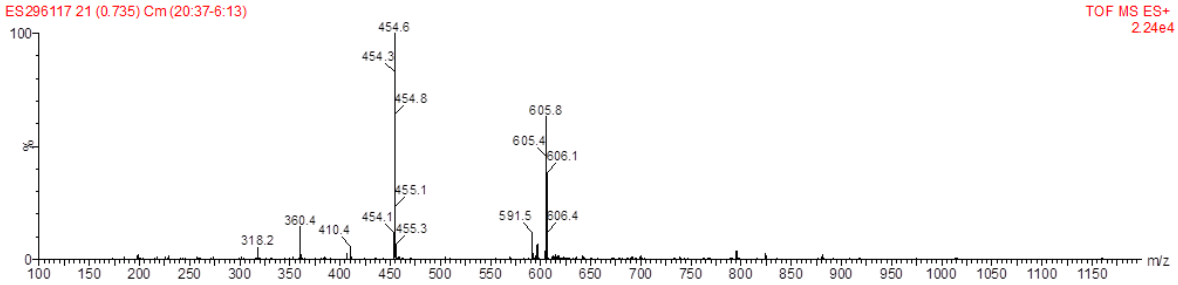

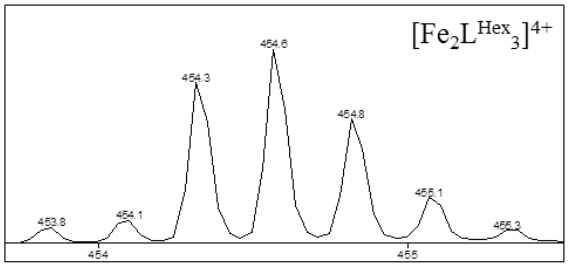

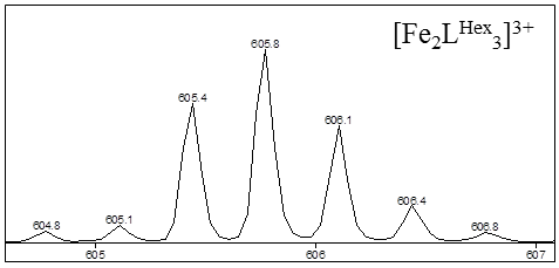

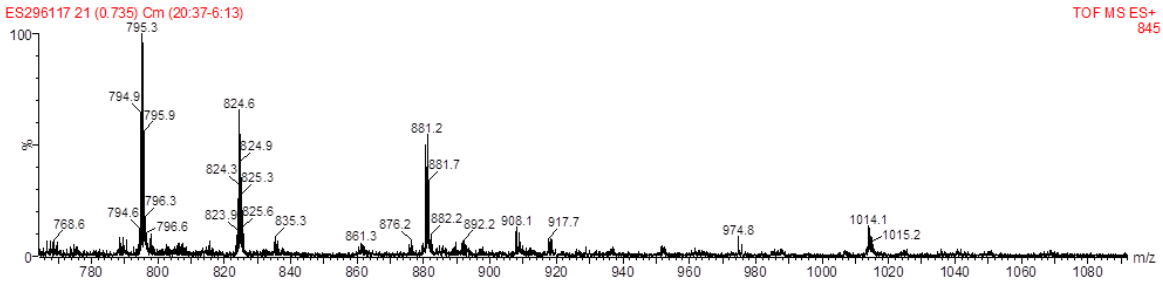

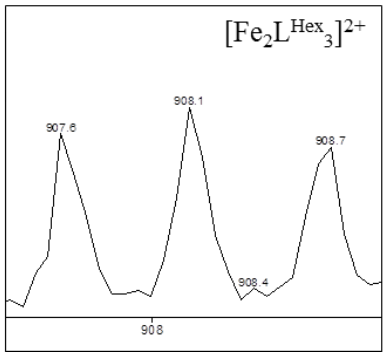

A.21 ESI mass spectrum of $[Fe_2L^{Phen}{}_3][BF_4]_4$

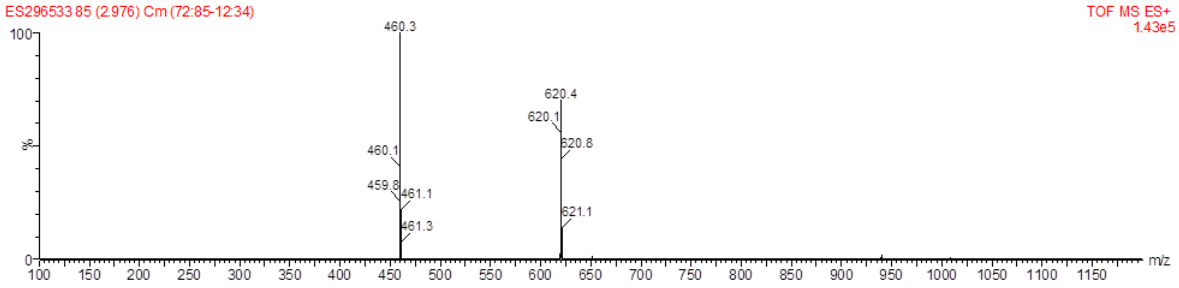

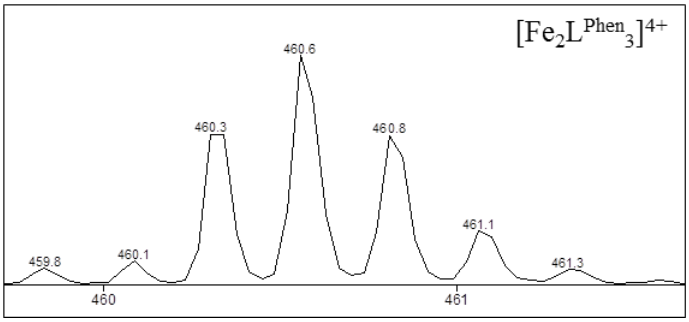

A.22 ESI mass spectrum of $[Fe_2L^{Test}_3][BF_4]_4$

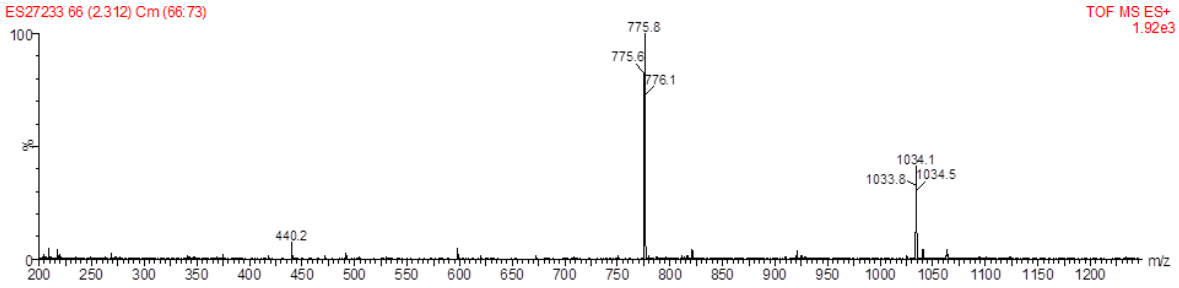

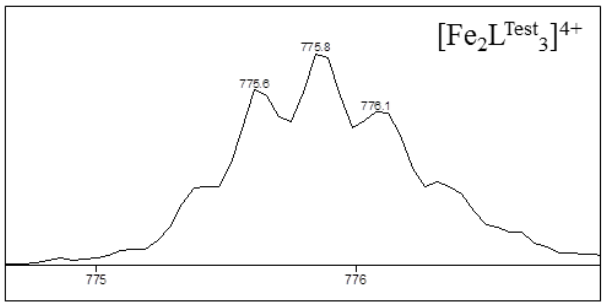

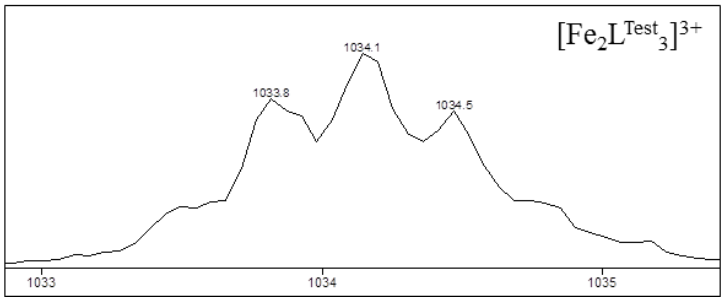

A.23 ESI mass spectrum of $[Fe_2L^{Estro}{}_3][BF_4]_4$

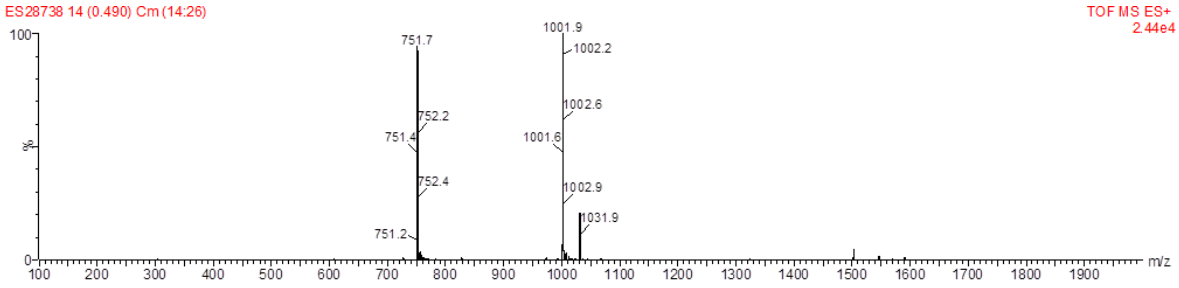

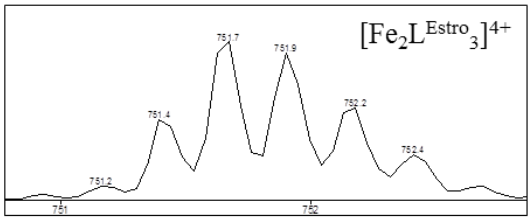

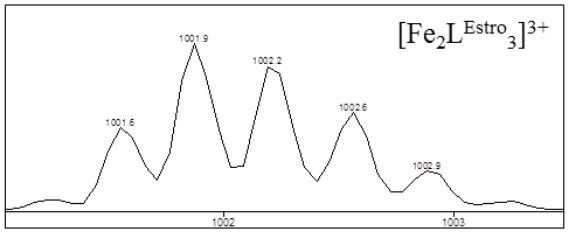

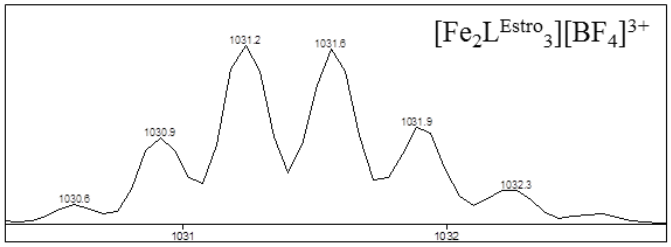

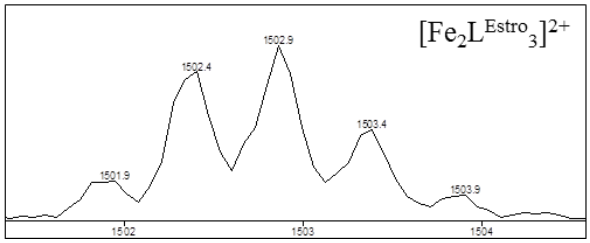

A.24 ESI mass spectrum of $[Fe_2L^{OAcSug}{}_3][BF_4]_4$

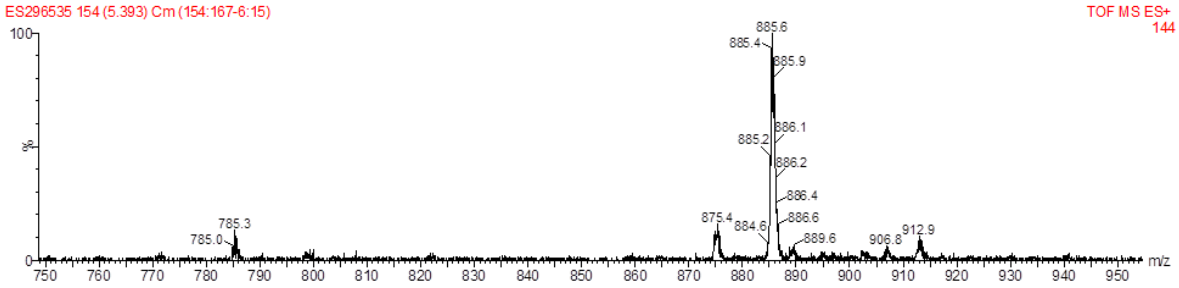

A.25 ESI mass spectra of $[Fe_2L^{OHSug_3}][BF_4]_4$

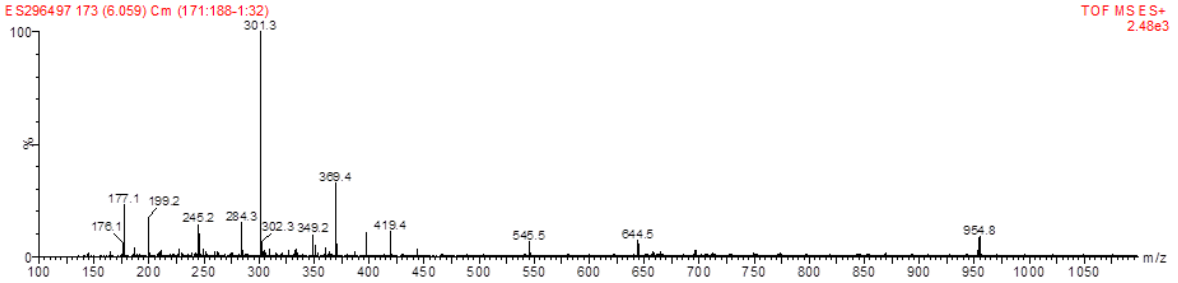

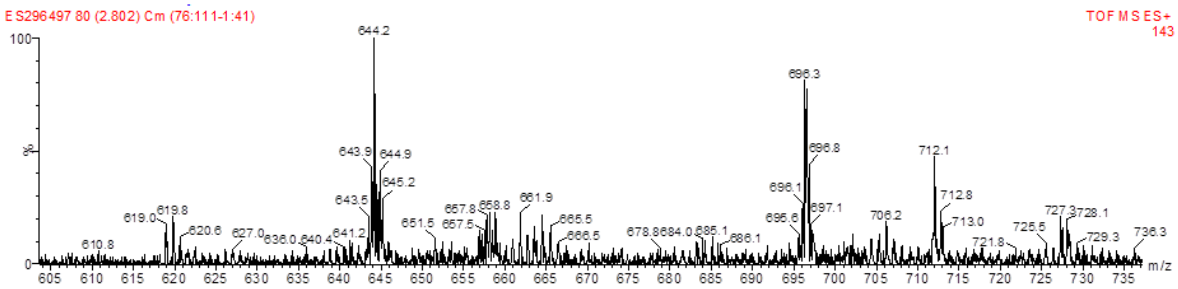

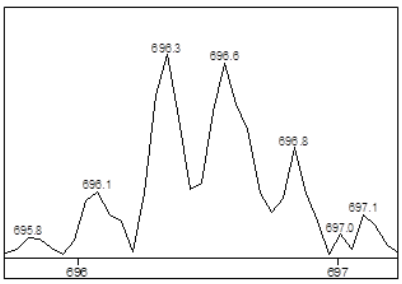

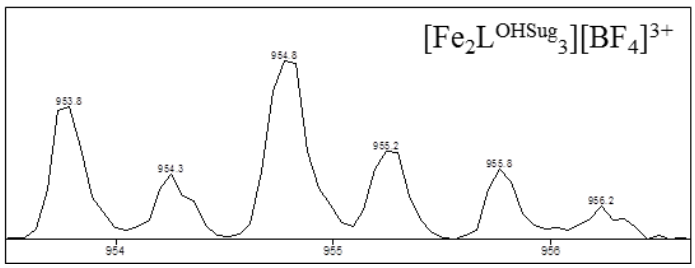

A.26 Autoradiogram of polyacrylamide gel run at 25 °C.

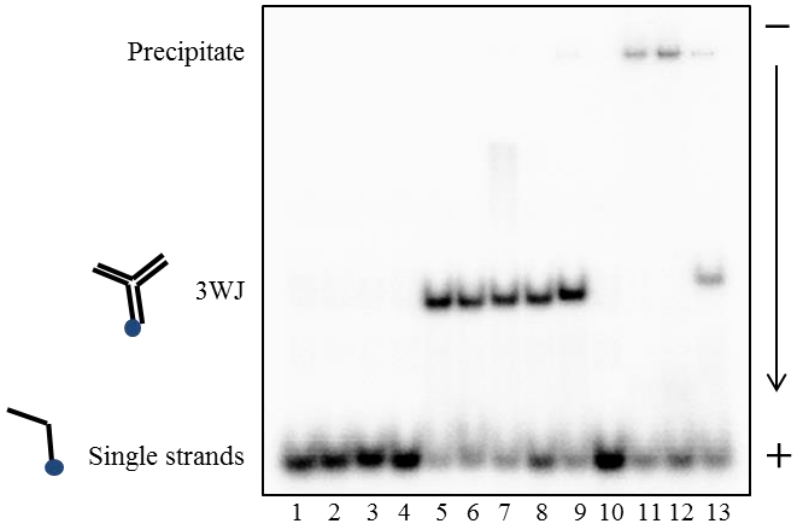

Lanes 1-3: S3*, S3*+S2, S3*+S2+S1 respectively; Lane 4: S3*+S2+S1+$MgCl_2$; Lanes 5-10: S3*+S2+S1 with $[Fe_2L^{P}{}_3][Cl]_4$, $[Fe_2L^{P}{}_3][BF_4]_4$, $[Fe_2L^{TB}{}_3][BF_4]_4$, $[Fe_2L^{PA}{}_3][BF_4]_4$, $[Fe_2L^{Hex}{}_3][BF_4]_4$, $[Fe_2L^{Phen}{}_3][BF_4]_4$, $[Fe_2L^{Test}{}_3][BF_4]_4$, $[Fe_2L^{Estro}{}_3][BF_4]_4$ and $[Fe_2L^{OAcSug}{}_3][BF_4]_4$ respectively. Ratio of three-way junction (S1+S2+S3*):complex of 1:1. Asterisk indicates ^{32}P labelled strand.